Quantification of Nutrients in a Few Real Food Samples by Developing Specific Sensors

Thesis submitted

By

Dipan Bandyopadhyay

Doctor of Philosophy (Engineering)

Department of Instrumentation and Electronics Engineering

Faculty Council of Engineering & Technology

Jadavpur University, Kolkata, India

2025

Jadavpur University

Kolkata-700 032

INDEX NO. 248/23/E

Faculty of Engg. & Tech. Department:	Department of Instrumentation and Electronics Engineering
Name of the Degree:	**Doctor of Philosophy (Engineering)**
Name of the Candidate:	**Dipan Bandyopadhyay**
Proposed title of the Ph.D. thesis:	Quantification of Nutrients in a Few Real Food Samples by Developing Specific Sensors
Dept./Inst. Lab. Where the research was conducted:	Department of Instrumentation and Electronics Engineering,Jadavpur University Salt Lake Campus Kolkata-700098, India.
Date of Registration:	**5th April, 2023**
Roll No.:	**PHDIEE24105**
Date of submission of thesis:	**24th September 2025**
Name & Complete Official address of the Supervisors:	**Prof. Runu Banerjee Roy** Professor Dept of Instrumentation and Electronics Engineering,Jadavpur University, Salt Lake Campus, Sector-III, Block-LB, Plot-8, Kolkata-7000 098, India. Phone: 033-2335-2587.

PUBLICATIONS

JOURNALS:

- Dipan Bandyopadhyay, Shreya Nag, Debangana Das, Srikanta Acharya, Bipan Tudu, Panchanan Pramanik, Rajib Bandyopadhyay, and Runu Banerjee Roy, "Voltammetric Detection of Inositol Using a Platinum-Based Electrode", NANOLIFE Journal, March 2022, doi: 10.1142/S1793984422500040.
- D. Bandyopadhyay, S. Acharya, S. Nag, D. Das, and R. B. Roy, "A Molecular-Imprinted Bipolymer Infused Capacitive Sensor for Inositol Detection in Fruits," *IEEE Transactions on Instrumentation and Measurement*, vol. 72, pp. 1-9, 2023, Art no. 9512409, doi: 10.1109/TIM.2023.3306839.
- D. Bandyopadhyay, S. Nag, D. Das, and R. B. Roy, "Detection of syringic acid in food extracts using molecular imprinted polyacrylonitrile infused graphite electrode," *Journal of food composition and analysis*, vol. 132, p. 106280, Aug. 2024, doi: 10.1016/j.jfca.2024.106280.
- D. Bandyopadhyay, S. Nag, D. Das, and R. B. Roy, "Electrochemical detection of Folic Acid in Food Extracts Using Molecularly Imprinted Polyacrylonitrile Imbued Graphite Electrode," *Analytica chimica acta*, vol. 1325, p. 343120, Aug. 2024, doi: 10.1016/j.aca.2024.343120.
- D. Bandyopadhyay, S. Nag, D. Das, and R. B. Roy, "A novel RGO-Decorated molecularly imprinted polyacrylic acid graphite electrode for the detection of quercetin in food," *IEEE Transactions on Instrumentation and Measurement*, vol. 73, pp. 1–8, Jan. 2024, doi: 10.1109/tim.2024.3398119.
- D. Bandyopadhyay, S. Nag, S. Acharya, D. Das and R. B. Roy, "A Novel Molecular Imprinted Dual-Polymer Infused Capacitive Sensor for Quercetin Detection in Agro Products," *IEEE Sensors Journal*, vol. 25, no. 21, pp. 39418-39425, 1 Nov.1, 2025, doi: 10.1109/JSEN.2025.3614749.
- D. Bandyopadhyay, S. Nag, J. Naskar, and R. B. Roy, "Towards the development of an integrated, user friendly, voltammetric electrode for the electrochemical sensing of food quality," *Measurement*, vol. 260, p. 119776, Nov. 2025, doi: 10.1016/j.measurement.2025.119776.

CONFERENCES:

- Dipan Bandyopadhyay, Shreya Nag, Runu Banerjee Roy, “Quantification of syringic acid in real samples based on uv-vis spectroscopy”, *IEEE Silchar Subsection Conference (IEEE SILCON-2022)*, Silchar, Assam, India

- D. Bandyopadhyay, S. Nag and R. B. Roy, "Prospect of UV-Vis Spectroscopy in Quantification of Folic Acid in Food Extracts," *2025 International Conference on Communication and Smart Devices (ICCoSD)*, Ranchi, India, 2025, pp. 1-5, doi: 10.1109/ICCoSD66074.2025.11348264.

Statement of Originality

I, Dipan Bandyopadhyay, registered on 5th April, 2023, do hereby declare that this thesis entitled "Quantification of Nutrients in a Few Real Food Samples by Developing Specific Sensors" contains a literature survey and original research work done by the undersigned candidate as part of Doctoral studies.

All information in this thesis has been obtained and presented in accordance with existing academic rules and ethical conduct. I declare that, as required by these rules and conduct, I have fully cited and referred all materials and results that are not original to this work.

I also declare that I have checked this thesis as per the "Policy on Anti-Plagiarism, Jadavpur University, 2019", and the level of similarity as checked by iThenticate software is 6%.

Dipan Bandyopadhyay

Dipan Bandyopadhyay
Index No. 248/23/E
Date: 25/03/2026

Professor
Dept. of Instrumentation & Electronics Engg
Jadavpur University
Saltlake, 2nd Campus
Kolkata-700 106

Prof. Runu Banerjee Roy
Professor
Dept. of Instrumentation and Electronics Engineering,
Jadavpur University, Salt Lake Campus, Kolkata- 700106. India

Certificate from the Supervisor

Date: 25/03/2026

This is to certify that the thesis entitled "Quantification of Nutrients in a Few Real Food Samples by Developing Specific Sensors" submitted by Dipan Bandyopadhyay, who got his name registered on 5th April, 2023 for the award of Ph.D. (Engineering) degree of Jadavpur University, is absolutely based upon his own work under the supervision of Prof. Runu Banerjee Roy, and that neither his thesis nor any part of the thesis has been submitted for any degree/diploma or any other academic award anywhere before.

Professor
Dept. of Instrumentation & Electronics Engg
Jadavpur University
Saltlake, 2nd Campus
Kolkata-700 106

Prof. Runu Banerjee Roy
Professor
Dept. of Instrumentation and Electronics Engineering,
Jadavpur University, Salt Lake Campus, Kolkata-700106. India

विद्वान्प्रशस्यते लोके विद्वान् सर्वत्र पूज्यते ।
विद्यया लभते सर्वं विद्या सर्वत्र पूज्यते ॥

Knowledge is extolled by everyone, knowledge is considered great everywhere, one can attain everything with the help of knowledge, and the person is respected everywhere.

This thesis is dedicated to
my parents
Late Pradip Kumar Bandyopadhyay
and
Smt. Bandana Bandyopadhyay
For their endless love, support, and encouragement

Acknowledgements

With a heart full of profound gratitude and a spirit humbled by the arduous journey, I stand on the precipice of submitting this thesis—a culmination of countless hours of relentless hard work, navigating through numerous setbacks, and overcoming significant struggles. This endeavor, sparked by the realization that a PhD is the cornerstone of a fulfilling research career, has been a transformative odyssey, made possible only by the unwavering support and invaluable guidance of truly remarkable individuals.

As a student within this esteemed institution, I have been exceptionally fortunate to avail myself of the state-of-the-art facilities and robust infrastructure provided by the Department of Instrumentation and Electronics Engineering (IEE), Jadavpur University, a privilege that has been indispensable to my progress.

A boundless debt of gratitude is owed to my exceptional supervisor, Prof. Runu Banerjee Roy. Her unwavering motivation, ceaseless assistance, and steadfast support have been the guiding stars through every intricate phase of this research. It is with immense gratitude that I also extend my most sincere thanks to Prof. Rajib Bandyopadhyay and Prof. Bipan Tudu of the Department of Instrumentation & Electronic Engineering at Jadavpur University. Their profound insights and immense support created an environment of warmth and intellectual camaraderie, allowing me to flourish. Their remarkable patience and flexibility in guiding my choice of research areas, alongside their firm integration into my academic journey, have sculpted this thesis into what it is. I pray for their continued blessings as I aspire to achieve even greater heights. Furthermore, I owe a significant debt to Dr. Panchanan Pramanik, the esteemed retired professor from the Department of Chemistry at IIT Kharagpur, whose expert guidance, particularly in the intricate chemistry-related aspects of my thesis, was truly invaluable.

I extend my heartfelt thanks to the following for their indispensable technical assistance: Dr. Dipankar Mandal from the Institute of Nano Science and Technology, Mohali, for the meticulous FTIR analysis; Dr. Ramdhan Majhi from the Indian Institute of Chemical Biology, Kolkata, for the precise HPLC analysis; the Department of Physics, Jadavpur University, Kolkata, for their support with FESEM and FTIR analysis; and the UGC DAE Consortium, Kolkata Centre, for their crucial XRD amenities. The dedicated technical and non-technical staff of the IEE department also rendered invaluable assistance throughout my study. A special note of appreciation goes to Mrs. Ruma De, whose ready availability and kindness were a constant source of comfort and support.

My profound appreciation and thanks extend to all my seniors, contemporary lab mates, and juniors who have shared this journey with me, fostering a supportive and collaborative atmosphere. Specifically, I acknowledge Debangana Das, Mr. Srikanta Acharya, Mrs. Madhurima Moulick, Mrs. Mahuya Bhattacharya, Mr. Deepam Gangopadhyay, Mrs. Samhita Dasgupta, Mr. Sumit Kundu, Mr. Mohasin Ali, Mr. Hemanta Naskar, Mr. Sourav Bagchi, Mr. Diganta Mondal, Mr. Nilabha Debabhuti, Jayanti Das, Ahana Patra, Indronil Mazumder, and all other colleagues who brightened my days and shared my burden. A special note of deepest gratitude goes to Ms. Shreya Nag and Mr. Jeet Naskar for their all-out support throughout my research journey.

My Eternal Pillars: Parents and Family

The adage that a supportive family is the cornerstone of success resonates deeply with me, and I am eternally grateful to God for bestowing upon me such a blessing.

To my dearest Late Pradip Kumar Bandyopadhyay, my revered father, and Bandana Bandyopadhyay, my cherished mother: words alone are insufficient to convey the depth of my gratitude. You are the very foundation upon which my dreams were built. Your unconditional love has been my shield through every storm, your sacrifices countless, and your faith in my abilities an unwavering beacon. Every step of this arduous journey, every moment of triumph, every struggle overcome, has been imbued with the essence of your boundless support and ceaseless prayers. You taught me resilience, the value of perseverance, and the profound meaning of striving for excellence. This thesis, born of my efforts, is also a testament to your enduring spirit and sacrifices, a humble offering to the two souls who shaped my world. Thank you for everything, from the deepest corners of my heart.

My heart is also filled with profound appreciation for the unwavering affection and steadfast encouragement bestowed upon me by my maternal uncles, Sarojit Chatterjee and Biswajit Chatterjee, and my beloved aunts, Nanda Mondal, Chanda Ghosal, and Tandra Mukherjee. And to my dearest maternal brothers and sisters—Soma Mondal, Suvo Mondal, Tua Chatterjee, Susmita Mukherjee, Basob Ghoshal, Tuna Chatterjee, Swarnodip Chatterjee, and Papiya Chatterjee—your collective presence has been a vibrant, continuous source of solace and immense strength, echoing love through every triumph and tribulation. Furthermore, my deepest gratitude extends to Sambhu Mondal, Pranab Mukherjee, Aparna Chatterjee, Suvankar Mondal, and Eliza Parvin, to the vast constellation of my paternal kin, my wider circle of cherished relatives, and all other well-wishers connected with me. I must also extend a special mention of heartfelt

thanks to Pampa Mondal, whose consistent dedication, hard work and support have brought immense comfort and invaluable assistance to my family life. Her unwavering kindness and boundless affection have illuminated my path throughout my life.

My Guiding Lights: The Teachers Who Shaped My Path

Beyond the confines of this research, my journey has been illuminated by the profound wisdom and boundless dedication of the educators who first ignited the flame of curiosity within me. To all my revered teachers from school life through college, your influence has been immeasurable. You did not merely impart knowledge; you instilled a love for learning, a discipline for inquiry, and a thirst for understanding that has ceaselessly driven my pursuits. Your patience, your passion, and your unwavering belief in your students, even in their formative years, laid the very bedrock upon which my academic aspirations were built. For these invaluable gifts, my heart overflows with eternal gratitude.

The Heartbeat of My Purpose: My Cherished Students

And to all my beloved students—each a testament to the future's bright promise—you have been a constant, resounding echo of purpose in my life. Spanning from the batches of 2013 through to those currently pushing towards their 2026, 2027 and 2028 pass-outs, your unwavering support, infectious enthusiasm, and boundless belief in me have not merely been inspiring but truly a wellspring for my spirit. Witnessing your vibrant growth and burgeoning potential has been a profoundly heartwarming experience—a daily reminder of the beautiful, reciprocal impact of education that touches my heart in the most profound ways. Thank you for enriching my life far beyond what words can capture.

This thesis is not just a document of research; it is a testament to the collective efforts, encouragement, and belief of every individual named here and many more unsung heroes. Thank you, from the depths of my heart.

Abstract

Food remains the fundamental source of nourishment, making the assurance of its safety and quality paramount. To address this, establishing efficient and reliable methods for food quality evaluation is essential. This thesis concentrates on the development of novel molecularly imprinted polymer (MIP) based sensors for the rapid and selective detection of key food nutrients: Inositol, Syringic Acid (SGA or SA), Folic Acid (FA), and Quercetin (QCN or QT). Furthermore, the work explores a portable, on-site detection system for Salicylic Acid (ScA).

The research details the fabrication, characterization, and analytical performance of various electrochemical and capacitive sensors. Using techniques such as Cyclic Voltammetry (CV) and Differential Pulse Voltammetry (DPV), the sensors' electrocatalytic properties were optimized by investigating critical factors like pH, buffer composition, and scan rate. These platforms were rigorously characterized for their size, structure, and morphology using diverse analytical tools.

The core findings include two distinct platforms for Inositol detection: a platinum-based electrochemical system and a sensitive MIP-based capacitive sensor, both successfully applied to orange juice samples. It also details a selective acrylonitrile MIP-on-graphite sensor for Syringic acid, validated against HPLC. For Folic acid, a polyacrylonitrile-imbued graphite electrode (MAN@G) demonstrated a remarkably low limit of detection in diverse food extracts. For Quercetin, an rGO-decorated MIP graphite electrode and a dual-polymer capacitive sensor were developed. Finally, an integrated pen-like tri-electrode system for on-site Salicylic acid detection is introduced, offering improved portability.

In conclusion, this thesis demonstrates the strategic use of MIPs and advanced materials to overcome the limitations of conventional techniques. The developed technologies offer a promising pathway toward cost-effective, portable, and reliable devices for real-time food quality assessment.

Contents

List of figures

List of tables

List of abbreviations

Abbreviation	Full Form
AA	Acrylic acid
Ag/AgCl	Silver/Silver chloride
AM	Acrylamide
AN	Acrylonitrile
ASV	Anodic stripping voltammetry
ATR	After template removal
Au	Gold
BOL	Black olives
BP	benzoyl peroxide
BTR	Before template removal
CA	Control amplifier
CE	Counter electrode
CF	Correlation factor
CHIT	Chitosan
CLF	Cauliflower
CNTs	Carbon nanotubes
CPE	Carbon paste electrode
C_{pis}	Parallel Capacitance (inositol, IS)
CSV	Cathodic stripping voltammetry
CV	Cyclic voltammetry
DPV	Differential pulse voltammetry
EGDMA	Ethylene glycol Di methacrylate
GA	Gallic acid
FA	Folic acid
FESEM	Field emission scanning electron microscope
FTIR	Fourier transform infrared spectroscopic
GC-MS	Gas Chromatography-Mass Spectrometry
GO	Graphene oxide
GCE	Glassy carbon electrode
LOD	Limit of detection
GC	Gas Chromatography
HPLC	High-Performance Liquid Chromatography

Abbreviation	Full Form
HRTEM	High-resolution transmission electron microscope
IEE	Department of Instrumentation and Electronics Engineering
IR	Infrared Spectroscopy
LSV	Linear sweep voltammetry
LOQ	Limit of Quantification
MAA	Methacrylic acid
MA	Maleic acid
M2P-QT@C	Polydopamine-polyethylene glycol (PDA-PEG) infused molecularly imprinted capacitive sensor
MAN@G	Molecularly imprinted polyacrylonitrile-imbued graphite-base electrode
MI-2P-IS@C	MIP-based PDA-PEG-coated capacitive sensor
M-AARGO@G	rGO decorated Molecularly Imprinted Polyacrylic Acid Graphite Electrode
MIP	Molecularly Imprinted Polymer
MIP(GA-ScA)/G	Gallic acid (GA) for MIP(GA-ScA)/G working electrode
MIP-AN@G	Molecularly imprinted polymer based electrochemical sensor using acrylonitrile (AN) MIP over graphite
MIS	Myo-inositol
MWCNT	Multiwalled carbon nanotube
NI-2P@C	Non-imprinted
NIP	Non imprinted polymer
NIP-AN@G	Non-imprinted polymer
NMR	Nuclear Magnetic Resonance Spectroscopy
NPV	Normal pulse voltammetry
ORG	Oregano
PAN	Polyacrylonitrile
PBS	Phosphate buffer solution
PCA	Principal component analysis
PCR	Principal component regression
PCs	Principal components
PDA	Polydopamine
PDA-PEG	Polydopamine-Polyethylene glycol
PLSR	Partial least squares regression

Abbreviation	Full Form
PMMA	Polymethylmethacrylate
Pt	Platinum nanoparticles
PV	Pulse voltammetry
PVDF	Polyvinyldene fluoride
QCN/QT	Quercetin
QCM	Quartz crystal microbalances
RE	Reference electrode
rGO	Reduced Graphene Oxide
RMSEV	Root mean square error of validation
RMSEP	Root mean square error of prediction
RMSEC	Root mean square error of calibration
SA or SGA	Syringic acid
ScA or SAc	Salicylic Acid
SCE	Saturated calomel electrode
SEM	Scanning electron microscope
SI	Separability index
SPE	Screen printed electrode
SV	Stripping voltammetry
SWV	Square wave voltammetry
TLC	Thin-Layer Chromatography
UV-Vis	Ultraviolet-Visible Spectroscopy
VNL	Vanillin
WE	Working electrode
WHO	World Health Organization
ppb	parts per billion
IS	inositol
TS	test solution
LOOCV	Leave-One-Out Cross-Validation
t-test	Student's t-test (Statistical test analysis)
DA	Dopamine
XRD	X-ray diffraction
Z_{pis}	Impedance
θ_{pis}	Phase angle

Introduction and scope of the thesis

1

1.1 Introduction:

The burgeoning understanding of the intricate relationship between diet and human health has ignited significant scientific inquiry into the multifaceted roles of vitamins and food nutrients. Beyond their fundamental functions in energy provision and tissue maintenance, these phytochemicals are increasingly recognized for their potent antioxidant, aromatic, anti-inflammatory, and a spectrum of other medically significant properties. This heightened awareness underscores the critical contribution of food-derived compounds to disease prevention, management, and the promotion of overall well-being. At the core of this nutritional paradigm lie six essential categories of nutrients: carbohydrates, the primary energy source; proteins, vital for tissue building and repair; fats, crucial for energy storage and vitamin absorption; vitamins, orchestrators of diverse bodily functions; minerals, supporting skeletal integrity and nerve transmission; and water, the indispensable medium for hydration and temperature regulation. An adequate and balanced intake of these nutrients, achievable through a varied diet rich in whole foods, bestows a multitude of health advantages as stated earlier. Embracing a dietary pattern abundant in fruits, vegetables, whole grains, lean proteins, and healthy fats is pivotal for sustaining healthy skin, hair, and nails, fostering mental acuity and emotional well-being, and mitigating the risk of debilitating chronic diseases such as cardiovascular disorders, diabetes, and certain cancers. Consequently, a substantial wave of scientific and public interest has emerged, focusing on the development of robust and reliable methods for quantifying these health-promoting compounds within our food supply. A central objective in this endeavor is the precise determination of key bioactive molecules, including inositol, syringic acid (SA), folic acid (FA), and quercetin (QCN). Inositol, a naturally occurring compound found in various food sources and supplements [1, 2], shows promise in managing conditions like depression and insulin resistance; however, adhering to safe intake levels, as exemplified by Codex Alimentarius guidelines for infant formula (4.0-40.0 mg/100 kcal for myo-inositol [3]), is important to prevent mild side effects. Syringic acid (SA), a phenolic compound present in numerous plants and foods [4-10], exhibits diverse therapeutic effects, including antioxidant and anti-inflammatory properties [6, 11-13], with potential in preventing chronic diseases and

generally considered non-toxic within suggested intake levels (1800–3200µg/person/day [14]). Folic acid (FA), a crucial B-vitamin for fundamental biological processes [15, 16] obtained through diet or supplements [17] with recommended intakes varying by life stage (e.g., 400-1000 µg DFE for adults [18]), carries risks of deficiency (anemia, neural tube defects [19]) and potential harm from excessive intake [20]. Quercetin (QCN), a flavonoid abundant in many plant-based foods [21], demonstrates significant antioxidant, anti-inflammatory, and anti-cancer activities [21-24], with generally mild side effects at high doses, highlighting its health-promoting potential.

Modern agriculture's reliance on pesticides and harmful chemicals poses a significant threat to the nutritional quality of food by potentially disrupting the biochemical processes responsible for vital health-beneficial compounds. Accurate quantification of these compounds is crucial for ensuring food quality and public health. Therefore, there is a compelling and urgent need for the development of simple, affordable, and rapid methodologies for accurately detecting and quantifying these crucial health-beneficial compounds in real food samples. While existing analytical methods like chromatography, spectroscopy, electrochemistry, and enzymatic/chemiluminescence techniques offer various advantages, they often suffer from limitations such as high cost, complex procedures, and environmental concerns. This thesis addresses the urgent need for simple, affordable, and rapid methodologies for quantifying these essential compounds in real food samples. It explores and develops improved detection methods, focusing on electrochemical and spectroscopic techniques integrated with advanced multivariate analysis, ultimately aiming to contribute to more accessible and sustainable tools for accurate nutritional assessment and enhanced food quality.

1.2 Selection of food nutrients

In the proposed work, sensors have been developed for the selective recognition of four types of health-beneficial food nutrient molecules as summarized in the Table. 1.

Table. 1

Selected health-beneficial food nutrient molecules

Sl. No.	Molecule category	Molecule name
1.	Sugar	Inositol
2.	Phytochemical (Phenolic acid)	Syringic acid
3.	Vitamin	Folic acid
4.	Phytochemical (Flavonol)	Quercetin

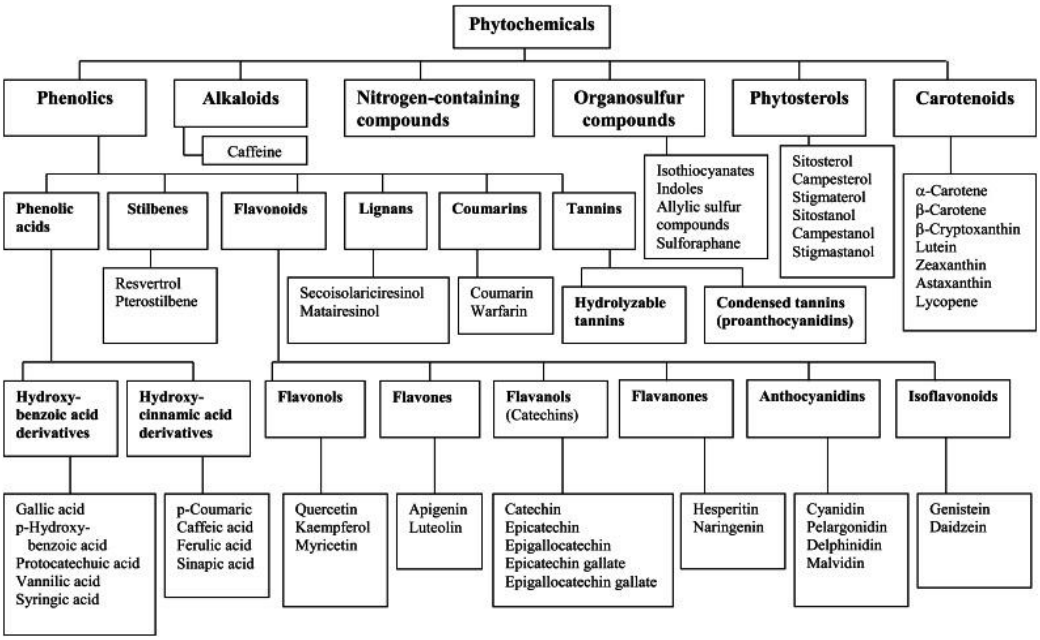

Fig. 1.1. Classification of phytochemicals

The pervasive use of pesticides and other harmful chemicals in modern agricultural practices presents a significant challenge to the nutritional integrity of our food supply. These agents can interfere with the intricate biochemical pathways governing the activity of these vital compounds, potentially diminishing their beneficial effects. This necessitates the development of reliable and accurate analytical methods for assessing food quality based on the precise quantification of the aforementioned health-beneficial compounds. Current methodologies for detecting and quantifying these compounds generally fall into several categories: (a) Chromatographic methods, such as gas chromatography (GC) and high-performance liquid chromatography (HPLC), offer high separation efficiency but often involve complex sample preparation and expensive instrumentation. (b) Spectroscopic methods, like UV-Vis spectroscopy, provide rapid and non-destructive analysis but may lack the required sensitivity for detecting low concentrations. (c) Electrochemical methods offer the potential for cost-effective and sensitive detection, but require careful selection and modification of electrode materials. (d) Enzymatic and chemiluminescent methods can provide good sensitivity but may be susceptible to interference from other compounds present in the food matrix. Despite their strengths, many of these existing analytical techniques suffer from limitations such as high cost, the use of toxic solvents, and the need for highly skilled operators.

The prime objective of developing dedicated sensors is to detect and quantify the content of these medically valuable compounds in real food samples, even if they occur in low quantities amid other compounds. This research focuses on developing robust nutrient-specific

sensors/sensor-based systems coupled with advanced machine learning algorithms to predict the quality attributes of specific food products in real-time, enabling proactive measures to maintain product integrity.

1.3 Qualitative assessment techniques for food-nutrients

Several qualitative assessment techniques for food nutrient detection have been discussed in section 1.1, which involve identifying and characterizing the nutrients present in a food sample. However, these common techniques can be broadly classified into:

1. Conventional methods

2. Electrochemical methods

1.3.1 Conventional Methods

Conventional methods for food nutrient analysis involve traditional laboratory techniques that have been used for decades to determine the nutritional content of food samples. These methods are often time-consuming, labor-intensive, and require specialized equipment and expertise. Analyzing the nutritional composition of food products relies on a variety of methodologies, each offering unique insights. Here are some conventional methods for food nutrient analysis:

- **Proximate Analysis**

Proximate analysis is a traditional method used to determine the moisture, ash, protein, fat, and carbohydrate content of food samples. This method involves various techniques such as:

- **Moisture content:** Determined by oven drying or vacuum drying.
- **Ash content:** Determined by incineration at high temperatures.
- **Protein content:** Determined by Kjeldahl method or Dumas method.
- **Fat content:** Determined by Soxhlet extraction or Babcock method.
- **Carbohydrate content:** Determined by difference calculation.

- **Chromatographic Techniques**

For more detailed and specific nutrient identification and quantification, Chromatographic Techniques are employed. High-Performance Liquid Chromatography (HPLC) allows for the separation and analysis of vitamins and amino acids, while Gas Chromatography (GC) is suited for fatty acids and volatile compounds. Thin-Layer Chromatography (TLC) provides a simpler method for separating and identifying vitamins and pigments.

➢ **Spectroscopic Techniques**

Spectroscopic techniques are used to analyze the interaction between light and nutrients in food samples. Common spectroscopic techniques used in food nutrient analysis include:

❖ **Infrared Spectroscopy (IR):** This technique is apposite for analyzing the molecular structure of nutrients such as proteins, carbohydrates, and fats.

❖ **Ultraviolet-Visible Spectroscopy (UV-Vis):** This technique is generally employed to analyze the absorption of light by nutrients, viz., vitamins and pigments.

❖ **Nuclear Magnetic Resonance Spectroscopy (NMR):** Like IR, this technique is employed to analyze the molecular structure of nutrients such as proteins, carbohydrates, and fats.

➢ **Titration Methods**

Titration methods involve the reaction between a nutrient and a reagent to determine the nutrient's concentration. Common titration methods used in food nutrient analysis include:

❖ **Acid-Base Titration:** Used to determine the acidity or alkalinity of food samples.

❖ **Redox Titration:** Used to determine the concentration of nutrients such as vitamins and minerals.

❖ **Complexometric Titration:** Used to determine the concentration of nutrients such as calcium and magnesium.

➢ **Microbiological Methods**

Microbiological methods involve the use of micro organisms to determine the nutrient content of food samples. Common microbiological methods used in food nutrient analysis include:

❖ **Microbial Assays:** Used to determine the concentration of nutrients such as vitamins and amino acids.

❖ **Bioassays:** Used to determine the biological activity of nutrients such as vitamins and hormones.

Pros and cons of conventional methods:

Traditional food nutrient analysis techniques are recognized for their reliability, offering high accuracy and precision in determining the composition of various food samples. These methods also exhibit a broad applicability, capable of analyzing a diverse array of nutrients across different food matrices. However, these established methodologies are not without their

drawbacks. They are often characterized by lengthy procedures and significant manual effort, making them time-consuming and labor-intensive. Furthermore, the implementation of these techniques necessitates specialized equipment and trained personnel, which can be a limiting factor for many laboratories. Lastly, the cost associated with these analyses, particularly for intricate nutrient profiles, can be substantial, posing a financial challenge.

In inference, conventional methods for food nutrient analysis are traditional laboratory techniques that have been used for decades to determine the nutritional content of food samples. While these methods have several advantages, they also have several limitations, including being time-consuming, labor-intensive, and expensive.

1.3.2 Electrochemical Methods

Electrochemical techniques are versatile and have a wide range of applications in various fields, including chemistry, industry, and environmental science. Understanding the fundamental principles of electrochemical cells and the nature of reactions occurring at electrodes is crucial for developing and utilizing these techniques effectively. The quest for rapid, selective, and sensitive food analysis has driven the exploration of innovative sensing technologies. Among these, capacitive sensors present a promising avenue.

- **Traditional electrochemical techniques**

Traditional analytical techniques have been employed for the detection of these compounds, each with its own strengths and limitations. Inositol Detection: Traditional detection methods for inositol encompass high-performance anion exchange chromatography with pulsed amperometric detection [25, 1], liquid chromatography [2], capillary electrophoresis with electrochemical detection [26,27,3], high-performance liquid chromatography coupled with electrochemical detection [28], HPLC and LC-MS/MS [29,30], capillary gas chromatography with flame ionization [31], voltammetric detection [32], ion chromatography [33], HPLC tandem mass spectrometry [34], and amperometric determination using modified glassy carbon electrodes [35]. Syringic Acid (SA) Detection: Similarly, SA detection has employed various methods: chemiluminescence [36], thin-layer chromatography (TLC) [37], chronoamperometry [38], flow injection analysis [39], and HPLC [40- 42]. HPLC methods have been used to quantify SA in herbal medicines and biological tissues [43- 45], and voltammetry has been applied to synthesized wine [46]. HPLC is also used for red wine analysis [47-52]. Folic Acid (FA) Detection: A plethora of conventional detection means, including electrophoresis [53], colorimetry [54], HPLC with mass spectroscopy [55, 56], fluorescence [57], UV spectrophotometry

[58], dual-emission fluorescence nanoprobe [59] HPLC–UV [60], RP-HPLC [61], FTIR spectroscopy [62], chemiluminescence detection [63], and green synthesized copper oxide nanoparticles and Electro-Poly(Methyl Orange) sensor [64], have been reported. Electrochemical sensors using carbon paste electrodes, CuO/SWCNTs nanocomposites, and Fe3O4@SiO2-graphite nanocomposites have been developed for FA detection [65, 66]. Optical FA sensors based on molecularly imprinted polymers on CdTe quantum dots have also been developed [67]. Molecularly imprinted polymer (MIP) technology has emerged as a promising approach for enhancing sensor selectivity [68-70]. MIP-based electrochemical sensors using molybdenum carbide modified glassy carbon electrodes [71], quantum dot-labeled hydrophilic MIP nanoparticles [72], SiO_2-coated Fe_3O_4 with surface MIP coating [73], and molecularly imprinted polydimethylsiloxane elastomer and magnetic molecular imprinted nanoparticles [74, 75] have been reported. Quercetin (QCN) Detection: Conventional detection methods, including fluorescence spectroscopy [76-78], electrophoresis [79], liquid chromatography–tandem mass spectroscopy [80], UHPLC-MS/MS [81], column chromatography [82], HPLC or rapid phase HPLC [83-87], chemiluminescence spectrophotometry [88], HPTLC [89,90], vortex assisted-ionic liquid dispersive liquid-liquid microextraction and spectrophotometry [91], switchable-hydrophilicity solvent liquid-liquid microextraction [92], and dispersive-micro-solid phase extraction [93], have been utilized. Electrochemical sensors using carbon paste electrodes [94], glassy carbon electrodes modified with porous nitrogen [95], $WS_2/GdCoO_3$ nanocomposites [96], porous polypyrrole modified GCE [97], poly(gallic acid)/MWNT-modified electrodes [98], carbon embedded $CuFeS_2$ hybrids [99], poly(9-(2-(pyren-1-yl)ethyl)-9h-carbazole) coated indium tin oxide electrodes [100], Co_3O_4 modified GCE [101], organic heterostructure modified carbon nitride biosensors [102], and carbon nanotubes modified electrodes with chemometric approaches [103] have been developed.

- **Capacitive technique**

Capacitive sensors operate by quantifying alterations in capacitance, which represents a conductor's capacity to hold an electrical charge. When a substance possessing dielectric characteristics, such as a food or real-world sample, approaches the sensor's electrodes, it perturbs the existing electric field, leading to a change in capacitance. This measured capacitance shift provides information about the material, including its makeup and the presence of specific molecules. Principle: The fundamental principle behind this type of sensing lies in the relationship between capacitance (C), the permittivity of the medium between the electrodes (ε), the area of the electrodes (A), and the distance between them (d), as described by the equation: $C=\varepsilon A/d$.

When a material with a different dielectric constant enters the electric field between the electrodes, it may effectively change the overall permittivity experienced by the sensor. This change in permittivity directly influences the capacitance. Furthermore, if the introduced material forms a layer on the electrode surface, it can also be perceived as a change in the effective distance (d) between the electrodes, thereby further altering the capacitance.

In practical applications, particularly for detecting specific molecules using modified electrode surfaces, the principle can be extended. For instance, if a sensor is designed with recognition sites for a target molecule, the adsorption of these molecules onto the sensor surface creates a thin layer with its own dielectric properties. The thickness of this adsorption layer is directly related to the concentration of the target molecule in the test solution and the interaction time. Since capacitance is inversely proportional to the effective separation distance created by this adsorption layer, an increase in the concentration of the target molecule leads to a thicker adsorbed layer and consequently a decrease in capacitance. Conversely, a lower concentration results in a thinner layer and a higher capacitance.

Therefore, by precisely measuring changes in capacitance, particularly in conjunction with impedance and phase measurements, it becomes possible to quantitatively determine the presence and concentration of specific molecules within a sample. The overall impedance (Z) of a capacitive sensor is related to the capacitance and the frequency (ω) of the applied AC signal by $Z = 1/j\omega C$, and the phase angle (θ) reflects the balance between the resistive and capacitive components of the sensor's impedance. Changes in capacitance due to analyte interaction will thus manifest as changes in both the impedance magnitude and the phase angle of the sensor's response.

1.3.3 Limitations of the standard techniques and importance of specific Sensors

- **Limitations of Standard Techniques:**

1. Time-consuming: Traditional methods can take hours or days to produce results.

2. Labor-intensive: Many techniques require skilled personnel and manual sample preparation.

3. Expensive: Specialized equipment and reagents can be costly.

4. Sample destruction: Some methods require sample destruction, making it impossible to retest.

5. Limited sensitivity: Standard techniques may not detect low levels of nutrients or contaminants.

- **Importance of Specific Sensors:**

1. Real-time monitoring: Molecule-specific sensors provide instant results, enabling timely decision-making.

2. Increased sensitivity: Molecule-specific Sensors can detect low levels of nutrients or contaminants, improving accuracy.

3. Reduced costs: Sensors can minimize equipment and personnel costs.

4. Non-destructive testing: Sensors allow for non-invasive testing, preserving the sample for further analysis.

5. Improved food safety: Sensors can quickly detect contaminants, ensuring safer food products.

Specific sensors, such as biosensors, nanosensors, and electrochemical sensors, offer innovative solutions to overcome the limitations of standard techniques, providing faster, more accurate, and cost-effective analysis of food nutrients.

1.4 Electrochemical Transduction Mechanism

The electrochemical transduction mechanism involves converting a chemical signal into an electrical signal. The process occurs in three stages:

1. Recognition: A biological or chemical receptor binds to the target analyte (e.g., nutrient, contaminant).

2. Conversion: The binding event triggers a chemical reaction, producing an electroactive species.

3. Transduction: The electro-active species is oxidized or reduced at an electrode, generating an electrical signal (viz. current, potential)**.**

1.5 Types of Electrochemical Techniques

A few important electroanalytical processes are listed below:

A. Coulometry

B. Potentiometry

C. Voltammetry

A. Coulometry

Coulometric methods rely on Faraday's law, which states that the total electrical charge or current passing through during electrolysis is directly proportional to the quantity of reactants and products involved in the redox reaction [104]. When the electrolysis is 100% efficient, indicating complete oxidation or reduction of the analyte, the total charge or current can be used to determine the analyte's concentration in the sample.

Performing coulometry (Fig. 1.2) requires the following instruments:

1. An electrochemical cell or electrolysis cell

2. A potentiostat for applying the necessary potential or voltage to the system

3. An integrator, either analog or digital, for determining the charge consumed

Electrochemical analysis typically employs one of two modes: potentiostatic (controlled-potential), in which current fluctuations are monitored at a constant potential, or galvanostatic (controlled-current), in which the total time required for complete analyte conversion is measured under a stable current.

Amperometric coulometry typically involves titrating the analyte at a constant current to generate a known amount of titrant electrochemically, and then detecting the analyte at a fixed potential.

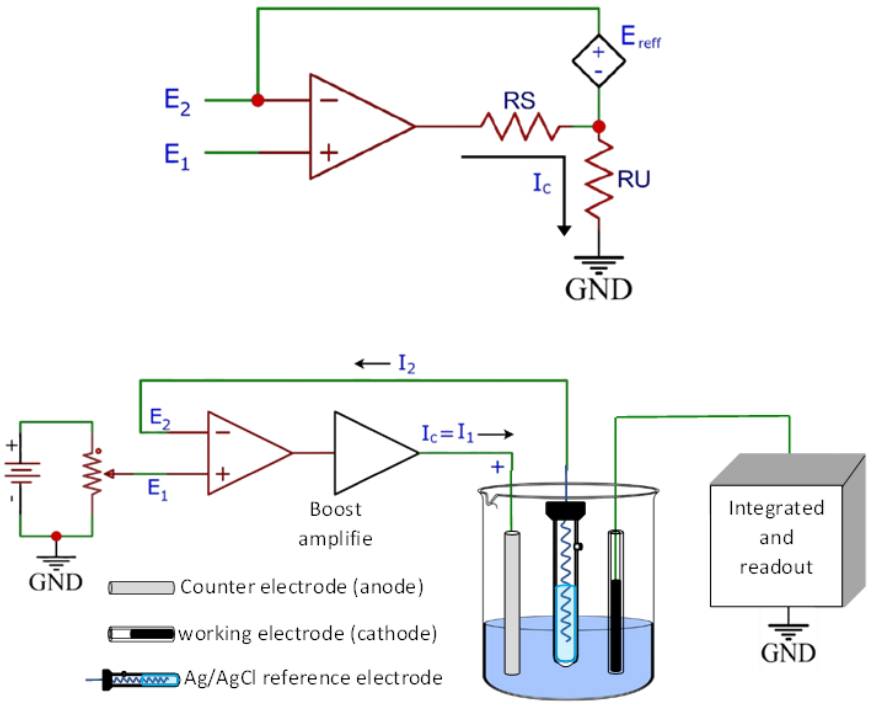

Fig. 1.2. Potentiostatic coulometry set up

B. Potentiometry

Potentiometry is a technique for measuring the concentration of an analyte by measuring the electrical potential of an electrode system (say electrochemical cell) (Fig. 1.3). The system consists of two electrodes, a reference electrode and an indicator electrode, and a solution of the analyte. The potential of the indicator electrode depends on the concentration of the analyte ions, while the potential of the reference electrode is stable and independent of the analyte concentration and temperature. The implicit difference between the two electrodes is measured using a potentiometer. In potentiometric sensors, the chemical recognition of a specific substance is translated into an electrical signal, the magnitude of which is directly proportional to the concentration of the substance being detected. This electrical signal, measured in volts, exhibits a logarithmic relationship to the substance's concentration. The Nernst equation establishes a logarithmic relationship between the measured electrode potential (E) and the relative activities of the redox species involved in the reaction of interest.

$$E = E^0 + \frac{RT}{nF} ln \frac{a^0}{a^R}$$

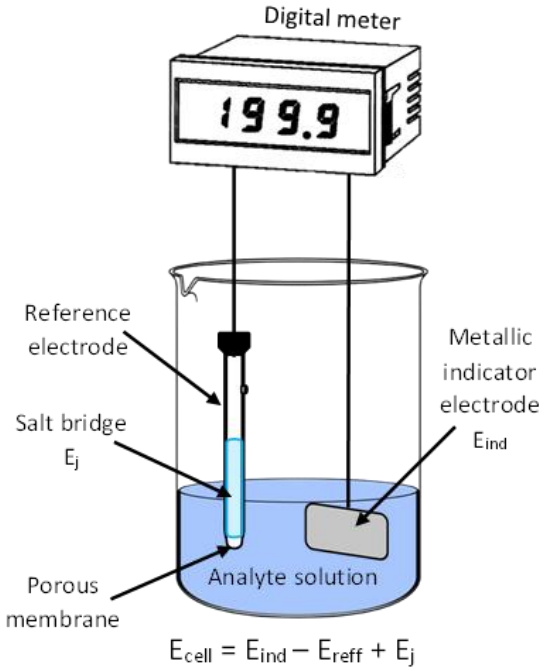

Fig. 1.3. Potentiometric set up

Where, E^0 - The standard electrode potential, measured under standard conditions relative to the Standard hydrogen electrode (SHE), and a^0 and a^R - activities of the oxidized and reduced species,*R* - universal gas constant; *T* - absolute temperature in Kelvin; *F* - Faraday constant; *n* -number of moles of electrons exchanged in the electrochemical reaction [104].

C. Voltammetry

The core of voltammetry lies in its ability to quantify target species by modulating the applied voltage. By measuring the current generated in response to a static or dynamic potential, researchers can precisely determine the concentration of analytes involved in specific recognition processes [105]. Common voltammetric techniques include cyclic voltammetry, differential pulse voltammetry, square wave voltammetry, and stripping voltammetry [106, 107]. Modern potentiostats can seamlessly switch between these techniques, blurring the distinctions between them. Stripping analysis stands out as one of the most sensitive voltammetric methods. In an amperometric setup, the potential is kept invariant to target specific redox transitions. This enables real-time monitoring of current fluctuations, providing a high-resolution temporal profile of the analyte's concentration as it interacts with the sensor surface. Hydrogen peroxide sensors and non-enzymatic glucose sensors are examples of amperometric sensors that have gained significant attention [108, 109].

Carbon paste, a mixture of carbon powder and a binding agent, has emerged over the past five decades as a popular carbon electrode material for sensors due to its suitability for screen printing, enabling mass production of electrodes. Researchers are increasingly exploring the use of new materials, particularly nanomaterials, in electrochemical sensors. Combining these nanomaterials to form novel composites holds particular promise, as synergistic effects often arise from such combinations [110, 111].

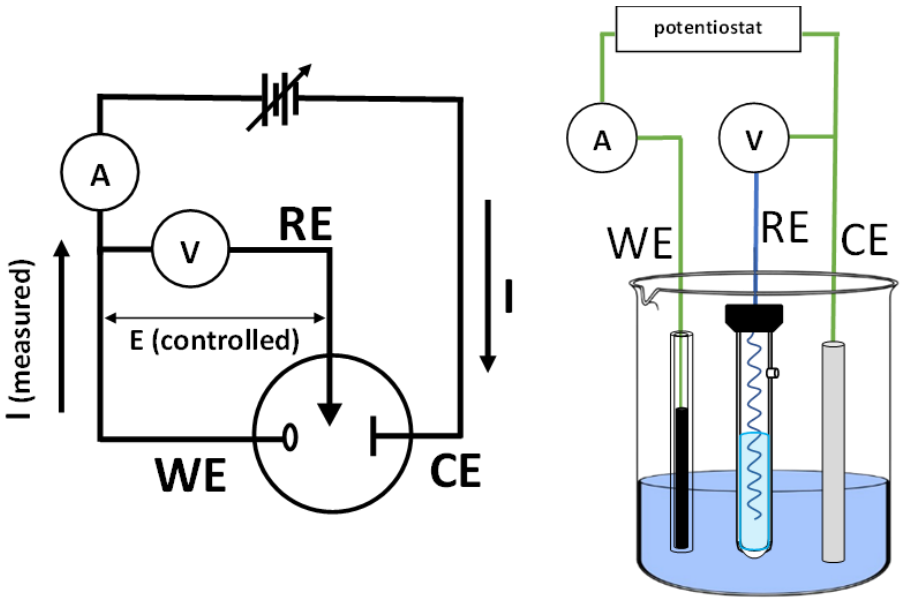

Fig. 1.4. Voltammetric set up

i. **Linear Sweep Voltammetry (LSV)**

Linear sweep voltammetry is similar to cyclic voltammetry, but it only involves a single potential sweep. This technique is often used to study the electrochemical behavior of a system.

ii. **Cyclic Voltammetry (CV)**

Electrochemical potentiodynamic measurements are commonly performed using Cyclic Voltammetry (CV), where the working electrode's potential is linearly changed over time. The process involves scanning the potential of the working electrode to a saturation point, followed by a brief reverse scan before returning to its initial value. A typical cyclic voltammogram, illustrated in Fig. 1.5 (a) and (b), displays the cathodic (i_{pc}) and anodic (i_{pa}) current responses to different time intervals, corresponding to oxidation and reduction processes. The reaction is initiated by a triangular pulse, as shown in Fig. 1.5. During the forward scan (t0-t1), the current increases with the input potential, as oxidation occurs rapidly due to the abundance of reactants. However, as the voltage is reapplied, the availability of reactants decreases, resulting in a constant or lower current value. The cathodic peak is observed during the reverse sweep (t1-t2), where the oxidized species are reduced.

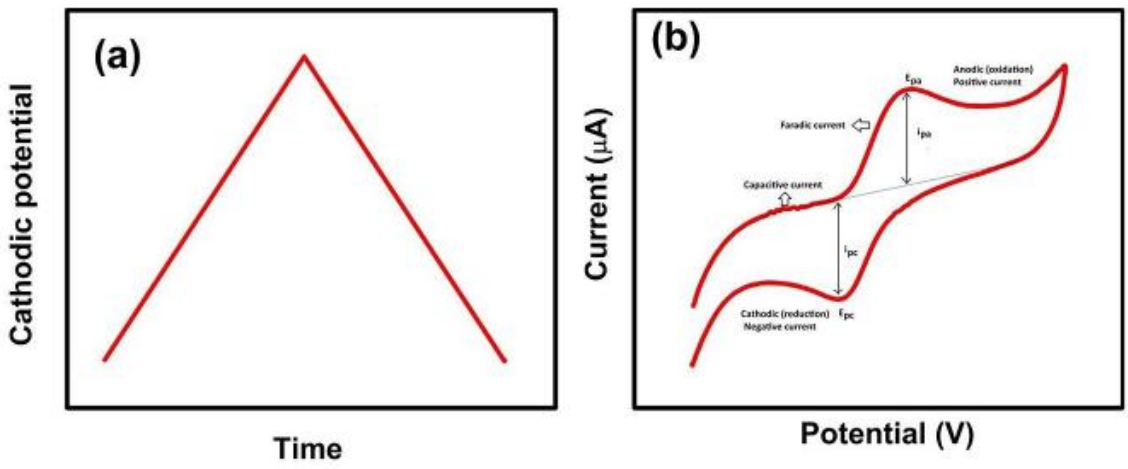

Fig. 1.5 (a) Waveform for cyclic voltammetry; (b) Parameters for a reversible reaction are shown on a typical cyclic voltammogram.

iii. **Pulse Voltammetry**

The operational principle of pulse voltammetry relies on the application of a potential pulse, which exploits the difference in decay rates between charging and Faradic currents. Specifically, the charging current decays exponentially, whereas the Faradic current decays more gradually, following a 1/(time)1/2 function. This disparity in decay rates enables the detection of analytes at concentrations as low as 10^{-8} M, as demonstrated by Barker and Jenkins' pioneering work [112] on this voltammetric approach.

a) **Normal Pulse Voltammetry (NPV)**

Normal Pulse Voltammetry (NPV) is a type of voltammetric technique that involves applying a series of potential pulses to the working electrode. The technique is widely used in electroanalytical chemistry to study the electrochemical behavior of molecules and to detect and quantify analytes.

b) **Differential Pulse Voltammetry (DPV)**

Differential pulse voltammetry involves applying a series of potential pulses to the working electrode. The resulting current-potential curve provides information about the electrochemical reaction, including the oxidation and reduction peaks.

c) **Square Wave Voltammetry (SWV)**

Square wave voltammetry involves applying a square wave potential pulse to the working electrode. This technique is often used to study the electrochemical behavior of a system.

d) **Stripping Voltammetry (SV)**

Stripping Voltammetry (SV) is a highly sensitive electroanalytical technique used to detect and quantify trace amounts of metal ions, organic compounds, and other electroactive species. The technique involves two main steps: preconcentration and stripping.

Comparison between voltammetry and potentiometry

Feature	Voltammetry	Potentiometry
Measured quantity	Current	Potential
Applied potential	Variable	Constant
Information obtained	Concentration and redox properties of analytes	Concentration of analytes
Sensitivity	High	Moderate
Selectivity	Moderate	High
Speed	Fast	Slow
Instrumentation	More complex	Less complex
Applications	Wide range of applications, including environmental monitoring, food safety, and clinical chemistry	Environmental monitoring, food safety, and clinical chemistry

1.6 Different Types of Electrodes for Electrochemical Sensing

Electrochemical sensing fundamentally relies on the materials constituting the electrodes, which dictate the efficiency of electron transfer, the operational potential range, and the overall sensitivity and selectivity of the sensor. Therefore, the selection of an appropriate electrode material is paramount in sensor design, tailored to the specific analyte and application. This section of the thesis will discuss various types of electrodes commonly employed in electrochemical sensing, highlighting their key characteristics and applications.

➢ Metal Electrodes

Historically, noble metals such as gold, platinum, and silver have been favored as electrode materials due to their high electrical conductivity, broad potential windows in aqueous environments, and catalytic activity towards diverse redox reactions. Gold electrodes, for example, are frequently utilized in biosensing due to their biocompatibility and ease of surface modification with biological molecules. Platinum electrodes exhibit excellent catalytic properties for reactions involving hydrogen and oxygen, making them suitable for fuel cells and certain biosensors. Silver electrodes find use in potentiometric sensors for halide ions and in some catalytic applications.

However, noble metal electrodes are costly and may experience surface contamination or necessitate specific pretreatments to maintain their activity. More recently, base metals like copper and nickel are being explored as more economical alternatives for particular

applications, especially in catalysis and some electrochemical sensors, often in modified forms to enhance their performance and stability.

- **Carbon-Based Electrodes**

Carbonaceous materials have emerged as highly versatile electrode materials owing to their low cost, wide potential window, chemical inertness, and ease of modification. Glassy carbon electrodes are a common choice, offering a favorable combination of these properties and a well-defined surface that can be readily polished and modified. Graphite electrodes, including highly ordered pyrolytic graphite and edge plane pyrolytic graphite, present distinct surface structures with varying electrochemical activities.

The rise of nanotechnology has led to the widespread adoption of nanomaterials like carbon nanotubes and graphene in electrode fabrication. Their high surface area to volume ratio and excellent electrical conductivity significantly improve sensor sensitivity. Carbon nanotubes can be used individually or incorporated into composite materials to enhance electron transfer kinetics. Graphene and its derivatives, such as graphene oxide and reduced graphene oxide, provide large surface areas for analyte interaction and can be functionalized to achieve high selectivity.

Screen-printed electrodes, often made from carbon inks, offer a cost-effective and scalable platform for disposable electrochemical sensors. These electrodes can be easily modified with various materials to tailor their sensing capabilities for specific analytes.

- **Metal Oxide Electrodes**

Metal oxides, such as indium tin oxide, titanium dioxide, zinc oxide, and various transition metal oxides, are increasingly utilized in electrochemical sensing, particularly for applications involving electrocatalysis, photocatalysis, and certain types of biosensing. These materials often exhibit unique electronic and catalytic properties that can be exploited for specific analyte detection. For instance, some metal oxides demonstrate high catalytic activity towards the oxidation or reduction of organic molecules. Nanostructured metal oxides can further increase the surface area and improve sensor performance.

- **Modified Electrodes (Including MIPs)**

A significant advancement in electrochemical sensing involves the modification of electrode surfaces with various materials to enhance sensitivity, selectivity, and stability. This can include the deposition of thin films of polymers, self-assembled monolayers,

enzymes, metal nanoparticles, or other nanomaterials. These modifications can introduce specific binding sites for target analytes, catalyze electrochemical reactions, or prevent electrode fouling. Molecularly imprinted polymers (MIPs) represent a powerful class of synthetic receptors that can be tailored to selectively recognize target analytes based on their size, shape, and chemical functionality. The fabrication of MIPs relies on stabilizing monomers around a template molecule during a polymerization step. Subsequent removal of the analyte creates physical and chemical footprints etched into the durable polymer base. This results in a selective sensing layer capable of identifying the target species through a lock-and-key fit. The integration of MIPs onto various electrode surfaces has revolutionized electrochemical sensing by providing a highly selective recognition element. MIPs can be directly electropolymerized onto the electrode surface, drop-cast as a thin film, or incorporated into composite materials. The selective binding of the target analyte to the MIP layer on the electrode surface can then be transduced into an electrochemical signal, which can be measured and correlated to the analyte concentration. MIP-modified electrodes have been developed for a wide range of analytes, including small organic molecules, pharmaceuticals, pesticides, and even proteins. The robustness, cost-effectiveness, and ease of preparation of MIPs make them attractive recognition elements for developing highly selective and stable electrochemical sensors.

1.6.1 Molecular Imprinted Polymer (MIP) Technique

Molecularly Imprinted Polymers (MIPs) are synthetic materials designed to specifically recognize and bind to a target molecule (template). They mimic the behavior of biological receptors such as enzymes and antibodies, offering advantages like high selectivity, stability, and reusability.

- **Template molecule:** The target molecule the MIP is designed to bind.
- **Functional monomers:** Building blocks of the polymer matrix that interact with the template through specific functional groups.
- **Cross-linkers:** Molecules that connect the functional monomers, forming a rigid 3D network around the template.
- **Binding sites:** Complementary cavities in the polymer matrix left behind after template removal, matching the shape and functional groups of the template.

Key steps in MIP synthesis:

1. **Template Selection:** Choosing the target molecule which one wants the MIP is to recognize.
2. **Monomer & Cross-linker Selection:** Selection of suitable functional monomers that interact with the template and cross-linkers to form a stable network.
3. **Polymerization:** Initiation of the reaction to form the polymer network around the template molecules.
4. **Template Removal:** Removal of the template molecules, leaving behind complementary binding sites.
5. **Activation:** Removal of any residual impurities that might hinder binding.
6. **Characterization:** Evaluation of the MIP's binding properties, selectivity, and capacity.

Applications:

MIP sensors are invaluable tools for environmental monitoring, ensuring food safety, and advancing medical diagnostics, where precise detection of specific compounds is crucial. Beyond sensing, MIPs are being explored for their capacity to revolutionize drug delivery systems. The ability to control drug release and target specific tissues holds immense promise for improving therapeutic efficacy and minimizing side effects. In the realm of separation science, MIPs are transforming chromatography, enabling the efficient separation and purification of target molecules, a process critical in various industries. Furthermore, the ability of MIPs to mimic enzymes opens up exciting possibilities in catalysis. By acting as artificial enzymes, MIPs offer enhanced stability and reusability, paving the way for more efficient and sustainable chemical reactions. This biomimetic approach to catalysis represents a significant advancement in the field, showcasing the broad applicability of MIPs in addressing diverse scientific and technological challenges.

Advantages of MIPs:

- **High Selectivity:** Specific binding to the target molecule, minimizing interference from others.
- **Stability:** Resistant to harsh chemicals and temperatures compared to biological counterparts.
- **Reusability:** Can be regenerated and used multiple times, reducing cost and waste.

- **Design Flexibility:** Tailorable for various target molecules and applications.

Limitations of MIPs:

- **Synthesis Complexity:** Requires careful selection of components and optimization of synthesis conditions.
- **Limited Binding Capacity:** May not bind as many target molecules as natural receptors.
- **Regeneration Challenges:** Regeneration efficiency can vary depending on the MIP and target molecule.

MIP technology offers a powerful tool for creating synthetic materials with specific recognition capabilities, finding applications in various fields ranging from environmental monitoring to healthcare.

Steps involved in MIP synthesis process (Fig. 1. 6):

1. **Template selection:** The template molecule is the key to MIP specificity. It should be well-defined and available in sufficient quantities. The size, shape, and functional groups of the template will determine the properties of the resulting binding sites.

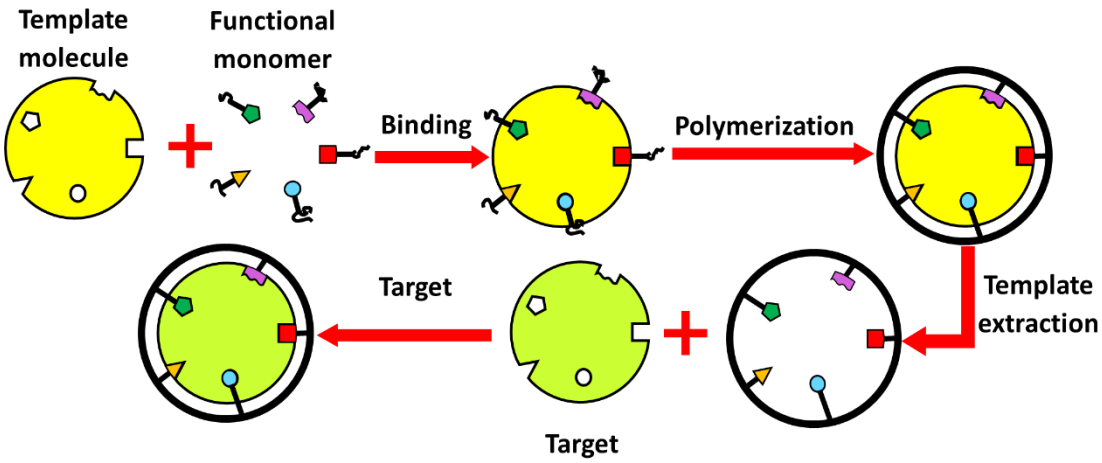

Fig. 1.6. Schematic of MIP technology.

2. Functional monomer selection: Functional monomers are the building blocks of the MIP polymer. They should be able to interact with the template through specific interactions like hydrogen bonding, ionic interactions, or π-π stacking. The choice of functional monomers will significantly impact the selectivity and affinity of the MIP.

3. Cross-linker selection: Cross-linkers are responsible for creating the rigid polymeric network around the template-monomer complex. They prevent the collapse of the binding sites after template removal and ensure the stability of the MIP.

4. Polymerization: Polymerization is the process of linking the functional monomers and cross-linkers together to form the polymer matrix. The specific polymerization method used will depend on the choice of monomers and cross-linkers.

5. Template removal: Template removal is crucial for creating binding sites in the MIP. The template molecule is usually removed by washing with solvents or extraction techniques that do not dissolve the polymer matrix.

6. MIP Activation: Activation is an optional step that can improve the binding performance of the MIP. Some MIPs require an activation step to remove any residual monomers or impurities that might interfere with binding. This can be performed by washing with specific solvents or treating with mild oxidizing agents.

7. Characterization: MIP characterization is essential for understanding its properties and performance. Various techniques like binding assays, chromatography, and spectroscopy are used to evaluate the binding capacity, selectivity, and affinity of the MIP.

1.6.1.1 Types of Imprinting Techniques

There are several types of imprinting techniques used in sensor development and molecular recognition:

A. Covalent Imprinting
B. Non-Covalent Imprinting
C. Semi-Covalent Imprinting
D. Spacer-Mediated Molecular Imprinting

1.6.1.1.1 Covalent Imprinting

This technique relies on establishing reversible chemical linkages between the target molecule and the monomeric precursors, allowing for the creation of well-defined and precise recognition sites. This is achieved through a chemical procedure that precedes polymerization, resulting in a template-monomer complex. A pre-polymerization step is used to create a derivative from the monomer and the template, followed by the polymerization process. The covalent bond between the polymer and the template is subsequently broken when the template is removed from the polymer after polymerization. Rebinding of the template molecule to the

MIP re-establishes a similar covalent bond. The key advantage of this method lies in the removal of the template molecule created during polymerization.

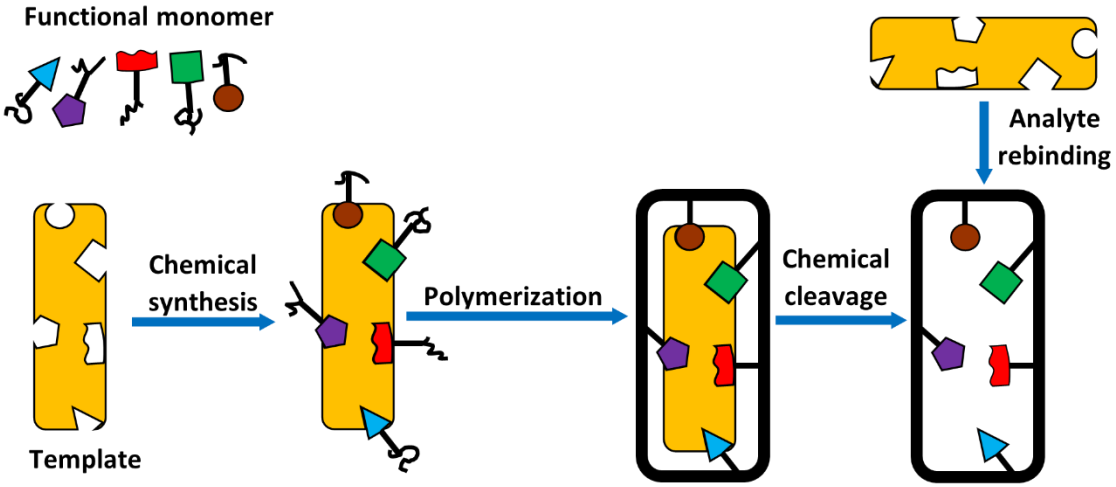

Fig.1.7. Schematic portraying the covalent imprinting process.

There are several types of Covalent Imprinting, like:

a) Imprinting with a readily reversible covalent bond
b) Covalent imprinting with boronate esters
c) Covalent imprinting with Schiff's bases
d) Covalent imprinting with acetals and ketals

a) Imprinting with a readily reversible covalent bond

Imprinting with readily reversible covalent bonds is a technique that utilizes quickly reversible binding reactions, such as boronate ester, ketal/acetal, and Schiff's base formation, to facilitate the design of template-monomer complexes. This approach requires the hydrolysis of the template molecule from the polymer under mild aqueous conditions to enhance the binding sites. However, the number of configurations that can be imprinted is limited by the specific auxiliary requirements of covalent methods, including 1) Diols (1,2- and 1,3-): Utilized for generating boronate esters, ketals, or acetals. 2)Carbonyls (Aldehydes/Ketones): Converted into acetal or ketal derivatives. 3)Amines: Reacted to produce stable yet reversible Schiff's bases. A significant benefit of this method is the reproducibility of the recognition sites, where the rebound state remains chemically identical to the pristine polymer. This ensures that the population of binding pockets maintains a highly homogeneous distribution across the matrix. Additionally, ambiguous binding may decrease as the amount of monomer decreases. Nevertheless, the requirement for the template

monomer to be covalently attached is considered a limitation of covalent imprinting techniques. Furthermore, the template monomer may be sensitive to the presence of water, and the steric requirements imposed by the processes in the imprinted polymer regions can hinder the system's ability to exchange the template molecule.

b) Covalent imprinting with boronate esters

The boronate ester strategy is considered one of the most effective reversible covalent techniques, particularly for the imprinting of carbohydrate or starch derivatives. This approach, originally developed by Gunter Wulff et al., involves the use of several formats such as glyceric acid, mannose, galactose, fructose, sialic acid, castasterone, and L-DOPA for the imprinting process [113-117]. Various studies have demonstrated the application of boronate esters in creating MIPs for fluorescent detection [118-120], imprinted polyelectrolyte hydrogels [121], functionalized polyaniline coatings for microtitre plates [122], and other applications. Additionally, this technique has been used to combine amino acids in an enantioselective manner. The use of boron ophthalide-based monomers has further expanded the technique, enabling the imprinting of monoalcohol forms and those with spatially segregated, distinct hydroxyl groupings [123-124]. The polymers synthesized using this method have also been successful in the specific derivatization of sterols by polymeric securing groups [125].

c) Covalent imprinting with Schiff's bases

Covalent imprinting with Schiff's bases involves the reaction between an essential amine and a carbonyl compound (typically an aldehyde), resulting in the formation of an imine. This chemistry makes Schiff's base a potentially useful method for imprinting templates bearing amine or aldehyde functional groups. Furthermore, this approach has been effectively employed to imprint amino acid derivatives [126]. However, a notable limitation of this method is that the exchange kinetics with the resulting enantioselective polymers is often too slow for practical applications in chromatographic separations.

d) Covalent imprinting with acetals and ketals

It uses acetal or ketal linkages to form covalent bonds between the mono- and di-ketone template molecule and the polymer, providing a reversible and selective binding site [127].

1.6.1.1.2 Non-Covalent Imprinting

Non-covalent imprinting is a method that overcomes the limitations of covalent imprinting. This approach was first reported in silica frameworks and later developed by Mosbach’s group

in the 1980s into a practical method for engineering imprinted receptors in synthetic polymers [128]. A schematic of the non-covalent imprinting procedure is shown in Fig. 1.8. In this approach, template-monomer complexes are formed in suitable solvents through various interaction forces, such as dipole-dipole interactions and Van der Waals forces. The template is then removed from the polymerized matrix and can rebind using the same interaction forces. Non-covalent imprinting is a widely used method today due to its flexibility in targeting various template features. The process involves the formation of pre-polymerization complexes between the target template and functional monomers, leading to the folding of polymer structures with diverse functional groups around the template particle. This results in a mutual influence due to the different interactions that occur compared to single monomer-template associations. As polymerization progresses, these structures continue to form and evolve, increasing the target molecule's affinity for the receptor site until a fully formed polymerized net is established. Non-covalent imprinting can be performed using a solo monomer or an amalgamation of monomers.

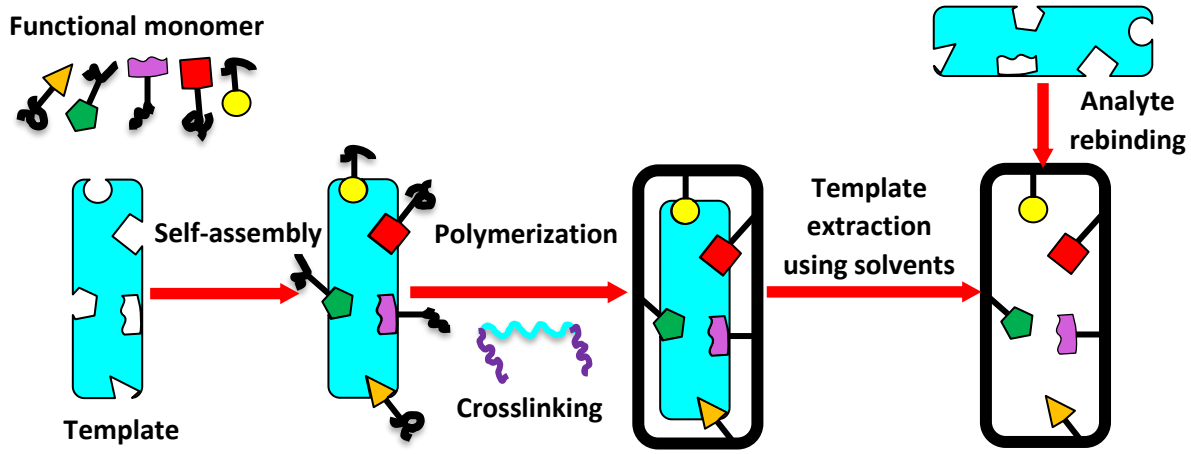

Fig. 1.8. Representation of non-covalent imprinting mechanism.

There are several types of Non-Covalent Imprinting, like:

a) Non-Covalent imprinting with a single functional monomer

b) Non-Covalent imprinting with a combination of monomers

a) **Non-Covalent imprinting with a single functional monomer**

This approach is the simplest and most extensively used strategy in non-covalent imprinting. It involves considering the concept of the existing polymerization complex, as well as the suitable interactions between the template and the monomer with the crosslinkers. The monomer

can alter the equilibrium of the ideal template-monomer complexes, while the template may play a crucial role in describing or improving usable receptors. However, issues may arise due to the monomer's propensity for self-association, such as dimerization in carboxylic acids. Additionally, potential interactions with the initiator should be taken into account, as they are often present at a fixation similar to the templates. Vinylbenzoic acid, although a desirable option due to its large bulk and aromatic ring's π electron configuration, often exhibits low reactivity with popular (methacrylate) cross-linkers, leading to problematic interactions with template molecules. The use of Phosphates and phosphate derivatives in imprinting depends on their ability to bind to metal particles. Vinyl pyridine, on the other hand, interacts strongly with electron-deficient aromatic rings and electron-rich π electron ring networks, making it an exceptionally productive monomer in imprinting. However, these monomers can occasionally be detrimental due to strong π-π exchanges during template rebinding in aqueous conditions, resulting in non-specific binding sites. Tertiary amino monomers are also necessary, although they are occasionally less favorable than acidic monomers due to their better chain flexibility and increased distance between the amine activity and the polymer backbone.

b) Non-Covalent imprinting with a combination of monomers

Combining multiple monomers with unique interface possibilities appears intriguing for specific projects. This approach is based on the idea that a pre-polymerization mixture has a large number of equilibria. Research by Spivak has shown that, when the crosslinker is properly functionalized, the monomers are not necessary for optimal imprinting [129]. For the bonds formed between the template and the helpful monomers to be effective, they must be stronger than interactions between them. Computational virtual imprinting has also predicted that combining imprinting strategies that worked effectively in tests would be successful.

1.6.1.1.3. Semi-Covalent Imprinting

As discussed in the previous sections, covalent imprinting requires the artificial modification of the template molecule with a functional monomer, followed by its removal through the breaking of covalent bonds. In contrast, the non-covalent approach is more practical, utilizing relatively weak forces of attraction, such as electrostatic contacts, hydrogen bonds, covalent bonds, and hydrophobic interactions, to attach the template to the monomer. This approach addresses the limitations of covalent imprinting by incorporating covalent attachment during polymerization and hydrogen bond formation during recognition. Semi-covalent imprinting, a

duo of non-covalent and covalent imprinting, involves the covalent binding of the functional monomer and template during polymerization and the rebinding process, respectively. For example, a mixture of monomers is co-polymerized with a methacrylate ester of the template. The template is then released by hydrolysis and rebinds to the polymer through interactions between its hydroxyl groups and methacrylic acid binders introduced into the imprinted site. However, this type of imprinting is not recognized due to the lack of direct template hydrolysis and the disparity in steric requirements of an acid and alcohol in hydrogen bonding contact compared to the corresponding ester.

1.6.1.1.4. Spacer-Mediated Molecular Imprinting

This modification addresses the inherent constraints of semi-covalent imprinting by introducing a cleavable cross-linking group between the template and the functional monomer. During the polymerization phase, this intermediary serves a dual role: it anchors the template to the monomeric unit while simultaneously providing a physical buffer. Upon template extraction and linker cleavage, the resulting cavity is less prone to steric congestion, thereby facilitating more efficient non-covalent analyte capture [130-132]. For instance, salicylate (2-hydroxybenzoate) was used as a spacer group between the primary amine of the template and the residue of polymerizable methacrylic acid [133]. Notably, the phenyl methacrylate ester is more readily cleaved than the amide due to intramolecular hydrogen bonding, which maintains a close contact between the ester oxygen and amide hydrogen during the non-covalent binding stage.

1.6.2. Capacitive - MIP Sensing Technology: The quest for rapid, selective, and sensitive food analysis has driven the exploration of innovative sensing technologies. Among these, the integration of MIPs with capacitive sensors presents a promising avenue. This approach leverages the inherent selectivity of MIPs, synthetic receptors tailored to specific target molecules, and the sensitive transduction capabilities of capacitive sensors. Capacitive sensors work by measuring changes in capacitance, which is the ability of a conductor to store electrical charge. When a material with dielectric properties (like a food sample) comes close to the sensor's electrodes, it affects the electric field and changes the capacitance. This change can be measured and used to infer information about the material, including its composition and the presence of specific molecules. Essentially, by immobilizing MIPs onto or within the architecture of a capacitive sensor, we create a system where the binding of a target food molecule induces a measurable change in capacitance. This change reflects the alteration in the dielectric properties of the sensing interface, directly correlating to the concentration of the analyte. This integration can manifest in several ways, from direct coating of electrodes with MIPs to

embedding MIPs within porous membranes or functionalizing micro- or nano-structures to maximize surface area and interaction.

Integration and Details: Several methods are being explored to integrate MIPs with capacitive sensors for food molecule detection:

- **MIP-coated electrodes:** The sensor electrodes are directly coated with a thin layer of MIP material. This allows the target molecule to bind to the MIP, leading to a measurable change in capacitance.
- **MIP-embedded membranes:** The MIP is incorporated into a porous membrane placed between the electrodes. The target molecule diffuses through the membrane and binds to the MIP, again affecting the capacitance.
- **MIP-functionalized micro- and nano-structures:** Micro- or nano-scale structures are fabricated on the sensor surface and functionalized with MIPs. This enhances the surface area and interaction with the target molecule, leading to higher sensitivity.

Advantages: The allure of this technology lies in its inherent advantages:

- **High selectivity:** MIPs enable detection of specific food molecules, even in complex matrices.
- **Label-free detection:** No need for additional labeling or markers, simplifying the process.
- **Real-time monitoring:** Changes in capacitance can be measured instantaneously, allowing for real-time detection.
- **Miniaturization potential:** Capacitive sensors can be miniaturized, leading to portable and compact devices.

Challenges:

- However, the realization of this technology is not without its challenges. Achieving optimal performance necessitates a delicate balance in both MIP and sensor design. Sensitivity, selectivity, and response time are intricately linked, demanding careful optimization. The complexity of food matrices, with their diverse constituents, poses a significant hurdle, potentially leading to interference and requiring robust control strategies. Ensuring the long-term durability and regenerability of the MIP, along with the reliable functioning of the sensor over time, is also paramount for practical applications.

Applications:

Despite these challenges, the potential applications are vast. In food safety, this technology can be deployed for the rapid detection of contaminants, allergens, and pathogens, safeguarding public health. In quality control, it can monitor freshness, ripeness, and other critical parameters, ensuring consistent product quality. In process control, real-time monitoring of key molecules can optimize food processing and manufacturing, leading to enhanced efficiency and reduced waste. Combining capacitive sensing and MIP technology holds great promise for the development of next-generation food molecule detection systems with high sensitivity, selectivity, and real-time capabilities**.** This technology can contribute to safer, healthier, and higher-quality food production. When it comes to integrating MIPs with capacitive sensors for food molecule detection, diverse approaches exist. Choosing the right sensor type depends on several factors like target molecule size, desired sensitivity, application requirements, and cost considerations. An overview of several promising approaches has been discussed below:

(a)Interdigitated Electrodes (IDEs): IDEs offer a miniaturized and cost-effective approach to capacitive sensing. By arranging two sets of comb-like electrodes in an interdigitated pattern, a high surface-to-volume ratio is achieved. Coating the IDE surface with an MIP layer enables the detection of target molecules through changes in capacitance. The binding of the analyte to the MIP alters the dielectric properties within the electrode gap, resulting in a measurable shift in capacitance. While IDEs boast high sensitivity and potential for miniaturization, their limited surface area can constrain the number of binding sites, and interference from non-target molecules remains a consideration.

(b)Planar Electrodes: Planar electrode configurations, typically comprising two parallel plates separated by a dielectric layer containing the MIP, provide a straightforward and fabrication-friendly approach. The interaction of target molecules with the MIP within the dielectric layer induces changes in its dielectric properties, leading to a measurable alteration in capacitance. This method is particularly well-suited for detecting larger molecules that can induce significant changes in the dielectric medium. However, the limited surface area of planar electrodes can restrict sensitivity, especially for smaller analytes.

(c)Dielectric Resonator Sensors: Dielectric resonator sensors leverage the sensitivity of microstrip antenna structures to changes in the surrounding dielectric medium. Integrating an MIP layer with the resonator allows for label-free detection of target molecules. The binding of the analyte to the MIP alters the resonance frequency of the antenna, providing a measurable signal.

This approach offers high sensitivity and the potential for remote sensing. However, the complex design and fabrication of dielectric resonators can pose challenges, and the associated costs may be higher compared to simpler electrode configurations.

(d)Field-Effect Transistors (FETs): FET-based sensors utilize the MIP layer as a gate dielectric, enabling the detection of target molecules through changes in drain current. The binding of the analyte to the MIP modifies the gate dielectric properties, modulating the flow of current between the source and drain. This approach offers high sensitivity and the potential for seamless integration with electronic circuitry. Nevertheless, the complex fabrication processes and potential cross-sensitivity issues require careful consideration.

(e)Microfluidic Capillary Sensors

Microfluidic capillary sensors combine the advantages of MIPs with the controlled flow of fluids in microchannels. By integrating MIP-coated surfaces within microfluidic channels, target molecules can be detected through changes in electrical conductivity as they interact with the MIP. This approach facilitates continuous or multiplexed detection and is particularly suitable for complex samples. However, the requirement for microfluidic infrastructure and potentially lower sensitivity compared to other methods should be considered.

Critical Factors in Sensor Design

The performance of MIP-based electrochemical sensors is significantly influenced by several factors. The choice of electrode material, whether metal or conductive polymer, impacts sensor performance and biocompatibility. Similarly, the MIP immobilization strategy, including covalent bonding, physical adsorption, or encapsulation, plays a crucial role in determining sensor stability and sensitivity. Furthermore, sophisticated signal processing and analysis techniques, such as lock-in amplification and chemometrics, are essential for enhancing sensitivity and specificity. The selection of an appropriate electrochemical sensing platform depends on the specific requirements of the application, including the target analyte, desired sensitivity, and operational environment. Each method offers unique advantages and limitations, and careful consideration of these factors is essential for the development of high-performance MIP-based sensors.

1.8. Literature Survey on various detection techniques

Table 1.2: An overview of the literature on various detection techniques

Nutrient/ Compound	Electrode/ Sensor	Techniques used	Linear range (ppm)	LOD(ppm/ µM/ µg/mL)	Refs
Inositol	CuS/GCE	Amperio-metric	0.09-1.53 ppm	0.04 ppm	[35]
Inositol	Cu-disk	CE	1-100 ppm	0.53 ppm	[26]
Inositol	SRM 1849a (for validation)	HPLC& LC-MS/MS	0.001-0.05 ppm	0.05 ppm	[29]
Inositol	-	HPLC–MS/MS	0-180.16 ppm	0.45 ppm	[34]
Syringic Acid	-	HPLC-UV	3-1000 µM	2.02 µM	[42]
Gallic acid, protocate-chuic acid, vanillic acid, and syringic acid	-	HPLC	0.5-20 µg/mL	0.309, 0.376, 0.213 and 0.388 µg/mL µg/mL	[134]
Ascorbic acid, Gallic acid	-	HPLC	-	0.96 µM	[135]
Folic Acid	-	Spectrophotometr-ic determination by coupling reac-tion	0.22-18.12 µM	0.1 µM	[58]
Folic Acid	-	Chemiluminometr-ic	13.59-258.26 µM	4.53 µM	[57]
Folic Acid	-	Capillary electro-phoresis	1.13-13.59 µM	0.67 µM	[53]
Folic Acid	-	Flow-injec-tion/chemilumi-nescence	0.3-2.5 µM	0.023 µM	[63]
Folic Acid	-	Facile approach (MIP based)	0.23–113 µM	0.048 µM	[71]
Folic Acid	Optical sensor (MIP) on quantum dots	fluorescence spec-troscopy	0.5-20 µM	0.032 µM	[67]
Folic Acid	Graphite SPE modified with Fe_3O_4@SiO_2	DPV	5-1000 µM	1 nM	[66]
Quercetin	[a]CPO/SPCE	DPV	0.08-129.83 µM	3 nM	[136]
Quercetin	Co_3O_4/GCE	DPV	0.01-3 µM	0.20 nM	[101]
Quercetin	[b]CNU-DAQx	DPV	0.015-230 µM	4 nM	[102]
Quercetin	[c]HOPNC	DPV	0.1-120 µM	30 nM	[95]
Quercetin	WS_2/$GdCoO_3$/GCE	DPV	0.001-329 µM	3 nM	[96]

[a]CPO/SPCE: cobalt phosphate/screen-printed carbon
[b]CNU-DAQx: carbon nitride urea-2,6-diamino anthraquinone;
[c]HOPNC: hierarchically ordered porous nitrogen-doped carbon;

This section summarizes advancements in different detection methods, organized by target analyte and application. Several detection techniques have been discussed in the introduction section 1.1. To illustrate the breadth of research in this area, Table 1.2 presents a compilation of few notable studies employing different detection strategies and rapid methodologies for detecting and quantifying these compounds in real food samples.

Despite the development of various sensors, challenges remain in terms of selectivity, fabrication complexity, and application specificity. Therefore, there is a need for simple, affordable, and rapid methodologies for detecting and quantifying these compounds in real food sample

1.9 Objectives and Scope

The current study is concentrated on the use of the MIP approach for the individual measurement of a few food nutrients, namely Inositol, SA, FA, and QCN. With regard to the development of the sensors, several exploratory factors have been thoroughly examined, including the effects of pH, buffer, and scan rate. The following summarizes the goals of this thesis work:

- The identification of monomers, cross-linkers, and initiators is necessary for the development of MIP sensors for inositol, SA, FA, and QCN.
- Identification of the sensor materials' size, structural, and morphological differences.
- Optimization of the experimental setup and investigation of the electrodes 'electrocatalytic characteristics.
- Analyze the electro-analytical characteristics of different electrodes.

The entire thesis has been organized into seven chapters in light of the aforementioned goals.

Below is a quick chapter-by-chapter dissection of the thesis.

Chapter 1: Introduction describes the causes of the problem and exemplifies the goals of this thesis study. The distinct transduction mechanisms inherent in electrochemical and capacitive sensing are then presented in the chapter. It also focuses on the numerous conventional techniques used recently for several food nutrient determinations, as well as their benefits and drawbacks. This is followed by a detailed description of how MIP-based recognition systems may be strategically used to overcome the significant challenges posed by conventional electrochemical identification techniques, particularly concerning selectivity in complex matrices. Here, a brief literature review of MIP-based sensing utilizing conventional electrochemical approaches is presented after a concise description of the MIP method itself. The chapter concludes with a summary of the work's overall goals and scope.

Chapter 2: Electrochemical Detection of Inositol in Food Samples delves into the development of two distinct sensing platforms for inositol, a crucial non-reducing sugar alcohol and significant nutrient. The chapter details the design and optimization of a platinum electrode-based electrochemical system, thoroughly characterizing its performance via techniques like Differential Pulse Voltammetry (DPV) and demonstrating its applicability in real orange juice samples. Additionally, it presents a novel, cost-effective molecularly imprinted polydopamine-polyethylene glycol (MIP-based) capacitive sensor, elucidating its fabrication, characterization, and exceptional sensitivity (achieving a limit of detection as low as 1.8 ppb), along with its impressive linearity, selectivity, and long-term stability for inositol detection in fruits.

Chapter 3: Quantification of Syringic Acid Using Novel Electrochemical Sensors explores two effective methods for quantifying syringic acid (SGA), a phenolic compound found in various plants that contributes to food quality. This chapter first discusses the application of Ultraviolet-visible (UV-Vis) spectroscopy coupled with multivariate analysis for initial assessment. It then elaborates on the development of a highly sensitive and selective molecularly imprinted polymer (MIP) based electrochemical sensor using an acrylonitrile (AN) MIP on graphite. The chapter covers the sensor's fabrication, comprehensive characterization, and its analytical performance, including its low detection limit (0.32 μM), excellent repeatability, reproducibility, and stability, with thorough validation against HPLC in various real food extracts.

Chapter 4: Molecularly Imprinted Polymer Electrode for Folic Acid Quantification in Food Extracts is dedicated to the effective quantification of folic acid (FA), an essential B vitamin vital for human health and a critical nutrient. This chapter details the comprehensive process of designing, fabricating, and characterizing a highly selective molecularly imprinted polyacrylonitrile-imbued graphite electrode (MAN@G). It thoroughly investigates the electrode's electrochemical response using DPV and Cyclic Voltammetry (CV), establishing its wide linear range, remarkably low limit of detection (18 nM), and robust analytical parameters, including high reproducibility and stability. The practical utility of the sensor is rigorously validated through accurate quantification of FA in diverse real food extracts, with results corroborated against HPLC.

Chapter 5: Advanced Electrochemical and Capacitive Sensors for Quercetin Detection in Food Products showcases the development of two innovative sensor designs for the precise detection of quercetin (QCN), a prominent flavonoid with significant antioxidant properties contributing to the nutritional profile of food. The chapter first describes a novel rGO-decorated

Molecularly Imprinted Polyacrylic Acid Graphite Electrode (M-AARGO@G), highlighting its enhanced electrochemical performance due to graphene integration, exceptionally low detection limits (0.13 nM), and wide linearity. Subsequently, it introduces a novel Molecular Imprinted Dual-Polymer Infused Capacitive Sensor (M2P-QT@C), detailing its unique architecture and demonstrating its impressive sensitivity (LOD of 0.035 μg/kg), high prediction accuracy through chemometric modeling, and excellent long-term stability for quercetin determination in agro-products.

Chapter 6: Development of a Pen-Like Trielectrode System for Salicylic Acid Detection introduces a novel, integrated pen-like trielectrode system for the electrochemical detection of salicylic acid (ScA), a phenolic phytohormone naturally present in many nutrient-rich plants and also utilized as a food preservative. This chapter focuses on the innovative design of the portable system, which maintains a fixed inter-electrode geometry for improved accuracy and reproducibility. It details comparative studies between this novel pen-like electrode and traditional setups, analyzing the effects of scan rate and concentration variation, establishing the system's analytical performance (LOD of 1.06 μM) across distinct linear ranges, and validating its potential through high recovery rates in real food samples, making it suitable for on-site assessment of food quality.

Chapter 7: Conclusions and Future Scopes provides a comprehensive summary of the major findings and contributions derived from the entire thesis. It discusses the broader implications of the developed sensor technologies for advancing food quality and nutrient assessment, highlighting the challenges successfully overcome. Furthermore, this chapter outlines promising avenues for future research, suggesting directions for further enhancing sensor economic viability, advancing predictive modeling, broadening analyte detection capabilities, and developing fully integrated, portable devices for real-time food analysis.

References

[1] Ellingson et al., "Determination of free and total myo-inositol in infant formula and adult/pediatric nutritional formula by high-performance anion exchange chromatography with pulsed amperometric detection, including a novel total extraction using microwave-assisted acid hydrolysis and enzymatic treatment: first action 2012.12.," *J. AOAC Int.*, vol. 96, no. 5, pp. 1068–1072, 2013, doi: 10.5740/jaoacint 13-128.

[2] K. Schimpf, L. Thompson, and S. Baugh, "Determination of myo-inositol (free and bound as phosphatidylinositol) in infant formula and adult nutritionals by liquid chromatography/pulsed amperometry with column switching: first action 2011.18.," *J. AOAC Int.*, vol. 95, no. 4, pp. 937–942, Aug. 2012, doi: 10.5740/jaoacint.cs2011_18.

[3] N. Bennani and H. Fabre, "Performances of a capillary electrophoresis method for the determination of meso-inositol in a tablet formulation," *Anal. Chim. Acta*, vol. 434, no. 1, pp. 67–73, Apr. 2001, doi: 10.1016/S0003-2670(01)00807-8.

[4] F. Liu, F.-B. Jiang, Y.-T. Li, R.-M. Liu, Z.-Y. Wu, and C.-W. Yan, "Cocrystallization with syringic acid presents a new opportunity for effectively reducing the hepatotoxicity of isoniazid," *Drug Development and Industrial Pharmacy*, vol. 46, pp. 988-995, 2020.

[5] M. M. Rob, K. Hossen, A. Iwasaki, K. Suenaga, and H. Kato-Noguchi, "Phytotoxic activity and identification of phytotoxic substances from Schumannianthus dichotomus," *Plants*, vol. 9, p. 102, 2020.

[6] C. Srinivasulu, M. Ramgopal, G. Ramanjaneyulu, C. Anuradha, and C. S. Kumar, "Syringic acid (SA)–a review of its occurrence, biosynthesis, pharmacological and industrial importance," *Biomedicine & Pharmacotherapy*, vol. 108, pp. 547-557, 2018.

[7] M. T. Bogert and J. Ehrlich, "The synthesis of certain substituted pyrogallol ethers, including a new acetophenetide derived from the ethyl ether of syringic acid," *Journal of the American Chemical Society*, vol. 41, pp. 798-810, 1919.

[8] J. M. Pezzuto, "Grapes and human health: a perspective," *Journal of agricultural and Food Chemistry*, vol. 56, pp. 6777-6784, 2008.

[9] L. A. Pacheco-Palencia, S. Mertens-Talcott, and S. T. Talcott, "Chemical composition, antioxidant properties, and thermal stability of a phytochemical enriched oil from Acai (Euterpe oleracea Mart.," *Journal of agricultural and Food Chemistry*, vol. 56, pp. 4631-4636, 2008.

[10] M. C. Gálvez, C. G. Barroso, and J. A. Pérez-Bustamante, "Analysis of polyphenolic compounds of different vinegar samples," *Zeitschrift für Lebensmittel-Untersuchung und Forschung*, vol. 199, pp. 29-31, 1994.

[11] M.-H. Lee et al., "The aerial part of Taraxacum coreanum extract has an anti-inflammatory effect on peritoneal macrophages in vitro and increases survival in a mouse model of septic shock," *Journal of Ethnopharmacology*, vol. 146, no. 1, pp. 1–8, Dec. 2012, doi: 10.1016/j.jep.2012.12.009.

[12] K. P. Chong, S. Rossall, and M. Atong, "In Vitro Antimicrobial Activity and Fungitoxicity of Syringic Acid, Caffeic Acid and 4-hydroxybenzoic Acid against Ganoderma Boninense," *Journal of Agricultural Science*, vol. 1, no. 2, Nov. 2009, doi: 10.5539/jas.v1n2p15.

[13] O. Cikman, O. Soylemez, O. F. Ozkan, H. A. Kiraz, I. Sayar, S. Ademoglu, et al., "Antioxidant activity of syringic acid prevents oxidative stress in L-arginine–induced acute pancreatitis: an experimental study on rats," *International surgery*, vol. 100, pp. 891-896, 2015.

[14] A. C. Mirza and S. S. Panchal, "Safety evaluation of syringic acid: subacute oral toxicity studies in Wistar rats," *Heliyon*, vol. 5, p. e02129, 2019.

[15] S. Akbar, A. Anwar, and Q. Kanwal, "Electrochemical determination of folic acid: A short review.," *Anal. Biochem.*, vol. 510, pp. 98–105, Oct. 2016, doi: 10.1016/j.ab.2016.07.002.

[16] C. Maynard, I. Cummins, J. Green, and D. Weinkove, "A bacterial route for folic acid supplementation.," *BMC Biol.*, vol. 16, no. 1, p. 67, Jun. 2018, doi: 10.1186/s12915-018-0534-3

[17] L. Bandžuchová, R. Šelešovská, T. Navrátil, and J. Chýlková, "Electrochemical behavior of folic acid on mercury meniscus modified silver solid amalgam electrode," *Electrochim. Acta*, vol. 56, no. 5, pp. 2411–2419, Feb. 2011, doi: 10.1016/j.electacta.2010.10.090.

[18] C. M. Pfeiffer, S. P. Caudill, E. W. Gunter, J. Osterloh, and E. J. Sampson, "Biochemical indicators of B vitamin status in the US population after folic acid fortification: results from the National Health and Nutrition Examination Survey 1999-2000.," *Am. J. Clin. Nutr.*, vol. 82, no. 2, pp. 442–450, Aug. 2005, doi: 10.1093/ajcn.82.2.442.

[19] T. N. Wien, E. Pike, T. Wisløff, A. Staff, S. Smeland, and M. Klemp, "Cancer risk with folic acid supplements: a systematic review and meta-analysis.," *BMJ Open*, vol. 2, no. 1, p. e000653, Jan. 2012, doi: 10.1136/bmjopen-2011-000653.

[20] S. Moazzen*et al.*, "Folic acid intake and folate status and colorectal cancer risk: A systematic review and meta-analysis.," *Clin. Nutr.*, vol. 37, no. 6 Pt A, pp. 1926–1934, Dec. 2018, doi: 10.1016/j.clnu.2017.10.010.

[21] S. Parasuraman, A. Anand David, and R. Arulmoli, "Overviews of biological importance of quercetin: A bioactive flavonoid," *Pharmacognosy Reviews*, vol. 10, no. 20, pp. 84-89, Nov 2016, doi: 10.4103/0973-7847.194044.

[22] S. C. Gupta, S. Prasad, and B. B. Aggarwal, *Drug Discovery from Mother Nature*. Springer, 2016.

[23] M. Abdelhalim, S. Moussa, and H. Qaid, "The protective role of quercetin and arginine on gold nanoparticles induced hepatotoxicity in rats," *International Journal of Nanomedicine*, vol. Volume 13, pp. 2821–2825, May 2018, doi: 10.2147/ijn.s160995.

[24] A. Ataie, R. Ataie, and M. Shadifar, "Polyphenolic Antioxidants and Neuronal Regeneration," *Basic and Clinical Neuroscience Journal*, vol. 7, no. 2, 2016, doi: 10.15412/j.bcn.03070201.

[25] Ellingson et al., "Analysis of free and total myo-inositol in foods, feeds, and infant formula by high-performance anion exchange chromatography with pulsed amperometric detection, including a novel total extraction using microwave-assisted acid hydrolysis and enzymatic treatment." *J. AOAC Int.*, vol. 95, no. 5, pp. 1469–1478, 2012, doi: 10.5740/jaoacint.12-028.

[26] L. Kong, Y. Wang, and Y. Cao, "Determination of Myo-inositol and d-chiro-inositol in black rice bran by capillary electrophoresis with electrochemical detection," *Journal of food composition and analysis*, vol. 21, no. 6, pp. 501–504, Sep. 2008, doi: 10.1016/j.jfca.2008.04.005.

[27] R. S. Clements and B. Darnell, "Myo-inositol content of common foods: development of a high-myo-inositol diet." *Am. J. Clin. Nutr.*, vol. 33, no. 9, pp. 1954–1967, Sep. 1980, doi: 10.1093/ajcn/33.9.1954.

[28] K. J. Schimpf, C. C. Meek, R. D. Leff, D. L. Phelps, D. J. Schmitz, and C. T. Cordle, "Quantification of myo-inositol, 1,5-anhydro-D-sorbitol, and D-chiro-inositol using high-performance liquid chromatography with electrochemical detection in very small volume clinical samples." *Biomed. Chromatogr.*, vol. 29, no. 11, pp. 1629–1636, Nov. 2015, doi: 10.1002/bmc 3470.

[29] J.-H. Shin, J.-M. Park, H.-J. Kim, J.-H. Ahn, B.-M. Kwak, and J.-M. Kim, "Development of Rapid Analytical Methods for Inositol as a Trace Component by HPLC and LC-MS/MS in Infant Formula," *Korean Journal for Food Science of Animal Resources*, vol. 35, no. 4, pp. 466–472, Aug. 2015, doi: 10.5851/kosfa 2015.35.4.466.

[30] G. Marolt and M. Kolar, "Analytical methods for determination of phytic acid and other inositol phosphates: A review." *Molecules*, vol. 26, no. 1, Dec. 2020, doi: 10.3390/molecules26010174.

[31] D. C. Woollard, C. Macfadzean, H. E. Indyk, A. McMahon, and S. Christiansen, "Determination of myo-inositol in infant formulae and milk powders using capillary gas chromatography with flame ionisation detection," *International Dairy Journal*, vol. 37, no. 2, pp. 74–81, Aug. 2014, doi: 10.1016/j.idairyj.2014.03.004.

[32] D. Bandyopadhyayet al., "Voltammetric detection of inositol using a platinum-based electrode," *Nano Life*, Mar. 2022, doi: 10.1142/S1793984422500040.

[33] G. Tagliaferri, G. Bonetti, and C. J. Blake, "Ion chromatographic determination of inositol in infant formulae and clinical products for enteral feeding." *J. Chromatogr. A*, vol. 879, no. 2, pp. 129–135, May 2000, doi: 10.1016/S0021-9673(00)00323-X.

[34] K.-Y. Leung, K. Mills, K. A. Burren, A. J. Copp, and N. D. E. Greene, "Quantitative analysis of myo-inositol in urine, blood and nutritional supplements by high-performance liquid chromatography tandem mass spectrometry." *J. Chromatogr. B Analyt. Technol. Biomed. Life Sci.*, vol. 879, no. 26, pp. 2759–2763, Sep. 2011, doi: 10.1016/j.jchromb.2011.07.043.

[35] R. Rajaram, M. Kiruba, C. Suresh, J. Mathiyarasu, S. Kumaran, and R. Kumaresan, "Amperometric determination of Myo-inositol using a glassy carbon electrode modified with nanostructured copper sulfide." *Mikrochim. Acta*, vol. 187, no. 6, p. 334, May 2020, doi: 10.1007/s00604-020-04300-z.

[36] X. Wang, J. Wang, and N. Yang, "Flow injection chemiluminescent detection of gallic acid in olive fruits," *Food Chemistry*, vol. 105, pp. 340-345, 2007.

[37] K. Dhalwal, V. Shinde, Y. Biradar, and K. Mahadik, "Simultaneous quantification of bergenin, catechin, and gallic acid from Bergenia ciliata and Bergenia ligulata by using thin-layer chromatography," *Journal of food composition and analysis*, vol. 21, pp. 496-500, 2008.

[38] R. de Queiroz Ferreira and L. A. Avaca, "Electrochemical determination of the antioxidant capacity: the ceric reducing/antioxidant capacity (CRAC) assay," *Electroanalysis: An International Journal Devoted to Fundamental and Practical Aspects of Electroanalysis*, vol. 20, pp. 1323-1329, 2008.

[39] W. Ma, D. Han, S. Gan, N. Zhang, S. Liu, T. Wu, et al., "Rapid and specific sensing of gallic acid with a photoelectrochemical platform based on polyaniline–reduced graphene oxide–TiO 2," *Chemical Communications*, vol. 49, pp. 7842-7844, 2013.

[40] L. Wang, M. S. Halquist, and D. H. Sweet, "Simultaneous determination of gallic acid and gentisic acid in organic anion transporter expressing cells by liquid chromatography–tandem mass spectrometry," *Journal of Chromatography B*, vol. 937, pp. 91-96, 2013.

[41] D. P. Singh, R. Govindarajan, A. Khare, and A. K. Rawat, "Optimization of a high-performance liquid chromatography method for the separation and identification of six different classes of phenolics," *Journal of chromatographic science*, vol. 45, pp. 701-705, 2007.

[42] F. Al-Rimawi and I. Odeh, "Development and validation of an HPLC-UV method for determination of eight phenolic compounds in date palms," *Journal of AOAC International*, vol. 98, pp. 1335-1339, 2015.

[43] D. Wen, C. Li, H. Di, Y. Liao, and H. Liu, "A universal HPLC method for the determination of phenolic acids in compound herbal medicines," *Journal of agricultural and Food Chemistry*, vol. 53, pp. 6624-6629, 2005.

[44] N. Sharma, U. K. Sharma, A. P. Gupta, and A. K. Sinha, "Simultaneous determination of epicatechin, syringic acid, quercetin-3-O-galactoside and quercitrin in the leaves of Rhododendron species by using a validated HPTLC method," *Journal of food composition and analysis*, vol. 23, pp. 214-219, 2010.

[45] C. Sun, Y. Yuan, E. Omari-Siaw, S. Tong, Y. Zhu, Q. Wang, et al., "An efficient HPLC method for determination of syringic acid liposome in rats plasma and mice tissues: Pharmacokinetic and biodistribution application," *Current Pharmaceutical Analysis*, vol. 14, pp. 41-52, 2018.

[46] W. Sordoń, A. Salachna, and M. Jakubowska, "Voltammetric determination of caffeic, syringic and vanillic acids taking into account uncertainties in both axes," *Journal of Electroanalytical Chemistry*, vol. 764, pp. 23-30, 2016.

[47] R. C. Minussi, M. Rossi, L. Bologna, L. v. Cordi, D. Rotilio, G. M. Pastore, et al., "Phenolic compounds and total antioxidant potential of commercial wines," *Food Chemistry*, vol. 82, pp. 409-416, 2003.

[48] R. J. Robbins and S. R. Bean, "Development of a quantitative high-performance liquid chromatography–photodiode array detection measurement system for phenolic acids," *Journal of chromatography A*, vol. 1038, pp. 97-105, 2004.

[49] M.-Á. Rodríguez-Delgado, G. González-Hernández, J.-E. a. Conde-González, and J.-P. Pérez-Trujillo, "Principal component analysis of the polyphenol content in young red wines," *Food Chemistry*, vol. 78, pp. 523-532, 2002.

[50] E. Kilinc and H. Kalkan, "High-performance liquid chromatographic determination of some phenolic acids of Turkish commercial wines: an electrochemical approach," *Journal of Wine Research*, vol. 14, pp. 17-23, 2003.

[51] M. Rossouw and J. Marais, "The phenolic composition of south African Pinotage, Shiraz and Cabernet Sauvignon wines," *South African Journal of Enology and Viticulture*, vol. 25, pp. 94-104, 2004.

[52] G. L. La Torre, M. Saitta, F. Vilasi, T. Pellicanò, and G. Dugo, "Direct determination of phenolic compounds in Sicilian wines by liquid chromatography with PDA and MS detection," *Food Chemistry*, vol. 94, pp. 640-650, 2006.

[53] S. Zhao, H. Yuan, C. Xie, and D. Xiao, "Determination of folic acid by capillary electrophoresis with chemiluminescence detection," *J. Chromatogr. A*, vol. 1107, no. 1–2, pp. 290–293, Feb. 2006, doi: 10.1016/j.chroma.2005.11.052.

[54] Z. Yang, F. Gong, Z. Yu, D. Shi, S. Liu, and M. Chen, "Highly sensitive folic acid colorimetric sensor enabled by free-standing molecularly imprinted photonic hydrogels," *Polym. Bull.*, vol. 79, no. 3, pp. 1857–1871, Mar. 2022, doi: 10.1007/s00289-021-03584-2.

[55] J. Jastrebova, C. Witthöft, A. Grahn, U. Svensson, and M. Jägerstad, "HPLC determination of folates in raw and processed beet-roots," *Food Chem.*, vol. 80, no. 4, pp. 579–588, Apr. 2003, doi: 10.1016/S0308-8146(02)00506-X.

[56] D. Sun *et al.*, "Modified EMR-lipid method combined with HPLC-MS/MS to determine folates in egg yolks from laying hens supplemented with different amounts of folic acid.," *Food Chem.*, vol. 337, p. 127767, Feb. 2021, doi: 10.1016/j.foodchem.2020.127767.

[57] P. Anastasopoulos, T. Mellos, M. Spinou, T. Tsiaka, and M. Timotheou-Potamia, "Chemiluminometric and fluorimetric determination of folic acid," *Anal. Lett.*, vol. 40, no. 11, pp. 2203–2216, Oct. 2007, doi: 10.1080/00032710701567022.

[58] R. Matias, P. R. S. Ribeiro, M. C. Sarraguça, and J. A. Lopes, "A UV spectrophotometric method for the determination of folic acid in pharmaceutical tablets and dissolution tests," *Anal. Methods*, vol. 6, no. 9, p. 3065, 2014, doi: 10.1039/c3ay41874j.

[59] Y. He, S. Wang, and J. Wang, "Detection and quantification of folic acid in serum via a dual-emission fluorescence nanoprobe.," *Anal. BioAnal. Chem.*, vol. 411, no. 28, pp. 7481–7487, Nov. 2019, doi: 10.1007/s00216-019-02121-5.

[60] A. Mahato, S. Vyas, and N. S. Chatterjee, "HPLC-UV Estimation of Folic Acid in Fortified Rice and Wheat Flour using Enzymatic Extraction and Immunoaffinity Chromatography Enrichment: An Interlaboratory Validation Study.," *J. AOAC Int.*, vol. 103, no. 1, pp. 73–77, Jan. 2020, doi: 10.5740/jaoacint.19-0207.

[61] R. Amidzic, J. Brboric, O. Cudina, and S. Vladimirov, "RP-HPLC determination of vitamins, folic acid and B12 in multivitamin tablets," *J. Serb. Chem. Soc.*, vol. 70, no. 10, pp. 1229–1235, 2005, doi: 10.2298/JSC0510229A.

[62] E. M. Mohammed, "Qualitative and quantitative determination of folic acid in tablets by FTIR spectroscopy.," *IJAPBC*, vol. 3, pp. 773–780, 2014.

[63] S. M. Wabaidur, S. M. Alam, S. H. Lee, Z. A. Alothman, and G. E. Eldesoky, "Chemiluminescence determination of folic acid by a flow injection analysis assembly.," *Spectrochim. Acta A Mol. Biomol. Spectrosc.*, vol. 105, pp. 412–417, Mar. 2013, doi: 10.1016/j.saa.2012.11.078.

[64] I. M. A. Hasan, K. M. Abd-Elsabur, F. H. Assaf, and M. Abd-Elsabour, "Folic Acid Determination in Food Samples Using Green Synthesized Copper Oxide Nanoparticles and Electro-Poly (Methyl Orange) Sensor," *Electrocatal.*, vol. 13, no. 6, pp. 759–772, Nov. 2022, doi: 10.1007/s12678-022-00756-0.

[65] H. Karimi-Maleh, F. Amini, A. Akbari, and M. Shojaei, "Amplified electrochemical sensor employing CuO/SWCNTs and 1-butyl-3-methylimidazolium hexafluorophosphate for selective analysis of sulfisoxazole in the presence of folic acid.," *J. Colloid Interface Sci.*, vol. 495, pp. 61–67, Jun. 2017, doi: 10.1016/j.jcis.2017.01.119.

[66] M. Safaei, H. Beitollahi, and M. R. Shishehbore, "Simultaneous determination of epinephrine and folic acid using the fe3o4@sio2/gr nanocomposite modified graphite," *Russ. J. Electrochem.*, vol. 54, no. 11, pp. 851–859, Nov. 2018, doi: 10.1134/S1023193518130402.

[67] A. A. Ensafi, P. Nasr-Esfahani, and B. Rezaei, "Simultaneous detection of folic acid and methotrexate by an optical sensor based on molecularly imprinted polymers on dual-color CdTe quantum dots.," *Anal. Chim. Acta*, vol. 996, pp. 64–73, Dec. 2017, doi: 10.1016/j.aca.2017.10.011.

[68] J.-L. Lu *et al.*, "Decaffeination of tea extracts by using poly(acrylamide-co-ethylene glycol dimethylacrylate) as adsorbent," *J. Food Eng.*, vol. 97, no. 4, pp. 555–562, Apr. 2010, doi: 10.1016/j.jfoodeng.2009.11.018.

[69] S. Nag, S. Pradhan, D. Das, B. Tudu, R. Bandopadhyay, and R. B. Roy, "Fabrication of A molecular imprinted polyacrylonitrile engraved graphite electrode for detection of formalin in food extracts," *IEEE Sens. J.*, pp. 1–1, 2021, doi: 10.1109/JSEN.2021.3128520.

[70] N. Leibl, K. Haupt, C. Gonzato, and L. Duma, "Molecularly imprinted polymers for chemical sensing: A tutorial review," *Chemosensors*, vol. 9, no. 6, p. 123, May 2021, doi: 10.3390/chemosensors9060123.

[71] S. Hussain, S. A. Zaidi, D. Vikraman, H.-S. Kim, and J. Jung, "Facile preparation of molybdenum carbide (Mo_2C) nanoparticles and its effective utilization in electrochemical sensing of folic acid via imprinting.," *Biosens. Bioelectron.*, vol. 140, p. 111330, Sep. 2019, doi: 10.1016/j.bios.2019.111330.

[72] Y. Yang, Z. Wang, H. Niu, and H. Zhang, "One-pot synthesis of quantum dot-labeled hydrophilic molecularly imprinted polymer nanoparticles for direct optosensing of folic acid in real, undiluted biological samples.," *Biosens. Bioelectron.*, vol. 86, pp. 580–587, Dec. 2016, doi: 10.1016/j.bios.2016.07.056.

[73] Y. Areerob, P. Sricharoen, N. Limchoowong, and S. Chanthai, "Core-shell SiO2-coated Fe_3O_4 with a surface molecularly imprinted polymer coating of folic acid and its applicable magnetic solid-phase extraction prior to determination of folates in tomatoes.," *J. Sep. Sci.*, vol. 39, no. 15, pp. 3037–3045, Aug. 2016, doi: 10.1002/jssc.201600342.

[74] A. Zengin, M. Utku Badak, M. Bilici, Z. Suludere, and N. Aktas, "Preparation of molecularly imprinted PDMS elastomer for selective detection of folic acid in orange juice," *Appl. Surf. Sci.*, vol. 471, pp. 168–175, Mar. 2019, doi: 10.1016/j.apsusc.2018.12.008.

[75] S. Hussain, S. Khan, S. Gul, M. I. Pividori, and M. Del Pilar Taboada Sotomayor, "A novel core@shell magnetic molecular imprinted nanoparticles for selective determination of folic acid in different food samples," *Reactive and Functional Polymers*, vol. 106, pp. 51–56, Sep. 2016, doi: 10.1016/j.reactfunctpolym.2016.07.011.

[76] S. Sadeghi and M. Hosseinpour-Zaryabi, "A sensitive fluorescent probe based on dithizone-capped ZnS quantum dots for quercetin determination in biological samples," *Luminescence*, vol. 35, no. 8, pp. 1391–1401, Aug. 2020, doi: 10.1002/bio.3903.

[77] Y. Hu, T. Feng, and G. Li, "A novel solid fluorescence method for the fast determination of quercetin in biological samples based on the quercetin–Al(III) complex imprinted polymer," *Spectrochimica Acta Part A: Molecular and Biomolecular Spectroscopy*, vol. 118, pp. 921–928, Jan. 2014, doi: 10.1016/j.saa.2013.09.076.

[78] Z. K. Alabri et al., "Fluorescence spectroscopy-partial least square regression method for the quantification of quercetin in Euphorbia masirahensis," *Measurement*, vol. 121, pp. 355–359, Jun. 2018, doi: 10.1016/j.measurement.2018.02.036.

[79] X. ZHOU, J. SUN, D. ZHU, B. YUAN, and T. YOU, "Quality Analysis of Herbal Medicine Products Prepared from Herba Sarcandrae by Capillary Electrophoresis with Electrochemical Detection," *Chemical Research in Chinese Universities*, vol. 24, no. 2, pp. 148–153, Mar. 2008, doi: 10.1016/s1005-9040(08)60031-8.

[80] L. WANG and M. MORRIS, "Liquid chromatography–tandem mass spectroscopy assay for quercetin and conjugated quercetin metabolites in human plasma and urine," *Journal of Chromatography B*, vol. 821, no. 2, pp. 194–201, Jul. 2005, doi: 10.1016/j.jchromb.2005.05.009.

[81] V. Pilařová et al., "Simultaneous determination of quercetin and its metabolites in rat plasma by using ultra-high-performance liquid chromatography tandem mass spectrometry," *Talanta*, vol. 185, pp. 71–79, Aug. 2018, doi: 10.1016/j.talanta.2018.03.033.

[82] S. Özbilgin, Ö. B. Acıkara, E. K. Akkol, I. Süntar, H. Keleş, and G. S. İşcan, "In vivo wound-healing activity of Euphorbia characias subsp. wulfenii: Isolation and quantification of quercetin glycosides as bioactive compounds," *Journal of Ethnopharmacology*, vol. 224, pp. 400–408, Oct. 2018, doi: 10.1016/j.jep.2018.06.015.

[83] J. Krňanová, N. Denderz, J. Lehotay, and M. Samohýl, "Determination of Some Flavonoids by HPLC Using Quercetin-Molecularly Imprinted Polymers," *Journal of Liquid Chromatography & Related Technologies*, vol. 38, no. 6, pp. 702–708, Oct. 2014, doi: 10.1080/10826076.2014.951768.

[84] M. Careri, L. Elviri, A. Mangia, and M. Musci, "Se ctrophotometric and coulometric detection in the high-performance liquid chromatography of flavonoids and optimization of sample treatment for the determination of quercetin in orange juice," *Journal of chromatography A*, vol. 881, no. 1–2, pp. 449–460, Jun. 2000, doi: 10.1016/s0021-9673(00)00256-9.

[85] M. Rahimi, S. Bahar, R. Heydari, and S. M. Amininasab, "Determination of quercetin using a molecularly imprinted polymer as solid-phase microextraction sorbent and high-performance liquid chromatography," *Microchemical Journal*, vol. 148, pp. 433–441, Jul. 2019, doi: 10.1016/j.microc.2019.05.032.

[86] O. A. A. Ahmed, H. M. El-Bassossy, H. M. El-Sayed, and S. S. A. El-Hay, "Rp-HPLC Determination of Quercetin in a Novel D-α-Tocopherol Polyethylene Glycol 1000 Succinate Based SNEDDS Formulation: Pharmacokinetics in Rat Plasma," *Molecules*, vol. 26, no. 5, p. 1435, Mar. 2021, doi: 10.3390/molecules26051435.

[87] V. S. Chaudhari, R. M. Borkar, U. S. Murty, and S. Banerjee, "Analytical method development and validation of reverse-phase high-performance liquid chromatography (RP-HPLC) method for simultaneous quantifications of quercetin and piperine in dual-drug loaded nanostructured lipid carriers," *Journal of Pharmaceutical and Biomedical Analysis*, vol. 186, p. 113325, Jul. 2020, doi: 10.1016/j.jpba.2020.113325.

[88] Qiu, C. Luo, M. Sun, F. Lu, L. Fan, and X. Li, "A novel chemiluminescence sensor for determination of quercetin based on molecularly imprinted polymeric microspheres," *Food Chemistry*, vol. 134, no. 1, pp. 469–473, Sep. 2012, doi: 10.1016/j.foodchem.2012.02.102.

[89] S. Gupta and R. Gupta, "Detection and quantification of quercetin in roots, leaves and flowers of Clerodendrum infortunatum L.," *Asian Pacific Journal of Tropical Disease*, vol. 2, pp. S940–S943, Jan. 2012, doi: 10.1016/s2222-1808(12)60296-5.

[90] P. K. Jain, S. Jain, S. Sharma, S. Paliwal, and G. Singh, "Evaluation of anti-diabetic and antihypertensive activity of Phoenix sylvestris (L.)Roxb leaves extract and quantification of biomarker Quercetin by HPTLC," *Phytomedicine Plus*, vol. 1, no. 4, p. 100136, Nov. 2021, doi: 10.1016/j.phyplu.2021.100136.

[91] N. Altunay, D. Bingöl, A. Elik, and R. Gürkan, "Vortex-assisted ionic liquid dispersive liquid-liquid microextraction and spectrophotometric determination of quercetin in tea, honey, fruit juice and wine samples after optimization based on response surface methodology," *Spectrochimica Acta Part A: Molecular and Biomolecular Spectroscopy*, vol. 221, p. 117166, Oct. 2019, doi: 10.1016/j.saa.2019.117166.

[92] M. Hassan, F. Uzcan, S. N. Shah, U. Alshana, and M. Soylak, "Switchable-hydrophilicity solvent liquid-liquid microextraction for sample cleanup prior to dispersive magnetic solid-phase microextraction for spectrophotometric determination of quercetin in food samples," *Sustainable Chemistry and Pharmacy*, vol. 22, p. 100480, Sep. 2021, doi: 10.1016/j.scp.2021.100480.

[93] A.Asfaram, M. Arabi, A. Ostovan, H. Sadeghi, and M. Ghaedi, "Simple and selective detection of quercetin in extracts of plants and food samples by dispersive-micro-solid phase extraction based on core–shell magnetic molecularly imprinted polymers," *New Journal of Chemistry*, vol. 42, no. 19, pp. 16144–16153, 2018, doi: 10.1039/c8nj03349h.

[94] Gomes, G. J. Mattos, B. Coldibeli, R. F. H. Dekker, A. M. Barbosa Dekker, and E. R. Sartori, "Covalent attachment of laccase to carboxymethyl-botryosphaeran in aqueous solution for the construction of a voltammetric biosensor to quantify quercetin," *Bioelectrochemistry*, vol. 135, p. 107543, Oct. 2020, doi: 10.1016/j.bioelechem.2020.107543.

[95] Y. Wang, M. Qiao, X. Mamat, X. Hu, and G. Hu, "Hierarchically ordered porous nitrogen doped carbon modified a glassy carbon electrode for voltammetry detection of quercetin," *Materials Research Bulletin*, vol. 136, p. 111131, Apr. 2021, doi: 10.1016/j.materresbull.2020.111131.

[96] V. Mariyappan, N. Karuppusamy, S.-M. Chen, P. Raja, and R. Ramachandran, "Electrochemical determination of quercetin using glassy carbon electrode modified with WS2/GdCoO3 nanocomposite," *Microchimica Acta*, vol. 189, no. 3, Feb. 2022, doi: 10.1007/s00604-022-05219-3.

[97] Ziyatdinova, E. Kozlova, and H. Budnikov, "Poly(gallic acid)/MWNT-modified electrode for the selective and sensitive voltammetric determination of quercetin in medicinal herbs," *Journal of Electroanalytical Chemistry*, vol. 821, pp. 73–81, Jul. 2018, doi: 10.1016/j.jelechem.2017.12.071.

[98] S. Bose, S. Radhakrishnan, B.-S. Kim, and H. W. Kang, "Formulation of amorphous carbon embedded CuFeS2 hybrids for the electrochemical detection of Quercetin," *Materials Today Chemistry*, vol. 26, p. 101228, Dec. 2022, doi: 10.1016/j.mtchem.2022.101228.

[99] W. Zhang, L. Zong, G. Geng, Y. Li, and Y. Zhang, "Enhancing determination of quercetin in honey samples through electrochemical sensors based on highly porous polypyrrole coupled with nanohybrid modified GCE," *Sensors and Actuators B: Chemical*, vol. 257, pp. 1099–1109, Mar. 2018, doi: 10.1016/j.snb.2017.11.059.

[100] S. Karakaya and İ. Kaya, "An electrochemical detection platform for selective and sensitive voltammetric determination of quercetin dosage in a food supplement by poly(9-(2-(pyren-1-yl)ethyl)-9h-carbazole) coated indium tin oxide electrode," *Polymer*, vol. 212, p. 123300, Jan. 2021, doi: 10.1016/j.polymer.2020.123300.

[101] N. H. Khand et al., "A new electrochemical method for the detection of quercetin in onion, honey and green tea using Co3O4 modified GCE," *Journal of Food Measurement and Characterization*, vol. 15, no. 4, pp. 3720–3730, May 2021, doi: 10.1007/s11694-021-00956-0.

[102] A. Hayat et al., "Organic heterostructure modified carbon nitride as apprehension for Quercetin Biosensor," *Synthetic Metals*, vol. 278, p. 116813, Aug. 2021, doi: 10.1016/j.synthmet.2021.116813

[103] M. Mosleh, S. M. Ghoreishi, S. Masoum, and A. Khoobi, "Determination of quercetin in the presence of tannic acid in soft drinks based on carbon nanotubes modified electrode using chemometric approaches," *Sensors and Actuators B: Chemical*, vol. 272, pp. 605–611, Nov. 2018, doi: 10.1016/j.snb.2018.05.172.

[104] D. A. Skoog, F. J. Holler, S.R.Crouch, *Principles of Instrumental Analysis*, 7th ed., Cengage learning , pp. 303-348 , January 2017.

[105] A.M. Bond, Broadening *electrochemical horizons: principles and illustration of voltammetric and related techniques*, Oxford University Press, Oxford, New York, 2002.

[106] A.F. Danet, *Metode electrochimice de analiza*, Editura Stiintifica, Bucuresti, 1996.

[107] A.W. Bott, *Practical problems in voltammetry* 2. Curr.Sep., 1993, Vol. 12(1), pp. 10-13.

[108] R.G. Compton and C.E. Banks, *Understanding voltammetry* (2nd Edition), World Scientific Publishing Co, New Jersey, London, Singapore, 2010.

[109] A. A. Behfar, N. Sadeghi, B. Jannat, and M. R. Oveisi, "Determination of L- ascorbic Acid in plasma by voltammetric method.," *PubMed*, Jan. 2010.

[110] H. Zhong, R. Yuan, Y. Chai, Y. Zhang, C. Wang, and F. Jia, "Non-enzymatic hydrogen peroxide amperometric sensor based on a glassy carbon electrode modified with an MWCNT/polyaniline composite film and platinum nanoparticles," *Microchimica Acta*, vol. 176, no. 3–4, pp. 389–395, Nov. 2011, doi: 10.1007/s00604-011-0731-z.

[111] A. M. Pisoschi, A. Pop, G. P. Negulescu, and A. Pisoschi, "Determination of ascorbic acid content of some fruit juices and wine by voltammetry performed at PT and carbon paste electrodes," *Molecules*, vol. 16, no. 2, pp. 1349–1365, Feb. 2011, doi: 10.3390/molecules16021349.

[112] H. H. Willard, Jr., L. L. Merrit, J. A. Dean, Jr., F. A. Settle, "*Instrumental methods of analysis*," 6th Edn. D. Van Nostrand, Princeton, 1981.

[113] G. Wulff, S. Schauhoff, "Enzyme-analog-built-polymers: 27 Racemic-resolution of free sugars with macroporous polymers prepared by molecular imprinting-selectivity dependence on the arrangement of functional group versus requirements," *J. Org. Chem*. vol.56, pp. 395-400, 1991.

[114] A. Kugimiya, J. Matsui, T. Takeuchi, K. Yano, H. Muguruma, A. V. Elgersma, I. Karube, "Recognition of sialic-acid using molecularly imprinted polymer," *Anal. Lett.*, vol.28, 2317-2323, 1995.

[115] A. Kugimiya, J. Matsui, H. Abe, M. Abrutani, T. Takeuchi, "Synthesis of castasterone selective polymers prepared by molecular imprinting," *Anal. Chim. Acta.*, vol.365, pp. 75-79, 1998.

[116] G. Wulff, J. Vietmeier, "Enzyme-analogue built polymers: 26. Enantioselective synthesis of amino acids using polymers possessing chiral cavities obtained by an imprinting procedure with template molecules," *Makromol. Chem.* vol.190, pp.1727-1735, 1989.

[117] N. Sallacan, M. Zayats, T. Bourenko, A. B. Kharitonov, I. Wilner, "Imprinting of nucleotide and monosaccharide recognition sites in acrylamide phenylboronic acid-acrylamide copolymer membranes associated with electronic transducers," *Anal. Chem*., vol. 74, pp.702-712, 2002.

[118] S. H. Gao, W. Wang, B. H. Wang, "Building fluorescent sensors for carbohydrates using template-directed polymerizations," *Bioorg. Chem.* vol.29, pp. 308-320, 2001.

[119] S. A. Piletsky, K. Piletskaya, E. V. Piletskaya, K. Yano, A. Kugimiya, A. V. Elgersma, R. Levi, U. Kahlow, T. Takeuchi, I. Karube, T. I. Panasyuk, A. V. Elskaya, "A biomimetic receptor system for sialic acid based on molecular imprinting," *Anal. Lett.*, vol.29, pp.157-170, 1996.

[120] W. Wang, S. H. Gao, B. H. Wang, "Building fluorescent sensors by template polymerization: the preparation of a fluorescent sensors for D-fructose," *Org. Lett.*, vol.1, pp. 1209-1212, 1999.

[121] Y. Kanekiyo, M. Sano, R. Iguchi, S. Shinkai, "Novel nucleotide-responsive hydrogels designed from copolymers of boronic acid and cationic units and their application as a QCM resonator system to nucleotide sensing," *J. Polym. Sci. A. Polym. Chem.* vol.38, pp.1302-1310, 2000.

[122] A. Bossi, S. A. Piletsky, E. V. Piletska, P. G. Righetti, A. P. F. Turner, "Surface-grafted molecularly imprinted polymers for protein recognition," *Anal. Chem*., vol. 73, pp. 5281-5286, 2001.

[123] G. Wulff, R. Dederichs, R. Grotstollen, C. Jupe, "On the chemistry of binding sites: II. Specific binding of substances to polymers by fast and reversible covalent interactions in: T.C.J. Gribnau, J. Visser, R.J.F. Nivard (Eds.)," *Affinity Chromatography and Related Tech.*, pp. 207-216, 1982.

[124] G. Wulff, "Selective binding to polymers via covalent bonds-the construction of chiral cavities as specific receptor sites," *Pure Appl. Chem.* vol. 54, pp. 2093-2102, 1982.

[125] C. Alexander, C. R. Smith, M. J. Whitecombe, E. N. Vulfson, "Imprinted polymers as protecting groups for regioselective modification of polyfunctional substrates," *J. Am. Chem. Soc.*, vol.121, pp. 6640-6651, 1999.

[126] G. Wulff, W. Best, A. Akelah, "Enzyme-analogue built polymers, 17 Investigations on the racemic resolution of amino acids," React. Polym. vol.2, pp. 167-174, 1984

[127] K. J. Shea, D. Y. Sasaki, "An analysis of small-molecule binding to functionalized synthetic polymers by C-13 CP/MAS NMR and FT-IR spectroscopy," *J. Am. Chem. Soc.*, vol.113, pp. 4109-4120, 1991.

[128] R. Arshady, K. Mosbach, "Synthesis of substrate-selective polymers by host-guest polymerization," *Makromol. Chem.* vol.182, pp. 687-692, 1981.

[129] M. Sibrian-Vazquez, D. A. Spivak, "Molecular imprinting made easy," *J. Am. Chem. Soc.*, vol. 126, pp. 7827-7833, 2004.

[130] A. Katz, M. E. Davis, "Molecular imprinting of bulk, microporous silica," *Nature*, vol.403, pp. 286-289, 2000.

[131] A. L. Graham, C. A. Carlson, P. L. Edmiston, "Development and characterization of molecularly imprinted sol-gel materials for the selective detection of DDT," *Anal. Chem.*, vol.74, pp. 458-467, 2002.

[132] C. J. Percival, S. Stanley, A. Braithwaite, M. I. Newton, G. McHale, "Molecular imprinted polymer coated QCM for the detection of nadrolone," *Analyst*, vol. 127, pp. 1024-1026, 2002.

[133] J. U. Klein, M. J. Whitecombe, F. Mulholl, E. N. Vulfson, "Template-mediated synthesis of a polymeric receptor specific to amino acid sequences," *Angew. Chem. Int. Ed.* vol.38, pp. 2057-2060, 1999.

[134] U. K. R. Jain Vandana Neeraj, "Novel hplc method for determination of polyphenols in agro-industrial waste of date fruits," *International Journal of Advanced Research*, vol. 8, pp. 626-634, 2020.

[135] T. Seal, "Quantitative HPLC analysis of phenolic acids, flavonoids and ascorbic acid in four different solvent extracts of two wild edible leaves, Sonchus arvensis and Oenanthe linearis of North-Eastern region in India," *Journal of Applied Pharmaceutical Science*, vol. 6, pp. 157-166, 2016.

[136] V. Vinothkumar, C. Koventhan, S.-M. Chen, M. Abinaya, G. Kesavan, and N. Sengottuvelan, "Preparation of three-dimensional flower-like cobalt phosphate as dual functional electrocatalyst for flavonoids sensing and supercapacitor applications," *Ceramics International*, vol. 47, no. 21, pp. 29688–29706, Jul. 2021, doi: 10.1016/j.ceramint.2021.07.140.

Electrochemical Detection of Inositol in Food Samples

2

2.1 Introduction

In fruits or fruit-based products, the leading natural sources of energy and nutrition are sugars such as sucrose, fructose, etc. Inositol or Hexa-hydroxyl cyclohexane ($C_6H_{12}O_6$; Fig. 2.1) is a type of non-reducing sugar alcohol that exists naturally in nine various stereoisomeric forms in various foods, animals, or human bodies. The most nutritionally significant, optically active, and popular among these nine forms of inositol is myo-inositol (MIS) or Cis-1, 2, 3, 5-trans-4, 6-cyclohexanehexol, which can influence various biological activities in the animal or human body. MIS can exist naturally in both free (as Myo-inositol) as well as in bounded (inositol phosphates (ISPs) or phosphatidyl inositol) forms [1]-[3]. Some of the natural sources of MIS include citrus fruits, cantaloupe, milk, and various fiber-rich foods, viz., sesame seed beans, wheat bran, brown rice, and corn [4]-[5]. MIS is also available in dietary supplements and can play a vital role in the complementary therapeutic treatment of various metabolic as well as mental disorders, anxieties, and depression by influencing serotonin (neurotransmitter). MIS can act as a fat-solubilizing agent and active intracellular messenger (phosphoinositides) that can stimulate the cell signaling process [6]-[9]. Few studies reveal that Inositol polyphosphate kinases and Inositol pyrophosphates play a pivotal role in nuclear regulation as well as development [10], apoptosis [11], and mammalian cell metabolism activities [12]-[14]. MIS can also be instrumental in blood sugar control and diabetes control as it can enhance insulin sensitivity. Moreover, it can act as a fertility supporter in both women and men [15]-[18]. Besides these, MIS and its derivatives find application in the food, pharmaceutical, feed, and cosmetics industries [19]. Several in vitro biosynthesis techniques have been reported for the efficient production of MIS from starches and Escherichia coli strains [20]-[22]. It is to be mentioned that MIS is nontoxic or nonhazardous for adults, but mild side effects in the form of dizziness, stomach pain, tiredness, nausea, and headache may be experienced owing to overdosing. For infants, the standard maximum permissible consumption limit of MIS ranges from 4 – 40 mg/100 kcal, while 27.0 to 67.5 mg/100 kcal for premature infants as standardized by Codex Alimentarius, FAO WHO (2007) [23]-[24]. Apart from MIS, some of the other inositol stereoisomers are also valuable health promoters. Patients with hyperglycemia, polycystic ovary

syndrome, and Alzheimer's disease have been proven to benefit from D-chiro-inositol (DCIS) and Scylla-inositol (SIS) [26]-[28]. Nowadays, various chemicals and pesticides are added to fruits, vegetables, and other food products, which have proven to be detrimental to health. The usage of these hazardous materials can rescind the nutritional or medical values of these vitamin-like sugar compounds. Thus, there is an indispensable need to assess the overall fruit and vegetable qualities by quantifying specifically the health-beneficial compounds like MIS (or IS). The prime objective of developing dedicated sensors is to detect and quantify the content of these medically valuable compounds in real food samples, even if they occur in low quantities amid other compounds.

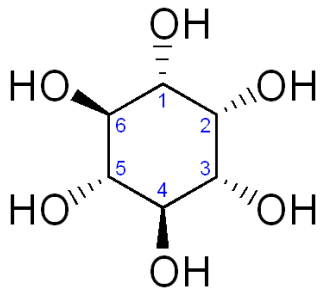

Fig. 2.1. Chemical structure of inositol.

Appreciating the medical and industrial significance of MIS as discussed earlier, there is an obligatory requirement to develop a cost-effective, reusable sensor for the detection as well as quantitative determination of MIS analytes in beverages, fruits, and vegetables. An extensive literature survey in last few decades reveals various conventional methods viz. high-performance anion exchange chromatography with pulsed ampere-metric detection [1]-[2], Liquid chromatography [3], capillary electrophoresis with electrochemical detection [4]-[6], high-performance liquid chromatography coupled with electrochemical detection [7], analytical methods by HPLC and LC-MS/MS [23]-[24], capillary gas chromatography with flame ionization [25], voltammetric detection [29], ion chromatographic method [30], HPLC tandem mass spectrometry[31] and amperometric determination technique employing glassy- carbon modified electrodes [32] were employed for the IS detection. Despite their utility, many of these methods remain hindered by prohibitive operational costs, a reliance on complex instrumentation, and the necessity for specialized technical expertise.

This chapter explores two distinct electrochemical approaches for inositol sensor development: a platinum-based electrode utilizing differential pulse voltammetry, and a novel molecularly imprinted bi-polymer infused capacitive sensor. These methods aim to provide robust, selective, and cost-effective solutions for the quantification of inositol in various food matrices.

2.2 Voltammetric detection of inositol using a platinum-based electrode

In this work, the electrochemical behavior of a platinum (Pt) based noble metal electrode for inositol detection is investigated. The electrode performance was studied using a three-electrode system, embracing a Pt working electrode (2.5 mm inner diameter), a steel counter electrode, and an Ag/AgCl reference electrode. Differential pulse voltammetry (DPV) was employed for its enhanced sensitivity and reduced charging currents compared to other voltammetric techniques. While previous studies have utilized various electrode materials for electrochemical sensing, for instance, quercetin-imprinted polymer graphite electrodes for epicatechin [33], nano cerium oxide modified graphite electrodes for formaldehyde [34] the application of a simple, robust Pt electrode specifically for inositol detection in food remains an area requiring further exploration to ensure cost-effectiveness and ease of implementation.

The electrochemical responses for various inositol concentrations (50 μM, 80 μM, 100 μM, 200 μM, 300 μM, and 400 μM) were analyzed. A satisfactory linear operating range was achieved from 50 - 400 μM, with a limit of detection (LOD) of 19.28 μM. Furthermore, chemometric tools, namely Principal Component Analysis (PCA) and Partial Least Squares Regression (PLSR), alongside Principal Component Regression (PCR), were utilized to analyze the electrochemical data. PCA enabled effective data clustering with a good class separability index (SI) of 142.91, demonstrating clear discrimination between different inositol levels. PLSR and PCR algorithms provided high prediction accuracies of 93.69% and 93.71%, respectively, for inositol content estimation. Crucially, the practical applicability of the Pt electrode was validated through its satisfactory recovery rate of 96.18% when applied to real orange juice samples. This demonstrates the potential of this electrochemical system for inositol detection in everyday food consumption, particularly in juices and beverages.

2.2.1 Experimental Section

2.2.1.1 Reagents and standards

Inositol was acquired from Sisco Research Laboratories Pvt. Ltd. (SRL) - India. Phosphate-buffer saline (PBS), Citrate Buffer Saline (CBS) of various pH (5, 6, 7), Acetate buffer saline (ABS), were prepared in the laboratory and used along with the solution of Inositol. The concentration of each of the buffers used in the experiments was 0.1M. All the chemicals used in this work were of pure and analytical grade. Millipore water was used for preparing experimental solutions, and at room temperature, the entire experiment

was performed. Between the experiments working electrode was cleaned by rinsing with Millipore water for surface regeneration.

2.2.1.2 Apparatus and Instruments

For the detection of inositol, a three-electrode assembly was interfaced with a Metrohm Autolab PGSTAT101 potentiostat. In this arrangement, the redox response was monitored at a Pt working electrode, while an Ag/AgCl electrode and a steel rod served as the reference and counter electrodes, respectively. Graphical illustrations of the DPV responses were presented by the NOVA software, provided by the Metrohom Autolab. An ultrasonicator (Labman Scientific instrument) was used to stir the solution to ensure proper blending of the solutes and solvents.

2.2.1.3 Experimental Set-up

The three-electrode system is connected with the potentiostat PGSTAT1010, which is interfaced with a lab computer. The voltammetric responses obtained from the NOVA user interface depict the electrochemical behavior of the inositol detection. The schematic diagram of the whole experimental setup is shown in Fig. 2.2.

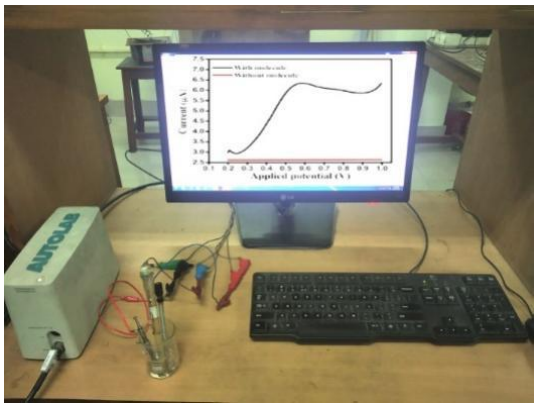

Fig. 2.2. Experimental set-up

2.2.1.4 Data Analysis

The electrochemical data obtained from the NOVA were analyzed using MATLAB (2017 version). The performance of the Pt electrode was examined using a data analysis tool-principal component analysis (PCA). Four sets of repetitions were noted for each of the six concentrations - 50 µM, 80 µM, 100 µM, 200 µM, 300 µM, and 400 µM of inositol. The electrochemical data were further analyzed by PLSR and PCR tools for estimating the prediction accuracies of the system.

2.2.2 RESULTS AND DISCUSSION

2.2.2.1 *Electrochemical conduct of the Pt working electrode*

To assess the electrochemical performance of the Pt electrode, measurements were carried out utilizing the DPV technique, ensuring high sensitivity for the detection process. For a fixed concentration of target analyte, inositol was subjected to electrochemical analysis in the presence of PBS-5 buffer solution. The electrochemical response of the Pt electrode was monitored within a potential window of 0.1 to 1.0 V using DPV. As illustrated in Fig. 2.3a, a distinct oxidation peak emerged at 0.575 V with a current magnitude of 6.35 µA upon the addition of inositol. Conversely, the absence of the target analyte resulted in a featureless voltammogram, confirming that the recorded faradaic process is specifically linked to the oxidation of the analyte at the electrode interface.

2.2.2.2 Effect of buffer variation

An investigation of the Pt electrode behavior was conducted with different buffer solutions, viz. PBS, CBS, and ABS. The maximum response was only obtained in the presence of PBS (6.35 µA, 0.57V) compared to the other two buffers, as displayed in Fig. 2.3. (b). The maximum current for PBS is 6.35 µA, which is approximately 1.16 and 1.55 times greater than that of ABS and CBS, respectively. Moreover, the effect of pH variation for PBS buffer was examined, and the optimum peak current was attained for pH 5 as shown in Fig. 2.3. (c).

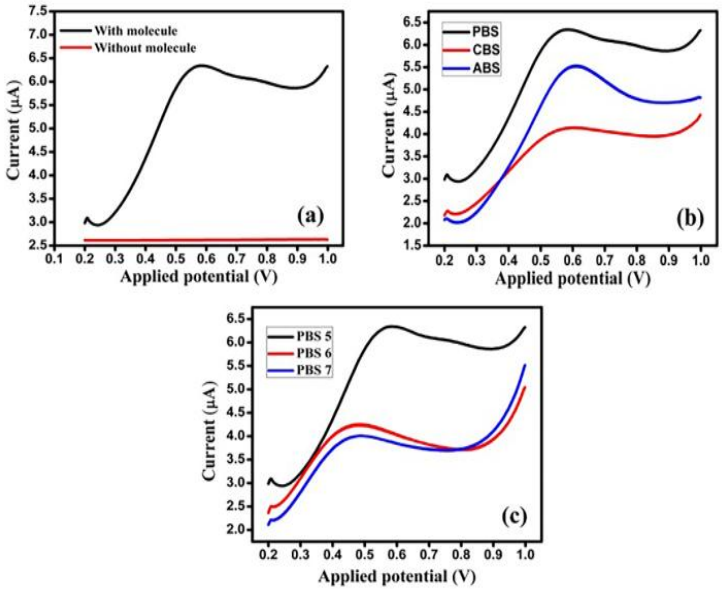

Fig. 2.3. DPV response of Pt electrode (a) with and without inositol in PBS-5. (b) for different types of buffer solutions(c)for different pH variations.

2.2.2.3 Effect of scan rate variation

Fig. 2.4 depicts the effect of scan rate variation on the electrochemical oxidation of the Pt electrode. Applying the DPV technique, the electrochemical responses were recorded within a potential range of 0.2 to 1 V. It is observed that with the increase of scan rates from 10 to 300mV/s, the oxidation peak current increases. Scan rate variation causes a change in equilibrium at the electrode surface. Fig. 2.4.b illustrates the linear plot of oxidation peak current versus scan rate. The regression equation obtained is $y = 0.0042x + 5.13; R^2 = 0.98$.The occurrence of an adsorption-controlled process is confirmed as there is an increase in oxidation peak current with the increase in scan rate [34].

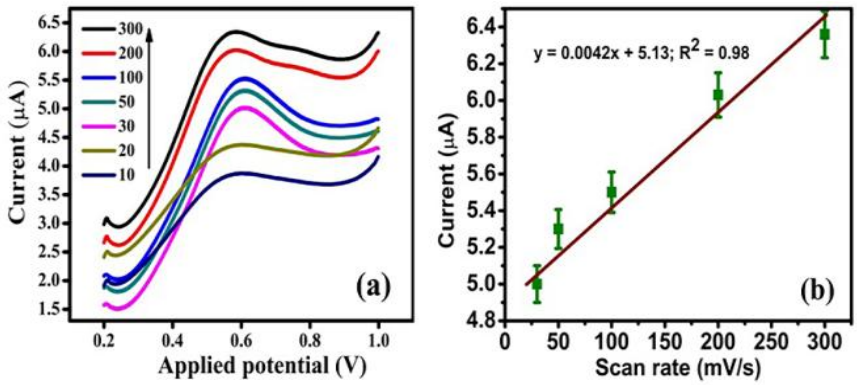

Fig. 2.4 (a) Scan rate dependence of inositol oxidation from 10 to 300 mV/s via DPV and (b) linear regression analysis of peak current as a function of scan rate in PBS-5 buffer.

2.2.2.4 Effect of concentration variation

The DPV responses were recorded in the potential range of 0.1 to 1 V with varying concentrations from 50 to 400 μM inositol in PBS solution. Increase of peak current with increase in inositol concentration is observed from Fig. 2.5. (a). Fig. 2.5. (b) represents the linear relationship of peak current with concentration variation, with the regression equation as-

$y = 0.0046x + 5.247; R^2 = 0.96$. The lowest limit of detection (LOD) was estimated as 19.28μM using the equation LOD = 3(Sy/x/)/m where Sy/x represents the standard deviation, while m is the calibration curve slope, respectively.

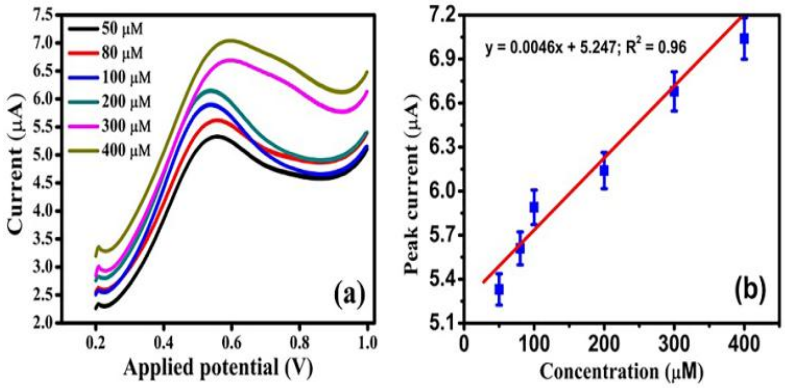

Fig. 2.5 (a) DPV profiles for inositol quantification at a Pt electrode across a range of concentrations in PBS and (b) the resulting linear calibration curve of peak current as a function of inositol concentration in pH 5.0 buffer.

2.2.2.5 Principal Component Analysis for discrimination of inositol concentrations

From a set of correlated data, PCA tool generates a set of non-correlated variables known as principal components (PCs) using orthogonal transformation [33]. For the first two or three PCs, the transformed data space facilitates a graphical interpretation of the multi-variate dataset by projecting the data onto a reduced-dimensional space. To provide a quantitative assessment of how effectively different inositol concentrations are distinguished, the Separability index (SI) is employed. This index is calculated as the ratio of the between-class (S_b) to the within-class (S_w) scatter matrix trace, as revealed in the following equation:

$$S_b = \sum_{i=1}^{c} n_i (m_i - m)(m_i - m)^T \quad (1)$$

$$S_w = \sum_{i=1}^{2} \left(\sum_{j=1}^{n_i} (x_{i,j} - m_i)(X_{i,j} - m_i)^T \right) \quad (2)$$

where c symbolizes the class count, n_i is the sample count in the ith class, m_i is the mean vector of the samples in the ith class, and m denotes the mean vector of the samples.

Since optimum peak current was obtained for PBS at pH 5, the DPV data for inositol spiked into PBS at pH 5 for different inositol concentrations- 50 µM, 80 µM, 100 µM, 200 µM, 300 µM and 400 µM (S1, S2, S3, S4, S5, and S6 respectively) were analyzed using PCA. Four repetitions were considered for each of the six concentrations. The number of data points obtained for individual observation was 328. Thus, the data matrix of size 328x4x6 was considered for data analysis. PCA plot with effective data clustering is depicted in Fig. 2.6. All the six different concentrations were effectively discriminated using PCA. PC1 and PC2 illustrated 86.01% and 13.72% of total variances respectively. On quantitative evaluation of the data

nature, high class separability index (SI) of 142.91 was obtained which indicates that the inter-class separability of the samples is reasonably good using this electrode.

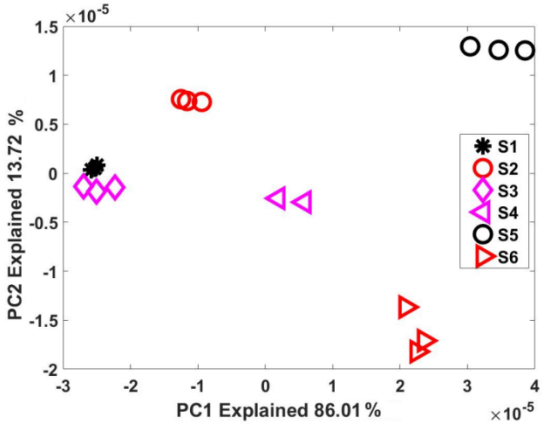

Fig. 2.6. Graphical representation of DPV data analysis using PCA

2.2.2.6 Partial least squares regression (PLSR) for prediction of inositol concentrations

In the PLSR algorithm, components with high correlation between predictors and response variables are extracted, thereby reducing the number of predictors [33]. In recent times, leave-one-out cross-validation techniques have been employed for the estimation of the predictive measurements of a sensor. To quantify the relationship between the estimated and actual values and evaluate the model's reliability, different parameters such as the correlation factor (CF) and the root mean square errors for both validation (RMSEV) and prediction (RMSEP) were employed. In this work, the prediction capability of the Pt electrode has been estimated using six different concentrations of inositol, S1-S6. For each concentration level, the collected data were partitioned into a training set (75%) and a test set (25%) to ensure a robust model evaluation. Using PSLR, a high prediction accuracy of 93.69% was obtained for the Pt electrode. The prediction parameters have been summarized in Table 2.1 and are shown below.

Table 2.1

Comparison of Actual and Predicted Inositol Contents Obtained Using PLSR

No. of samples	Actual Inositol Content (µM)	Predicted Inositol content (µM)	Prediction Accuracy (%)
1	50	56.12	87.75
2	80	84.80	93.99
3	100	95.30	95.29
4	200	213.34	93.32
5	300	298.05	99.34
6	400	369.89	92.47
Average Prediction Accuracy-			**93.69%**

2.2.2.7 Principal Component Regression (PCR) for prediction of inositol concentrations

In this approach, the predictors are aligned to capture maximum variance in directions that correspond to the response variable magnitudes. Similar to the PLSR framework, a leave-one-out cross-validation strategy was implemented to evaluate predictive performance. The system's capacity to quantify inositol across six distinct concentrations (S1–S6) was subsequently validated using statistical benchmarks, including the correlation factor (CF), RMSEV, and RMSEP. Data partitioning was done in the same ratio as in PLSR. prediction accuracy of 93.71% was obtained for the Pt electrode. Table 2.2 (shown below) comprises the prediction measures of the Pt electrode-based electrochemical system.

Table 2.2

Predictive performance of the PCR model: A comparative plot of actual versus estimated inositol content.

No. of samples	Actual Inositol Content (µM)	Predicted Inositol content (µM)	Prediction Accuracy (%)
1	50	56.13	87.73
2	80	84.76	94.05
3	100	95.31	95.31
4	200	213.38	93.3
5	300	298.14	99.37
6	400	369.88	92.47

Average prediction accuracy- 93.71%

2.2.2.8 Comparative Validation and Prediction by Regression Models

Table 2.3 provides a comparative performance summary of PLSR and PCR models used for the quantitative validation and prediction of the Pt electrode's sensing accuracy.

Table 2.3

Performance Comparison of the Two Regression Models

Method	Before Prediction		After Prediction	
	CF	RMSECV	CF	RMSEP
PLSR	0.99	0.181	0.987	11.43
PCR	0.988	0.183	0.988	11.42

2.2.2.9 Real Sample Analysis

Real-sample analysis was conducted by applying the standard addition method to orange juice extracts diluted with Millipore water, requiring no further pre-treatment. The extracts were spiked with a 300 µM inositol solution and subsequently evaluated via the DPV technique [34]. As summarized in Table 2.4, the recovery rate was determined to be 96.18% with a precision of 1.01% RSD. These findings validate the robustness of the sensor and affirm that the electrode interface is effectively free from matrix effects during inositol quantification in complex biological media.

Table 2.4.

Determination of inositol in fresh orange juice extract using Pt-based electrode

Sample	Spiking (µM)	Detected µM)	Recovery rate[a] (%)	± R.S.D[b] (%) (n=4)
Orange juice extracted pure	0	81.02	-	0.97
Orange juice extracted spiked	300	369.56	96.18	1.01

[a]Recovery rate = [Detected(µM)-Diluted Sample(µM)]/Spiking(µM)

[b]R.S.D (%)= 100 *Standard Deviation/Mean

PUBLICATION STATUS

JOURNAL

- Dipan Bandyopadhyay, Shreya Nag, Debangana Das, Srikanta Acharya, Bipan Tudu, Panchanan Pramanik, Rajib Bandyopadhyay, and Runu Banerjee Roy," Voltammetric Detection of Inositol Using a Platinum-Based Electrode", NANOLIFE Journal, March 2022, doi:10.1142/S1793984422500040.

2.3 Molecular imprinted bi-polymer infused capacitive sensor for inositol detection

This section presents the development of a cost-effective, reusable, and highly stable molecularly imprinted polymer (MIP) technology-based capacitive sensor for the specific detection of inositol (IS) in fruits. While electrochemical sensors offer advantages in terms of simplicity and cost, issues such as lack of selectivity, poor lifetime, and cross-sensitivity often pose limitations for conventional amperometric determination techniques using glassy carbon electrodes [32] and ion chromatographic methods [30]. Owing to the inherent attractive properties of high

selectivity and reusability, molecular imprint polymer (MIP) technology has evolved over the years [33]. Several studies encouraged the application of MIP-based electrochemical detection techniques for the detection of several compounds in various real samples [34]-[39]**.** Since capacitive sensors emerge as comparatively better performers in terms of stability, sensitivity, reproducibility, and power consumption, one can think of coupling MIP technology with capacitive sensor technology. In [40], a reduced graphene oxide (RGO)/ polymethylmethacrylate (PMMA) coated copper-based (Cu) capacitive sensor was proposed to detect formaldehyde in milk and water. The variation of the electrical parameters, viz., impedance and phase, with frequency has been explored in this work. A MIP-based polydimethyl siloxane (PDMS) coated capacitive sensor for the detection of 2-Furfuraldehyde (2-FAL) in transformer oil had been put forward in [41]. The sensitivity of the proposed sensor had been investigated in terms of electrical parameters (capacitance, impedance, and phase angle) variation for different 2-FAL concentrations in transformer oil. MIP-based capacitive sensor based on gold-coated silicon electrodes had been introduced in another study for the detection of sulphanilamide (SN) in milk as well as water [42].In recent years, bio-mimic materials have emerged as potential surface-coating specialists (on various substrates) in sensor fabrication and device engineering. Derivatives of 3, 4-dihydroxyphenylalanine (DOPA) and Dopamine (DA) or polydopamine (PDA) exhibit remarkable adhesive properties courtesy of substrate-ligand (embracing catechol, phenyl, and amine groups) interactions via hydrophobic interactions, hydrogen bond formation, and electrostatic interactions [43]-[54]. To improve the wetting ability and enhance the performance of the sensor, some works recommended the usage of PDA co-deposited with polyethylene glycol (PEG) like polymers [47],[55]. Realizing the advantages of MIP, PDA-PEG, and capacitive sensor technology, in this envisaged work, a MIP-based PDA-PEG-coated capacitive sensor (MI-2P-IS@C) has been proposed for the detection of inositol specifically. To the best of the author's knowledge, no previous work has been reported in this regard. As mentioned earlier, molecular imprinted PDA-PEG has been considered as the inositol-sensitive layer for the proposed sensor. Frequency variation and influence of inositol concentration variation on primary electrical parameters of the sensors, viz. capacitance (C_{pis}), impedance (Z_{pis}), and phase angle (θ_{pis}), have been investigated in the present work. For a further comprehensive study (linearity, stability, and selectivity), the parallel capacitance C_{pis} has been adjudged as the pivotal parameter. Comparative performance of molecular imprinted (MI-2P-IS@C) and non-imprinted (NI-2P@C) based sensors in terms of C_{pis} variation has also been studied in this work.

The novelty of this present work is borne in the fact that it propounds a cost-effective and highly stable sensor with excellent selectivity for the recognition of Inositol (IS) in fruits, viz.

Orange and Kiwi. In addition, this sensor, being of a capacitive type, can be immersed directly in any infusion during experimentation without any pre-treatment. The regression models - PLSR and PCR have been employed for evaluating the predictive potential of the developed capacitive sensor. It will be established by the end of this paper that this fabricated capacitive sensor can be a viable candidate for the recognition and determination of IS in fruits or other real samples.

2.3.1 Experimental section

2.3.1.1 Necessary Materials for developing the sensor

Copper-cladded FR-4 sheet (thickness: 0.15 cm) and IS were purchased from local retailers and TCI, respectively. 3-Hydroxytyramine hydrochloride, alternatively known as dopamine hydrochloride (DA-HCl), was supplied by Tokyo Chemical Industry (TCI) (CAS RN: 62-31-7). DA was oxidized to form a chemically more reactive PDA, which behaves as a surface-coating agent. The presence of ligands such as catechol, amine, and phenyl in PDA favors interaction with Cu substrates via electrostatic and hydrophobic interactions through hydrogen bonds, which makes PDA more chemically reactive. Sandpaper of zero sizes, Millipore water, as well as a filter, were used for substrate-surface cleaning purposes, and the coating was performed primarily using polyethylene glycol (PEG MW 400) acquired from Merck Millipore.

2.3.1.2 Fabrication Methodology

The proposed sensor (dimensionality: 5.9 cm × 1.6 cm × 0.15 cm) as depicted in Fig. 2.7(a), consisting of a copper-cladded FR-4 sheet, was smoothened with sandpaper and filed on the edges. The strips were ultrasonicated in acetone at 60 °C for 15 minutes and then washed with Millipore water. Thereafter, the washed plates were dried at 70 °C in the chamber of a thermally-controlled oven for around 10 minutes. The copper strips are dipped in PEG solution for about 15 minutes to form PEG-coated Cu strips.

MIP material was prepared using IS and DA as a template and functional monomer molecule. A solution was formed by mixing 8 mg IS and DA-HCl of 2 mg ml-1 in Millipore water of 90 ml. The pH value of the solution is tuned to 9 by the gradual addition of tris-ammonium buffer solution. PEG-coated Cu strips were dipped in this solution and stirred using a magnetic stirrer for 48 hours. After 48 hours, it was noticed that DA-HCl undergoes single-step self-polymerization, thereby forming PDA, which gets deposited on both sides of the copper strip.

Thereafter, the developed MI-2P-IS@C sensor was dried for 30 minutes in a furnace at a constant furnace temperature of 40 °C. To wash out the loosely bound particles and IS molecules, the sensor was dipped into Millipore water once again for about 5 minutes. This leads to the

formation of template-shaped cavities on the polymer surface. Once again, drying at the same furnace temperature for the same time, the sensor is finally ready for testing experiments. Preparation of NI-2P@C based sensor follows the same steps as MIP except for the addition of IS in the solution prior to the stirring process. For electrical connection purposes, copper wires were connected on both sides of the Cu strip by soldering technique.

2.3.1.3 Experimental set-up

As depicted in Fig. 2.8, the sensor was dipped (dip-length: 4.4cm) in the test sample contained in a 100 ml Borosil beaker. For the evaluation of the electrical parameters of the sensor, an impedance analyzer (KEYSIGHT, E4990A, 20 Hz-50MHz) was connected to the sensor via the electrical contacts. For testing, the sensor was dipped into five test samples of varying IS concentrations (0.125 ppm, 0.25 ppm, 0.5 ppm, 1 ppm, and 2 ppm) at room temperature. Eight repetitions were performed for the data acquisition of the three electrical parameters, viz. capacitance (C_{pis}), impedance (Z_{pis}), and phase angle (θ_{pis}) corresponding to each test sample. After eight repetitions for one test sample, the sensor was dipped in Millipore water for around 5 minutes for washing purposes. Prior to the commencement of experimentation with another test sample, the sensor was subjected to incubation in the test solution (TS) for about 10 minutes. Since all the experiments have been performed under ambient temperature and the breaker size was chosen to be the same in every case, these parameters did not perturb the measured electrical parameters, especially parallel capacitances. The washing time between the testing runs was optimized to be 5 minutes, as a minimum error of 0.17% (Table 2.5) was achieved for 5 minutes, comparing the maximum capacitances obtained prior to testing and post-testing washing in regular time intervals.

Table 2.5

Optimization of washing time

Sl No.	**Pre-Testing (Max. Capacitance (nF)**	**Post-Testing**		**Error (%)**
1	163.06	**Washing Time (min)**	**Max. Capacitance (nF)**	0
2		0	82.39	49.47
3		2	133.18	18.32
4		**5**	**163.34**	**0.17**
5		10	163.36	0.18
6		15	163.37	0.19

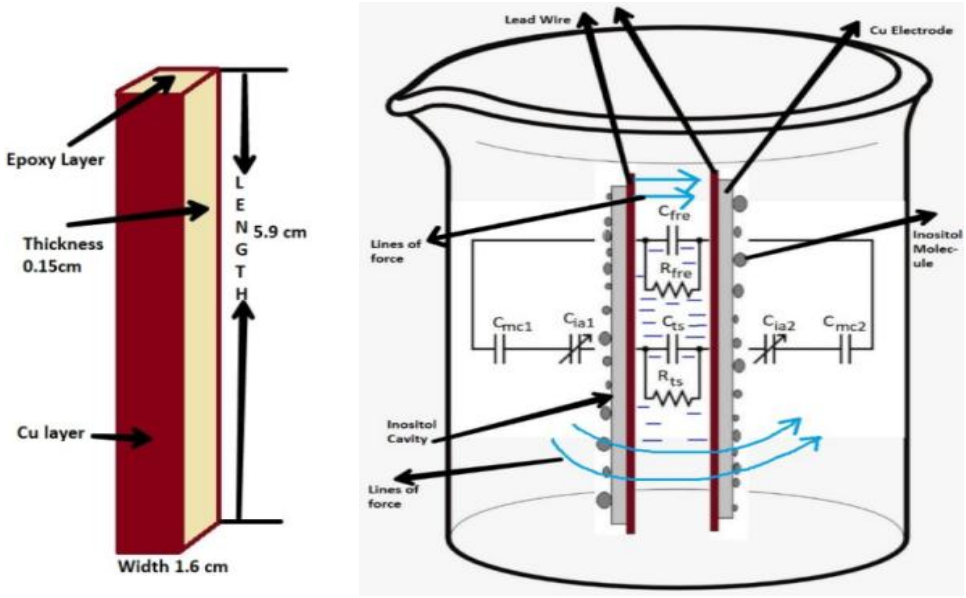

Fig. 2.7. (a) Schematic of Cu strip, (b) Equivalent circuit of the sensor along with MI-2P-IS coated Cu strip.

Fig. 2.8. Experimental Testing setup: impedance analyzer connected with the electrode.

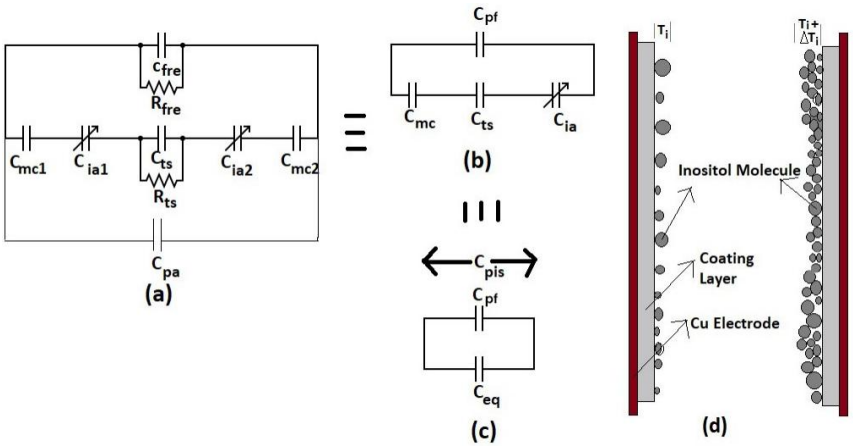

Fig. 2.9. (a) Comprehensive and (b)–(c) stepwise circuit simplifications, and (d) MIP-coated Cu strips portraying widening of IS-layer on the electrode surface.

2.3.1.4 Electrical equivalent model of the proposed sensor

1) Equivalent electrical circuit model: MI-2P-IS@C sensor

As reported in earlier studies, the following equivalent electrical model can be developed for the sensor [40], [56]-[57]. The sensor consists of FR4 fiberglass epoxy (EP) sandwiched between the bilayer of copper plates. The electrical model was developed using circuit elements, viz. C_{pa}, C_{fre}, R_{fre}, C_{mc1}, C_{mc2}, C_{ia1}, C_{ia2}, C_{ts} and R_{ts} which are depicted in Fig. 2.9(a) and Fig. 2.9(b). As soon as the sensor is dipped in the TS and the signal is applied, a dual path is followed by the electric lines of force a) Path 1: directly through FR4 epoxy giving rise to C_{fre} and R_{fre} between the two Cu electrodes (b) Path 2: through TS (emanates from the fringing fields developed at the edges of the sensor) in which the sensor is dipped leading to two parameters viz. C_{ts} and R_{ts}. Besides these, coating capacitances (C_{mc1} and C_{mc2}) arise from MIP coatings, and variable capacitances (C_{ia1} and C_{ia2}) originate owing to the adsorption of IS molecules in the MIP sensitive layers on both sides of the Cu electrodes. Owing to the high values of R_{fre} and R_{ts}, the corresponding paths act as open circuits, therefore can be eliminated from the circuit model (Fig. 2.9(b) and Fig. 2.9(c)) [40]. It is to be mentioned that C_{pf} is the equivalent capacitance of C_{pa} and $C_{fre,}$ where C_{pa} is the parasitic capacitance of the sensor. The overall parallel capacitance, $C_{pis,}$ can be obtained from the following expressions-

$$C_{pis} = C_{pf} + C_{eq} \quad (1)$$

Where $C_{pf} = C_{pa} + C_{fre}$ (2)

and $C_{eq} = \frac{C_{mc} \times C_{ts} \times C_{ia}}{(C_{mc} \times C_{ts}) + (C_{ts} \times C_{ia}) + (C_{ia} \times C_{mc})}$ (3)

$$\frac{C_{mc} \times C_{ts}}{C_{mc} + C_{ts} + \left(\frac{C_{mc} \times C_{ts}}{C_{ia}}\right)} \quad (4)$$

Here, the variable capacitance due to the adsorption of IS molecules, C_{ia} is given by

$$C_{ia} = \frac{C_{ia_1} \times C_{ia_2}}{C_{ia_1} + C_{ia_2}} = \frac{\in_o \times \in_{io} \times A}{2 \times T_{ia}} = f\left(\frac{1}{T_{ia}}\right) \quad (5)$$

where, T_{ia} - The thickness of the absorbed IS molecule layer on the MIP surface and $\in_{io}$ - dielectric constant of IS

On the other hand, overall coating capacitance, C_{mc} is given by

$$C_{mc} = \frac{C_{mc_1} \times C_{mc_2}}{C_{mc_1} + C_{mc_2}} = \frac{\in_o \times \in_m \times A}{2 \times T_{mip}} \quad (6)$$

where, T_{mip} -thickness of MIP coating on both sides of the Cu electrode, $\in_o$- Dielectric constant of vacuum, $\in_m$- Dielectric constant of MIP coating and A- Surface area of the electrode

Hence,

$$C_{pis} = C_{pf} + C_{eq} = C_{pa} + C_{fre} + \frac{C_{mc} \times C_{ts}}{C_{mc} + C_{ts} + \left(\frac{C_{mc} \times C_{ts}}{f\left(\frac{1}{T_{ia}}\right)} \right)} \quad (7)$$

Table 2.6

Capacitance dependency on concentration and layer thickness

Case	Concentration	T_{ia}	C_{ia}	C_{Pis}
1	↑	↑	↓	↓
2	↓	↓	↑	↑

2) Theoretical Aspect-Capacitance dependency on IS concentration

I. As already mentioned earlier, the detection principle of the MI-2P-IS@C sensor is based on MIP technology. The template recognition sites, formed in the PDA-PEG layer, resemble the IS molecules and thereby favor IS molecule adsorption from the TS. The moment the sensor is dipped in TS, the adsorption mechanism initiates, resulting in the formation of the IS layer on the surface of the electrode. The adsorption layer thickness depends both on the IS concentration on the TS and the dipping time. Depending on the degree of molecular adsorption, the surface density varies near the solid-liquid interface based on concentration and dipping time, which might alter the overall thickness of the corresponding interface. Since capacitance varies inversely with layer thickness, C_{ia1} and C_{ia2} also vary with IS concentration (Table 2.6). As illustrated in Fig. 2.9(d), the adsorption layer increases as the IS concentration increases (say T_{ia} to $T_{ia} + \Delta T_{ia1}$), thereby resulting in a fall in the capacitance values C_{ia1} and C_{ia2}. A decrease in these variable capacitances decreases the equivalent adsorption capacitances (C_{ia}). The overall parallel capacitance, $C_{pis,}$ is a function of C_{pa}, $C_{fre,}$ $C_{mc1,}$ $C_{mc2,}$ $C_{ia1,}$ $C_{ia2,}$ and C_{ts} as represented by (7), among which only C_{ia1} and C_{ia2} vary while others remain constant once fabricated. Hence, after sensor fabrication, C_{pis} solely depends on C_{ia1} and $C_{ia2,}$ and if inositol concentration varies in TS, the overall effect will be on C_{pis}.

2.3.2 **Results and discussions**

2.3.2.1 SEM Analysis

To study surface morphology, SEM analysis was performed. Fig. 2.10 presents the SEM images of MI-2P-IS@C and NI-2P@C materials. It can be inferred with pellucidity that more globular, as well as big uniform-size particles, are evident in the case of MI-2P-IS@C (Fig. 2.10(a)) than that of NI-2P@C (Fig. 2.10(b)) which suggests better dispersion of the molecules

on the surface of the sensor [58]-[59]. This can lead to more IS binding sites over the sensor surface, and hence, IS molecules may get sheltered easily in those sites**.**

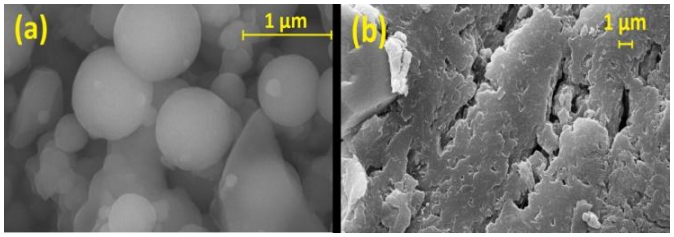

Fig. 2.10. SEM morphology of (a) MI-2P-IS@C material, (b) NI-2P@C material.

2.3.2.2 XRD Analysis

The X-ray diffraction (XRD) profile of the MI-2P-IS@C material has been presented in Fig. 2.11. A couple of broad peaks were significant at 13.85° and 29.88°(2θ values), with considerably higher peaks for the former one. This ensures the formation of a strongly-bonded polymer chain with multiple DA ring units entangled with each other. Thus, it is quite clear from the figure that an amorphous polymer of DA (PDA) was formed, which is quite in accordance with what was reported in [60].

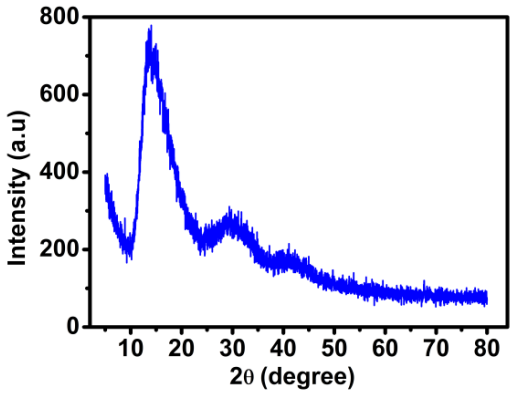

Fig. 2.11. X-ray diffraction profile of synthesized MI-2P-IS@C material.

2.3.2.3 Comparative study on capacitance variation for MI-2P-IS@C and NI-2P@C

While synthesizing the MIP material, when PEG and DA are blended, the following mechanism occurs. PEG has ether groups that come in proximity to the catechol group present in DA through hydrogen bonding. The uniform distribution of PDA aggregates (formed due to self-polymerization of DA) over PEG yields a PDA-PEG composite. This composite offers satisfactory adhesivity on copper (Cu) plates. PDA has the dual inherent ability to chelate and reduce the metallic ions (Cu^{2+}) to their metallic state in an alkaline ambiance courtesy of the catechol and amino groups. Further, an add-on advantage is that owing to the higher affinity of

Cu^{2+} ions toward amino groups, there is a higher plausibility of coordination between Cu^{2+} and the amino group of PDA [54]. The variation of the sensor capacitance (C_{pis}) as a function of operating frequency is portrayed in Fig.2.12 for MI-2P-IS@C and NI-2P@C. In the case of MI-2P-IS@C, owing to the abundance of IS-recognition sites, analyte adsorption increases, thereby widening the adsorption layer thickness (T_{ia}). An increase in T_{ia} decreases the C_{ia} as per equation (5), which in turn results in a lower value of C_{pis}. On the contrary, for NI-2P@C, there is negligible molecular adsorption owing to the absence of IS-recognition sites. Since there is negligible adsorption, it is quite implicit that adsorption thickness (T_{ia}) will be less, leading to a higher value of C_{pis}. Hence, as expected significantly lower value of C_{pis} (approx.14.3% of that of NI-2P@C) was experienced for MI-2P-IS@C in comparison to that of the NI-2P@C sensor. To illustrate clearly the variation of the C_{pis} and other electrical parameters, the subsequent data plots are limited to 100 Hz.

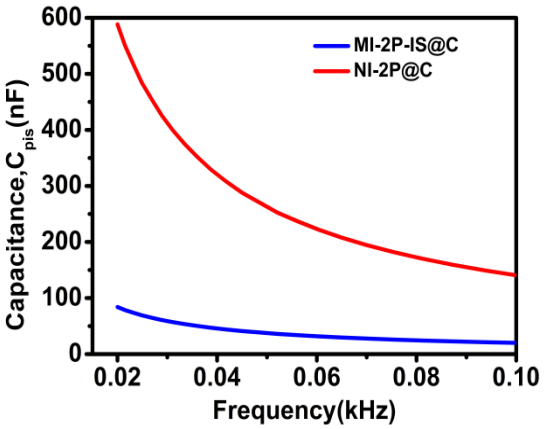

Fig. 2.12. Capacitance (C_{pis}) variation with frequency for MI-2P-IS@C and NI-2P@C sensors.

2.3.2.4 Capacitance (C_{pis}) variation profile with frequency for different IS concentrations

As it is evident from Fig. 2.13 (a) that the parallel capacitance of the sensor C_{pis} falls with the increase in operating frequency. Further, it was observed that C_{pis} also varies inversely with the IS concentration, as C_{pis} falls with the increase in IS concentration in the test sample. This is quite consistent with the remarks inferred from the proposed electrical model conferred in section II and those reported in [40]. Equation (7) governs the dependency of C_{pis} on IS concentration (P_{is}) in the TS.

2.3.2.5 Linearity investigation with LOD estimation

A linear plot of maximum parallel capacitance (C_{pism}) with variation in IS concentration (P_{is} in ppm) is depicted in Fig. 2.13(b). This calibration curve illustrates satisfactory linearity from 0.125 to 1 ppm of IS concentration, governed by the linear regression equation

$$C_{pism} = -80.333P_{is} + 90.183 \quad (8)$$

$$R^2 = 0.995 \quad (9)$$

The limit of detection (LOD) of the MI-2P-IS@C was obtained as 1.8 ppb using the equation LOD= $3\sigma_c/ m_c$, where σ_c and m_c represent the standard deviation of the capacitance (C_{pis}) and slope of the calibration curve [36], [61]. The estimated LOD value (1.8 ppb) significantly improves on that reported in [29].

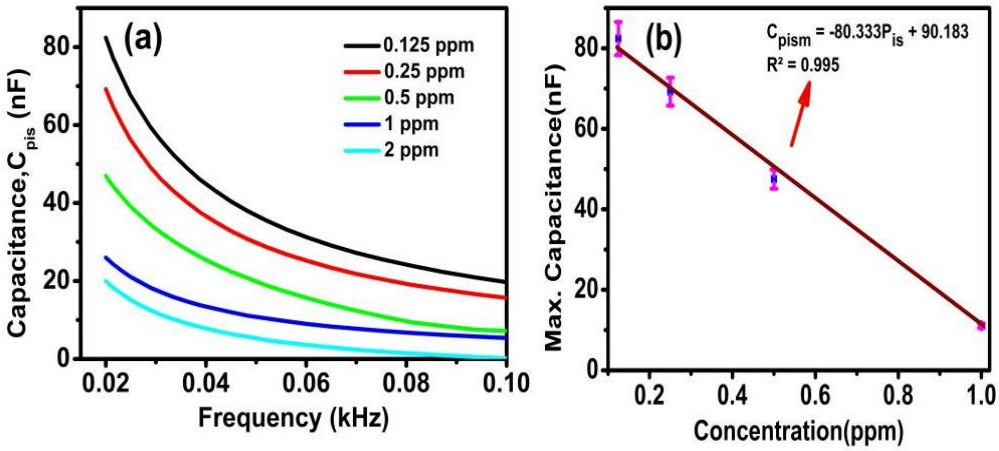

Fig. 2.13. (a) Dependency of C_{pis} as a function of IS concentration in the TS within the frequency window of 20-100 Hz and (b) Maximum capacitance (C_{pism}) deviation with IS concentration.

2.3.2.5 Frequency variation of Sensor impedance and phase angle for different IS concentration

It is well-known that the equivalent admittance (Y_{pis}) of an RC parallel circuit (R_{pis}- resistance, C_{pis}-capacitance) can be expressed as

$$Y_{pis} = \frac{1}{Z_{pis}} = j\omega C_{pis} + \frac{1}{R_{pis}} \quad (10)$$

Since impedance is the reciprocal of admittance, so equivalent sensor impedance (Z_{pis}) can be readily obtained from the above equation.

$$Z_{pis} = \frac{R_{pis}}{1+j\omega C_{pis}R_{pis}} = \frac{R-j\omega C_{pis}{R_{pis}}^2}{1+\omega^2 C^2 {R_{pis}}^2} \quad (11)$$

The real part and the imaginary part of Z_{pis} can be obtained as $Z_r = \frac{R_{pis}}{1+\omega^2 {C_{pis}}^2 {R_{pis}}^2}$

(12)

$$Z_i = \frac{-j\omega C_{pis}{R_{pis}}^2}{1+\omega^2 {C_{pis}}^2 {R_{pis}}^2} \quad (13)$$

Equations 10-13 represent the relationship between C_{pis} and Z_{pis}. The variation of the sensor impedance (Z_{pis} in kΩ) with frequency (limited up to 100 Hz) for different IS concentrations is depicted in Fig. 2.14(a). A couple of observations are revealed from the frequency characteristics: (a) sensor impedance, $Z_{pis,}$ increases as the IS concentration increases, and (b) Z_{pis} negligibly decreases in the low-frequency range corresponding to each concentration. Both these observations are quite well in accordance with the above equations.

Since the phase angle (θ_{pis}) is a function of frequency and other electrical parameters, it is quite obvious that it will change with the frequency as well as with the concentration of the analyte [40]. Phase angle versus frequency plot for different IS concentrations is depicted in Fig. 2.14(b). From the figure, it is quite evident that the phase angle gradually decreases as the frequency increases, corresponding to each concentration of IS. Further, quite expectedly for the same frequency window, the phase angle increases when the IS concentration is raised in the TS. This can be attributed to the change in electrical parameters of the sensors as the analyte concentration changes.

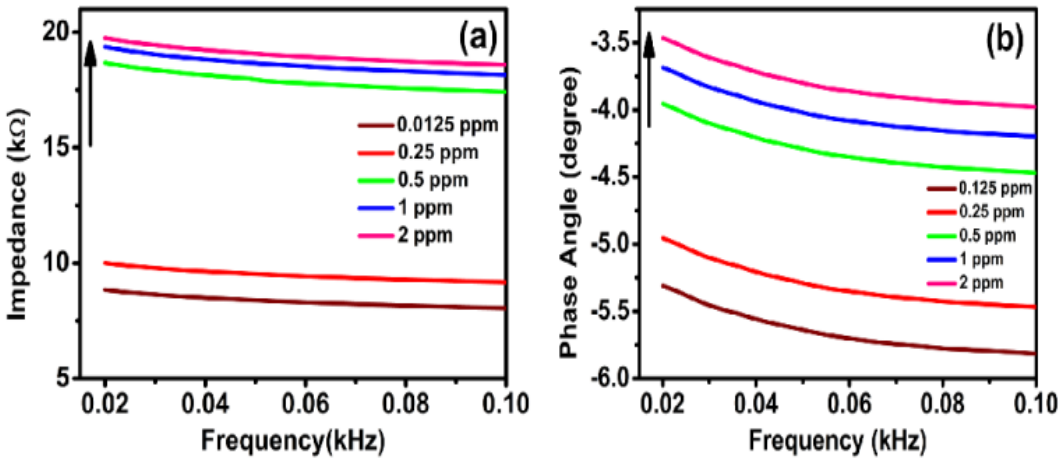

Fig. 2.14. (a)Sensor impedance (Z_{pis}) versus frequency plot and (b) Phase angle (θ_{pis})-frequency plot of different IS concentrations in the TS.

2.3.2.6 *Stability Analysis of MI-2P-IS@C Capacitive Sensor*

The stability of the sensor was investigated by performing testing experiments periodically, and a quite satisfactory performance was exhibited by the sensor. Frequent testing for three months reveals that the maximum parallel capacitance (C_{pism}) hardly changes in the first 30 days, and after 90 days, it increases only by 0.5% (Fig. 2.15) at 0.125 ppm IS concentration, thereby ensuring high reliability. The slight increase in C_{pism} can be attributed to a slight decrease in MIP coating layer thickness due to aging, which somehow slightly banishes the

template recognition sites from the surface. To avoid atmospheric contaminations, the MI-2P-IS@C sensors were cautiously preserved in zip-lock pouches at room temperature after wrapping carefully wrapped with tissue papers.

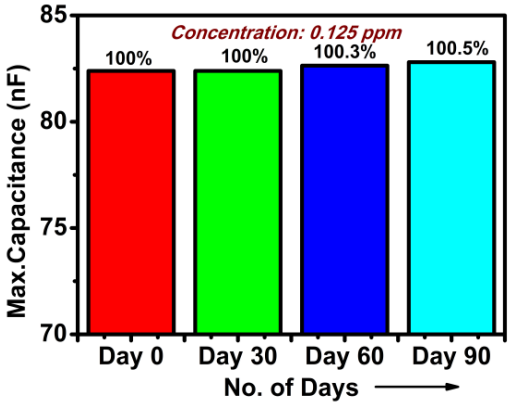

Fig. 2.15. Stability Profile of the MI-2P-IS@C Sensor.

2.3.2.7 *Selectivity Study of MI-2P-IS@C Sensor*

To explore the selectivity of the MI-2P-IS@C sensor, it was tested by dipping in 0.125 ppm solution of IS, Gallic acid (GA), caffeine, catechin, and Epigallocatechin gallate (EGCG) one after the other with a dipping time of 10 minutes in between. The selectivity profile in Fig. 2.16 reveals that the best response of the sensor corresponds to IS in terms of C_{pism}. This can be attributed to the fact that, owing to the presence of the same number of hydrogen bond-forming donors, IS molecules fit in well in the surficial cavities of the MI-2P-IS@C sensor. Since the adsorption of IS molecules increases, the adsorption layer (T_{ia}) increases, which in turn decreases the maximum capacitance C_{pism}. Thus, it may be inferred that the MI-2P-IS@C sensor can offer good selectivity towards IS.

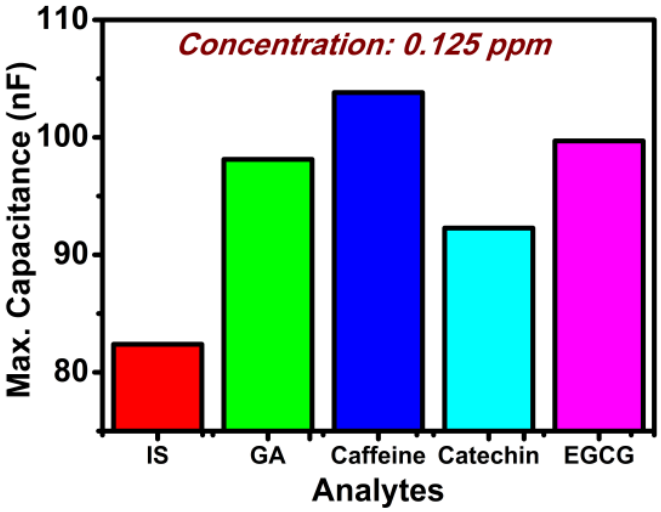

Fig. 2.16. MI-2P-IS@C Sensor Capacitive Sensor exhibiting selectivity.

2.3.2.8 Real Sample Study

The MI-2P-IS@C sensor was employed to determine IS content in a couple of fruits, viz., orange and kiwi. Here, the fruit extracts were diluted (1:10) and brewed to form a 200 ml solution, which was subjected to testing through an impedance analyzer. For each of the two real samples, immersing the MI-2P-IS@C electrode in TS, eight responses were acquired, considering the entire frequency range of 0.02 Hz-50 kHz, which leads to a data matrix of size [201 × 8 × 2]. Prediction data analysis was carried out by implementing PLSR and PCR regression models in MATLAB R2017b, and the results are summarized in Tables 2.7 and 2.8. The results, when compared with those obtained from HPLC analysis, yield high average prediction accuracies of greater than 99% for both techniques.

Table 2.7

Inositol content: PLSR and PCR model

Sl No.	Actual IS (mg/g) (HPLC)	Predicted IS (mg/g)		Prediction Accuracy (%)	
		PLSR	PCR	PLSR	PCR
Orange	61.77	61.71	61.80	99.90	99.95
Kiwi	50.29	50.34	50.35	99.90	99.88
	Average prediction accuracy			**99.90**	**99.91**

Table 2.8

Prediction of inositol concentration in an unknown sample

Technique used	Calibration		Validation		Prediction	
	RMSEC	Rc^2	RMSEV	Rv^2	RMSEP	Rp^2
PLSR	0.0008	1	0.0554	0.99	0.0558	1
PCR	0.0008	1	0.0551	0.99	0.0552	1

2.3.2.9 Comparative Study: Present Technique with Previous works on IS detection

A comparative study of findings assembled from previous works on IS detection is summarized in Table 2.9. The proposed sensor offers a lower LOD value with excellent prediction capability, in comparison to that achieved in the prior works. In fruits viz. orange and kiwi, the minimum IS content in 0.1µL is found to be 0.307 ppm and 0.136 ppm (as per stated by the Inositol

Australia organization) respectively, which are much higher than that of the LOD value offered by this sensor. Moreover, since the sensor fabrication methodology is quite simple and less time-consuming, this highly stable capacitive sensor stands out to be a commercially superior candidate for IS detection in the industries.

Table 2.9

Comparative summary: existing techniques vs present work

Electrode/ Sensor	Techniques used	Linear range (ppm)	LOD (ppm)	Max. Prediction accuracy (%)	Refs
CuS/ GCE	Amperio-metric	0.09-1.53	0.04	-	[32]
Cu-disk	CE	1-100	0.53	-	[4]
Pt	CV and DPV	9.01-72.06	3.47	93.71	[29]
SRM 1849a (for validation)	HPLC& LC-MS/MS	0.001-0.05	0.05	-	[23]
-	HPLC–MS/MS	0-180.16	0.45	-	[31]
MI-2P-IS@C	**Capacitive Sensing**	**0.125-1**	**0.0018**	**99.91**	**This work**

PUBLICATION STATUS

JOURNAL

- D. Bandyopadhyay, S. Acharya, S. Nag, D. Das, and R. B. Roy, "A Molecular-Imprinted Bipolymer Infused Capacitive Sensor for Inositol Detection in Fruits," *IEEE Transactions on Instrumentation and Measurement*, vol. 72, pp. 1-9, 2023, Art no. 9512409, doi: 10.1109/TIM.2023.3306839.

2.4 Summary of Developed Electrochemical Sensors

This chapter explored two distinct electrochemical sensor designs for the detection of inositol, a crucial non-reducing sugar alcohol with significant health implications. Both approaches demonstrated promising results for quantitative analysis in various matrices.

2.4.1 Voltammetric Detection using a Platinum-Based Electrode

The first approach involved the development and optimization of a platinum (Pt) electrode-based electrochemical system for rapid inositol detection. This system utilized Differential

Pulse Voltammetry (DPV), proving its efficacy over a wide linear range of operation from 50 to 400 µM, with a limit of detection (LOD) of 19.28 µM. This LOD is notably lower than the recommended inositol limit for children (27.7 µM, equivalent to 50mg/kg per day) [19], indicating its sensitivity for practical applications. Chemometric analysis using Principal Component Analysis (PCA) successfully discriminated between different inositol concentrations, yielding an impressive class separability index (SI) of 142.91. Furthermore, Partial Least Squares Regression (PLSR) and Principal Component Regression (PCR) models exhibited high prediction accuracies of 93.69% and 93.71%, respectively. The sensor's practical utility was validated by achieving a satisfactory recovery rate of 96.18% when tested on real orange juice samples. These results collectively highlight the potential of the Pt electrode-based electrochemical system for reliably detecting varying traces of inositol in everyday food items like fruits and fruit juices.

2.4.2 Molecular Imprinted Bi-Polymer Infused Capacitive Sensor

The second approach presented a novel, inexpensive, reusable, and stable molecularly imprinted polymer (MIP) technology-based capacitive sensor designed for inositol (IS) detection in fruits. The sensitive material comprised molecular imprinted polydopamine-polyethylene glycol (PDA-PEG) introduced onto copper (Cu)-clad FR-4 plates. The sensor's performance was rigorously investigated across an IS concentration range of 0.125 - 2 ppm. A key finding was the sensor's exceptional linearity from 0.125-1 ppm and a significantly lower LOD of 1.8 ppb, which is superior to many previously reported methods for inositol detection in infusions. Experimental analysis revealed a consistent reduction in parallel capacitance (C_{pis}) with increasing IS concentration, aligning well with the sensor's equivalent circuit model. The study also elucidated the distinct variations in (C_{pis}) with frequency for both the MI-2P-IS@C (molecularly imprinted) and NI-2P@C (non-imprinted) sensors, along with the impact of frequency on sensor impedance and phase. Predictive modeling using PCR and PLSR techniques yielded remarkably high average prediction accuracies of 99.91% and 99.90%, respectively. Beyond its high sensitivity and accuracy, the sensor demonstrated excellent selectivity for IS and maintained high stability even after three months of usage. These attributes position the proposed MI-2P-IS@C capacitive sensor as a highly feasible and promising prospect for the quantitative detection of inositol in fruits and other food samples.

2.5 Conclusion

This chapter successfully demonstrated the development of two distinct yet effective electrochemical sensor platforms for the accurate and reliable detection of inositol. The voltammetric

system employing a Pt electrode offers a robust and adaptable solution, providing a satisfactory linear range and recovery rate, making it suitable for routine screening in various food and beverage samples. Concurrently, the novel MIP-based capacitive sensor showcases a significant advancement in sensitivity, achieving an exceptionally low LOD of 1.8 ppb, coupled with remarkable prediction accuracy, high selectivity, and impressive long-term stability. Both methodologies leverage chemometric tools like PCA, PLSR, and PCR to enhance data interpretation and predictive capabilities. The collective findings from these studies underscore the immense potential of electrochemical sensing as a cost-effective, rapid, and straightforward alternative to conventional analytical techniques for ensuring food quality and safety by precisely quantifying inositol content. These developments pave the way for practical, real-time inositol detection in a wide array of food products, contributing to better public health surveillance and adherence to nutritional guidelines.

References

[1] D. Ellingson et al., "Analysis of free and total myo-inositol in foods, feeds, and infant formula by high-performance anion exchange chromatography with pulsed amperometric detection, including a novel total extraction using microwave-assisted acid hydrolysis and enzymatic treatment." *J. AOAC Int*., vol. 95, no. 5, pp. 1469–1478, 2012, doi: 10.5740/jaoacint.12-028.

[2] D. Ellingson et *al.*, "Determination of free and total myo-inositol in infant formula and adult/pediatric nutritional formula by high-performance anion exchange chromatography with pulsed amperometric detection, including a novel total extraction using microwave-assisted acid hydrolysis and enzymatic treatment: first action 2012.12.," *J. AOAC Int.*, vol. 96, no. 5, pp. 1068–1072, 2013, doi: 10.5740/jaoacint 13-128.

[3] K. Schimpf, L. Thompson, and S. Baugh, "Determination of myo-inositol (free and bound as phosphatidylinositol) in infant formula and adult nutritionals by liquid chromatography/pulsed amperometry with column switching: first action 2011.18.," *J. AOAC Int.*, vol. 95, no. 4, pp. 937–942, Aug. 2012, doi: 10.5740/jaoacint.cs2011_18.

[4] L. Kong, Y. Wang, and Y. Cao, "Determination of Myo-inositol and d-chiro-inositol in black rice bran by capillary electrophoresis with electrochemical detection," *Journal of food composition and analysis*, vol. 21, no. 6, pp. 501–504, Sep. 2008, doi: 10.1016/j.jfca.2008.04.005.

[5] R. S. Clements and B. Darnell, "Myo-inositol content of common foods: development of a high-myo-inositol diet." *Am. J. Clin. Nutr.*, vol. 33, no. 9, pp. 1954–1967, Sep. 1980, doi: 10.1093/ajcn/33.9.1954.

[6] N. Bennani and H. Fabre, "Performances of a capillary electrophoresis method for the determination of meso-inositol in a tablet formulation," *Anal. Chim. Acta*, vol. 434, no. 1, pp. 67–73, Apr. 2001, doi: 10.1016/S0003-2670(01)00807-8.

[7] K. J. Schimpf, C. C. Meek, R. D. Leff, D. L. Phelps, D. J. Schmitz, and C. T. Cordle, "Quantification of myo-inositol, 1,5-anhydro-D-sorbitol, and D-chiro-inositol using high-performance liquid chromatography with electrochemical detection in very small volume clinical samples." *Biomed. Chromatogr.*, vol. 29, no. 11, pp. 1629–1636, Nov. 2015, doi: 10.1002/bmc 3470.

[8] A. H. Drummond, L. A. Joels, and P. J. Hughes, "The interaction of lithium ions with inositol lipid signalling systems." *Biochem. Soc. Trans.*, vol. 15, no. 1, pp. 32–35, Feb. 1987, doi: 10.1042/bst0150032.

[9] M. L. Croze and C. O. Soulage, "Potential role and therapeutic interests of myo-inositol in metabolic diseases." *Biochimie*, vol. 95, no. 10, pp. 1811–1827, Oct. 2013, doi: 10.1016/j.biochi.2013.05.011.

[10] A. M. Seeds, J. P. Frederick, M. M. K. Tsui, and J. D. York, "Roles for inositol polyphosphate kinases in the regulation of nuclear processes and developmental biology." *Adv. Enzyme Regul.*, vol. 47, pp. 10–25, Jan. 2007, doi: 10.1016/j.advenzreg.2006.12.019.

[11] MP. W. Majerus, J. Zou, J. Marjanovic, M. V. Kisseleva, and M. P. Wilson, "The role of inositol signaling in the control of apoptosis." *Adv. Enzyme Regul.*, vol. 48, pp. 10–17, Apr. 2008, doi: 10.1016/j.advenzreg.2008.04.001.

[12] M. Bennett, S. M. N. Onnebo, C. Azevedo, and A. Saiardi, "Inositol pyrophosphates: metabolism and signaling." *Cell. Mol. Life Sci.*, vol. 63, no. 5, pp. 552–564, Mar. 2006, doi: 10.1007/s00018-005-5446-z.

[13] A. Chakraborty, S. Kim, and S. H. Snyder, "Inositol pyrophosphates as mammalian cell signals." *Sci. Signal*, vol. 4, no. 188, p. re1, Aug. 2011, doi: 10.1126/scisignal 2001958.

[14] M. S. C. Wilson, T. M. Livermore, and A. Saiardi, "Inositol pyrophosphates: between signalling and metabolism." *Biochem. J.*, vol. 452, no. 3, pp. 369–379, Jun. 2013, doi: 10.1042/BJ20130118.

[15] R. Gambioli, G. Forte, G. Buzzaccarini, V. Unfer, and A. S. Laganà, "Myo-Inositol as a Key Supporter of Fertility and Physiological Gestation." *Pharmaceuticals (Basel)*, vol. 14, no. 6, May 2021, doi: 10.3390/ph14060504.

[16] J. Brown, T. J. Crawford, J. Alsweiler, and C. A. Crowther, "Dietary supplementation with myo-inositol in women during pregnancy for treating gestational diabetes." *Cochrane Database Syst. Rev.*., vol. 9, p. CD012048, Sep. 2016, doi: 10.1002/14651858.CD012048.pub2.

[17] C. Stern, "Dietary supplementation with myo-inositol in women during pregnancy for treating gestational diabetes." *Int. J. Nurs. Pract.*, vol. 24, no. 6, p. e12684, Dec. 2018, doi: 10.1111/ijn.12684.

[18] R. A. Condorelli et *al.*, "Myo-inositol as a male fertility molecule: speed them up!" *Eur. Rev. Med. Pharmacol. Sci.*, vol. 21, no. 2 Suppl, pp. 30–35, Jun. 2017.

[19] Y. Li, P. Han, J. Wang, T. Shi, and C. You, "Production of myo-inositol: Recent advance and prospective.," *Biotechnol. Appl. Biochem.*, vol. 69, no. 3, pp. 1101–1111, Jun. 2022, doi: 10.1002/bab 2181.

[20] C. You, T. Shi, Y. Li, P. Han, X. Zhou, and Y.-H. P. Zhang, "An in vitro synthetic biology platform for the industrial biomanufacturing of myo-inositol from starch." *Biotechnol. Bioeng.*, vol. 114, no. 8, pp. 1855–1864, Aug. 2017, doi: 10.1002/bit 26314.

[21] T. Fujisawa, S. Fujinaga, and H. Atomi, "An in vitro enzyme system for the production of myo-inositol from starch." *Appl. Environ. Microbiol.*, Jun. 2017, doi: 10.1128/AEM.00550-17.

[22] R. You *et al.*, "Efficient production of myo-inositol in Escherichia coli through metabolic engineering." *Microb. Cell Fact.*, vol. 19, no. 1, p. 109, May 2020, doi: 10.1186/s12934-020-01366-5.

[23] J.-H. Shin, J.-M. Park, H.-J. Kim, J.-H. Ahn, B.-M. Kwak, and J.-M. Kim, "Development of Rapid Analytical Methods for Inositol as a Trace Component by HPLC and LC-MS/MS in Infant Formula," *Korean Journal for Food Science of Animal Resources*, vol. 35, no. 4, pp. 466–472, Aug. 2015, doi: 10.5851/kosfa 2015.35.4.466.

[24] G. Marolt and M. Kolar, "Analytical methods for determination of phytic acid and other inositol phosphates: A review." *Molecules*, vol. 26, no. 1, Dec. 2020, doi: 10.3390/molecules26010174.

[25] D. C. Woollard, C. Macfadzean, H. E. Indyk, A. McMahon, and S. Christiansen, "Determination of myo-inositol in infant formulae and milk powders using capillary gas chromatography with flame ionisation detection," *International Dairy Journal*, vol. 37, no. 2, pp. 74–81, Aug. 2014, doi: 10.1016/j.idairyj.2014.03.004.

[26] J. Larner, "D-chiro-inositol--its functional role in insulin action and its deficit in insulin resistance." *Int. J. Exp. Diabetes Res.*, vol. 3, no. 1, pp. 47–60, Jan. 2002, doi:10.1080/15604280212528.

[27] J. E. Nestler, D. J. Jakubowicz, P. Reamer, R. D. Gunn, and G. Allan, "Ovulatory and metabolic effects of D-chiro-inositol in the polycystic ovary syndrome." *N. Engl. J. Med.*, vol. 340, no. 17, pp. 1314–1320, Apr. 1999, doi: 10.1056/NEJM199904293401703.

[28] J. McLaurin et *al.*, "Cyclohexanehexol inhibitors of Abeta aggregation prevent and reverse Alzheimer phenotype in a mouse model." *Nat. Med.*., vol. 12, no. 7, pp. 801–808, Jul. 2006, doi: 10.1038/nm1423.

[29] D. Bandyopadhyay et *al.*, "Voltammetric detection of inositol using a platinum-based electrode," *Nano Life*, Mar. 2022, doi: 10.1142/S1793984422500040.

[30] E. G. Tagliaferri, G. Bonetti, and C. J. Blake, "Ion chromatographic determination of inositol in infant formulae and clinical products for enteral feeding." J. Chromatogr. A, vol. 879, no. 2, pp. 129–135, May 2000,doi: 10.1016/S0021-9673(00)00323-X.

[31] K.-Y. Leung, K., Mills, K. A., Burren, A. J. Copp, and N. D. E. Greene, "Quantitative analysis of myo-inositol in urine, blood and nutritional supplements by high-performance liquid chromatography tandem mass spectrometry." *J. Chromatogr. B Analyt. Technol. Biomed. Life Sci.*, vol. 879, no. 26, pp. 2759–2763, Sep. 2011, doi: 10.1016/j.jchromb.2011.07.043.

[32] R. Rajaram, M. Kiruba, C. Suresh, J. Mathiyarasu, S. Kumaran, and R. Kumaresan, "Amperometric determination of Myo-inositol using a glassy carbon electrode modified with nanostructured copper sulfide." *Mikrochim. Acta*, vol. 187, no. 6, p. 334, May 2020, doi: 10.1007/s00604-020-04300-z.

[33] D. Das *et al.*, "Amine Functionalized MWCNTs Modified MIP-Based Electrode for Detection of Epicatechin in Tea," *IEEE Sens. J.*, vol. 22, no. 11, pp. 10323–10330, Jun. 2022, doi: 10.1109/JSEN.2022.3169169.

[34] S. Nag *et al.*, "A simple nano cerium oxide modified graphite electrode for electrochemical detection of formaldehyde in mushroom," *IEEE Sensors J*., vol. 21, no. 10, pp. 12019–12026, May 2021

[35] N. Leibl, K. Haupt, C. Gonzato, and L. Duma, "Molecularly imprinted polymers for chemical sensing: A tutorial review," *Chemosensors*, vol. 9, no. 6, p. 123, May 2021, doi: 10.3390/chemosensors9060123.

[36] S. Nag, S. Pradhan, D. Das, B. Tudu, R. Bandyopadhyay and R. Banerjee Roy, "Fabrication of a Molecular Imprinted Polyacrylonitrile Engraved Graphite Electrode for Detection of Formalin in Food Extracts," in *IEEE Sens. J.*, vol. 22, no. 1, pp. 42-49, 1 Jan.1, 2022, doi: 10.1109/JSEN.2021. 3128520.

[37] S. Nag, D. Das, H. Naskar, B. Tudu, R. Bandyopadhyay, and R. Banerjee Roy, "Detection of metanil yellow adulteration in turmeric powder using nano nickel cobalt oxide modified graphite electrode," *IEEE Sens. J.*, vol. 22, no. 13, pp. 12515–12521, Jul. 2022, doi: 10.1109/JSEN.2022.3178768.

[38] S. Nag et al., "Formalin Detection using Platinum Electrode-Based Electrochemical System," *J. Inst. Eng. IndiaSer. B*, vol. 103, no. 4, pp. 1159–1165, Feb. 2022, doi: 10.1007/s40031-022-00712-y.

[39] T. Nandy Chatterjee et *al.*, "Molecular imprinted polymer based electrode for sensing catechin (+C) in green tea," *IEEE Sens. J.*, vol. 18, no. 6, pp. 2236–2244, Mar. 2018, doi: 10.1109/JSEN.2018.2791661.

[40] S. Biswas, M. Chakraborty, and K. Biswas, "Detection of formaldehyde by an A RGO/PMMA coated sensor," in *2020 IEEE International Instrumentation and Measurement Technology Conference (I2MTC)*, May 2020, pp. 1–6, doi: 10.1109/I2MTC43012.2020.9129118.

[41] MD. M. Nezami, S. A. Wani, S. A. Khan, N. Khera, and S. Sohail, "An MIP-Based Novel Capacitive Sensor to Detect 2-FAL Concentration in Transformer Oil," *IEEE Sens. J.*, vol. 18, no. 19, pp. 7924–7931, Oct. 2018, doi: 10.1109/JSEN.2018.2864793.

[42] A. K. Prusty and S. Bhand, "Molecularly imprinted polyresorcinol-based capacitive sensor for sulphanilamide," *Electroanalysis*, vol. 31, no. 9, pp. 1797–1808, Jun. 2019, doi: 10.1002/elan 201900099.

[43] J. H. Waite, "Adhesion a la moule." *Integr. Comp. Biol.*, vol. 42, no. 6, pp. 1172–1180, Dec. 2002, doi: 10.1093/icb/42.6.1172.

[44] H. G. Silverman and F. F. Roberto, "Understanding marine mussel adhesion." *Mar. Biotechnol.*, vol. 9, no. 6, pp. 661–681, Dec. 2007, doi: 10.1007/s10126-007-9053-x.

[45] H. Lee, S. M. Dellatore, W. M. Miller, and P. B. Messersmith, "Mussel-inspired surface chemistry for multifunctional coatings." *Science*, vol. 318, no. 5849, pp. 426–430, Oct. 2007, doi: 10.1126/science 1147241.

[46] J. Yu et al., "Adaptive hydrophobic and hydrophilic interactions of mussel foot proteins with organic thin films." ProcNatlAcadSci USA, vol. 110, no. 39, pp. 15680–15685, Sep. 2013, doi: 10.1073/pnas 1315015110.

[47] S.-C. Chou, W.-A. Chung, T.-L. Fan, Y. Dordi, J. Koike, and P.-W. Wu, "Polydopamine and its composite film as an adhesion layer for cu electroless deposition on SiO2," *J. Electrochem. Soc.*, vol. 167, no. 4, p. 042507, Mar. 2020, doi: 10.1149/1945-7111/ab7aa2.

[48] J. Wang et al., "Electropolymerization of dopamine for surface modification of complex-shaped cardiovascular stents.," Biomaterials, vol. 35, no. 27, pp. 7679–7689, Sep. 2014, doi: 10.1016/j.biomaterials.2014.05.047.

[49] W. Wang, Y. Jiang, S. Wen, L. Liu, and L. Zhang, "Preparation and characterization of polystyrene/Ag core-shell microspheres--a bio-inspired poly(dopamine) approach.," *J. Colloid Interface Sci.*, vol. 368, no. 1, pp. 241–249, Feb. 2012, doi: 10.1016/j.jcis.2011.10.047.

[50] W. Wang, A. Zhang, L. Liu, M. Tian, and L. Zhang, "Dopamine-Induced Surface Functionalization for the Preparation of Al–Ag Bimetallic Microspheres," *J. Electrochem. Soc.*, vol. 158, no. 4, p. D228, 2011, doi: 10.1149/1.3551496.

[51] C. Xu, M. Tian, L. Liu, H. Zou, L. Zhang, and W. Wang, "Fabrication and properties of silverized glass fiber by dopamine functionalization and electroless plating," *J. Electrochem. Soc.*, vol. 159, no. 4, pp. D217–D224, 2012, doi: 10.1149/2.056204jes.

[52] Z. Tapsir and S. Saidin, "Synthesis and characterization of collagen–hydroxyapatite immobilized on polydopamine grafted stainless steel," *Surface and Coatings Technology*, vol. 285, pp. 11–16, Jan. 2016, doi: 10.1016/j.surfcoat.2015.11.024.

[53] P. Qi, M. F. Maitz, and N. Huang, "Surface modification of cardiovascular materials and implants," *Surface and Coatings Technology*, vol. 233, pp. 80–90, Oct. 2013, doi: 10.1016/j.surfcoat.2013.02.008.

[54] L. Huang, J. Yi, Q. Gao, X. Wang, Y. Chen, and P. Liu, "Carboxymethyl chitosan functionalization of CPED-treated magnesium alloy via polydopamine as intermediate layer," *Surface and Coatings Technology*, vol. 258, pp. 664–671, Nov. 2014, doi: 10.1016/j.surfcoat.2014.08.020.

[55] D. Schaubroeck, L. Mader, P. Dubruel, and J. Vanfleteren, "Surface modification of an epoxy resin with polyamines and polydopamine: Adhesion toward electroless deposited copper," *Appl. Surf. Sci.*, vol. 353, pp. 238–244, Oct. 2015, doi: 10.1016/j.apsusc.2015.06.114.

[56] A. Bose and K. Biswas, "Performance Study of Urease-PMMA-Based Aqueous Urea Sensor," *IEEE Sens. J.*, vol. 17, no. 21, pp. 6850–6858, Nov. 2017, doi: 10.1109/JSEN.2017.2751502.

[57] J.-L. Gong, F.-C. Gong, Y. Kuang, G.-M. Zeng, G.-L. Shen, and R.-Q. Yu, "Capacitive chemical sensor for fenvalerate assay based on electropolymerized molecularly imprinted polymer as the sensitive layer." *Anal. BioAnal. Chem.*, vol. 379, no. 2, pp. 302–307, May 2004, doi: 10.1007/s00216-004-2568-3.

[58] S. Mo, Y. Li, S. Shan, L. Jia, and Y. Chen, "Synthesis and properties of inositol nanocapsules." *Materials (Basel)*, vol. 14, no. 19, Sep. 2021, doi: 10.3390/ma14195481.

[59] A. H. Kamel*et al.*, "Novel Solid-State Potentiometric Sensors Using Polyaniline (PANI) as A Solid-Contact Transducer for Flucarbazone Herbicide Assessment," *Polymers (Basel)*, vol. 11, no. 11, Nov. 2019, doi: 10.3390/polym11111796.

[60] M. Maruthapandi, M. Natan, G. Jacobi, E. Banin, J. H. T. Luong, and A. Gedanken, "Antibacterial Activity Against Methicillin-Resistant Staphylococcus aureus of Colloidal Polydopamine Prepared by Carbon Dot Stimulated Polymerization of Dopamine," *Nanomaterials (Basel)*, vol. 9, no. 12, Dec. 2019, doi: 10.3390/nano9121731.

[61] M. Moulick, S. Nag, D. Das, B. Tudu, R. Bandyopadhyay and R. B. Roy, "Detection of Tannic Acid using Nd2O3 Modified Graphite Electrode," *2022 2nd International Conference on Emerging Frontiers in Electrical and Electronic Technologies (ICEFEET)*, 2022, pp. 1-5, doi: 10.1109/ICEFEET51821.2022.9848155.

Quantification of Syringic Acid Using Novel Electrochemical Sensors

3

3.1 Introduction

In recent years, various phenolic compounds have drawn the attention of medical, food experts, and scientists owing to their antioxidant, fragrant aromatic, and anti-inflammatory properties. Realizing the importance of human health and medicinal value, the usage of phytochemicals for controlling human diseases is of considerable scientific and public interest. Syringic acid (SA, $C_9H_{10}O_5$), one of the naturally occurring phenolic compounds, also known as 4-Hydroxy-3, 5-dimethoxybenzoic acid, is a dimethoxybenzene, which is a 3, 5-dimethyl ether of gallic acid. SA, being a member of the benzoic acid group and conjugate acid of a syringate, finds its significant role as a nutraceutical and plant metabolite [1]. The natural occurrence of SA is reported in a wide variety of plants, namely Raphanus sativus, Annona squamosa, Tagetes erecta, Ardisia elliptica, Hemidesmus indicus, Schumannianthus dichotomus, and Catunaregam [2-3]. SA is also found in abundance in several fruits, vegetables, and beverages, including dates, olives, grapes, pumpkins, cauliflower, spices, acai palm, honey, red wine, and vinegar [3-7]. SA possesses anti-angiogenic, anti-oxidant, anti-hyperglycaemic, antimicrobial, anti-inflammatory, antiendotoxic, and memory-enhancing, neuro and hepatoprotective properties [3] [8]. Among the therapeutic applications, SA is instrumental in the prevention of cancer, diabetes, cerebral ischemia, and CVDs. SA's therapeutic property is owing to the existence of methoxy groups on the aromatic ring at the 3rd and 5th positions as shown in the chemical structure in Fig. 3.1. SA has the potential to regulate protein dynamics, modulate enzymatic activities as well as diverse transcription factors associated with cancer, diabetes, angiogenesis, and inflammation [3]. According to the report of TGSC Information System, the Good Scents Company, for an adult, the maximum permissible daily intake limit of SA is 1800µg/person/day, although there are no reports of adverse toxicity of SA in any study [9]. Apart from biomedical and clinical applications, SA has considerable usage in industrial applications. SA being present in lignin promotes laccase-based catalysis and thereby plays an important role in pulp and bioremediation industries [10]. As reported in [11-12], SA is instrumental in photocatalytic ozonation activities, and industries utilize the caries reduction property of SA in dental cement preparation.

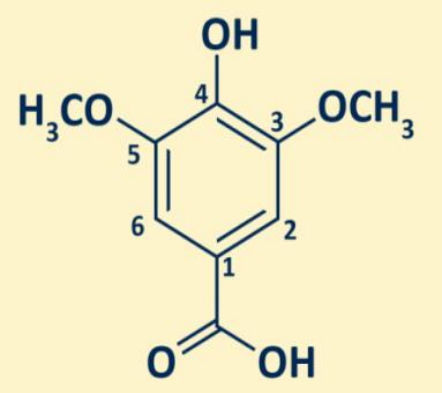

Fig. 3.1. Chemical Structure of SA.

Nowadays, a wide variety of pesticides and chemicals are used in fruits and vegetables, which can be detrimental to health. The application of these harmful agents can inhibit pharmacological activities or can obliterate the medical and nutritional values of phenolic compounds like SA by modulating their composition through biochemical reactions. Thus, it is necessary to assess the overall quality of the fruits and vegetables based on the quantification of specific health-beneficial compounds like SA. The primary objective of developing dedicated sensors is to detect and determine the content of these health-beneficial compounds in real food samples, even if they may be present in very low concentrations. Comprehending the wide availability, industrial and medical importance of SA, there is an obligatory need for a reusable, at the same time, cost-effective sensor for quantitative analysis of SA analytes in fruits, vegetables, and beverages. As already mentioned, SA is a phenolic compound and a derivative of gallic acid, one can think of using conventional detection methods including chemiluminescence [13], thin-layer chromatography (TLC)[14] and chronoamperometry [15], flow injection analysis [16] and reversed phase high- performance liquid chromatography (HPLC) [17-19]. Quantification of SA in herbal medicines leaves of Rhododendron species, plasma of rats and mice tissues using HPLC methods was reported in some literature [20-22]. Micromolar concentrations of SA in artificially synthesized wine and laboratory samples had been estimated using an indirect analytical voltammetric technique [23]. In several works, quantitative analysis of SA in a wide variety of red wines had been performed employing HPLC methods [24-29]. However, these methods involve the usage of toxic organic solvents during experiments, costly high-end instruments, long operation time, and the requirement of highly skilled expert laborers for performing the experiments. Electrochemical detection can turn out to be a potential alternative in such instances since it is a simple, cost-effective as well and less time-consuming process. The electrochemical sensors find their application in the field of food detection

analysis [30]– [32], biomolecules [33]– [36], and the determination of environmental pollutants [37]. Phytochemicals are widely used for the treatment of several human diseases, viz., diabetes, cancer, cerebral ischemia, etc.

This chapter explores two distinct analytical approaches for the detection and quantification of syringic acid in real samples: Ultraviolet-visible (UV-Vis) spectroscopy coupled with multivariate analysis, and a molecularly imprinted polymer (MIP) based electrochemical sensor. These investigations aim to provide rapid, reliable, and cost-effective solutions for assessing SA content in various food matrices.

3.2 Quantification of Syringic Acid in Real Samples Based on UV-Vis Spectroscopy

In this work, a rapid and reliable Ultraviolet-visible (UV-Vis) spectroscopy technique was employed for assessing syringic acid (SA) content in real food samples, specifically cauliflower (CLF), oregano (ORG), and black olive (BOL). UV-Vis spectrophotometry offers a direct, non-destructive method that measures the absorbance of light in the UV-Vis spectrum, produced by electronic transitions within the sample [38]. This technique avoids the use of chemical solvents, distinguishing it from many conventional methods.

Data measurements were performed using a UV Spectrophotometer operating in the wavelength range of 200-400 nm. To analyze and distinguish between different samples, Principal Component Analysis (PCA) was applied to the UV-Vis absorbance data. The PCA plot confirmed effective clustering of the samples, demonstrating clear qualitative discrimination. A high-class separability index of 313.52 was obtained, further validating the distinct spectral profiles of the samples. For quantitative prediction and correlation of SA levels, Principal Component Regression (PCR) and Partial Least Squares Regression (PLSR) analyses were performed. These prediction algorithms exhibited high average prediction accuracies of 99.78% and 99.69%, respectively, and achieved an almost identical correlation factor (CF) as high as 0.99 for both models. The primary investigation results strongly suggest that the UV-Vis spectroscopy technique, when coupled with multivariate data analysis, represents a viable and effective approach for detecting and quantitatively assessing SA contents in real food samples.

3.2.1 Materials and methods

3.2.1.1 Preparation of samples

Cauliflower (CLF), black olives (BOL), and oregano (ORG) were selected as real samples, which were purchased from a local market. Samples, weighing 1 g each, were blended in 90mL of water. Thereafter, filtration was performed using Whatman UNIFLO disposable sterile

syringe filters of 25mm diameter and 0.22µM pore size. The filtered solutions thus extracted were used for the UV-Vis spectroscopy method. As a reference solvent, Millipore water (resistance = 18 MΩ) was used while experimenting. Concentration values of 46.84 µM, 73.86 µM, and 79.84 µM corresponding to cauliflower (CLF), black olive (BOL), and oregano (ORG) were obtained as reference values from HPLC analysis.

3.2.1.2 Spectral data acquisition process

UV Spectrophotometer (UV-1800 SHIMADZU) was operated in the laboratory to acquire the UV-Vis absorbance spectral data. The entire spectrophotometer setup comprises a light source, detector, monochromator, and two cuvettes for holding the sample solution and the reference solution through which beams pass. A schematic UV-vis experimental setup has been depicted in Fig. 3.2, similar to that reported in [39]. After pouring the samples in the crystal cuvettes made of quartz, the cuvettes containing the samples were placed within the dark chamber to prevent stray light from passing. The UV-Probe user interface provides the recorded spectral data. The entire experiment was performed at room temperature, setting the wavelength range of the spectrometer from 200 to 400 nm. Firstly, base corrections were performed by introducing water-filled cuvettes into the spectrophotometer chamber. Secondly, choosing one cuvette as a reference, the sample solution was poured into the other. Absorbance data were recorded for 10 µM SA concentration as well as for three real samples, viz. CLF, BLO, and ORG. 1001 data points were obtained for each repetition, and in total, eight repetitions were acquired within the wavelength window for each of the samples. Before performing each experiment to acquire UV-Vis absorbance spectral data for each of the sample solutions, the cuvette containing the sample solution was rinsed and dried using dry tissue papers.

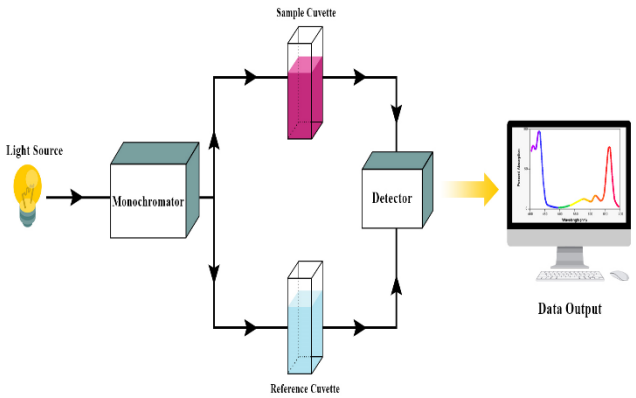

Fig. 3.2. Schematic of the experimental set-up of UV-Vis spectroscopy [39].

3.2.1.3 Data analysis techniques

An initial investigation of the spectral data of UV-Vis corresponding to each sample was performed using ORIGIN 8 without applying any data pre-processing techniques. Using MATLAB R2017 version, the absorbance spectra were analyzed. Principal component analysis (PCA) was employed on UV-Vis spectra for qualitative analysis of the data. For quantitative data estimation and analysis of SA content in real samples, partial least squares regression (PLSR) and principal component regression (PCR) were applied. Eight sets of data for 10 µM SA concentration and three real sample solutions corresponding to CLF, BLO, and ORG were subjected to quantitative analysis. Six repetition sets and two repetition sets (3:1) were considered as the training set and the testing set, respectively.

a) Principal component analysis (PCA)

PCA is a dimensionality reduction method where a large set of variables is reduced into small, detailed data sets without significant loss of information [40]-[41]. Orthogonal transformation of uncorrelated variables, known as principal components (PC), to correlated variables is performed in this technique. Simpler and faster analysis of the spatial distribution profile of the multivariate data is possible by perceiving PCA score plots. The first principal component gives the maximum variance, and the total variance is obtained from all the principal components. Class separability Index (SI) represents the degree of data clustering for different samples and is calculated from the ratio of trace of the 'between class scatter matrix' (S_b) to that of the 'within class scatter matrix' (S_w), where the S_b and S_w are given by the following expressions (1) and (2) respectively [42].

$$S_b = \sum_{i=1}^{c} n_i (m_i - m)(m_i - m)^T \quad (1)$$

$$S_w = \sum_{i=1}^{2} \left(\sum_{j=1}^{n_i} (x_{i,j} - m_i)(X_{i,j} - m_i)^T \right) \quad (2)$$

where c symbolizes the class count, n_i is the sample count in the i^{th} class, m_i is the mean vector of the samples in the i^{th} class, and m denotes the mean vector of the samples.

of the samples.

b) Partial least squares regression (PLSR)

The fundamental goal of PLSR is to establish a multivariate linear relationship that maps the predictor matrix to the corresponding response variables by maximizing the covariance between them.[43]. The leave-one-out cross-validation technique was considered as a performance metric in the current study. In order to reduce the number of predictors, PLSR eliminates

a set of components having highly correlated predictors and response variables. Statistical parameters, viz. correlation factor (CF), root mean square error of validation (RMSEV) and root mean square error of prediction (RMSEP), and average prediction accuracy, were calculated, which signify the correspondence level between predicted and actual values.

c)Principal Component Regression (PCR)

PCR, a multi–collinearity reduction algorithm, aims at estimating the principal components by applying the PCA algorithm on the gathered data matrix [44]. In the same direction corresponding to that of the output variables, the highest variance is exhibited by the predictors. The LOOCV technique is also employed here, similar to that used for PLSR, for performance measurement and prediction improvement.CF, RMSEV, RMSEP, and average prediction accuracy were estimated once again to analyze the extent of prediction.

3.2.2 **Results and Discussion**

3.2.2.1 UV-Vis absorbance spectra

The UV-Vis absorbance spectra of SA had been studied for the wavelength window of 200-400 nm for a 10 µM SA concentration. Fig. 3.3 depicts the absorbance peaks around 220 nm and 270 nm observed during the experiment, which is quite consistent with that reported in previous works [45]-[46].

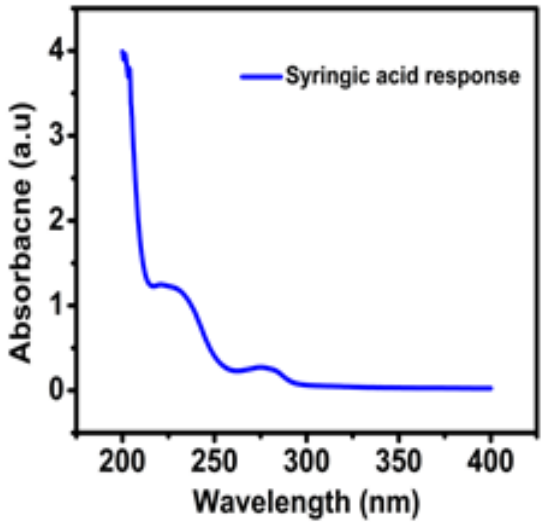

Fig. 3.3. UV-Vis spectra of absorbance for SA Concentration of 10 µM.

3.2.2.2 Principal component analysis (PCA)

In this work, the recorded UV-Vis spectral data were analysed employing the PCA tool. Three different real samples - cauliflower (CLF), black olives (BOL), and oregano (ORG) solutions

were considered for data clustering representation. Fig. 3.4 represents the test score plot for PCA, which indicates 85.18%, 14.78% and 0.0083 % of the total explained variances, respectively. The separability index (SI) represents the quantitative measurement of discrimination, and the measured SI value was as high as 313.52.

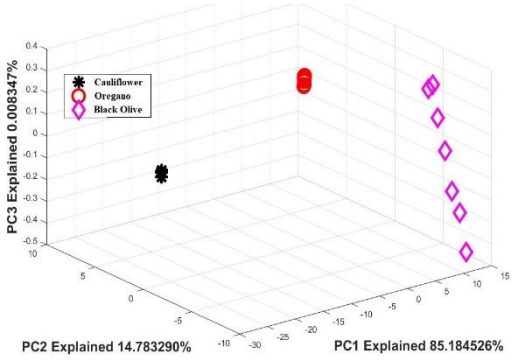

Fig. 3.4. Graphical depiction of UV-Vis data analysis for the three real samples using PCA test score plot.

3.2.2.3 Partial least squares regression (PLSR) analysis

Spectral data recorded for three different real samples - cauliflower (CLF), oregano (ORG), and black olives (BOL) were analyzed using the PLSR tool. As discussed earlier, eight repetitions were recorded in total, among which six repetitions were set and two repetitions were set (3:1) were considered for developing the training set and testing set, respectively. Component 6 was selected as the optimum one for prediction analysis as the minimum RMSEC was found at component 6 through cross-validation. Prediction analysis result yielded a high correlation factor, CF of 0.99, and it can be observed that there is negligible variation in the prediction accuracies. Table 3.1 depicts a comparative study of actual SA content, obtained from HPLC analysis, with that of the predicted values. The average prediction accuracy was found to be 99.78 %.

Table 3.1

Comparative study on actual and predicted SA contents obtained using PLSR

Sample	Actual SA Content (µM)	Predicted SA Content(µM)	Prediction Accuracy (%)
CF	46.84	46.96	100.25
	46.84	46.86	100.04
ORG	79.84	79.86	100.02
	79.84	79.80	99.94
BLO	73.86	73.59	99.63
	73.86	72.98	98.80
Average prediction accuracy = 99.78 %			

3.2.2.4 Principal component regression (PCR) analysis

For further quantitative analysis of the UV-Vis spectral data obtained for the three samples, the PCR analysis tool was used. In this case minimum RMSEC value was obtained for component 9, and the CF was 1. Therefore, 9 components were selected for the prediction analysis, and after prediction analysis, a high CF value of 0.99 and an average prediction accuracy of 99.69 % were obtained, which is represented in Table 3.2.

Table 3.2

Comparative study on actual and predicted SA contents obtained using PCR

Sample	Actual SA Content (µM)	Predicted SA Content(µM)	Prediction Accuracy (%)
CF	46.84	46.88	100.08
	46.84	46.81	99.93
ORG	79.84	79.89	100.06
	79.84	79.81	99.96
BLO	73.86	73.47	99.47
	73.86	72.87	98.65
Average prediction accuracy = 99.69%			

3.2.2.5 Comparative study on the performance of the regression models

In this study, two different regression models, namely PLSR and PCR had were employed as regression models for the prediction analysis of SA concentrations in real samples. The comparative performance parameters are summarized in Table 3.3 for both the regression models. All the parameters were estimated prior to the prediction process as well as after the prediction process, as shown in Table 3.3. PLSR and PCR exhibited highly satisfactory average prediction accuracy of 99.78% and 99.69% respectively.

Table 3. 3

Comparative summary on regression model performance

Method	Prior to Prediction		Post Prediction	
	CF	***RMSECV***	***CF***	***RMSEP***
PLSR	1	0.0038	0.99	0.046
PCR	1	0.0044	0.99	0.038

PUBLICATION STATUS

CONFERENCE

- Dipan Bandyopadhyay, Shreya Nag, Runu Banerjee Roy, "Quantification of syringic acid in real samples based on uv-vis spectroscopy", IEEE Silchar Subsection Conference (IEEE SILCON-2022), Silchar, Assam, India.

3.3 Detection of Syringic Acid in Food Extracts Using Molecular Imprinted Polyacrylonitrile Infused Graphite Electrode

This section details the development of a highly sensitive and selective molecularly imprinted polymer (MIP) based electrochemical sensor for the detection of syringic acid (SA) in food extracts. The overarching objective is to assess the overall quality of fruits and vegetables by quantifying specific health-beneficial compounds like SA. This cost-effective and reproducible sensor was fabricated by creating an acrylonitrile (AN) molecularly imprinted polymer (MIP) over a graphite electrode, termed the MIP-AN@G electrode. The novelty of this work lies in introducing a facile, cost-effective electrochemical sensor with enhanced selectivity for SA, marking the first reported application of voltammetry coupled with MIP technology for SA detection.

The fabricated MIP-AN@G electrode material was characterized using UV-visible (UV-Vis) spectroscopy, Fourier transform infrared (FTIR) spectroscopy, and scanning electron microscopy (SEM). Its analytical performance was investigated using a three-electrode system employing Differential Pulse Voltammetry (DPV) and Cyclic Voltammetry (CV) techniques. Rigorous analysis under optimized experimental conditions revealed a wide linearity window from 10 μM to 100 μM concentrations, demonstrating a satisfactory lower limit of SA detection (LOD) of 0.32 μM. The electrode demonstrated attractive features such as high repeatability (RSD: 1.11%), high reproducibility (RSD: 1.16%), and reasonable stability (RSD: 1.89%). Its practical application in real food extracts (cauliflower, oregano, black olives) yielded high accuracies (above 99%) when validated against HPLC analysis, with supporting t-test results. These findings firmly establish the MIP technique and the MIP-AN@G electrode-based sensor as a viable and promising candidate for SA detection in real food samples within industrial applications.

3.3.1 Experimental section

3.3.1.1. Chemical reagents and standards

SA (>97%) was bought from TCI (Tokyo Chemical Industry) Chemicals Pvt. Ltd., India. Fine Graphite powder of 99% purity, acrylonitrile (AN), acrylic acid (AA), acrylamide (AM), and ethylene glycol dimethyl acrylate (EGDMA) were procured from Sigma Aldrich, USA. Benzoyl peroxide was bought from Merck Specialities Private Limited (India). Acetate buffer

saline (ABS), Phosphate buffer saline (PBS), and citrate buffer saline (CBS) of PH 5, 6, as well as 7, were prepared in the laboratory. Ethanol and Binder (paraffin oil) were provided by Merck & Co. (India). Chemicals being of analytical grade, they are not subjected to any purification process. For washing the electrode and other accessories, distilled water (R=18 MΩ), acquired from a system of Millipore water purification, was used while experimenting.

3.3.1.2 Characterization details and equipment specifications

A tri-electrode system was implemented to examine the electrode performance employing Autolab Potentiostat/ Galvanostat PGSTAT101 (Metrohom Autolab, Netherlands). In the electrochemical cell, MIP-AN@G served as the working electrode, while the potential was regulated against an Ag/AgCl reference electrode and a platinum (Pt) counter electrode. For both differential pulse voltammetry (DPV) as well as cyclic voltammetry (CV) measurements, the voltage range was set as 0.4 V to 0.9 V. Fourier transform infrared spectroscopic (FTIR) analysis of the powder samples was performed using a NicoletTM iS20, Thermo Fisher Scientific using potassium bromide (KBr) pellets for calibration purpose. The measurements of Ultraviolet-visible (UV-Vis) absorption were performed employing a double-beam Shimadzu (UV-3600). To estimate SA in real samples, the HPLC analysis was performed using the Agilent Infinity preparative HPLC system- DEABG05977, G7161B. A scanning electron microscope (SEM, ZEISS EVO 18, US), operating at 15 kV accelerating voltage, was utilized for investigating the chemical composition and surface morphology characteristics of the synthesized materials.

3.3.1.3 Non-imprinted polymer (NIP-AN@G) and molecular imprinted polymer (MIP-AN@G) preparation

Graphite powder weighing 0.95 g was blended with 15 mL of ethanol, and sonication was performed for 1 hour in an ultrasonicator. Then, 0.05 g of AN (monomer) and 0.05 g of SA (template) were added to that mixture, thereby creating a new mixture which was sonicated for another hour. Thereafter, EGDMA of 400µL along with 1 mg of Benzoyl peroxide (as polymerization initiator) was added to the mixture, and further sonication was carried out for about 45 minutes. Polymerization was performed in a water bath by regulating the water bath temperature from 30-40 ^{o}C. Next, the acquired polymerized material was subjected to a washing-out process using an ethanol-water mixture in the ratio of 70:30 for removing the SA molecules. By filtration process, traces of SA were leached out from the polymerized sample, thereby synthesizing the MIP-AN@G material. The synthesized material was preserved after drying at room temperature to develop the MIP-AN@G electrode. The process of NIP sample synthesis is quite similar to that of MIP, except for mixing the template, SA for preparing NIP-AN@G.

3.3.1.4 MIP- AN @G and NIP- AN @G electrodes fabrication

Synthesized powdered polymerized materials, weighing 300 mg, were mortared in succession, adding 3-4 drops of paraffin oil (binder), resulting in a smooth, yet fine paste which is suitable for the development of the electrodes. This fine paste was stuffed into glass capillary glass tubes (1.25 mm inner dia.) using a thin metallic rod. For providing the electrical contacts, copper wires were connected to these electrodes.

3.3.1.5 Real sample extract preparation

Three samples, namely cauliflower, oregano, and black olives, were purchased from the nearby market. Each sample, weighing 1 g, was blended in 100 mL of water. After filtration with a disposable sterile syringe filter of Whatman UNIFLO (diameter and pore size of 25 mm and 0.22μM respectively) comprising of filter membrane of polyvinylidene fluoride (PVDF) in a polypropylene platform, the resultant extracted solution was used for HPLC as well as DPV analysis. Agilent 1260 infinity II DAD detector, column BioSute C 18 of dimension 4.6 x 150 mm, having a silica particle size of 3μm, was used during HPLC analysis of the aliquots at ambient temperature. The mobile phases used were i) 0.1% Trifluoroacetic acid (TFA) in H2O and ii) 100% acetonitrile (ACN), maintaining a 1ml min^{-1} flow rate for the entire run time of 10 minutes.

3.3.2 Results with discussions

3.3.2.1 Optimization of the monomer

Three diverse monomers, namely acrylonitrile (AN), acrylamide (AM), and acrylic acid (AA), have been chosen for synthesizing the MIP samples as well as the corresponding electrodes. The detailed fabrication process has already been discussed in the experimental section. CV responses were recorded for these three electrodes, which reveal the presence of an irreversible redox peak around 0.65 V in the presence of a 100μM solution containing buffer and analyte molecule (SA) at 50 mV/s. It can be inferred from Fig. 3.5 that the highest peak current of oxidation was obtained for the MIP-AN@G electrode (4.01 and 1.85 times higher in comparison to that of AA and AM imprinted corresponding electrodes, respectively). The CV plots for different monomers have been depicted in the inset of Fig. 3.5. The electrochemical performance of the MIP may be influenced by the dipole-dipole, monomer-template interaction in the pre-polymerization step, which governs the SA recognition process at the MIP-AN@G electrode surface [47]. Therefore, AN was chosen as a prospective monomer, and the corresponding electrode was used for the detection of SA in the further experimental processes.

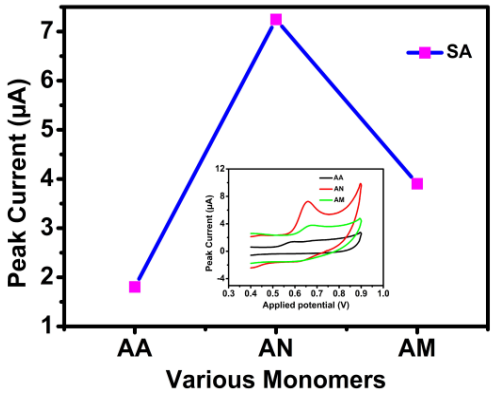

Fig. 3.5. Plot of maximum oxidation peak currents versus different monomers (insets showing CV plots for different monomers).

3.3.2.2 Synthesized Polymer Material Characterization

3.3.2.2.1 *FTIR Spectroscopic Analysis*

Using FTIR spectroscopy, the spectral investigation of the polymerized material after template removal (ATR) and before template removal (BTR) was performed which is illustrated in Fig. 3.6. The spectra present in the region of 953 cm^{-1}, 1067 cm^{-1}, 1150 cm^{-1}, 1244 cm^{-1}, 1380 cm^{-1}, 1464 cm^{-1}, 1652 cm^{-1}, 2893 cm^{-1} and 2940 cm^{-1} attributes the formation of polyacrylonitrile (PAN) [48-49]. The –CH bending gives rise to a peak at 1380 cm^{-1}. The vibrations for stretching, symmetric stretching as well as bending of the methylene group ($-CH_2$) were witnessed at the bands centering at 2893 cm^{-1}, 1067 cm^{-1}, and 1464 cm^{-1}[50-52]. A small Peak centered at 1652 cm^{-1} related to the nitryl group (C ≡ N) [53-55]. The presence of a sharp peak at 1710 cm^{-1} unveils the carbonyl stretching frequency of the carboxyl group (C = O) of the SA [56] [57]. As expected, this peak intensity was considerably reduced after template removal (ATR). Moreover, the presence of the methoxy group associated with the aromatic ring of SA leads to a sharp band centered at 2967 cm^{-1} [58].

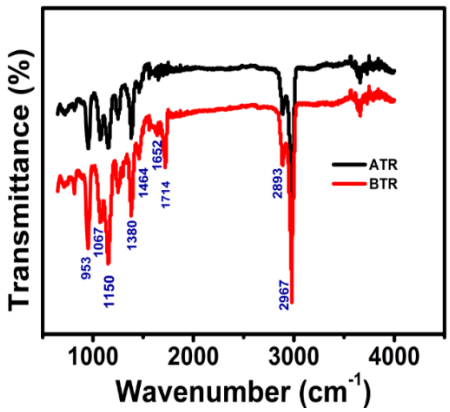

Fig. 3.6. MIP FTIR spectra before template removal along with after template removal.

3.3.2.2.2 *UV-Vis spectroscopy analysis*

The UV-Vis spectroscopic study, corresponding to the wavelength window of 200-400 nm confirms complete leaching out process of the SA molecule Fig. 3.7. The spectral observation depicted a sharp absorption peak at 273.50 nm (well in accordance with that reported in [45]) in case of before wash material (MIP- BW) which was absent in case of after wash material (MIP-AW). This affirms the complete SA template removal from the MIP material.

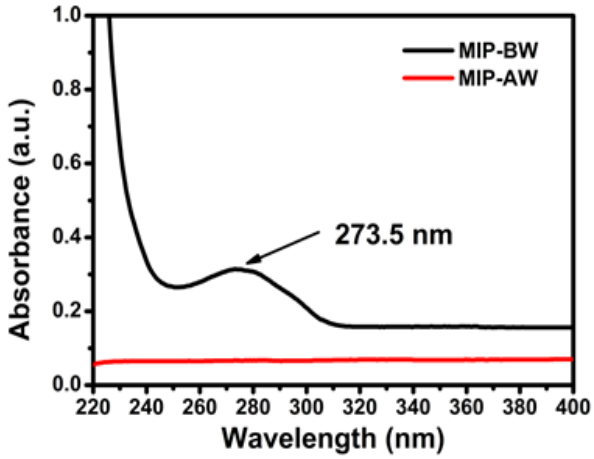

Fig. 3.7. Spectra of UV-vis absorption corresponding to the MIP material before (BW) as well as after template washing (AW).

3.3.2.2.3 SEM measurements for morphological insights

The surface morphologies of the MIP-AN@G and NIP-AN@G synthesized materials are shown in the SEM images of Fig. 3.8.(a) and Fig. 3.8.(b), respectively. MIP-AN@G surface appears to be considerably wrinkled, rugged as well, and rough in comparison to that of the NIP-AN@G, which can be attributed to the imprinted cavities.

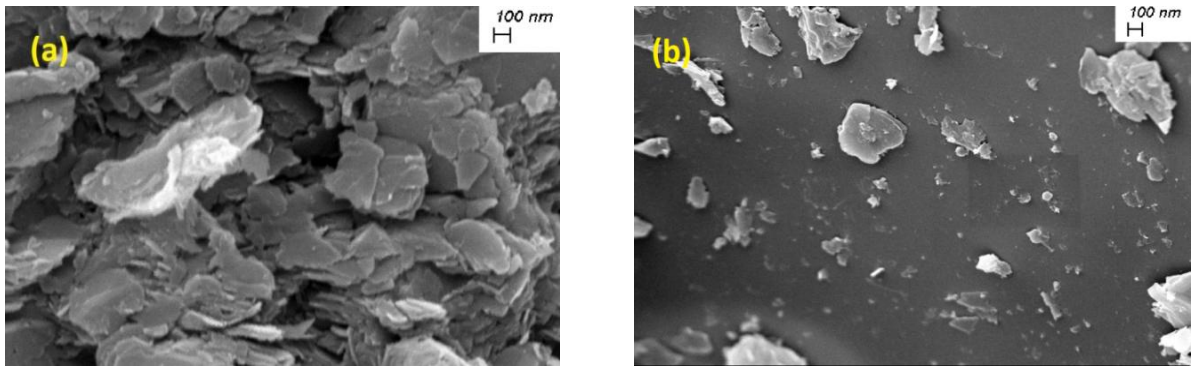

Fig. 3.8. Morphological images obtained from SEM measurements for (a) MIP-AN@G and (b) NIP-AN@G electrode materials.

3.3.2.3 Buffer and pH optimization

To study the influence of buffer as well as pH, the MIP-AN@G electrode was subjected to 1 ml of SA and 9 ml of various buffers, viz. Acetate buffered saline (ABS), citrate buffered saline (CBS), and phosphate buffered saline (PBS). CV responses revealed maximum oxidation peak current (7.249µA) was achieved for PBS (Fig. 3.9.(a)). Moreover, the effect of pH on MIP-AN@G was inspected using PBS of three different pH values, viz., 5, 6, and 7. It is quite clear from Fig. 3.9.(b) that the electrode offers the best response in terms of maximum oxidation peak current under PBS of pH 5. Owing to sufficient phenolate ion production at PBS 5 due to the ionization phenomenon of the phenolic group of SA through dissociation, electrochemical detection of SA is more favored. Thus, PBS 5 was chosen as a suitable buffer-solution for the subsequent experiments.

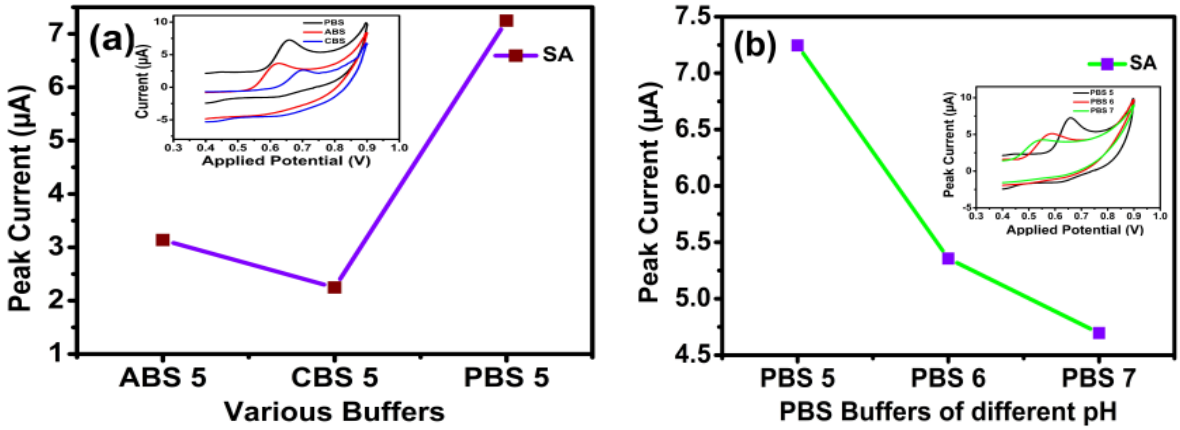

Fig. 3.9. Peak currents obtained for 100 µM SA solution (a) in ABS, CBS, as well as PBS 5 and (b) with PBS having pH values of 5, 6, and 7(insets showing CV plots for buffer variation and pH variation).

3.3.2.4 Electrochemical performance of MIP-AN@G electrode

The MIP-AN@G electrode's electrocatalytic performance was examined in two stages. In the first stage, a study on comparative analysis was performed at the surface of MIP-AN@G and NIP-AN@G electrodes based on the electrochemical oxidation of SA. The CV data were acquired in the presence of PBS 5 for the voltage range of 0.4 - 0.9 V, maintaining a 50 mV/s scan rate. A boosted oxidation peak at MIP-AN@G compared to the NIP-AN@G electrode is observed, which is depicted in Fig. 3.10 (a). It was found out that the MIP-AN@G electrode exhibited almost 2.358 times (peak currents for MIP-AN@G and NIP-AN@G electrodes were 7.287 μA and 3.090 μA, respectively) the highest peak current for oxidation in comparison to that of the NIP-AN@G electrode. The probable reason behind this is enhanced analyte

adsorption favored by the molecule recognition sites embedded within the MIP materials, which eventually increases the SA oxidation at the MIP-AN@G electrode. Another study was performed to investigate the MIP-AN@G electrode behavior. Again, CV responses were investigated in the presence as well as in the absence of SA molecules, considering PBS 5 as a buffer solution. The experiment was carried out in the presence of 100 µM SA in 0.1 M PBS 5, and a clearly defined oxidation peak was witnessed as illustrated in Fig. 3.10 (b), which was absent in the absence of the target analyte under the same ambient conditions.

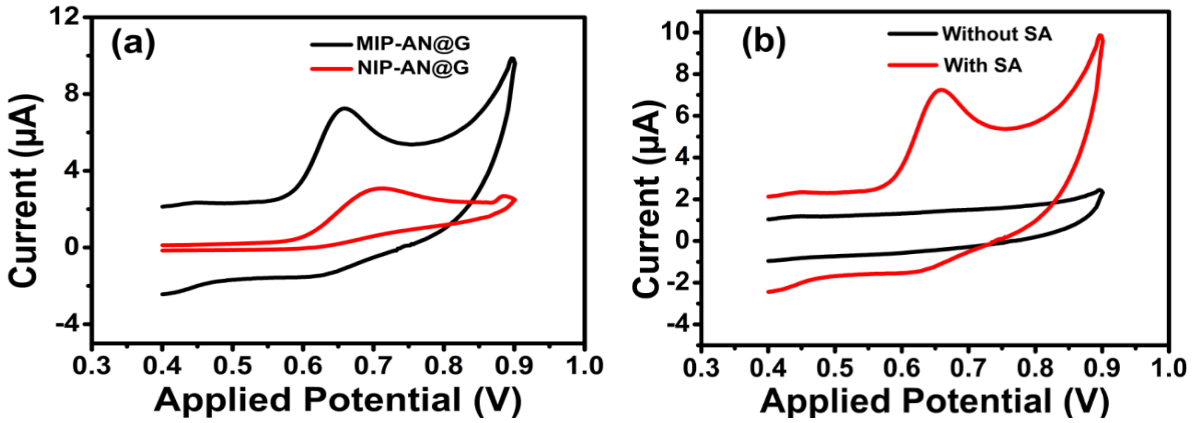

Fig. 3.10. CV responses of (a) MIP-AN@G as well as NIP-AN@G electrode in 100 µM solution containing 1 ml SA (b) MIP-AN@G in the presence and the absence of target analyte, SA molecule.

3.3.2.5 *Influence of scan rate variation*

The influence of scan rate on the electrochemical response of the MIP-AN@G electrode in the presence of 100 µM of the SA molecule is depicted in Fig. 3.11 (a). CV responses were investigated for the scan rate variation of 10 mV/s to 400 mV/s. Analyzing this figure, it can be concluded that increasing the scan rate increases the oxidation peak current of SA, thereby affirming that the surface-controlled oxidation process of SA is occurring at the interface of the MIP electrode surface [59]. Moreover, the plot of the anodic peak current (I_{SA}) variation with scan rate (Fig. 3.11.(b)) portrays linearity following a linear equation of regression (1).

$$I_{SA} = 0.178\upsilon + 9.343; R^2 = 0.99 \quad (1)$$

The number of transferred electrons throughout the electrochemical oxidation process of SA was calculated from the equation, described by Langmuir Isotherm (2) [32] [60], where *F, n*, Q, υ, *T,* and *R* symbolize Faraday's constant, no. of transferred electrons, the quantity of consumed charge, scan rate, room temperature, and the universal gas constant, respectively.

$$I_p = \frac{nFQ\upsilon}{4RT} \quad (2)$$

The value of n was estimated to be around unity, which is attributed to a single electron adsorption mechanism.

The linearity in the relationship between the peak potential of oxidation (E_P) and the logarithm of scan rate ($log\upsilon$) is illustrated in Fig.8. (c). It is evident from Fig. 3.11.(c) that there is a positive shift of peak potential (E_P) which also increases linearly along with $log\upsilon$. The corresponding linear equation of regression (3) can be expressed as

$$E_P = 0.067log\upsilon + 0.754; R^2 = 0.999 \quad (3)$$

The charge transfer coefficient t($\alpha = 0.88$) was computed from the slope of this equation

$$Slope = \frac{2.303RT}{\alpha nF} \quad (4)$$

for irreversible process, and the value is well in accordance with the existing reports related to the electrochemical redox mechanism of phenolic compounds [61].

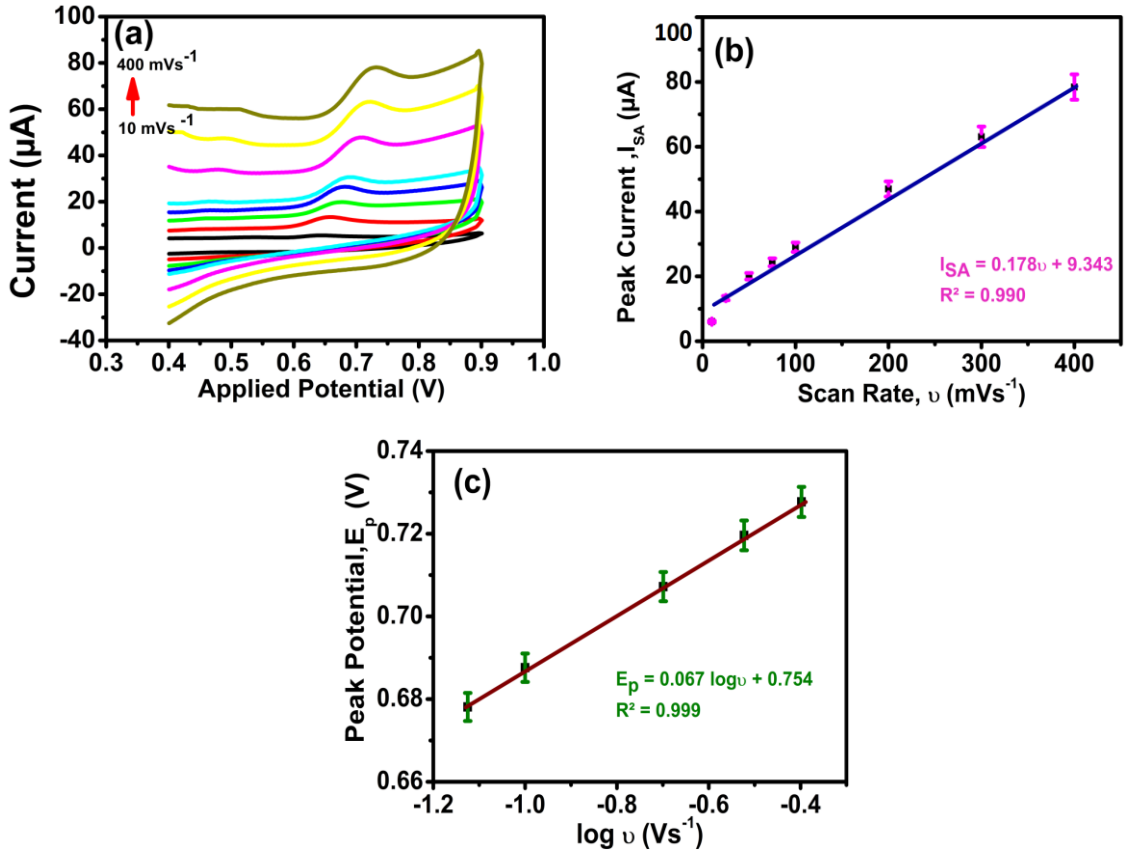

Fig. 3.11. CV responses of MIP-AN@G electrode in PBS 5 (a) Influence of scan rate variation (10 – 400 mVs^{-1}) on peak current of oxidation (b) Peak current - scan rate variation (Linear plot) (c) Linear variation of peak potential E_P With a log of scan rate.

3.4 Calibration analysis and limit of detection

The impact of various SA concentrations (C_{SA}Near the MIP-AN@G electrode surface is portrayed in Fig. 3.12. The extremely sensitive DPV responses were acquired for diverse SA contents in PBS 5 solution, optimizing the potential window from 0.4 to 0.9 V. Progressive hikes in oxidation peak currents at 50 mV/s for gradual SA concentration rise from 10 to 100µM were observed, which is depicted in Fig. 3.12.(a). Further, it can be inferred from Fig. 3.12.(b) that the calibration plot exhibits linearity in the concentration window of 10 to 100µM, obeying the equation of regression (5).

$$I_{SA} = 0.041C_{SA} + 8.169; R^2 = 0.999 \quad (5)$$

where C_{SA} -corresponding SA concentration, I_{SA} - peak current. The lower limit of detection, popularly designated as LOD for SA, was calculated to be 0.32 µM using $LOD = 3\frac{\sigma_{SA}}{m_{SA}}$ [51] where σ_{SA}- peak currents standard deviation corresponding to the lowest detected SA concentration and m_{SA} - slope of the calibration plot for SA. This low LOD value affirms the efficient detection capability of the MIP-AN@G electrode. The low LOD value affirms the efficient detection capability of the MIP-AN@G electrode. Further, the limit of quantification (LOQ) was computed to be 1.06 µM by the equation $LOQ = 10\frac{\sigma_{SA}}{m_{SA}}$ [62], where m_{SA} and σ_{SA}Indicate the calibration line slope and the peak current standard deviation for the lowest quantified SA concentration.

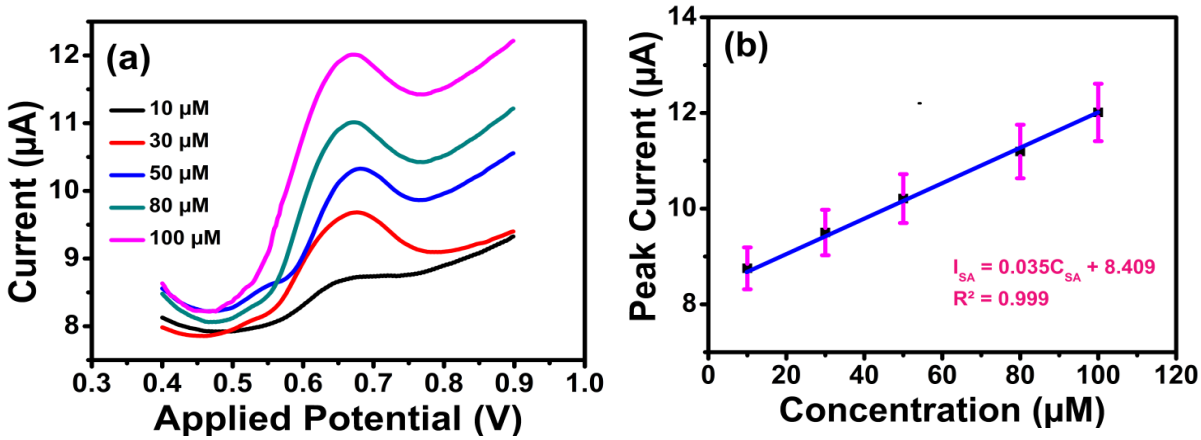

Fig. 3.12. DPV responses for SA using MIP-AN@G electrode surface in PBS 5 (subjected to 15s dipping time between each measurement) (a) for different SA concentrations and (b) Peak current vs SA concentration (Linear plot).

3.3.2.6 Repeatability, stability, and reproducibility investigation

In this work, the studies of repeatability, stability, along with reproducibility have been performed in a 100μM solution containing SA in 0.1 M PBS 5 to evaluate the MIP-AN@G sensor characteristics. Firstly, for the repeatability analysis, five consecutive CV measurements were recorded for the MIP-AN@G electrode. The deviation of peak currents for the five runs (R1-R5) is represented in Fig. 3.13 (a). Since the variation is minimal with a relative standard deviation (RSD) of 1.11%, it can be concluded that the proposed MIP sensor is exhibiting satisfactory repeatability. For the reproducibility analysis, three different sensors (E1, E2, and E3) were fabricated using the same technique discussed earlier. Three CV responses were procured using these electrodes, and subsequent analysis revealed an extremely satisfactory reproducibility with an acceptable RSD of 1.16% as depicted in Fig. 3.13.(b). Lastly, for the stability analysis, the same test was conducted with the same electrode for one month at 15-day intervals. It is to be noted that the electrode is preserved at normal room temperature in this interval. The MIP-AN@G electrode exhibited quite satisfactory stable behavior with an RSD of 1.89%, offering negligible peak current variation as illustrated in Fig. 3.13.(c). Moreover, the anodic peak potential position of the SA molecule hardly deviates for the MIP-AN@G electrode. Thus, these highly acceptable values of the sensor parameters elucidate the high efficacy of the proposed sensor.

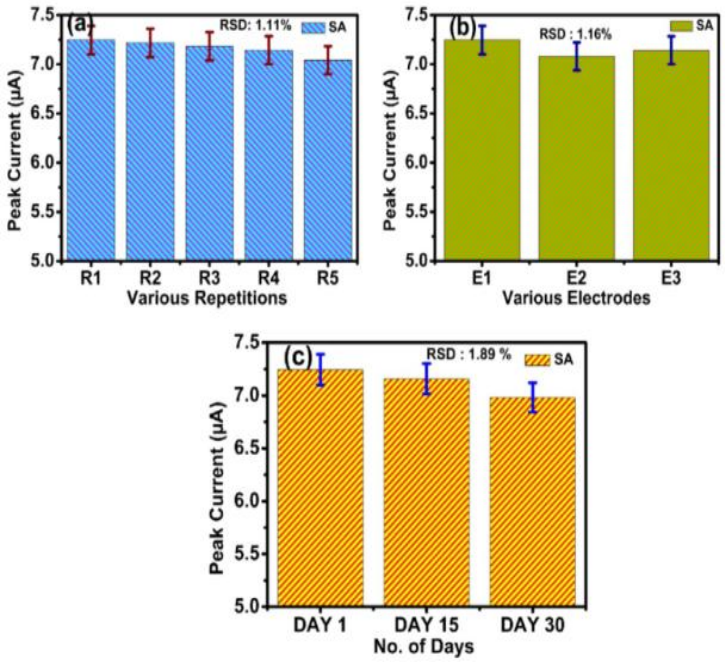

Fig. 3.13. (a) Repeatability, (b) reproducibility, and (c) stability of the MIP-AN@G electrode at 100 μM concentration.

3.3.2.7 Interference study

For the interference study, the MIP-AN@G electrode was exposed to five interfering agents, namely Vanillic acid (VA), Gallic acid (GA), Methyl Salicylate (MS), Salicylic Acid (SAc), Calcium (Ca^{2+}), and Chlorine (Cl^-) ions. 100µM of target analyte (SA) was subjected to these interfering species, and CV responses were acquired. The interference profile in terms of maximum peak current variation is illustrated in Fig. 3.14. The relatively negligible peak current change within a tolerance limit of 5% implies high selectivity of this MIP-AN@G electrode amid phenolic and other interfering species.

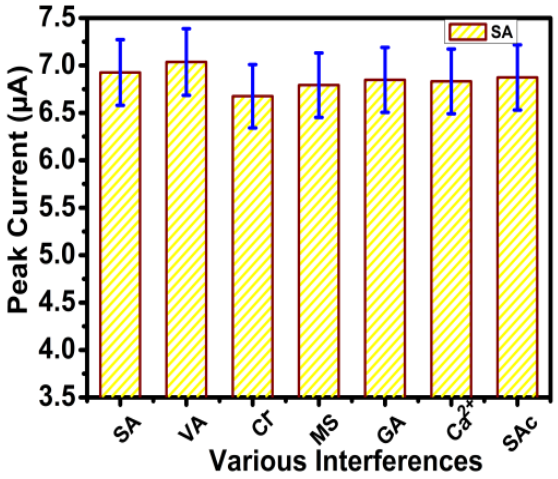

Fig. 3.14. Interference profile of MIP-AN@G electrode in the presence of six interfering species, namely VA, GA, MS, SAc, $Ca^{2+,}$ and Cl^- ions.

3.3.2.8 Real sample analysis

The quantitative analysis of SA in three samples, namely cauliflower, oregano, and black olives, was investigated, and a comparative study was performed with that of HPLC analysis. The analysis results are summarized in Table 3.3, where r (no. of observations corresponding to the three sample extracts) = 4. The MIP-AN@G electrode exhibited elevated accuracy of 99.34%, 99.79%, and 99.15% corresponding to cauliflower, oregano, and black olives samples, respectively. Moreover, the accuracy of this detection technique was evaluated by performing a t-test analysis considering the HPLC method as a reference. The mean difference ($\overline{X_d}$) and the standard deviation of the difference (S_d) were calculated to be 0.366 and 0.237, respectively, for 3 samples (number of samples, =3). The absolute 't' (A_t) value was estimated to be 2.673 usig $T = \frac{\overline{X_d}}{S_d/\sqrt{N}}$ [63]. Based on the 't' distribution table, the critical 't' (C_t)value of 4.303 was obtained for a 95% confidence level, degree of freedom 2, and significance level of 0.05.

Since A_t is less than C_t, it can be inferred that there is no substantial deviation of the detection results of the proposed method in comparison to that of the reference HPLC method corresponding to the mean SA concentrations present in the three real samples.

Table 3.3

SA detection using the proposed MIP-AN@G electrode

Sample	Detected SA(μM)		[a]Error (%)	[b]Accuracy (%)
	Proposed method (Measured)	Ref. (HPLC) method (Actual)		
Cauliflower (CF)	46.53	46.84	0.66	99.34
Oregano (OG)	79.67	79.84	0.20	99.79
Black Olives (BO)	73.24	73.86	0.84	99.15

% [a] Error =[|Measured- Actual|)/Actual]100 ; % [b] Accuracy = 100- Error %

3.3.2.9 Comparative study- present method versus existing techniques

After a comprehensive literature survey, it was revealed that mostly HPLC techniques were used for the determination of SA. The LODs obtained from some of the studies are summarized in Table 3.4. It can be affirmed that the MIP-AN@G-based sensor offers the lowest LOD (0.32μM) as seen from the comparative summary presented in Table 3.4, where LOD is chosen as the primary parameter. Moreover, the HPLC methods have certain drawbacks, which have already been discussed earlier. Thus, one can think of deploying MIP-AN@G-based sensors for the determination of SA in real food samples in the industry.

Table 3.4

Comparative summary- present technique and existing methods

Techniques employed	LOD (μM)	Correlation Coefficient (R^2)	Refs
HPLC-UV	2.02	0.99	[16]
HPLC	1.95	0.997	[63]
HPLC	0.96	0.996	[64]
CV and DPV using MIP-AN@G	0.32	0.999	This work

3.4 Summary of Developed Syringic Acid Detection Methods

This chapter meticulously investigated two distinct methodologies for the accurate and efficient quantification of syringic acid (SGA) in various food samples. Both approaches underscore the growing demand for reliable and accessible analytical tools for phytochemical analysis.

3.4.2 UV-Vis Spectroscopy for Syringic Acid Quantification

The first method employed a UV-Vis spectroscopy technique coupled with multivariate analysis for the rapid and reliable assessment of SGA. This non-destructive method, operating in the 200-400 nm wavelength range, demonstrated its capability to effectively differentiate between samples. Principal Component Analysis (PCA) confirmed strong data clustering, achieving a high-class separability index of 313.52, indicating a clear qualitative distinction. For quantitative analysis, Principal Component Regression (PCR) and Partial Least Squares Regression (PLSR) models yielded exceptional average prediction accuracies of 99.78% and 99.69%, respectively, both with a high correlation factor (CF) of 0.99. This approach offers a simple and solvent-free method for the preliminary screening and quantification of SGA in complex matrices like cauliflower, oregano, and black olives.

3.4.3 Electrochemical Detection using MIP-AN@G Electrode

The second method focused on developing a highly sensitive and selective molecularly imprinted polymer (MIP) based electrochemical sensor, specifically the MIP-AN@G electrode, for syringic acid detection. This cost-effective and reusable sensor, characterized by UV-Vis, FTIR, and SEM, utilized DPV and CV techniques for analytical performance. The electrode demonstrated a wide linear range of 10 μM to 100 μM and a remarkably low LOD of 0.32 μM, showcasing significant sensitivity. Beyond its detection limits, the sensor exhibited high repeatability (RSD: 1.11%), reproducibility (RSD: 1.16%), and satisfactory stability (RSD: 1.89%). Its practical application in real food extracts (cauliflower, oregano, black olives) yielded high accuracies (above 99%) when validated against HPLC analysis, with supporting t-test results. This marks a significant advancement, being the first report of voltammetry combined with MIP technology for SA detection, offering a robust and selective solution for food quality assessment.

3.5 Conclusion

This chapter successfully showcased the development and validation of two distinct, yet highly effective, analytical platforms for the quantification of syringic acid in real food samples. The UV-Vis spectroscopy approach, enhanced by multivariate analysis, provides a rapid, non-

destructive, and solvent-free method with strong qualitative discrimination and high predictive accuracy, making it suitable for initial screening and routine analysis. Complementing this, the molecularly imprinted polyacrylonitrile-infused graphite electrode (MIP-AN@G electrode) represents a significant advancement in electrochemical sensing. This innovative sensor combines high sensitivity (exceptionally low LOD), excellent selectivity, and robust stability with a cost-effective and reproducible fabrication process. Its proven high accuracy in real food extracts, validated against established HPLC methods, underscores its potential for precise quantitative determination of SGA. Together, these methodologies offer versatile and practical solutions for the assessment of syringic acid content, addressing the critical need for efficient and accessible tools in food quality control and health-beneficial compound analysis.

References

[1] F. Liu, F.-B. Jiang, Y.-T. Li, R.-M. Liu, Z.-Y. Wu, and C.-W. Yan, "Cocrystallization with syringic acid presents a new opportunity for effectively reducing the hepatotoxicity of isoniazid," *Drug Development and Industrial Pharmacy*, vol. 46, pp. 988-995, 2020.

[2] M. M. Rob, K. Hossen, A. Iwasaki, K. Suenaga, and H. Kato-Noguchi, "Phytotoxic activity and identification of phytotoxic substances from Schumannianthus dichotomus," *Plants*, vol. 9, p. 102, 2020.

[3] C. Srinivasulu, M. Ramgopal, G. Ramanjaneyulu, C. Anuradha, and C. S. Kumar, "Syringic acid (SA)–a review of its occurrence, biosynthesis, pharmacological and industrial importance," *Biomedicine & Pharmacotherapy*, vol. 108, pp. 547-557, 2018.

[4] M. T. Bogert and J. Ehrlich, "The synthesis of certain substituted pyrogallol ethers, including a new acetophenetide derived from the ethyl ether of syringic acid," *Journal of the American Chemical Society*, vol. 41, pp. 798-810, 1919.

[5] J. M. Pezzuto, "Grapes and human health: a perspective," *Journal of agricultural and Food Chemistry*, vol. 56, pp. 6777-6784, 2008.

[6] L. A. Pacheco-Palencia, S. Mertens-Talcott, and S. T. Talcott, "Chemical composition, antioxidant properties, and thermal stability of a phytochemical enriched oil from Acai (Euterpe oleracea Mart.," *Journal of agricultural and Food Chemistry*, vol. 56, pp. 4631-4636, 2008.

[7] M. C. Gálvez, C. G. Barroso, and J. A. Pérez-Bustamante, "Analysis of polyphenolic compounds of different vinegar samples," *Zeitschrift für Lebensmittel-Untersuchung und Forschung*, vol. 199, pp. 29-31, 1994.

[8] O. Cikman, O. Soylemez, O. F. Ozkan, H. A. Kiraz, I. Sayar, S. Ademoglu, et al., "Antioxidant activity of syringic acid prevents oxidative stress in L-arginine–induced acute pancreatitis: an experimental study on rats," *International surgery*, vol. 100, pp. 891-896, 2015.

[9] A. C. Mirza and S. S. Panchal, "Safety evaluation of syringic acid: subacute oral toxicity studies in Wistar rats," *Heliyon*, vol. 5, p. e02129, 2019.

[10] T. Abe, E. Masai, K. Miyauchi, Y. Katayama, and M. Fukuda, "A tetrahydrofolate-dependent O-demethylase, LigM, is crucial for catabolism of vanillate and syringate in Sphingomonas paucimobilis SYK-6," *Journal of bacteriology*, vol. 187, pp. 2030-2037, 2005.

[11] G. Brauer and J. Stansbury, "Materials science cements containing syringic acid esters-o-Ethoxybenzoic acid and zinc oxide," *Journal of Dental Research,* vol. 63, pp. 137-140, 1984.

[12] O. Gimeno, L. A. Fernandez, M. Carbajo, F. Beltran, and J. Rivas, "Photocatalytic ozonation of phenolic wastewaters: Syringic acid, tyrosol and gallic acid," *Journal of Environmental Science and Health, Part A*, vol. 43, pp. 61-69, 2007.

[13] X. Wang, J. Wang, and N. Yang, "Flow injection chemiluminescent detection of gallic acid in olive fruits," *Food Chemistry*, vol. 105, pp. 340-345, 2007.

[14] K. Dhalwal, V. Shinde, Y. Biradar, and K. Mahadik, "Simultaneous quantification of bergenin, catechin, and gallic acid from Bergenia ciliata and Bergenia ligulata by using thin-layer chromatography," *Journal of food composition and analysis*, vol. 21, pp. 496-500, 2008.

[15] R. de Queiroz Ferreira and L. A. Avaca, "Electrochemical determination of the antioxidant capacity: the ceric reducing/antioxidant capacity (CRAC) assay," *Electroanalysis: An International Journal Devoted to Fundamental and Practical Aspects of Electroanalysis*, vol. 20, pp. 1323-1329, 2008.

[16] W. Ma, D. Han, S. Gan, N. Zhang, S. Liu, T. Wu, et al., "Rapid and specific sensing of gallic acid with a photoelectrochemical platform based on polyaniline–reduced graphene oxide–TiO 2," *Chemical Communications*, vol. 49, pp. 7842-7844, 2013.

[17] L. Wang, M. S. Halquist, and D. H. Sweet, "Simultaneous determination of gallic acid and gentisic acid in organic anion transporter expressing cells by liquid chromatography–tandem mass spectrometry," *Journal of Chromatography B*, vol. 937, pp. 91-96, 2013.

[18] D. P. Singh, R. Govindarajan, A. Khare, and A. K. Rawat, "Optimization of a high-performance liquid chromatography method for the separation and identification of six different classes of phenolics," *Journal of chromatographic science*, vol. 45, pp. 701-705, 2007.

[19] F. Al-Rimawi and I. Odeh, "Development and validation of an HPLC-UV method for determination of eight phenolic compounds in date palms," *Journal of AOAC International*, vol. 98, pp. 1335-1339, 2015.

[20] D. Wen, C. Li, H. Di, Y. Liao, and H. Liu, "A universal HPLC method for the determination of phenolic acids in compound herbal medicines," *Journal of agricultural and Food Chemistry*, vol. 53, pp. 6624-6629, 2005.

[21] N. Sharma, U. K. Sharma, A. P. Gupta, and A. K. Sinha, "Simultaneous determination of epicatechin, syringic acid, quercetin-3-O-galactoside and quercitrin in the leaves of Rhododendron species by using a validated HPTLC method," *Journal of food composition and analysis*, vol. 23, pp. 214-219, 2010.

[22] C. Sun, Y. Yuan, E. Omari-Siaw, S. Tong, Y. Zhu, Q. Wang, et al., "An efficient HPLC method for determination of syringic acid liposome in rats plasma and mice tissues: Pharmacokinetic and biodistribution application," *Current Pharmaceutical Analysis*, vol. 14, pp. 41-52, 2018.

[23] W. Sordoń, A. Salachna, and M. Jakubowska, "Voltammetric determination of caffeic, syringic and vanillic acids taking into account uncertainties in both axes," *Journal of Electroanalytical Chemistry*, vol. 764, pp. 23-30, 2016.

[24] R. C. Minussi, M. Rossi, L. Bologna, L. v. Cordi, D. Rotilio, G. M. Pastore, et al., "Phenolic compounds and total antioxidant potential of commercial wines," *Food Chemistry*, vol. 82, pp. 409-416, 2003.

[25] R. J. Robbins and S. R. Bean, "Development of a quantitative high-performance liquid chromatography–photodiode array detection measurement system for phenolic acids," *Journal of chromatography A*, vol. 1038, pp. 97-105, 2004.

[26] M.-Á. Rodríguez-Delgado, G. González-Hernández, J.-E. a. Conde-González, and J.-P. Pérez-Trujillo, "Principal component analysis of the polyphenol content in young red wines," *Food Chemistry*, vol. 78, pp. 523-532, 2002.

[27] E. Kilinc and H. Kalkan, "High-performance liquid chromatographic determination of some phenolic acids of Turkish commercial wines: an electrochemical approach," *Journal of Wine Research*, vol. 14, pp. 17-23, 2003.

[28] M. Rossouw and J. Marais, "The phenolic composition of south African Pinotage, Shiraz and Cabernet Sauvignon wines," *South African Journal of Enology and Viticulture*, vol. 25, pp. 94-104, 2004.

[29] G. L. La Torre, M. Saitta, F. Vilasi, T. Pellicanò, and G. Dugo, "Direct determination of phenolic compounds in Sicilian wines by liquid chromatography with PDA and MS detection," *Food Chemistry*, vol. 94, pp. 640-650, 2006.

[30] S. Nag, D. Das, H. Naskar, B. Tudu, R. Bandyopadhyay, and R. B. Roy, "Detection of Metanil Yellow Adulteration in Turmeric Powder Using Nano Nickel Cobalt Oxide Modified Graphite Electrode," *IEEE Sens. J.*, vol. 22, pp. 12515-12521, 2022.

[31] S. Nag, H. Naskar, S. Pradhan, R. Chatterjee, V. Sharma, B. Tudu, et al., "Formalin Detection using Platinum Electrode-Based Electrochemical System," *Journal of The Institution of Engineers (India): Series B*, pp. 1-7, 2022.

[32] S. Nag, S. Pradhan, H. Naskar, R. B. Roy, B. Tudu, P. Pramanik, et al., "A simple nano cerium oxide modified graphite electrode for electrochemical detection of formaldehyde in mushroom," *IEEE Sens. J.*, vol. 21, pp. 12019-12026, 2021.

[33] H. Karimi-Maleh, M. Alizadeh, Y. Orooji, F. Karimi, M. Baghayeri, J. Rouhi, et al., "Guanine-based DNA biosensor amplified with Pt/SWCNTs nanocomposite as analytical tool for nanomolar determination of daunorubicin as an anticancer drug: a docking/experimental investigation," *Industrial & Engineering Chemistry Research*, vol. 60, pp. 816-823, 2021.

[34] H. Karimi-Maleh, Y. Orooji, F. Karimi, M. Alizadeh, M. Baghayeri, J. Rouhi, et al., "A critical review on the use of potentiometric based biosensors for biomarkers detection," *Biosensors and Bioelectronics*, vol. 184, p. 113252, 2021.

[35] S. Tajik, H. Beitollahi, H. W. Jang, and M. Shokouhimehr, "A screen printed electrode modified with Fe3O4@ polypyrrole-Pt core-shell nanoparticles for electrochemical detection of 6-mercaptopurine and 6-thioguanine," *Talanta*, vol. 232, p. 122379, 2021.

[36] Y. Orooji, P. N. Asrami, H. Beitollahi, S. Tajik, M. Alizadeh, S. Salmanpour, et al., "An electrochemical strategy for toxic ractopamine sensing in pork samples; twofold amplified nano-based structure analytical tool," *Journal of Food Measurement and Characterization*, vol. 15, pp. 4098-4104, 2021.

[37] S. Tajik, H. Beitollahi, F. G. Nejad, Z. Dourandish, M. A. Khalilzadeh, H. W. Jang, et al., "Recent developments in polymer nanocomposite-based electrochemical sensors for detecting environmental pollutants," *Industrial & Engineering Chemistry Research*, vol. 60, pp. 1112-1136, 2021.

[38] D. A. Skoog, F. J. Holler, S.R.Crouch, Principles of Instrumental Analysis, 7th ed., Cengage learning , pp. 303-348 , January 2017.

[39] S. Nag, D. Das, B. Tudu and R. B. Roy, "Multivariate Analysis of Formalin Using UV-Vis Spectroscopy," *2021 IEEE Second International Conference on Control, Measurement and Instrumentation (CMI)*, pp. 133-137, March 2021.

[40] P. B. Garcia-Allende, O. M. Conde, J. Mirapeix, A. M. Cubillas, and J. M. Lopez-Higuera, "Data processing method applying principal component analysis and spectral angle mapper for imaging spectroscopic sensors," *IEEE Sens. J.*, vol. 8, pp. 1310–1316, July 2008.

[41] S. Nag. et al. "Formalin detection using platinum electrode-based electrochemical system," J. Inst. Eng. (India): B, pp.1-7, February 2022.

[42] D. Bandyopadhyay et al. ," Voltammetric Detection of Inositol Using a Platinum Based Electrode," *Nano LIFE*, vol. 12, pp. 2250004-1 -2250004-8, March 2022.

[43] F. Harrou, Y. Sun, M. Madakyaru, and B. Bouyedou, "An improvedmultivariate chart using partial least squares with continuous ranked probability score," *IEEE Sens. J.*, vol. 18, pp. 6715–6726, June 2018.

[44] U. Depczynski, V. J. Frost, and K. Molt, "Genetic algorithms applied to the selection of factors in principal component regression," *Anal. Chim. Acta*, vol. 420, pp. 217–227, September 2000.

[45] N. Yang, F. Qiu, F. Zhu, Feng & L. Qi , " Therapeutic potential of zinc oxide-loaded syringic acid against in vitro and in vivo model of lung cancer," *Int. J. Nanomedicine*., vol. 15, pp. 8249-8260 , October 2020.

[46] R. Holser, "Lipid Encapsulated Phenolic Compounds by Fluidization," *J. encapsulation adsorpt*. sci., vol. 3, pp. 13-15, March 2013.

[47] H. Naskar, S. Biswas, B. Tudu, R. Bandyopadhyay, and P. Pramanik, "Voltammetric detection of thymol (THY) using polyacrylamide embedded graphite molecular imprinted polymer (PAM@ G-MIP) electrode," *IEEE Sens. J.*, vol. 19, pp. 8583-8589, 2019.

[48] S. Nag, S. Pradhan, D. Das, B. Tudu, R. Bandyopadhyay, and R. B. Roy, "Fabrication of a Molecular Imprinted Polyacrylonitrile Engraved Graphite Electrode for Detection of Formalin in Food Extracts," *IEEE Sens. J.*, vol. 22, pp. 42-49, 2021.

[49] A. Jenab, R. Roghanian, N. Ghorbani, K. Ghaedi, and G. Emtiazi, "The efficacy of electrospun PAN/Kefiran nanofiber and kefir in mammalian cell culture: promotion of PC12 cell growth, anti-MCF7 breast cancer cells activities, and cytokine production of PBMC," *International Journal of Nanomedicine*, vol. 15, p. 717, 2020.

[50] F. Nacimiento, R. Alcántara, J. R. González, and J. L. Tirado, "Electrodeposited polyacrylonitrile and cobalt-tin composite thin film on titanium substrate," *Journal of The Electrochemical Society*, vol. 159, p. A1028, 2012.

[51] H.-l. Wu, D. H. Bremner, H.-y. Li, Q.-q. Shi, J.-z. Wu, R.-q. Xiao, et al., "A novel multifunctional biomedical material based on polyacrylonitrile: Preparation and characterization," *Materials Science and Engineering: C*, vol. 62, pp. 702-709, 2016.

[52] M. A. Al Faruque, R. Remadevi, A. Guirguis, A. Kiziltas, D. Mielewski, and M. Naebe, "Graphene oxide incorporated waste wool/PAN hybrid fibres," *Scientific reports*, vol. 11, pp. 1-12, 2021.

[53] A. B. D. Nandiyanto, R. Oktiani, and R. Ragadhita, "How to read and interpret FTIR spectroscope of organic material," *Indonesian Journal of Science and Technology*, vol. 4, pp. 97-118, 2019.

[54] T. N. Chatterjee, D. Das, R. B. Roy, B. Tudu, A. K. Hazarika, S. Sabhapondit, et al., "Development of a nickel hydroxide nanopetal decorated molecular imprinted polymer based electrode for sensitive detection of epigallocatechin-3-gallate in green tea," *Sensors and Actuators B: Chemical*, vol. 283, pp. 69-78, 2019.

[55] B. Balan, A. S. Dhaulaniya, R. Jamwal, K. K. Sodhi, S. Kelly, A. Cannavan, et al., "Application of Attenuated Total Reflectance-Fourier Transform Infrared (ATR-FTIR) spectroscopy coupled with chemometrics for detection and quantification of formalin in cow milk," Vibrational Spectroscopy, vol. 107, p. 103033, 2020.

[56] S. S. Hassan, H. I. A. Shafy, M. S. Mansour, and H. E. Sayour, "Quercetin recovery from onion solid waste via solid-phase extraction using molecularly imprinted polymer nanoparticles," *International Journal of Food Engineering*, vol. 15, 2019.

[57] I. Degen, "Detection of the methoxyl group by infrared spectroscopy," *Applied Spectroscopy*, vol. 22, pp. 164-166, 1968.

[58] A. Peyravi, M. P. Gashti, and S. H. Hosseini, "Chemical grafting of disperse dyes onto polyacrylonitrile: A novel method for coloration of fibers," *Fibers and Polymers*, vol. 15, pp. 2307-2312, 2014.

[59] N. Yang, F. Qiu, F. Zhu, and L. Qi, "Therapeutic potential of zinc oxide-loaded syringic acid against in vitro and in vivo model of lung cancer," *International Journal of Nanomedicine*, vol. 15, p. 8249, 2020.

[60] E. Laviron, "General expression of the linear potential sweep voltammogram in the case of diffusionless electrochemical systems," *Journal of Electroanalytical Chemistry and Interfacial Electrochemistry*, vol. 101, pp. 19-28, 1979.

[61] X. Li, Y. Gao, H. Xiong, and Z. Yang, "The electrochemical redox mechanism and antioxidant activity of polyphenolic compounds based on inlaid multi-walled carbon nanotubes-modified graphite electrode," *Open Chemistry*, vol. 19, pp. 961-973, 2021.

[62] S. Ngamchana and W. Surareungchai, "Sub-millimolar determination of formalin by pulsed amperometric detection," *Analytica chimica acta*, vol. 510, pp. 195-201, 2004.

[63] U. K. R. Jain Vandana Neeraj, "Novel hplc method for determination of polyphenols in agro-industrial waste of date fruits," *International Journal of Advanced Research*, vol. 8, pp. 626-634, 2020.

[64] T. Seal, "Quantitative HPLC analysis of phenolic acids, flavonoids and ascorbic acid in four different solvent extracts of two wild edible leaves, Sonchus arvensis and Oenanthe linearis of North-Eastern region in India," *Journal of Applied Pharmaceutical Science*, vol. 6, pp. 157-166, 2016.

PUBLICATION STATUS

JOURNAL

- D. Bandyopadhyay, S. Nag, D. Das, and R. B. Roy, "Detection of syringic acid in food extracts using molecular imprinted polyacrylonitrile infused graphite electrode," *Journal of food composition and analysis*, vol. 132, p. 106280, Aug. 2024, doi:10.1016/j.jfca.2024.106280.

Electrochemical detection of Folic Acid in Food Extracts Using Molecularly Imprinted Polyacrylonitrile Imbued Graphite Electrode

4

4.1 Introduction

Water-soluble vitamin B-complex, like folic acid (FA) or folate derivatives, has grabbed the attention of researchers and medical sectors owing to their immense health benefits [1]-[2]. As depicted in Fig. 4.1, the molecular structure of FA(IUPAC name :(2S)-2-[[4-[(2-amino-4-oxo1Hpteridinyl) methylamino] benzoyl] amino] pentanedioic acid) reveals the presence of tri-components: a pteridine section linked through p-aminobenzoic acid to L-glutamic acid [3]. FA must be acquired through dietary supplements or other sources, namely green leafy vegetables, liver, yolk, kidney beans, and fresh fruits [4]. FA plays a pivotal role in the synthesis, methylation, and repair of DNA, cell proliferation, regeneration, cell assimilation, and biological methylation [5]-[6]. As per the guidelines from the Harvard T.H. Chan School of Public Health, the recommended daily allowance of FA for adults above 19 years, lactating and pregnant women, varies from 400-1000 µg of dietary folate equivalents (DFE) [7]. The deficiency of FA may lead to vitamin deficits in the body and may cause many degenerative conditions like megaloblastic anemia and neural tube defects during embryo development [8]. While FA in acceptable amounts in supplements can be used in the treatment of psoriasis [9], dermatomyositis [10], polymyositis [11], and rheumatoid arthritis [12] but high dosages may boost the risk of cancer, and stimulate preneoplastic as well as undiagnosed neoplastic lesions progression [13]. Daily consumption of FA through commercially accessible supplements is recommended for pregnant women to combat neural disorders in developing fetuses [14]. FA can not only decrease the threat of cardiovascular abnormalities by decreasing the level of blood homocysteine [15] but also can promote red blood cell (RBC) formation in the body [16].

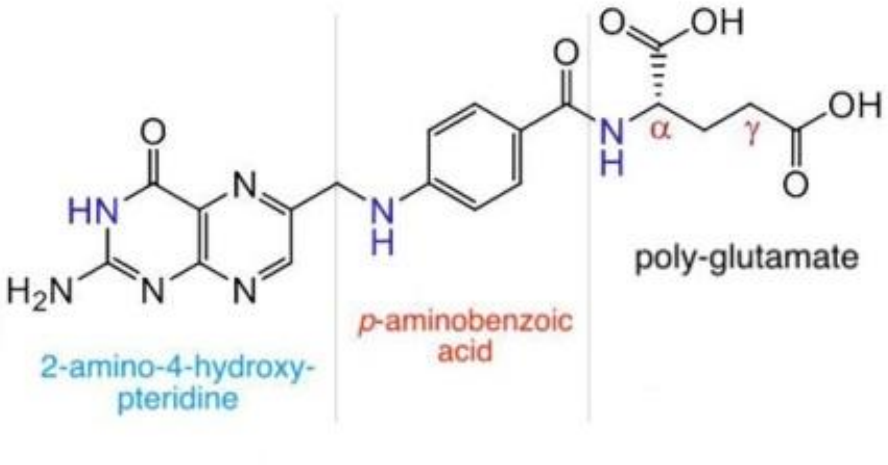

Fig. 4.1. FA: Chemical structure

In today's economy, hazardous chemicals are routinely used during harvest and nurturing seasons to increase profits. As these hazardous species modulate different pharmacological processes on biochemical reactions, they can impede the nutritional and medical value of vitamins like FA. Consequently, it is the need of the hour to nourish and assess fruits, multivitamin dietary supplements, vegetables, and other fortified food qualities by quantifying the concentrations of specific health-valuable molecules like FA, albeit their concentration may be very low in the real food samples. Appreciating the colossal medical significance of FA, there is an obligatory requisite for cost-effective and at the same time stable, sensitive, reusable, and easy-to-use sensors for the quantitative assessment of FA in real food extracts. The plethora of various conventional detection methods, employing laboratory instrumentations viz. electrophoresis [17], colorimetry [18], high-performance liquid chromatography(HPLC) [19] with mass spectroscopy [20], fluorescence [21], UV spectrophotometric method [22], Dual-emission fluorescence nanoprobe [23], HPLC–UV method [24], RP-HPLC determination[25], FTIR spectroscopy[26], chemiluminescence detection [27], and green synthesized copper oxide nanoparticles and Electro-Poly (Methyl Orange) Sensor[28] have been reported in last few decades. However, most of these methods suffer from drawbacks such as the involvement of exorbitantly high-end sophisticated instrumentation, the application of organic toxic solvents throughout the experiments, and the obligation of highly skilled operators for experimentation. Contrary, one of the potential cost-effective yet fast and simple solutions in such instances turns out to be the electrochemical detection of health-beneficial compounds. Few electrochemical sensors were reported where carbon paste electrodes, copper oxide (CuO) nanoparticle-infused single-walled carbon nanotubes (CuO/SWCNTs) nano-composites, along with 1-butyl-3-methylimidazolium hexafluorophosphate and Fe_3O_4@SiO_2-graphite nanocomposite modified

graphite were employed for the detection of folate [29]-[30]. An optical FA sensor was introduced by Ensafi et al. [31] in 2017 based on molecularly imprinted polymers on dual-color CdTe quantum dots. However, some of the sensors exhibit moderate selectivity and involve complex fabrication processes. Moreover, the application areas of those sensors are quite different. In recent times, numerous studies have divulged that molecularly imprinted polymer (MIP) technology can be widely used to boost the selectivity, reproducibility, and repeatability of the sensors [32]. Specific active recognition sites bearing cross-linked polymers known as MIPs are formed by synthetic or natural monomer polymerization [33]. MIP technology embracing molecular memory offers the intrinsic advantages of manufacturing simplicity, reusability, high selectivity, and high mechanical strength, and is thus employed nowadays for several food constituents' detection applications [34]. Few studies report the employment of MIP technology in the electrochemical detection of FA [35]-[36]. Molybdenum carbide (Mo_2C) modified glassy carbon electrode (GCE) had been utilized in electrochemical sensing of folic acid by imprinting technology [37]. In [38], FA was opto-sensed using quantum dot-labeled hydrophilic MIP nanoparticles in real biological samples. A sol-gel method was employed for the determination of FA in tomatoes by core-shell SiO_2-coated Fe_3O_4 having surface MIP coating [39]. A molecularly imprinted dimethylsiloxane elastomer and novel core@shell magnetic molecular imprinted nanoparticle had been proposed in [40]-[41] for FA recognition in different food samples. While several well-calibrated sensors have been developed, their application areas are specific and vary greatly from one sensor to another. Moreover, some of these techniques are complex, time-consuming, and suffer from a narrow linearity range, poor reproducibility, and the likelihood of chemical contamination.

This chapter emphasizes fabrication and detection characteristics assessment of poly-acrylonitrile (PAN) based MIP electrode (MAN@G) for the detection of FA traces in real food samples. This research has brought scientific innovation by introducing cost-effective yet sensitive electrochemical sensors based on MIPs for the selective quantification of FA. Among the three monomers, acrylic acid (AA), acrylonitrile (AN), and acrylamide (AM), the AN-based MIP electrode, i.e., MAN@G, offered the highest peak oxidation current. AN is one of the highly reactive monomers owing to the existence of a nitrile functional group, which promotes the template and monomer interaction during the pre-polymerization stage [34]. So, AN was chosen to be a suitable monomer for the development of the electrode. The fabricated MAN@G electrode could exhibit a widespread linearity range with an acceptable LOD compared to that reported in existing works. Rigorous analyses of the analytical performances of the electrode

revealed enduring stability, satisfactory repeatability, and reproducibility. Furthermore, the detection proficiency of the electrode was affirmed after testing in real food extracts, specifically orange, spinach, papaya, soybean, and cooked rice, as an average accuracy of 99% was achieved when compared to the HPLC method. Moreover, satisfactory results were observed when analyzed using the statistical tool t-test method. It has been established that the proposed electrode can be a promising candidate for the detection of FA in real food samples in the food industry.

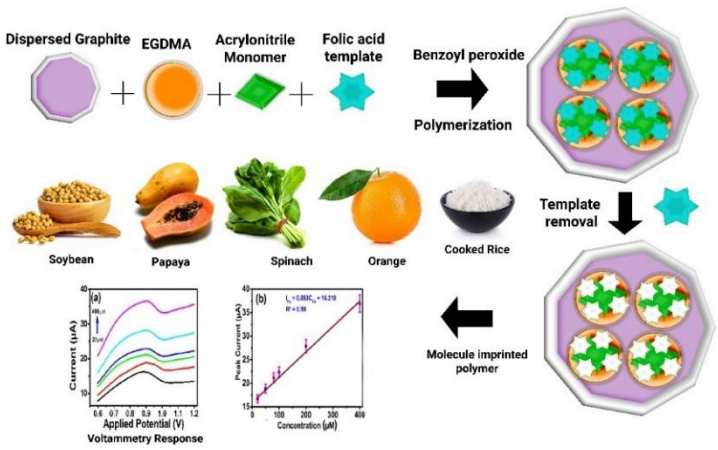

4.2 Experimental section

4.2.1 Chemical reagents and standards

Tokyo Chemical Industry Chemicals Pvt. Ltd., India, provided the FA ($C_{19}H_{19}N_7O_6$). The monomers (acrylic acid (AA), acrylonitrile (AN), acrylamide (AM)), fine graphite triturate (99% pure), as well as ethylene glycol dimethyl acrylate (EGDMA), were procured from Sigma Aldrich, USA. Benzoyl peroxide was supplied by Merck Specialities Pvt. Ltd. (India). The preparations of acetate buffer saline (ABS), citrate buffer saline (CBS), and phosphate buffer saline (PBS), having pHs 5, 6 as well and 7, were carried out in the laboratory. Paraffin oil and ethanol, offered by Merck & Co., were used as a binder and solvent, respectively, during the sensor development and testing. Since analytical grade chemicals are involved, no prior purification processes are required. Distilled water (Resistance value: 18 MΩ) was amassed from a Millipore water-purification system to wash the electrodes and supplementary chemical utensils during the experimentations.

4.2.2 Characterization details and equipment specifications

To investigate and evaluate the performance of the developed electrodes, a tri-electrode system coupled with Autolab (Metrohom Autolab, Netherlands) Potentiostat/Galvanostat

PGSTAT101 was employed. Platinum (Pt) electrode, Ag/AgCl electrode, and most importantly, MAN@G electrode were preferred as counter, reference, and working electrodes, respectively. Even though the measurement analysis has been pursued for the voltage window of 0.1 to 1.2V through differential pulse voltammetry (DPV) and cyclic voltammetry (CV), for a clear depiction of the oxidation peaks, it was restricted from 0.6 V to 1.2 V. For examining surface morphologies along with the chemical composition characteristics of the synthesized sample, a scanning electron microscope (SEM, ZEISS EVO 18, US), operated at an acceleration voltage of 15 kV was introduced. Moreover, a double-beam Shimadzu (UV-3600) was employed to inspect the Ultraviolet-visible (UV-Vis) absorption spectra.

4.2.3 Non-imprinted polymer (NAN@G) and molecularly imprinted polymer (MAN@G) preparation

0.9 g of graphite powder was dispersed in ethanol (15 ml), and the solution was subjected to 1-hour sonication using an ultrasonicator. Thereafter, monomer AN and template FA, each weighing 0.05 g, were poured into it, and the solution was subjected to a further 1 hr sonication. Then, a polymerization initiator (PI), Benzoyl peroxide (1 mg), along with 400 µL of crosslinker EGDMA, was added to the mixture, and re-sonication was performed for nearly 45 minutes. The amount of monomer, PI, and crosslinker was optimized in the earlier studies [33]. The mixture was transferred to a water bath later, and a temperature of 35 °C was set to initiate the polymerization process. Next, to wash and leach out the traces of FA molecules, the resultant polymerized material was periodically filtered (5 - 10 minutes interval) by washing in an ethanol-water mixture (ratio of 70:30) for an optimized duration of 48 hrs. The preservation of the electrode MIP material has been done at room temperature after drying. The electrode material is now ready for sensor development. The synthesizing procedure of the NIP follows the same steps as MIP, except for template (FA) amalgamation in the second step.

4.2.4 MAN@G and NAN@G electrodes fabrication

The working electrode was developed by stuffing smooth, fine MIP/NIP powdered paste in capillary glass tubes (1.25 mm inner dia.) using thin metallic rods. The powdered paste was obtained by mortaring the synthesized material for about 1 hr. 3-4 drops of paraffin oil were added while mortaring for binding purposes. Copper wires were connected from the capillary tubes for the sake of electrical connections.

4.2.5 Real sample extract preparation

Five samples, namely orange, spinach, papaya, soybean, and rice, were procured from the local market. The rice was boiled prior to making the test solutions. Each sample, weighing 1 g, was

blended in 100 mL of water. Filtration was performed thereafter with a disposable sterile syringe filter of Whatman UNIFLO (diameter: 25 mm, pore size: 0.22 µm), which consists of a polyvinylidene fluoride (PVDF) filter membrane in a polypropylene base. The extracted solution was subjected to HPLC and DPV analysis. In the HPLC analysis of the aliquots, column BioSute C 18 (4.6 x 150 mm) with 5 µm particle size Agilent 1290 infinity II DAD detector was employed and operated at ambient temperature. The mobile phases involved were a) 0.1% Trifluoroacetic acid (TFA) in H_2O and b) 90% acetonitrile (ACN). The flow rate of 1 ml min^{-1} was set for the entire 15 minutes of run-time.

4.3 Results with discussions

4.3.1 Optimization of the monomer

To prepare the MIP samples of the corresponding electrodes, three sundry monomers, acrylic acid (AA), acrylonitrile (AN), and acrylamide (AM) have been selected. A comprehensive fabrication procedure has been discussed in the preceding section. For all the electrodes, an irreversible redox peak has been observed around 0.85 V, as shown in Fig. 2; the CV characteristics were obtained in the presence of 100 µM analyte FA molecule-buffer solution at 50 mV/s. A meticulous observation from Fig. 4.2 reveals that the MAN@G electrode offers the highest peak oxidation current, almost 4.01 and 1.85 times higher in comparison to that of AA and AM electrodes, respectively. In the pre-polymerization stages, monomer-analyte or dipole-dipole interactions influence the electrochemical behavior of the MIP, which aids the FA recognition course near the MAN@G electrode surface [34]. Hence, the monomer AN and the corresponding MAN@G were elected as apposite candidates for the recognition and quantification of FA in the subsequent experimental steps.

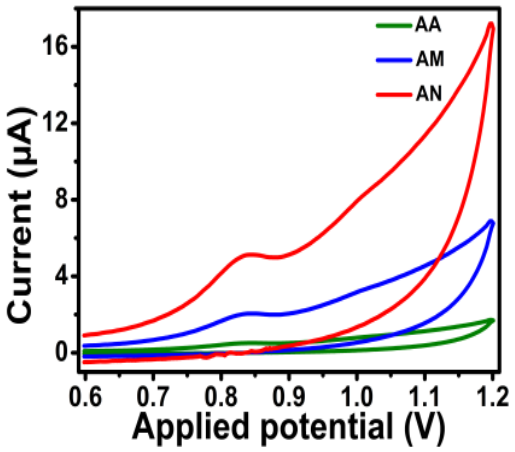

Fig. 4.2. Plot of current versus applied potential (CV) for different monomers (AA, AM, and AN) recorded for 100 µM FA solution at room temperature.

4.3.2 Synthesized Polymer Material Characterization

4.3.2.1 UV-Vis spectroscopy analysis

The UV-Vis spectroscopy analysis has been performed for the wavelength window of 220 nm -400 nm to endorse the leaching out of the FA molecule after wash. The spectral surveillance of Fig. 4.3 portrayed multiple absorption peaks at 256.2 nm, 278.1 nm, and 368.8 nm (close to that testified in [42]) for before-wash (MBW) material which was lacking in the case of after-wash (MAW) material. Based on the presence of absorption peak, it was inferred whether there is any presence of QCN molecule in the polymerised material. It has been observed that after 48-hours, almost complete leaching-out of the FA molecule occurred. Thus, it was affirmed that there are no or minimal traces of FA in the MIP material.

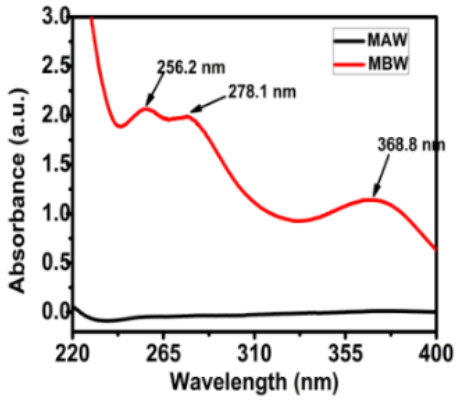

Fig. 4.3. Plot of UV-vis absorption spectra for MIP material before (MBW) and after template washing (MAW).

4.3.2.2 SEM studies for morphological insights

SEM studies explored the surface morphological insights of the MAN@G and NAN@G synthesized electrode materials. Fig. 4.4(b) reveals the MAN@G surface is noticeably creased compared to that of the NAN@G in Fig. 4.4(a). This may be due to the formation of imprinted craters.

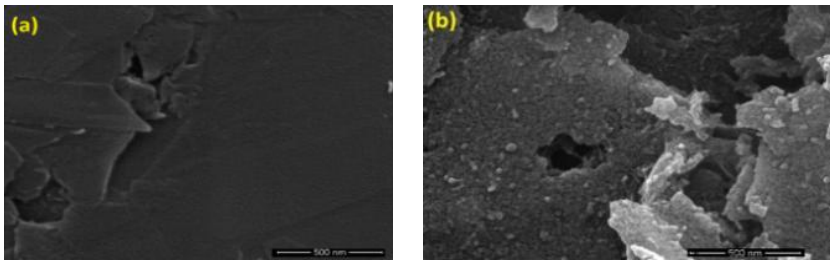

Fig. 4.4. Surface morphological images acquired from SEM measurements for (a) NAN@G and (b) MAN@G electrode materials.

4.3.2.3 Buffer and pH optimization

Primarily, three different buffers namely phosphate-buffered saline (PBS), acetate-buffered saline (ABS), and citrate-buffered saline (CBS) each of 9 ml and 1 ml of analyte, FA were employed to investigate the effect of buffers on the electrochemical characteristics of the MAN@G electrode. The CV characteristics (Fig. 4.5(a)) divulged a maximum oxidation peak current of 5.129 µA for PBS buffer. Furthermore, the influence of pH on MAN@G electrode characteristics was investigated for three different pH values (5, 6, and 7) of PBS buffer. Fig. 4.5(b) reveals that the optimum electrode response was recorded for PBS 7 in terms of maximum oxidation peak current. Hence, PBS 7 was used for the following experiments.

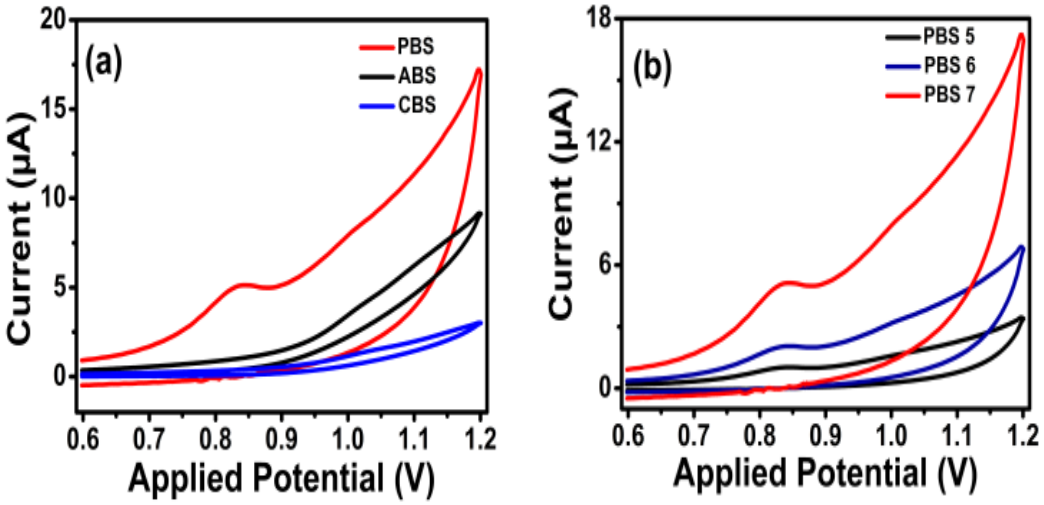

Fig. 4.5. CV plots for (a) buffer variation (PBS, ABS, and CBS) and (b)PBS pH variation 5, 6, and 7) recorded for 100 µM FA solution at room temperature.

4.3.2.4 Electrochemical performance of MIP-AN@G electrode

The electrochemical characteristics of the MAN@G electrode was evaluated in two stages. The first phase deals with the investigation of the electrochemical activities of the MAN@G and NAN@G electrodes in the post-oxidation stage of FA. The CV data were recorded in the voltage window of 0.6 V – 1.2 V with a 50 mV/s scan rate. Peak currents of about 5.129 µA and 2.306 µA were recorded for MAN@G and NAN@G electrodes, respectively. Fig. 4.6(a) depicts a heightened oxidation peak in the case of MAN@G (2.224 times greater) compared to the NAN@G electrode at the oxidation potential of 0.85 V. This may be attributed to enhanced FA oxidation owing to more analyte adsorption promoted by the molecule-specific recognition sites entrenched within the MIP material. In the second phase, to further explore the electrochemical performance of the MAN@G electrode, CV responses were acquired both in the presence (100 µM FA) and in the absence of the FA molecules in the 0.1 M PBS 7 buffer solution.

Under similar ambient conditions, a more distinct noticeable oxidation peak, as portrayed in Fig. 4.6(b), was detected in the presence of the FA compared to that obtained in the absence of FA.

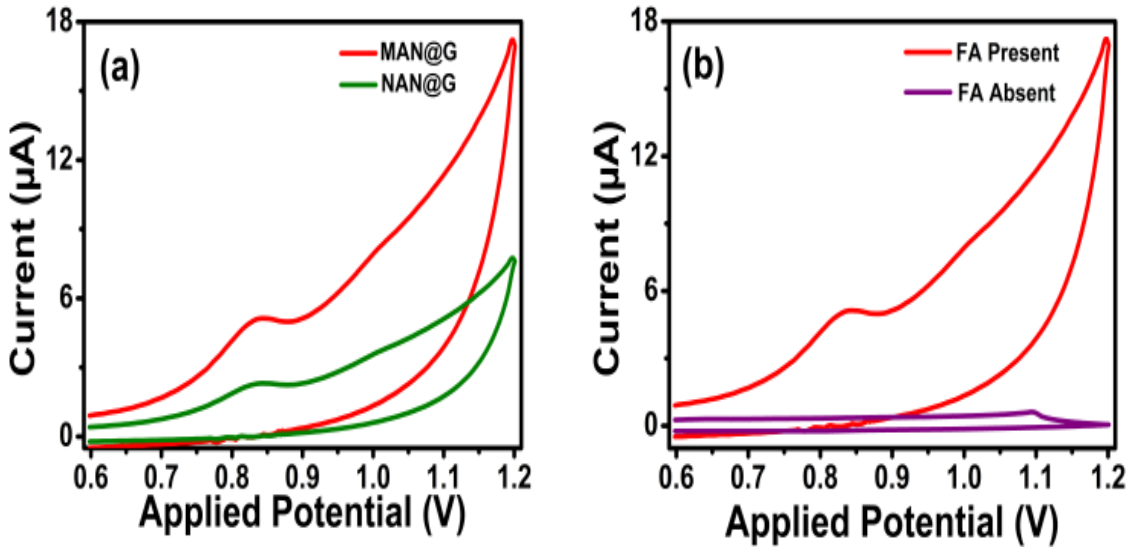

Fig. 4.6. CV responses of (a) MAN@G and NAN@G electrode in 100 μM solution containing 1 ml target analyte, FA (b) MAN@G in the presence and absence of FA molecule. The experimentation has been performed at room temperature.

4.3.2.5 Influence of scan rate variation

The impact of scan rate variation on the CV characteristics of the MAN@G electrode interface in the presence of 100 μM FA concentration is portrayed in Fig. 4.7(a). CV responses were recorded for a range of scan rates from 10 mV/s to 400 mV/s. It can be inferred from the figure that the oxidation peak current of FA increases with the increase in the scan rate. This asserts the occurrence of a surface-controlled oxidation process of FA at the MIP electrode surface. Further, Fig. 4.7(b) depicts a linear variation of anodic peak current (I_{FA}) with the scan rate obeying a linear regression equation (1).

$$I_{FA} = 15.432\upsilon + 2.514; R^2 = 0.99 \quad (1)$$

Langmuir Isotherm equation quantifies the number of electrons transported during the electrochemical oxidation of FA (2) [43].

$$I_{FA} = \frac{nFQ\upsilon}{4RT} = \frac{n^2F^2A\upsilon\Gamma_c}{4RT} \quad (2)$$

where R, T, n, Q, F, υ, and Γ_c represent universal gas constant, room temperature, no. of transferred electrons, consumed charge quantity during the oxidation, Faraday's constant, no. of transferred electrons, scan rate, and surface concentration of FA respectively. The value of Γ_c

and 'n' was computed to be 5.562×10^{-6} mole/cm² and 2, thereby asserting the occurrence of a double electron adsorption process [44]. The linear variation of the peak oxidation potential (E_p) with the logarithm of scan rate ($log\upsilon$) is illustrated in Fig. 4.7(c). It was witnessed that it varies linearly along with log, conforming to a linear regression equation (3)

$$E_P = 0.037log\upsilon + 0.879; R^2 = 0.99 \quad (3)$$

For an irreversible process, the gradient (G) of this equation can be alternatively expressed as

$$G = \frac{2.303RT}{\alpha nF} \quad (4)$$

The rate of electron transfer was estimated to be $0.747s^{-1}$ using Laviron's equation (5), which signifies the extent of chemical reversibility of the electrochemical phenomenon.

$$gk_s = \alpha log(1-\alpha) + (1-\alpha)log\alpha - \left(\frac{logRT}{nFv}\right) - \left(\frac{nF\Delta E_P\alpha(1-\alpha)}{2.303RT}\right) \quad (5)$$

From equation (4), the product of 'n' and charge transfer coefficient 'α', i.e., 'αn', was estimated to be 1.6, which complies with that reported in existing literature [44].

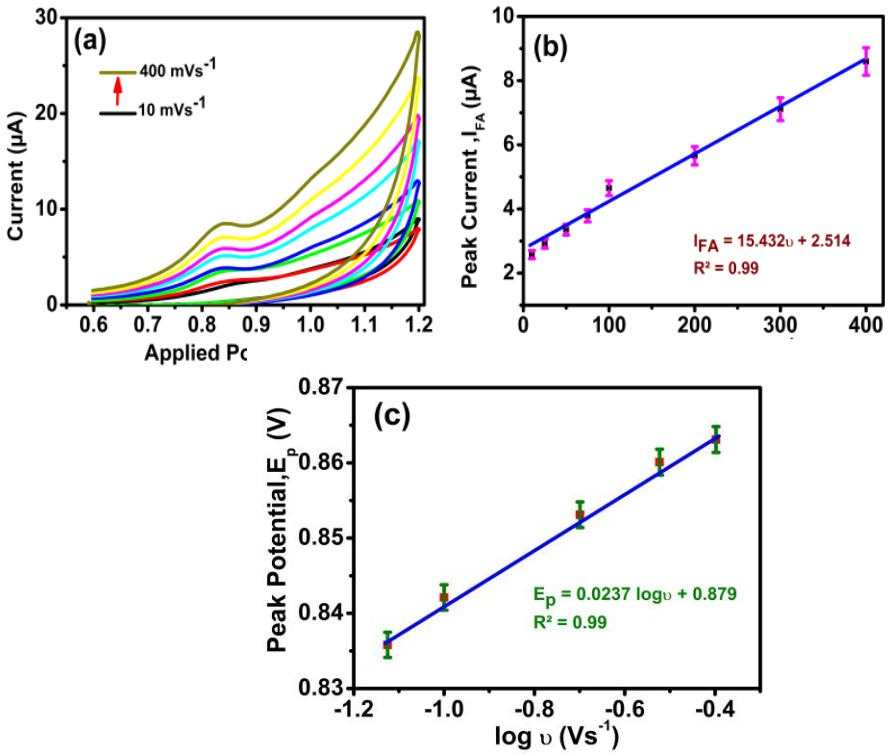

Fig. 4.7. (a).CV responses of MAN@G electrode in PBS of pH 7 at room temperature (b) peak oxidation current variation under the influence of scan rate (SR) when SR varied from 10 – 400 mVs^{-1} (b) Peak current (I_{FA}) - SR variation (Linear plot) (c) Linear plot of peak potential (E_p) versus logarithm of SR.

4.3.2.6 Calibration analysis and limit of detection

The concentration variation of FA (C_{FA}) in the test solution also turned out to be modulating the MAN@G electrode characteristics. Fig. 4.8(a) depicts the DPV responses within the optimized potential window of 0.6 V to 1.2 V for different FA concentrations in PBS 7 solution. With the increase in FA concentration (C_{FA}) from 20 to 400 µM, a progressive ascent in anodic peak current (I_{FA}) was noticed at 50 mV/s which is portrayed in Fig. 4.8(a). Moreover, the calibration plot of Fig. 4.8(b) unveils linear anodic peak current variation for 10 µM to 100 µM FA concentration variation. The corresponding linear regression equation (6) can be expressed as

$$I_{FA} = 0.053C_{FA} + 16.210; R^2 = 0.99 \quad (6)$$

With reference to equation (6), the lower limit of FA detection (LOD) and the lower limit of FA quantification (LOQ) were computed to be 18 nM and 60 nM, employing the following well-known expressions: $LOD = 3\frac{\sigma_{FA}}{m_{FA}}$ and $LOQ = 10\frac{\sigma_{FA}}{m_{FA}}$[45]-[46] where m_{FA} and σ_{FA} symbolize the gradient of the calibration line and the standard deviation of the peak current for the lowest quantified FA concentration. The low value of LOD connotes the FA detection efficacy of the MAN@G electrode.

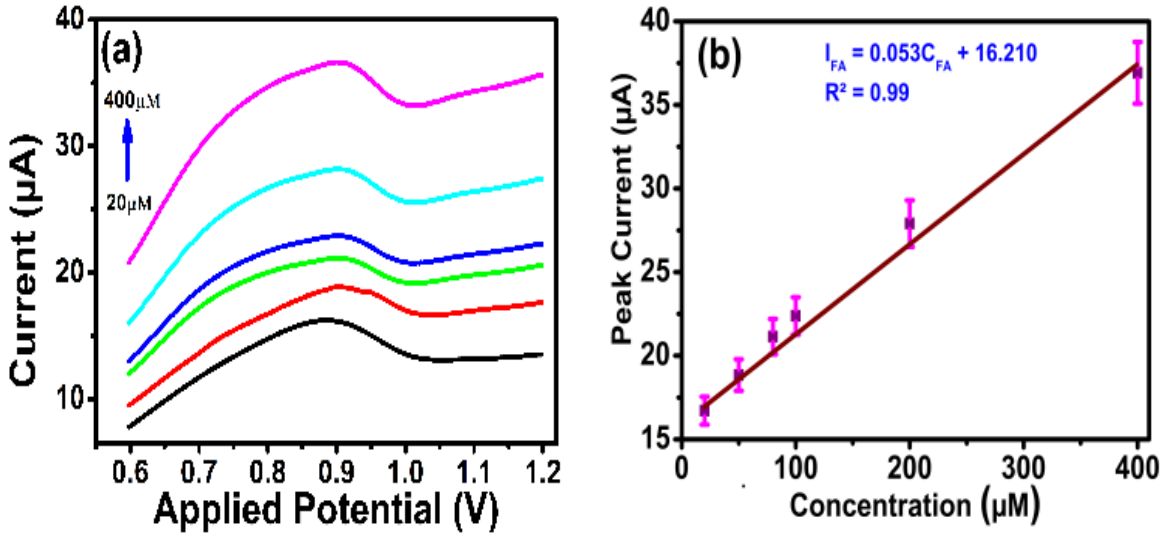

Fig. 4.8. (a). DPV profile of MAN@G electrode surface recorded in PBS 7 (for different FA and (b)Linear concentrations (dipping time was considered to be 2 minutes between two runs) at room temperature, profile of Peak current (I_{FA}) versus FA concentration (C_{FA}).

4.3.2.7 Investigations on Repeatability, Stability, and Reproducibility

To investigate the MAN@G sensor reliability, repeatability, reproducibility, and most importantly, stability studies have been explored in a 100 µM solution of FA in 0.1M PBS 7. In the first phase, repeatability analysis was carried out with five successive CV measurements corresponding to the MAN@G electrode. Fig. 4.9(a) represents the anodic peak current deviation corresponding to five runs-R1, R2, R3, R4, and R5. The nominal relative standard deviation (RSD) variation of about 1.19% reveals satisfactory repeatability of the proposed MIP sensor. Three different sensors, S1, S2, and S3, were fabricated to investigate the reproducibility of the sensor. The fabrication technique followed is the same for all the sensors as discussed earlier. The CV responses were recorded and peak anodic currents were estimated for each of these electrodes (Fig. 4.9(b)). The subsequent analysis affirmed a satisfactory reproducibility of the sensor with a low RSD of 1.72 %. Moreover, the same experiment was repeated twice in a zip lock packet at a 15-day interval for 45 days to investigate the sensor stability. It is noteworthy that the MAN@G electrode was maintained under ambient temperature conditions throughout the storage period. The negligible variations in peak anodic current (Fig. 4.9(c)) endorse fairly satisfactory stable behavior of the sensor with an acceptable RSD of 1.32 %. Furthermore, minimal deviation of the anodic peak potential point corresponding to the FA molecule was observed. Hence, it can be stated that the proposed sensor is quite reliable in terms of stability, reproducibility, and repeatability.

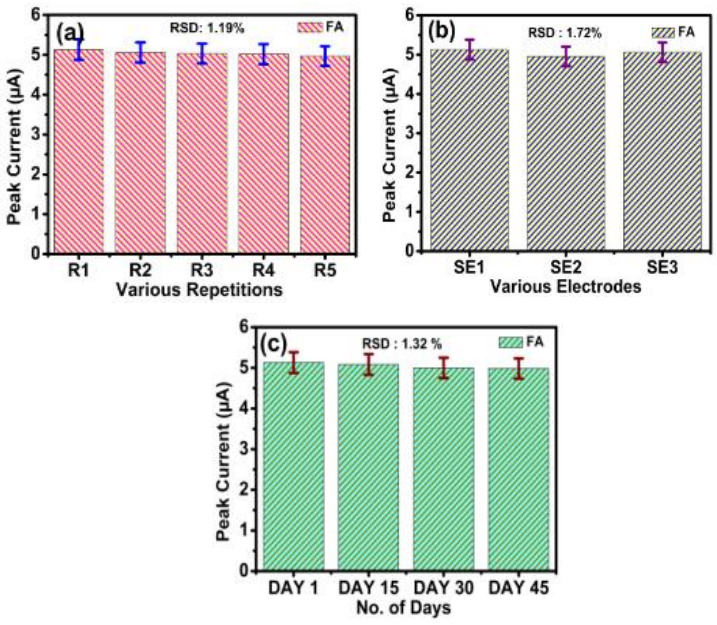

Fig. 4.9. Study of (a) Repeatability, (b) reproducibility, and (c) stability of the MAN@G electrode current acquired in PBS 7 for 100 µM FA concentration at room temperature.

4.3.2.8 Interference study

To investigate the influence of the external agents or interfering molecules, the MAN@G electrode was subjected to five interfering species agents, namely Vanillic acid (VA), Chlorine (Cl^-) ions, Urea (UR), Calcium (Ca^{2+}), and Ascorbic acid (AcA). 100 µM of FA solution was exposed to 5-fold of each interferent, and corresponding CV responses were recorded. Fig. 4.10 demonstrates the interference profile highlighting the maximum anodic current variation. The peak anodic current shows insignificant fluctuation (remaining within a 5% tolerance limit) in the presence of each phenolic and other interfering species, which elucidates the satisfactory selectivity of the MAN@G sensor.

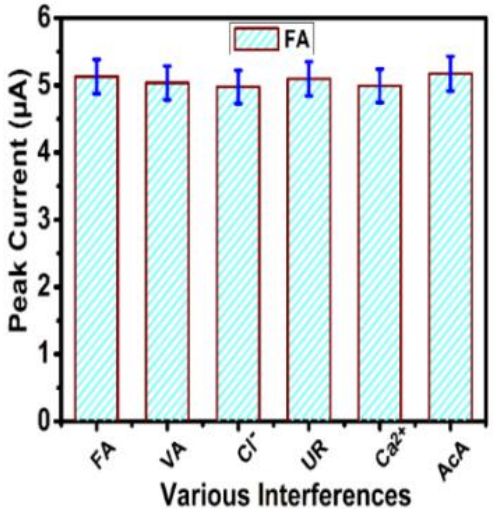

Fig. 4.10. Interference characteristics of MAN@G electrode amid five interfering species, namely VA, Cl^-, UR, Ca^{2+}, and AcA.

4.3.2.9 Real sample analysis

The quantitative analysis of FA content was carried out using the calibration curve method in five samples, namely orange, spinach, papaya, soybean, and cooked rice was carried out followed by a comparative study, which was explored with that of HPLC analysis. The findings from that analysis are abridged in Table 4.1, where r (no. of observations corresponding to the three sample extracts) =4. In the detection of orange, spinach, papaya, soybean, and cooked rice samples, the MAN@G electrode demonstrated preeminent accuracy of 99.86%, 99.96%, 99.92%, 99.24%, and 99.73% corresponding to orange, spinach, papaya, soybean, and cooked rice samples, respectively. Employing HPLC analysis as a reference, the accuracy of this detection method was further assessed by t-test analysis. The standard deviation of the difference (S_d) and the mean difference ($X_{d)}$ were estimated to be 0.258 and 0.293, respectively for 5 samples (number of samples, N=5). The absolute 't'(A_t) value was calculated to be 1.963 from

$T = \frac{\overline{X_d}}{S_d/\sqrt{N}}$[47]. Referring 't' distribution table, the critical 't' (C_t)value was obtained to be 2.132 for a degree of freedom (D_F) of 4, 95% confidence level, and 0.05 significance (alpha) level. The result showed that 'A_t' is less than 'C_t', and thus it can be concluded that the detection results almost comply with those of the reference HPLC method for the mean FA concentrations present in the five real samples.

Table 4.1

Detection of FA using the proposed MAN@G electrode

Sample	Detected FA(μM)		[a]Error (%)	[b]Accuracy (%)
	Proposed method (Measured)	Ref. (HPLC) method (Actual)		
Orange	89.37	89.23	0.16	99.84
Spinach	82.97	83.01	0.04	99.96
Papaya	92.61	92.53	0.08	99.92
Soybean	224.23	224.99	0.34	99.66
Cooked rice	124.72	124.99	0.22	99.78

% [a] Error =[|Measured- Actual|)/Actual]100 ; % [b] Accuracy = 100- Error %

4.3.2.10 Comparative study- present method versus existing techniques

An inclusive literature survey revealed that various techniques were employed for the determination of FA in diverse real samples. The LODs of FA offered by various sensors and methods, as reported in some of the existing studies, are summarized in Table 4.2 along with other parameters. A comparative study shown in Table 4.2 unveils that the proposed MAN@G-based sensor is offering a satisfactory LOD of about 18 nM. The low value of LOD signifies more FA detection efficacy and sensitivity of the sensor. Besides, the conventional methods employed in many studies either have different application areas or certain limitations, already discussed earlier. Hence, MAN@G-based sensors can be deployed in the industries for the determination of FA in real food samples considered here.

Table 4.2

Comparative insight- present methods and a few conventional techniques

Techniques employed	Linear range(µM)	LOD (µM)	Refs
Spectrophotometric determination by coupling reaction	0.22-18.12	0.1	[22]
Chemiluminometric	13.59-258.26	4.53	[21]
Capillary electrophoresis	1.13-13.59	0.67	[17]
Flow-injection/chemiluminescence	0.3-2.5	0.023	[27]
Facile approach (MIP-based)	0.23–113	0.048	[37]
Optical sensor (MIP) on quantum dots	0.5-20	0.032	[31]
Graphite SPE modified with Fe_3O_4@SiO_2	5-1000	1	[30]
DPV using MAN@G	**20-400**	**0.018**	**This work**

4.4 Summary of Developed Folic Acid Detection Method

This chapter detailed the development and characterization of a novel molecularly imprinted polyacrylonitrile-imbued graphite-base electrode (MAN@G) aimed at selective and sensitive detection of folic acid (FA) in various food samples. Recognizing the critical role of FA as a water-soluble B-complex vitamin in human health, the primary objective was to provide a cost-effective, reproducible, and durable solution for its quantification, especially considering the potential degradation of nutritional value by harmful chemicals in food production.

The MAN@G electrode was fabricated using acrylonitrile (AN) as the functional monomer and FA as the template molecule, capitalizing on AN's high reactivity due to its nitrile functional group. Characterization of the synthesized electrode material was performed using UV-visible (UV-vis) spectroscopy and scanning electron microscopy (SEM). The analytical performance was thoroughly investigated using a three-electrode system with Differential Pulse

Voltammetry (DPV) and Cyclic Voltammetry (CV) techniques. Rigorous analysis revealed that the electrode exhibited a wide linearity window ranging from 20 μM to 400 μM concentrations. Crucially, it demonstrated an impressively low LOD of 18 nM and a LOQ of 60 nM, signifying its high sensitivity for trace FA detection. Furthermore, the electrode exhibited excellent analytical stability with high reproducibility (RSD: 1.72%), good stability (RSD: 1.32%), and high repeatability (RSD: 1.19%) even after extensive usage. The practical efficacy of the proposed electrode was validated in real food extracts, including orange, spinach, papaya, soybean, and cooked rice. The results consistently endorsed high accuracy (over 99% relative accuracy) when compared to the established high-performance liquid chromatography (HPLC) method. Additionally, statistical validation through t-test analysis yielded satisfactory results for the mean FA concentrations in these five samples, confirming the reliability of the MAN@G electrode. This work stands as a significant contribution by introducing a sensitive, selective, and cost-effective electrochemical sensor based on MIP technology for FA quantification, addressing limitations of conventional methods such as high cost, complex procedures, and toxic solvent usage.

4.5 Conclusion

The current study successfully proposes and validates the molecularly imprinted polyacrylonitrile-imbued graphite-base electrode (MAN@G) as a highly effective electrochemical sensor for the practical detection and quantification of folic acid (FA). Experimental results unequivocally affirm the electrode's ability to exhibit a widespread linearity window, spanning from 20 μM to 400 μM, with an exceptionally low LOD of 18 nM and a LOQ of 60 nM. These figures highlight the sensor's remarkable sensitivity, enabling the reliable measurement of even minute concentrations of FA.

Beyond its sensitivity, the MAN@G electrode demonstrates robust analytical performance characteristics: high reproducibility (RSD of 1.72%), good stability (RSD of 1.32%), and high repeatability (RSD of 1.19%), even following extensive and repeated usage. The practical utility and detection efficacy of the proposed sensor were rigorously investigated in real food extracts, including orange, spinach, papaya, soybean, and cooked rice samples. The results consistently ratified high relative accuracies, exceeding 99%, when compared against the gold-standard HPLC reference method. Furthermore, statistical analysis using the t-test method yielded satisfactory comparative results for the mean FA concentrations across all five real samples, solidifying the reliability of the electrochemical sensor.

In conclusion, this work unequivocally avows that the developed stable, cost-effective, sensitive, and highly selective MIP-decorated electrochemical sensor is a feasible and promising contender for the recognition and quantitative determination of folic acid in folate-rich food samples within both food industries and the broader research community.

References

[1] A. Andlid, M. R. D'Aimmo, and J. Jastrebova, "Folate and Bifidobacteria," *Bifidobacteria and related organisms, Elsevier*, 2018, pp. 195–212.

[2] W. C. Langston, W. J. Darby, C. F. Shukers, and P. L. Day, "NUTRITIONAL CYTOPENIA (VITAMIN M DEFICIENCY) IN THE MONKEY," *The Journal of Experimental Medicine*, vol. 68, no. 6, pp. 923–940, Dec. 1938, doi: 10.1084/jem.68.6.923.

[3] G. P. Talwar, *Textbook of biochemistry, biotechnology, allied and molecular medicine*. PHI Learning Pvt. Ltd., 2015.

[4] L. Bandžuchová, R. Šelešovská, T. Navrátil, and J. Chýlková, "Electrochemical behavior of folic acid on mercury meniscus modified silver solid amalgam electrode," *Electrochim. Acta*, vol. 56, no. 5, pp. 2411–2419, Feb. 2011, doi: 10.1016/j.electacta.2010.10.090.

[5] S. Akbar, A. Anwar, and Q. Kanwal, "Electrochemical determination of folic acid: A short review.," *Anal. Biochem*., vol. 510, pp. 98–105, Oct. 2016, doi: 10.1016/j.ab.2016.07.002.

[6] C. Maynard, I. Cummins, J. Green, and D. Weinkove, "A bacterial route for folic acid supplementation.," BMC Biol., vol. 16, no. 1, p. 67, Jun. 2018, doi: 10.1186/s12915-018-0534-3

[7] C. M. Pfeiffer, S. P. Caudill, E. W. Gunter, J. Osterloh, and E. J. Sampson, "Biochemical indicators of B vitamin status in the US population after folic acid fortification: results from the National Health and Nutrition Examination Survey 1999-2000.," Am. J. Clin. Nutr., vol. 82, no. 2, pp. 442–450, Aug. 2005, doi: 10.1093/ajcn.82.2.442.

[8] T. N. Wien, E. Pike, T. Wisløff, A. Staff, S. Smeland, and M. Klemp, "Cancer risk with folic acid supplements: a systematic review and meta-analysis.," *BMJ Open*, vol. 2, no. 1, p. e000653, Jan. 2012, doi: 10.1136/bmjopen-2011-000653.

[9] I. M. G. J. Bronckers*et al.*, "Safety of systemic agents for the treatment of pediatric psoriasis.," *JAMA Dermatol.*, vol. 153, no. 11, pp. 1147–1157, Nov. 2017, doi: 10.1001/jamadermatol.2017.3029.

[10] G. A. Cobos, A. Femia, and R. A. Vleugels, "Dermatomyositis: an update on diagnosis and treatment.," *Am. J. Clin. Dermatol.*, vol. 21, no. 3, pp. 339–353, Jun. 2020, doi: 10.1007/s40257-020-00502-6.

[11] F. C. Arnett, J. C. Whelton, T. M. Zizic, and M. B. Stevens, "Methotrexate therapy in polymyositis.," *Ann. Rheum. Dis.*, vol. 32, no. 6, pp. 536–546, Nov. 1973, doi: 10.1136/ard.32.6.536.

[12] E. Nogueira, A. C. Gomes, A. Preto, and A. Cavaco-Paulo, "Folate-targeted nanoparticles for rheumatoid arthritis therapy.," *Nanomedicine*, vol. 12, no. 4, pp. 1113–1126, May 2016, doi: 10.1016/j.nano.2015.12.365.

[13] S. Moazzen*et al.*, "Folic acid intake and folate status and colorectal cancer risk: A systematic review and meta-analysis.," *Clin. Nutr.*, vol. 37, no. 6 Pt A, pp. 1926–1934, Dec. 2018, doi: 10.1016/j.clnu.2017.10.010.

[14] N. A. Shlobin, M. A. LoPresti, R. Y. Du, and S. Lam, "Folate fortification and supplementation in prevention of folate-sensitive neural tube defects: a systematic review of policy.," *J. Neurosurg. Pediatr.*, vol. 27, no. 3, pp. 294–310, Dec. 2020, doi: 10.3171/2020.7.PEDS20442.

[15] Y. Peng *et al.*, "Synergistic Effect of Atorvastatin and Folic Acid on Cardiac Function and Ventricular Remodeling in Chronic Heart Failure Patients with Hyperhomocysteinemia.," *Med. Sci. Monit.*, vol. 24, pp. 3744–3751, Jun. 2018, doi: 10.12659/MSM.906893.

[16] J. Rodríguez Flores, G. C. Peñalvo, A. E. Mansilla, and M. J. R. Gómez, "Capillary electrophoretic determination of methotrexate, leucovorin and folic acid in human urine," *Journal of Chromatography B*, vol. 819, no. 1, pp. 141–147, May 2005, doi: 10.1016/j.jchromb.2005.01.039.

[17] S. Zhao, H. Yuan, C. Xie, and D. Xiao, "Determination of folic acid by capillary electrophoresis with chemiluminescence detection.," *J. Chromatogr. A*, vol. 1107, no. 1–2, pp. 290–293, Feb. 2006, doi: 10.1016/j.chroma.2005.11.052.

[18] Z. Yang, F. Gong, Z. Yu, D. Shi, S. Liu, and M. Chen, "Highly sensitive folic acid colorimetric sensor enabled by free-standing molecularly imprinted photonic hydrogels," *Polym. Bull.*, vol. 79, no. 3, pp. 1857–1871, Mar. 2022, doi: 10.1007/s00289-021-03584-2.

[19] J. Jastrebova, C. Witthöft, A. Grahn, U. Svensson, and M. Jägerstad, "HPLC determination of folates in raw and processed beetroots," *Food Chem.*, vol. 80, no. 4, pp. 579–588, Apr. 2003, doi: 10.1016/S0308-8146(02)00506-X.

[20] D. Sun *et al.*, "Modified EMR-lipid method combined with HPLC-MS/MS to determine folates in egg yolks from laying hens supplemented with different amounts of folic acid.," *Food Chem.*, vol. 337, p. 127767, Feb. 2021, doi: 10.1016/j.foodchem.2020.127767.

[21] P. Anastasopoulos, T. Mellos, M. Spinou, T. Tsiaka, and M. Timotheou-Potamia, "Chemiluminometric and fluorimetric determination of folic acid," *Anal. Lett.*, vol. 40, no. 11, pp. 2203–2216, Oct. 2007, doi: 10.1080/00032710701567022.

[22] R. Matias, P. R. S. Ribeiro, M. C. Sarraguça, and J. A. Lopes, "A UV spectrophotometric method for the determination of folic acid in pharmaceutical tablets and dissolution tests," *Anal. Methods*, vol. 6, no. 9, p. 3065, 2014, doi: 10.1039/c3ay41874j.

[23] Y. He, S. Wang, and J. Wang, "Detection and quantification of folic acid in serum via a dual-emission fluorescence nanoprobe.," *Anal. BioAnal. Chem.*, vol. 411, no. 28, pp. 7481–7487, Nov. 2019, doi: 10.1007/s00216-019-02121-5.

[24] A. Mahato, S. Vyas, and N. S. Chatterjee, "HPLC-UV Estimation of Folic Acid in Fortified Rice and Wheat Flour using Enzymatic Extraction and Immunoaffinity Chromatography Enrichment: An Interlaboratory Validation Study.," *J. AOAC Int.*, vol. 103, no. 1, pp. 73–77, Jan. 2020, doi: 10.5740/jaoacint.19-0207.

[25] R. Amidzic, J. Brboric, O. Cudina, and S. Vladimirov, "RP-HPLC determination of vitamins, folic acid and B12 in multivitamin tablets," *J. Serb. Chem. Soc.*, vol. 70, no. 10, pp. 1229–1235, 2005, doi: 10.2298/JSC0510229A.

[26] E. M. Mohammed, "Qualitative and quantitative determination of folic acid in tablets by FTIR spectroscopy.," *IJAPBC*, vol. 3, pp. 773–780, 2014.

[27] S. M. Wabaidur, S. M. Alam, S. H. Lee, Z. A. Alothman, and G. E. Eldesoky, "Chemiluminescence determination of folic acid by a flow injection analysis assembly.," *Spectrochim. Acta A Mol. Biomol. Spectrosc.*, vol. 105, pp. 412–417, Mar. 2013, doi: 10.1016/j.saa.2012.11.078.

[28] I. M. A. Hasan, K. M. Abd-Elsabur, F. H. Assaf, and M. Abd-Elsabour, "Folic Acid Determination in Food Samples Using Green Synthesized Copper Oxide Nanoparticles and Electro-Poly (Methyl Orange) Sensor," *Electrocatal.*, vol. 13, no. 6, pp. 759–772, Nov. 2022, doi: 10.1007/s12678-022-00756-0.

[29] H. Karimi-Maleh, F. Amini, A. Akbari, and M. Shojaei, "Amplified electrochemical sensor employing CuO/SWCNTs and 1-butyl-3-methylimidazolium hexafluorophosphate for selective analysis of sulfisoxazole in the presence of folic acid.," *J. Colloid Interface Sci.*, vol. 495, pp. 61–67, Jun. 2017, doi: 10.1016/j.jcis.2017.01.119.

[30] M. Safaei, H. Beitollahi, and M. R. Shishehbore, "Simultaneous determination of epinephrine and folic acid using the fe3o4@sio2/gr nanocomposite modified graphite," *Russ. J. Electrochem.*, vol. 54, no. 11, pp. 851–859, Nov. 2018, doi: 10.1134/S1023193518130402.

[31] A. A. Ensafi, P. Nasr-Esfahani, and B. Rezaei, "Simultaneous detection of folic acid and methotrexate by an optical sensor based on molecularly imprinted polymers on dual-color CdTe quantum dots.," *Anal. Chim. Acta*, vol. 996, pp. 64–73, Dec. 2017, doi: 10.1016/j.aca.2017.10.011.

[32] J.-L. Lu *et al.*, "Decaffeination of tea extracts by using poly(acrylamide-co-ethylene glycol dimethylacrylate) as adsorbent," *J. Food Eng.*, vol. 97, no. 4, pp. 555–562, Apr. 2010, doi: 10.1016/j.jfoodeng.2009.11.018.

[33] S. Nag, S. Pradhan, D. Das, B. Tudu, R. Bandopadhyay, and R. B. Roy, "Fabrication of A molecular imprinted polyacrylonitrile engraved graphite electrode for detection of formalin in food extracts," *IEEE Sens. J.*, pp. 1–1, 2021, doi: 10.1109/JSEN.2021.3128520.

[34] N. Leibl, K. Haupt, C. Gonzato, and L. Duma, "Molecularly imprinted polymers for chemical sensing: A tutorial review," *Chemosensors*, vol. 9, no. 6, p. 123, May 2021, doi: 10.3390/chemosensors9060123.

[35] F. M. de Oliveira, M. G. Segatelli, and C. R. T. Tarley, "Evaluation of a new water-compatible hybrid molecularly imprinted polymer combined with restricted access for the selective recognition of folic acid in binding assays," *J. Appl. Polym. Sci.*, vol. 133, no. 21, Jun. 2016, doi: 10.1002/app.43463.

[36] M. Hussain, N. Iqbal, and P. A. Lieberzeit, "Acidic and basic polymers for molecularly imprinted folic acid sensors—QCM studies with thin films and nanoparticles," *Sensors and Actuators B: Chemical*, vol. 176, pp. 1090–1095, Jan. 2013, doi: 10.1016/j.snb.2012.09.082.

[37] S. Hussain, S. A. Zaidi, D. Vikraman, H.-S. Kim, and J. Jung, "Facile preparation of molybdenum carbide (Mo2C) nanoparticles and its effective utilization in electrochemical sensing of folic acid via imprinting.," *Biosens. Bioelectron.*, vol. 140, p. 111330, Sep. 2019, doi: 10.1016/j.bios.2019.111330.

[38] Y. Yang, Z. Wang, H. Niu, and H. Zhang, "One-pot synthesis of quantum dot-labeled hydrophilic molecularly imprinted polymer nanoparticles for direct optosensing of folic acid in real, undiluted biological samples.," *Biosens. Bioelectron.*, vol. 86, pp. 580–587, Dec. 2016, doi: 10.1016/j.bios.2016.07.056.

[39] Y. Areerob, P. Sricharoen, N. Limchoowong, and S. Chanthai, "Core-shell SiO2 -coated Fe3 O4 with a surface molecularly imprinted polymer coating of folic acid and its applicable magnetic solid-phase extraction prior to determination of folates in tomatoes.," *J. Sep. Sci.*, vol. 39, no. 15, pp. 3037–3045, Aug. 2016, doi: 10.1002/jssc.201600342.

[40] A. Zengin, M. Utku Badak, M. Bilici, Z. Suludere, and N. Aktas, "Preparation of molecularly imprinted PDMS elastomer for selective detection of folic acid in orange juice," *Appl. Surf. Sci.*, vol. 471, pp. 168–175, Mar. 2019, doi: 10.1016/j.apsusc.2018.12.008.

[41] S. Hussain, S. Khan, S. Gul, M. I. Pividori, and M. Del Pilar Taboada Sotomayor, "A novel core@shell magnetic molecular imprinted nanoparticles for selective determination of folic acid in different food samples," *Reactive and Functional Polymers*, vol. 106, pp. 51–56, Sep. 2016, doi: 10.1016/j.reactfunctpolym.2016.07.011.

[42] A. S. Novikova, T. S. Ponomaryova, and I. Y. Goryacheva, "Fluorescent AgInS/ZnS quantum dots microplate and lateral flow immunoassays for folic acid determination in juice samples.," *Mikrochim. Acta*, vol. 187, no. 8, p. 427, Jul. 2020, doi: 10.1007/s00604-020-04398-1.

[43] E. Laviron, "General expression of the linear potential sweep voltammogram in the case of diffusionless electrochemical systems," *J. ElectroAnal. Chem. Interfacial Electrochem.*, vol. 101, no. 1, pp. 19–28, Jul. 1979, doi: 10.1016/S0022-0728(79)80075-3.

[44] M. Arvand, A. Pourhabib, and M. Giahi, "Square wave voltammetric quantification of folic acid, uric acid and ascorbic acid in biological matrix," *Journal of Pharmaceutical Analysis*, vol. 7, no. 2, pp. 110–117, Apr. 2017, doi: 10.1016/j.jpha.2017.01.002.

[45] S. Nag, D. Das and R. B. Roy, "Voltammetry Application of Molecularly Imprinted Polyacrylamide as Vanillin Receptor in Desserts," *IEEE Sens. J.*, vol. 23, no. 4, pp. 3446-3452, 15 Feb.15, 2023, doi: 10.1109/JSEN.2023.3235933.

[46] S. Kar, B. Tudu, A. K. Bag and R. Bandyopadhyay, "Application of near-infrared spectroscopy for the detection of metanil yellow in turmeric powder", *Food Anal. Methods*, vol. 11, pp. 1291-1302, May 2018.

[47] S. Nag, D. Das, H. Naskar, B. Tudu, R. Bandyopadhyay and R. B. Roy, "A Novel Molecular Imprinted Polymethacrylic Acid Decorated Graphite Electrochemical Sensor for Analyzing Metanil Yellow Adulteration in Food," in *IEEE Sens. J.*, doi: 10.1109/JSEN.2023.3300732

PUBLICATION STATUS

JOURNAL

- D. Bandyopadhyay, S. Nag, D. Das, and R. B. Roy, "Electrochemical detection of Folic Acid in Food Extracts Using Molecularly Imprinted Polyacrylonitrile Imbued Graphite Electrode," *Analytica chimica acta*, vol. 1325, p. 343120, Aug. 2024, doi: 10.1016/j.aca.2024.343120.

Advanced Electrochemical and Capacitive Sensors for Quercetin Detection in Food Products

5

5.1 Introduction

Quercetin (QCN or QT), a prominent flavonoid and a member of the polyphenolic compounds group, is widely present in various fruits, vegetables, and beverages, including apples, berries, citrus fruits, onions, nuts, red wine, tea, and leafy green vegetables [1]. As depicted in Fig. 5.1, QCN ($C_{15}H_{10}O_7$) is well-known for its potent antioxidant properties, playing a crucial role in protecting cells from damage by neutralizing free radicals in the body [1]. Beyond its antioxidant capabilities, QCN also exhibits a range of beneficial biological activities, including anti-inflammatory, anti-bacterial, and anti-viral properties, immune-modulating activities, cardiovascular benefits, and promising anti-cancer properties [1-4]. Interestingly, some research suggests QCN could be considered in the preventive medical treatment of recurrent kidney stones [5]. While QCN-rich foods generally offer health benefits, high dose levels (typically ranging from 13 to 800 mg/day) may lead to mild side effects such as digestive issues, headaches, or tingling sensations, though these are uncommon at typical dietary intake levels [6]. In modern agricultural practices, the widespread application of hazardous chemicals during cultivation and harvest seasons is common, primarily to enhance crop yields and maximize profits. These chemicals can, unfortunately, disrupt various biochemical processes, potentially compromising the nutritional value of essential health-friendly compounds like QCN. Consequently, there is a pressing need for robust and reliable methods to accurately assess and quantify QCN levels in fruits, vegetables, and multivitamin supplements. The development of molecule-specific sensors offers a promising approach for precise and sensitive detection of QCN, even at low concentrations in complex food matrices. Given QCN's crucial role in human health, the endeavor to develop cost-effective, stable, sensitive, reusable, and user-friendly QCN sensors is of significant importance.

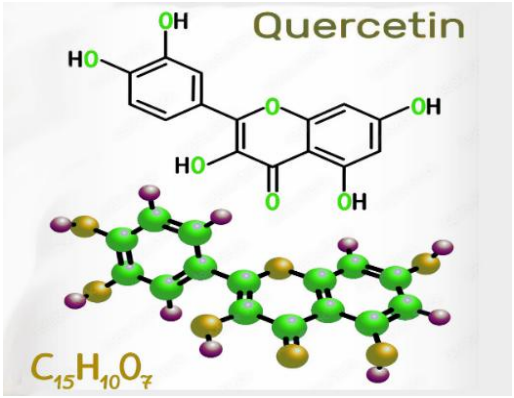

Fig. 5.1. Chemical structure of QCN

Traditional detection and isolation methods for QCN, such as fluorescence spectroscopy [7], electrophoresis [8], liquid chromatography–tandem mass spectrometry [9], column chromatography [11], high-performance liquid chromatography (HPLC) [12, 13], rapid phase HPLC [13], chemiluminescence spectrophotometry [14], liquid-liquid microextraction [15], and vortex-assisted ionic liquid dispersive liquid-liquid microextraction combined with spectrophotometry [16], are well-established. However, these methods often come with substantial drawbacks, including high instrumentation costs, the necessity for toxic organic solvents, and the requirement for highly skilled operators, limiting their widespread applicability in routine analysis. Electrochemical detection offers a more striking alternative owing to its lucrative, simpler, and faster facets [17 – 19]. Researchers have explored various electrochemical sensors for QT detection from food supplements to vegetables in the antecedent studies. These sensors have employed different nanocomposites viz. carbon embedded $CuFeS_2$ hybrids [20], polypyrrole coupled with nanohybrids [21], $WS_2/GdCoO_3$, [22] and various electrodes including glassy carbon electrodes (GCE) or unmodified carbon pastes [23 – 24] poly (gallic acid)/MWNT-altered electrodes [25] modified carbon nitride modified Organic heterostructure based biosensor [26], Co_3O_4 modified GCE [27] and dummy molecules [28]. While these advancements are notable, some existing sensors exhibit moderate selectivity or involve complex fabrication processes, thereby restricting their practical application. Recent studies have increasingly highlighted the transformative potential of molecularly imprinted polymer (MIP) technology to significantly enhance the selectivity, reproducibility, and repeatability of sensors [29-31]. MIPs are synthetic or natural polymers characterized by cross-linked structures that possess "molecular memory" or specific recognition sites tailored for target molecules [32-34]. MIP technology offers several intrinsic advantages, including simplified fabrication, reusability, high selectivity, and

robust mechanical strength, making it particularly well-suited for the detection of various food constituents [35]. While several studies have explored the use of imprinting technologies for electrochemical detection of QCN and other molecules [36-39], challenges remain in achieving broad applicability, wide linearity ranges, consistent reproducibility, and minimizing the risk of chemical contamination.

The current study delves into two distinct, innovative approaches for quercetin detection.

5.2 A Novel rGO Decorated Molecularly Imprinted Polyacrylic Acid Graphite Electrode for the Detection of Quercetin in Food

The first investigation focuses on the fabrication and evaluation of a reduced graphene oxide (rGO) decorated Molecularly Imprinted Polyacrylic Acid Graphite Electrode (M-AARGO@G) for selective QCN detection in real food samples. This work introduces a cost-effective yet sensitive MIP-based electrochemical sensor for selective quantification of QCN. The usage of MIP modifiers (rGO) can favor electrocatalytic activities owing to the high surface area and higher number of active sites that encourage additional molecular adsorption and fast electron transfer [41]. Among the three monomers evaluated—acrylic acid (AA), acrylonitrile (AN), and acrylamide (AM)—the AA-based MIP electrode, i.e., M-AARGO@G, exhibited the highest peak oxidation current. The monomers were selected based on their functional group compatibility and reactivity with the template (QCN) molecule. AA, being a weak acid with a dissociation constant (pKa) of 4.26, can dissociate in water to produce hydrogen ions (H+) and acrylate ions (CH2=CHCOO-), which are responsible for the crosslinking of acrylic monomers, providing strength and durability to acrylic polymers [40]. Moreover, AA acts as a good nucleophile, facilitating the template-monomer reaction process in the pre-polymerization stage [42]. Therefore, AA was chosen as a suitable monomer for electrode development. The fabricated M-AARGO@G electrode demonstrated two broad linearity windows (0.001 μM to 1 μM; 1 μM to 400 μM) with an acceptable LOD and LOQ compared to existing methods. Rigorous analysis of the electrode's analytical performance revealed excellent stability, satisfactory repeatability, and reproducibility. The detection proficiency of the electrode was evaluated in real food extracts of onion, oregano, and spinach. The results demonstrated an average accuracy of 99% when compared to the HPLC method. Furthermore, satisfactory results were obtained using the statistical tool t-test method.

5.2.1 Materials and Methodology

5.2.1.1 Chemical reagents and standards

QCN of purity >97% was procured from Tokyo Chemical Industry Chemicals Pvt. Ltd., India. Fine graphite powder with a purity of 99%, acrylonitrile (AN), acrylic acid (AA), acrylamide (AM), and ethylene glycol dimethyl acrylate (EGDMA as crosslinker) were obtained from Sigma Aldrich, USA. Benzoyl peroxide (binder) was sourced from Sisco Research Laboratories Private Limited, India. The reduced graphene oxide (RGO) was synthesized by a well-known standard modified Hummers' method [41]. Acetate buffer saline (ABS), citrate buffer saline (CBS), and phosphate buffer saline (PBS), with pH values of 3, 4, 5, 6, 7, and 8, were prepared in the laboratory. In the process of developing and testing the sensor, ethanol and paraffin oil from Merck & Co. were utilized as binders and solvents, respectively. There is no need for previous purification procedures because analytical grade compounds are involved. During experiments, distilled water (resistance(R) approx. 18 MΩ) of the Millipore water purification system was used for washing electrodes and chemical utensils.

5.2.1.2 Characterization details and equipment specifications

A tri-electrode system, interfaced with a Metrohm Autolab PGSTAT101 potentiostat was employed to examine and assess electrode performance. In this arrangement, the redox response was monitored at a M-AARGO@G working electrode, while an Ag/AgCl electrode and a Pt rod served as the reference and counter electrodes, respectively. The voltage window of 0.1 V-1 V was set for the measurements of cyclic voltammetry (CV) and differential pulse voltammetry (DPV). To examine the Ultraviolet-visible (UV-Vis) absorption spectra, UV-visible absorption measurements were accomplished by a double-beam Shimadzu UV-3600 spectrophotometer. Surface morphology of synthesized materials was examined using a scanning electron microscope (SEM, ZEISS EVO 18, US) operating at 15 kV accelerating voltage.

5.2.1.3 Non-imprinted polymer (N-AARGO@G) and molecularly imprinted polymer (M-AARGO@G) preparation

To prepare M-AARGO@G, initially 0.95 g graphite powder was dissolved in 15 mL of ethanol and sonicated employing an ultrasonicator for 1 h. Subsequently, 0.05 g of AA (monomer) and 0.05 g of QCN (template) were added, and the mixture was again sonicated for an additional 1 h. Thereafter, 400 µL of EGDMA and 1 mg of benzoyl peroxide (polymerization initiator) were added, and re-sonication was continued for 45 mins. Later, the sonicated mixture was placed in a water bath with the temperature adjusted to 30–40°C to commence the polymerization

process. Subsequently, the polymerized material was periodically filtered and immersed in a 70:30 ethanol-to-water mixture for 48 h to remove any remaining traces of QCN molecules. The electrode MIP material was then dried and preserved at room temperature. This concludes the synthesis process of the electrode material. Except for template (QCN) amalgamation in the second step, the NIP synthesizing process follows the same steps as the MIP process.

5.2.1.4 M-AARGO@G and N-AARGO@G electrodes fabrication

The working electrode was developed by stuffing fine graphene-MIP/NIP powdered paste in capillary glass tubes (1.25 mm inner dia.) using thin metallic rods. The powdered paste was obtained by blending the mixture of synthesized material and rGO (9:1 ratio) using a mortar and pestle for about 1 h. For binding purposes, 3-4 drops of paraffin oil were added during mortaring. For electrical connections, copper wires were crowned from the capillary tubes.

5.2.1.5 Real sample extract preparation

Oregano, onion, and spinach (1 g each), procured from the neighborhood market, were blended in 100 mL of water. The samples were crushed prior to making the test solutions. The resultant solutions were filtered through disposable sterile syringe filters (Whatman UNIFLO, diameter: 25 mm, pore size: 0.22 μm) with polyvinylidene fluoride (PVDF) membranes in polypropylene platforms. The filtrates were analyzed using DPV and HPLC investigations. HPLC analysis was performed employing an Agilent 1290 Infinity II detector and a BioSute C18 column (4.6 x 150 mm, particle size: 5 μm) at ambient temperature. The mobile phases used were i) 0.1% Trifluoroacetic acid (TA) in H2O and ii) 90% acetonitrile (ACN), with a flow rate of 1 ml min^{-1} for a total run time of 15 mins.

5.2.2 Results And Discussions

5.2.2.1 Optimization of the monomer and the electrode selection

For synthesizing the MIP samples and corresponding electrodes, three distinct monomers, namely acrylonitrile (AN), acrylamide (AM), and acrylic acid (AA), were selected. The detailed procedure for fabrication has been previously elucidated in the experimental section. Consequently, CV responses were recorded for these three electrodes, revealing the presence of an irreversible redox peak at approximately 0.22 V when subjected to a 100μM solution containing buffer PBS 6 and the analyte molecule (QCN) at a scan rate of 50 mV/s. The CV plots of Fig. 5.2.1 depict that the M-AARGO@G electrode exhibited the highest peak current for oxidation, which was 1.53 times and 1.39 times greater than the corresponding rGO-modified electrodes imprinted with AM and AN, respectively. The electrochemical performance of

the MIP electrode may be influenced by the dipole-dipole interactions and monomer-template interactions during the pre-polymerization stage, aiding the QCN recognition process at the M-AARGO@G electrode surface [42]. Consequently, AA was selected as the most promising monomer, and its corresponding electrode was subsequently employed for QCN detection in subsequent experimental processes.

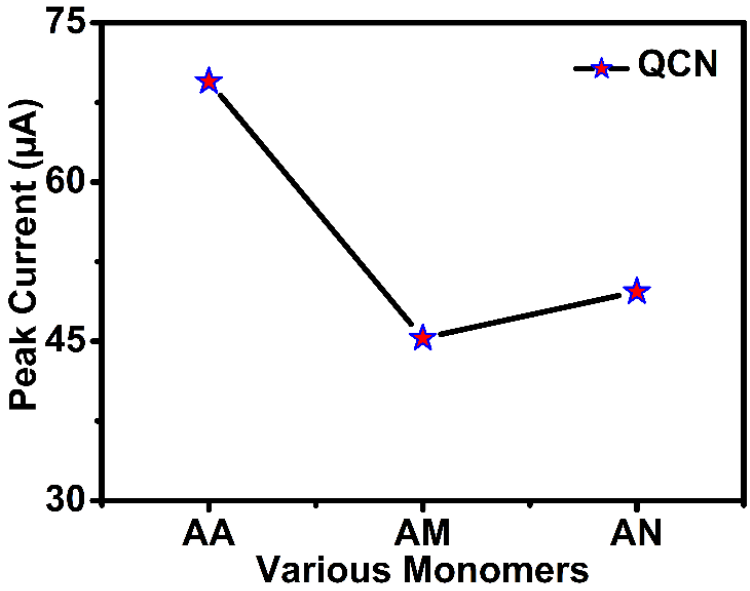

Fig. 5.2.1. Plot of peak currents at the same peak potential for different monomers (AA, AM, and AN).

Four different types of electrodes (CP@G, rGO@G, M-AA@G, M-AARGO@G) were fabricated and subjected to CV measurements. CP@G, rGO@G, and M-AA@G represent carbon paste electrodes, reduced graphene oxide (rGO) modified graphite electrodes, and molecularly imprinted acrylic acid engraved graphite-base electrodes. Among the four diverse electrodes, the M-AARGO@G electrode exhibits the highest current (69.60 μA) at 0.22 V, as summarized in Table 5.2.1. The incorporation of rGO with the MIP perhaps enhances the effective surface area of the M-AARGO@G, facilitating a more efficient electron transfer between the electrode surface and the analyte molecules. Thus, the M-AARGO@G electrode was opted for the detection of QCN in this study.

Table 5.2.1

Comparative Insight- Different Electrodes

Electrodes employed	Anodic peak potential (V)	Anodic peak current (I_{Qm}), µA
CP@G	0.22	14.81
rGO@G	0.22	33.12
M-AA@G	0.22	55.36
M-AARGO@G	**0.22**	**69.06**

5.2.2.2 Synthesized Polymer Material Characterization: UV-Vis Spectroscopy Analysis

For the wavelength window of 280 nm - 400 nm, UV-Vis spectroscopy analysis has been carried out to affirm the leaching-out of the QCN molecule following wash. Consistent with the prior report [43], the spectral surveillance reveals a distinct absorption peak at 287.5 nm (Fig. 5.2.2) for the the unwashed material only, suggesting the successful removal of the QCN species.

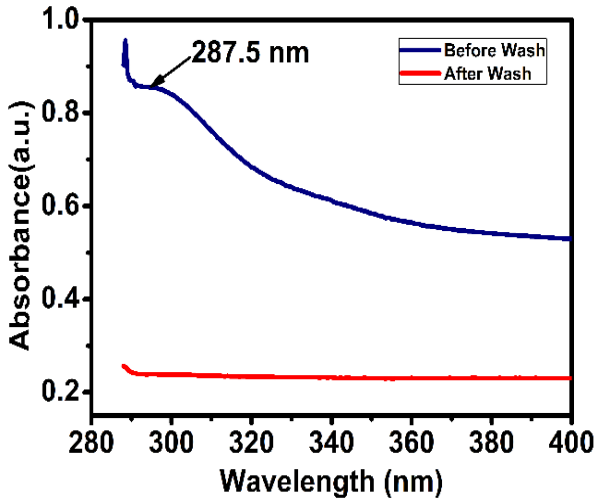

Fig. 5.2.2. The UV-vis absorption spectra of MIP material are plotted both before (MBW) and after template washing (MAW).

5.2.2.3 SEM studies for morphological insights

SEM images of the synthesized materials: M-AARGO@G and N-AARGO@G are presented in Fig. 5.2.3(a) and Fig. 5.2.3(b), respectively, to illustrate their surface morphologies. The M-

AARGO@G surface appears notably wrinkled and rugged when compared to N-AARGO@G (Fig. 4(b)), owing to the formation of imprinted cavities on the M-AARGO@G surface.

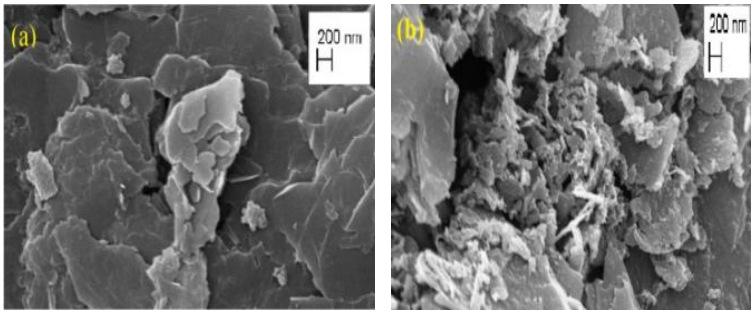

Fig. 5.2.3. Images of surface morphology corresponding to the electrode materials (a)N-AARGO@G and (b)M-AARGO@G obtained from SEM investigations.

5.2.2.4 Buffer and pH optimization

To examine the impact of different buffers and pH levels, firstly, the M-AARGO@G electrode was exposed to 1 ml of QCN and 9 ml of various buffers, including acetate buffered saline (ABS), citrate buffered saline (CBS), and phosphate-buffered saline (PBS). CV responses showed that the maximum oxidation peak current (69.60 µA) was achieved with PBS (Fig. 5.2.4(a)). Additionally, the effect of pH on the M-AARGO@G electrode was assessed using PBS at six different pH values: 3 - 8. The results demonstrated in Fig. 5.2.4(b) unequivocally indicate that PBS 6 proved to be the most favorable test solution for electrode function, as it elicited the highest oxidation peak current.

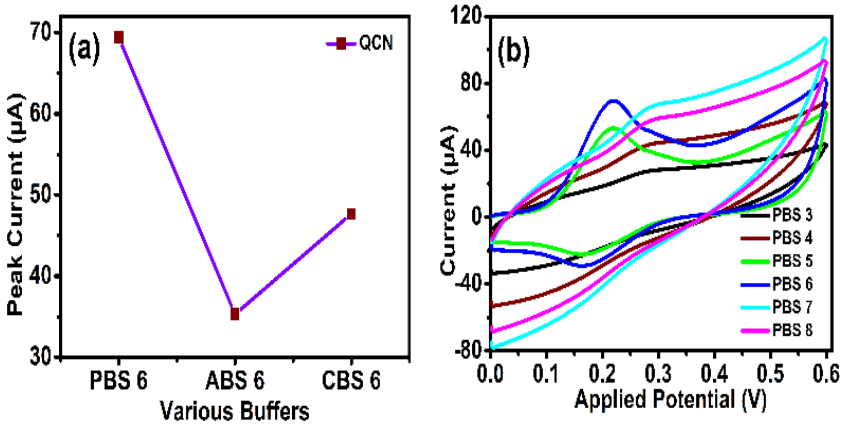

Fig. 5.2.4. (a)Plot of peak currents obtained for a 100 µM QCN solution corresponding to PBS, ABS, and CBS at pH 6, and (b) PBS pH variation 3- 8.

5.2.2.5 Electrochemical performance of M-AARGO@G electrode

The electrocatalytic performance of the M-AARGO@G electrode was assessed in two stages. Initially, a comparative analysis was conducted on the surfaces of both M-AARGO@G and N-

AARGO@G electrodes, focusing on the electrochemical oxidation of QCN. CV data was acquired in the presence of PBS 6 within a voltage range of 0 V - 0.6 V, at a scan rate (SR) of 50 mV/s. Notably, the M-AARGO@G electrode exhibited a peak oxidation current (Fig. 5.2.5(a)) of almost 6.46 times higher than that of the N-AARGO@G electrode (with peak currents of 69.60 µA and 10.77 µA, respectively). This substantial increase in peak current can be attributed to the enhanced adsorption of the analyte, facilitated by the molecule recognition sites embedded within the MIP materials. Additionally, another study was conducted to investigate the behavior of the M-AARGO@G electrode. CV responses were recorded both in the presence (100 µM) and absence of QCN molecules, employing 0.1 M PBS6 solution. As illustrated in Fig. 5.2.5(b), the results boasted a well-demarcated oxidation peak for the solution containing QCN.

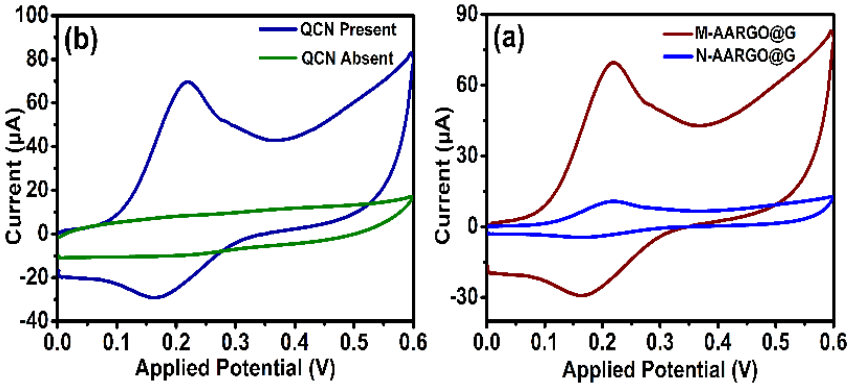

Fig. 5.2.5. CV responses of the following electrodes:(a) M-AARGO@G and N-AARGO@G electrode in 100 µM solution with 1 ml target analyte, QCN, and (b) M-AARGO@G with and without the QCN molecule.

5.2.2.6 Influence of scan rate variation

The effect of SR change on the CV characteristics of the M-AARGO@G electrode interface is portrayed in Fig. 5.2.6(a) at 100 µM QCN concentration. CV responses at scan rates ranging from 10 mV/s - 400 mV/s were recorded. The figure reveals a striking correlation – as the scan rate increases, the QCN oxidation peak current surges, implying a surface-controlled QCN oxidation process at the MIP electrode surface. In addition, Fig. 5.2.6(b) portrays how the anodic peak current (I_{Qm}) varies linearly while the scan rate follows a linear regression equation:

$$I_{Qm} = 0.466\upsilon + 39.628; R^2 = 0.996 \quad (1)$$

The quantity of transferred electrons during the electrochemical oxidation of QCN is estimated from the Langmuir Isotherm equation (2) [44].

$$I_{QCN} = \frac{nFQ\upsilon}{4RT} \quad (2)$$

Where T, R (8.314 $Jmol^{-1}k^{-1}$), Q, n, F (96,480 $Cmol^{-1}$), and υ signify room temperature, universal gas constant, consumed charge quantity, no. of transferred electrons, Faraday's constant, and scan rate, respectively. The double electron adsorption mechanism was corroborated by calculating the value of "n," which resulted in approximately 2 [45]. Fig. 5.2.6(c) shows the linear fluctuation of the peak oxidation potential (E_P) with the logarithm of the scan rate ($log\upsilon$). It was revealed that E_P varies linearly along with $log\upsilon$ in accordance with a linear regression equation (3) expressed as:

$$E_P = 0.016log\upsilon + 0.240; R^2 = 0.999 \quad (3)$$

The gradient (G) of this equation can be represented for an irreversible process as:

$$G = \frac{2.303RT}{\alpha nF} \quad (4)$$

Employing equation (4), the product of charge transfer coefficient 'α' and 'n' ('αn') was computed to be 3.693. These obtained parametric values align closely with those reported in previous studies [45].

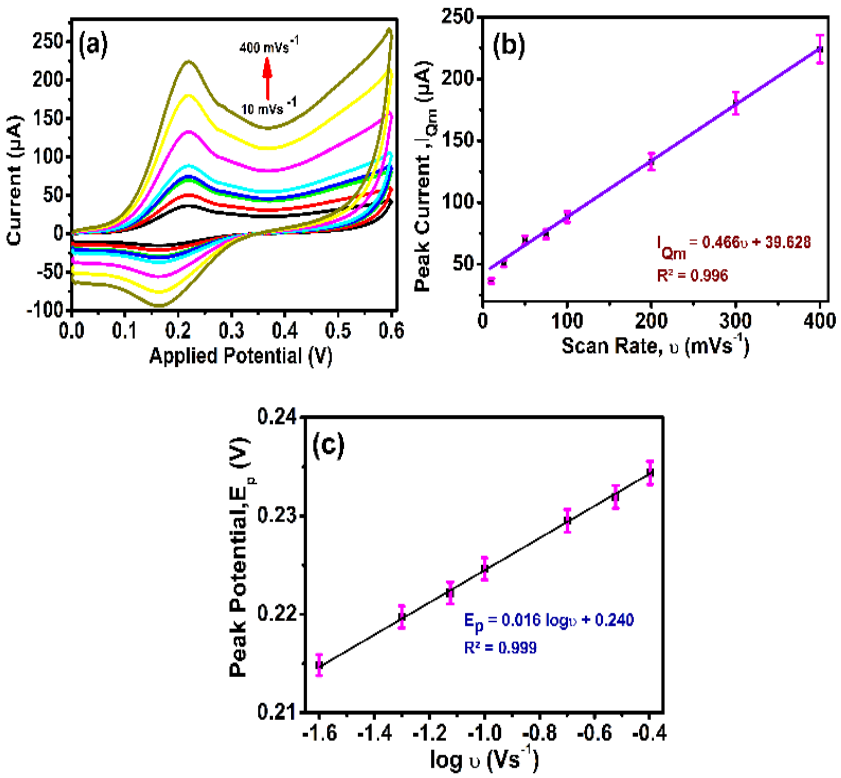

Fig. 5.2.6.(a)CV profile recorded for M-AARGO@G electrode in PBS of pH 6 (b) effect of scan rate (SR) variation (10 mVs^{-1} – 400 mVs^{-1}) on maximum oxidation current I_{Qm}) (Linear plot) (c) peak potential (E_P)- logarithm of SR in a linear plot.

5.2.2.7 Calibration analysis and limit of detection

It also revealed that the M-AARGO@G electrode properties were modulated by the fluctuation in QCN ($C_Q$concentration in the test solution. The DPV responses within the optimum potential window of 0 V- 1 V for various QCN concentrations in PBS 6 solution are shown in Fig. 5.2.7(a). Anodic peak current (I_{Qm}) was observed to gradually ascend at 50 mV/s when QCN concentration (C_Q) increased from 0.001 µM to 400 µM, as shown in Fig. 5.2.7(a). Furthermore, two linear segments are seen in the QCN calibration plots for: 0.001 µM - 1 µM (Fig. 5.2.7(b)); and 1 µM - 400 µM (Fig. 5.2.7(c)). The respective linear regression equations (5 and 6) can be expressed as

$$I_{Qm} = 13.777C_Q + 17.936; R^2 = 0.995 \quad (5)$$

$$I_{Qm} = 0.1779C_Q + 32.347; R^2 = 0.995 \quad (6)$$

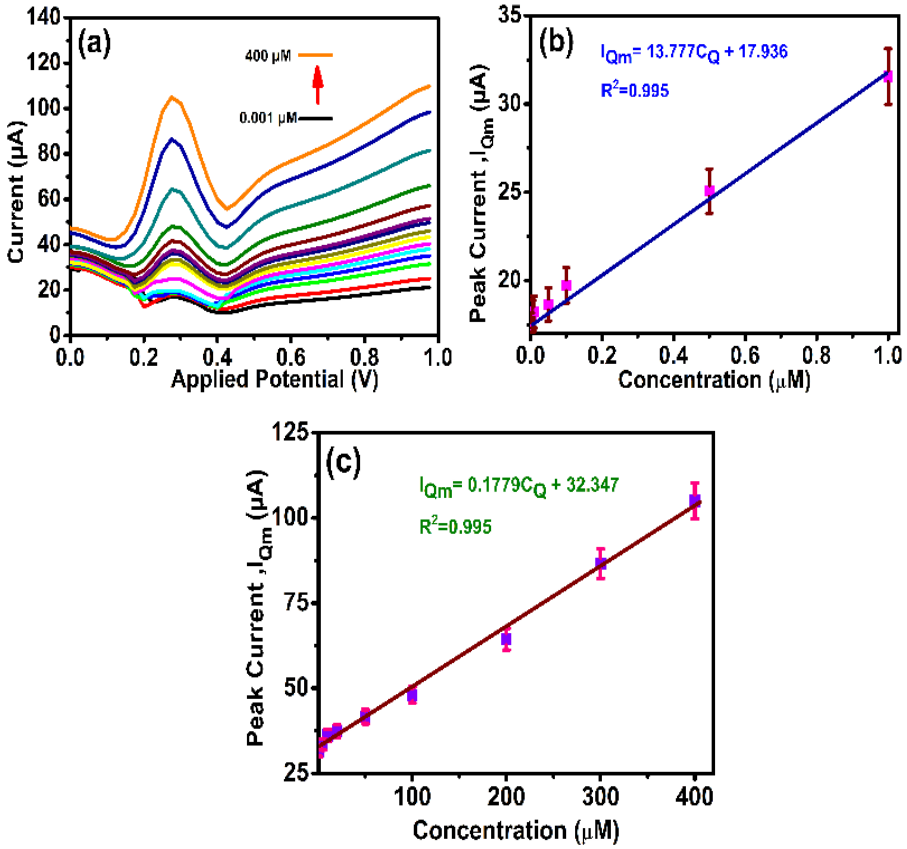

Fig. 5.2.7. (a) DPV responses of M-AARGO@G electrode surface in PBS 6 acquired for different QCN concentrations, considering dipping time of 30 s between two successive runs, and Peak current (I_{Qm}) versus QCN concentration (C_Q) Linear plot for (b) 0.001 µM to 1 µM, and (c) 1 µM to 400 µM.

By utilizing equation (5), the lower limit of QCN detection (LOD) was calculated to be 0.13 nM from $LOD = 3\frac{\sigma_Q}{m_Q}$[46], [47]. The limit of QCN quantification (LOQ) was estimated to be 0.43 nM employing $LOD = 10\frac{\sigma_Q}{m_Q}$ [48], [49] where m_Q and $\sigma_Q$represent the gradient of the calibration line and the peak current standard deviation for the lowest quantified QCN concentration. The M-AARGO@G electrode's effectiveness in detecting QCN is indicated by the obtained low value of LOD.

5.2.2.8 Repeatability, stability, and reproducibility investigation to assess the reusability of the sensor

Studies on stability, repeatability, and reproducibility have been conducted in a 100 µM QCN-0.1 M PBS 6 solution to explore the M-AARGO@G sensor reliability and reusability. Firstly, repeatability analysis was performed using five consecutive CV measurements for the M-AARGO@G electrode. The proposed MIP sensor exhibits satisfactory repeatability, as evidenced by its nominal anodic peak current deviation (relative standard deviation (RSD): 1.17%) for the five repetitions T1, T2, T3, T4, and T5 (Fig. 5.2.8(a)). The reproducibility of the sensor was investigated by fabricating three distinct electrodes- ET1, ET2, and ET3. As was previously mentioned, the same fabrication process is employed for all of the sensors. For every one of these electrodes, the peak anodic currents were estimated and the CV responses were noted (Fig. 5.2.8(b)). With a low RSD of 1.47%, the subsequent analysis confirmed the sensor's satisfactory reproducibility. Furthermore, with an acceptable RSD of 1.82%, the sensor's reasonably satisfactory and stable behaviors were endorsed by the minimal variations in peak anodic current and potential (Fig. 5.2.8(c)). The electrode maintained its functionality after a month of dormancy in a ziplock bag at room temperature, thereby highlighting impressive durability. Consequently, this sensor stands out as a prime candidate for food applications and long-term resource-conscious research.

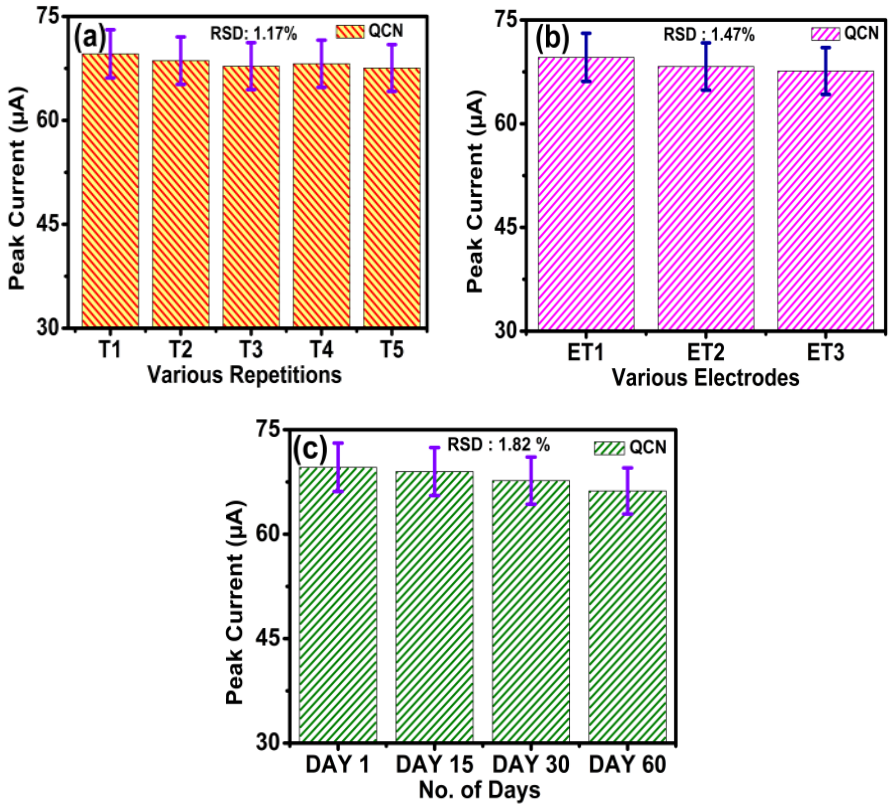

Fig. 5.2.8. (a) Repeatability, (b) reproducibility, and (c) stability profile of the M-AARGO@G electrode with respect to maximum anodic current at a concentration of 100 µM QCN.

5.2.2.9 Interference study

Practical applications demand investigations of the interference study of the electrode because inorganic compounds or biologically active co-agents may influence the detection of QCN. In this work, five different potentially interfering species agents, each 5-fold were applied to the M-AARGO@G electrode at 100 µM of the target analyte: syringic acid (SA), salicylic acid (SCA), magnesium (Mg^{2+}), potassium (K^{+}), and cinnamic acid (CA). The interference profile with the maximum anodic current variation is shown in Fig. 5.2.9. The peak anodic current barely fluctuates (within the 5% tolerance limit level) among all phenolic and other interfering species, indicating that the M-AARGO@G sensor's selectivity is satisfactory.

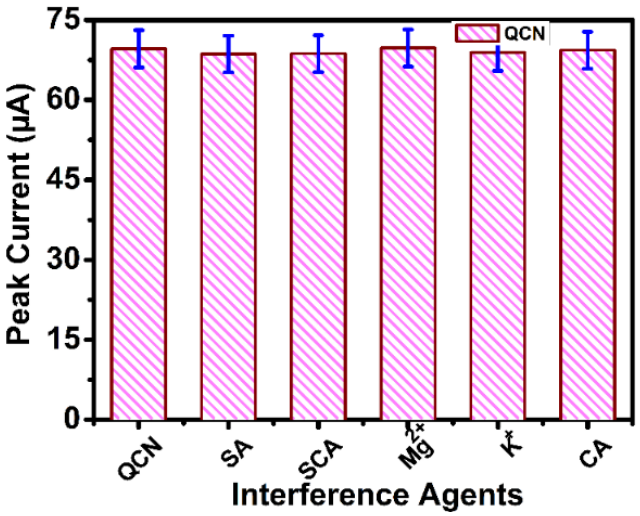

Fig. 5.2.9. Interference profile of M-AARGO@G electrode subjected to five interfering agents (syringic acid (SA), salicylic acid (SCA), magnesium (Mg^{2+}), potassium (K^{+}), cinnamic acid (CA).

5.2.2.10 Real Sample Study

Three samples—onion, oregano, and spinach were subjected to a quantitative measurement of QCN level, followed by comparison research using an HPLC analysis. Table 5.2.2 summarizes the results of that study, where r (number of observations corresponding to the three sample extracts) =3. The M-AARGO@G electrode exhibited superior accuracy of 99.93%, 99.67%, and 99.92% in detecting QCN for oregano, onion, and spinach samples, respectively. Further, from the t-test analysis, the estimated values for the standard deviation of the difference (σ_d) and the mean difference ($\overline{M_d}$) were 0.147 and 0.160, respectively, for three samples (number of samples, N = 3). Utilizing $T = \frac{\overline{M_d}}{\sigma_d/\sqrt{N}}$[42], it was estimated that the absolute value of "t" (A_t) was 1.88. With reference to the "t" distribution table, the critical "t" (C_t) value for a degree of freedom (DF) of 2, a 95% confidence level, and a 0.05 significance (alpha) level was obtained to be 2.92. Since "A_t" is smaller than "C_t", it can be inferred that the detection results almost comply with those of the reference HPLC technique for the mean QCN concentration present in those three samples.

TABLE 5.2.2

Detection Of QCN Using M-AARGO@G Electrode

Sample	Detected QCN(μM)		[a]Error (%)	[b]Accuracy (%)
	Proposed method (Measured)	Ref. (HPLC) method (Actual)		
Oregano	49.36	49.29	0.07	99.93
Onion	64.46	64.13	0.33	99.67
Spinach	33.98	34.06	0.08	99.92

[a]Error(%)=[|Measured- Actual|)/Actual]100; [b]Accuracy (%) = 100- Error %

PUBLICATION STATUS

JOURNAL

- D. Bandyopadhyay, S. Nag, D. Das, and R. B. Roy, "A Novel rGO-Decorated Molecularly Imprinted Polyacrylic Acid Graphite Electrode for the detection of Quercetin in Food," IEEE Transactions on Instrumentation and Measurement, vol. 73, pp. 1–8, Jan. 2024, doi:10.1109/tim 2024.3398119.

5.3 A Novel Molecular Imprinted Dual-Polymer Infused Capacitive Sensor for Quercetin Detection in Agro Products

The second study introduces a novel Molecular Imprinted Dual-Polymer Infused Capacitive Sensor (M2P-QT@C) for precise QT detection in agro-products. As per the authors' research inspection, this is the first reported use of a capacitive sensor for QT detection. Capacitive sensors offer several advantages over other types of sensors, including stability, sensitivity, reproducibility, low power consumption, and ease of fabrication. A study proposed a capacitive sensor using a copper electrode coated with reduced graphene oxide (RGO) and polymethylmethacrylate (PMMA) for detecting formaldehyde in milk and water [50]. Another study presented an MIP-based sensor using a PDMS (polydimethylsiloxane) coating on a capacitive sensor for detecting 2-Furfuraldehyde (2-FAL) in transformer oil. The sensor's sensitivity was evaluated by measuring changes in capacitance, impedance, and phase angle for varying concentrations of 2-FAL in the oil [51]. Researchers also introduced a MIP-based capacitive sensor with gold-coated silicon electrodes for detecting sulphanilamide (SN) in milk and water [52].

Recent research has explored the application of bio-mimic materials like derivatives of 3, 4-dihydroxyphenylalanine and Dopamine (also known as polydopamine or PDA) for surface

coatings in sensor fabrication. These materials offer excellent adhesion properties owing to the combination of hydrophobic interactions, hydrogen bonding, and electrostatic interactions between the substrate and ligand groups (clasping catechol, phenyl, and amine groups) [53 – 64]. Some studies suggest that co-depositing PDA with polymers like polyethylene glycol can ameliorate the wettability of the sensor surface and amend its overall performance [53, 64].

The proposed sensor combines the advantages of MIPs, Polydopamine-Polyethylene Glycol (PDA-PEG), and capacitive sensor technology. The influence of frequency and the concentration of QT on parallel capacitance (C_{pqt}) was examined along with other electrical parameters like impedance (Z_{pqt}) and phase angle (θ_{pqt}). C_{pqt} has been chosen as the key parameter for further in-depth studies on the sensor's linearity, stability, and selectivity. The performance of the M2P-QT@C sensor was compared to a non-imprinted version (NI-2P@C) by examining the variation of capacitance values C_{pqt} with QT concentration. This study highlights the novelty in introducing a promising repeatable, selective, cost-effective, and highly stable capacitive sensor for discerning recognition of QT in Oregano (OGN), onion (ON), and spinach (SN). The sensor's efficacy lies in its ability to be directly immersed in any infusion during experimentation without any pre-treatment, due to its capacitive nature. To assess the sensor's potential for predicting QT concentration, this study employs partial least squares regression (PLSR) and principal component regression (PCR) models. Both methods achieved exceptionally high accuracy, exceeding 90% in predicting QT content. The sensor showed a linear response to QT concentrations ranging from 10 to 50 ppm (parts per million) with a LOD and LOQ as low as 0.035 µg/kg and 0.116 µg/kg, respectively. It has been demonstrated that this synthesized capacitive sensor can stand out to be a worthwhile contender for recognizing and determining QT in agro-products.

5.3.1 Experimental Section

5.3.1.1 Essential Materials for sensor development and testing

Tokyo Chemical Industry (TCI) supplied both QT and 3-Hydroxytyramine hydrochloride, also known as dopamine hydrochloride (DA-HCl) (CAS RN: 62-31-7). DA-HCl was oxidized to create a more reactive surface coating substance known as PDA. The ligands (catechol, amine, and phenyl) of PDA aid bonding with Cu substrates through electrostatic and hydrophobic interactions, courtesy of hydrogen bonds. The copper-clad FR-4 (0.15 cm thick) sheet, sandpaper (zero sizes), Millipore water, and filter paper were obtained from a local retailer. Keysight Technologies is the vendor for the Impedance Analyzer (E4990A, 20 Hz-50 MHz), which was

employed for sensor-testing purposes. The disposable sterile syringe filters (Whatman UNI-FLO, 25 mm diameter, 0.22 µm pore size) equipped with polyvinylidene fluoride (PVDF) membranes were supplied by Whatman. Finally, polyethylene glycol (PEG MW 400) acquired from Merck Millipore was employed for PDA-coating purposes.

A. Fabrication Procedure

A copper-clad FR-4 sheet (measuring 5.9 cm × 1.6 cm × 0.15 cm as represented by Fig. 5.3.1 (a), (b)) was smoothed with sandpaper (zero sizes), and its edges were filed. Then, the sheet was cleaned by ultrasonically cleaning it in acetone at 60°C for 15 min, followed by rinsing with Millipore water. The cleansed sheet was then dried in a controlled-temperature oven at 70°C for 10 min. Finally, the Cu strips were coated with PEG solution by dipping them in the solution for 15 min. The MIP material was synthesized engaging dopamine hydrochloride (DA-HCl) as the efficient monomer, and QT as the analyte molecule. 2 mg mL^{-1} of DA-HCl, along with 8 mg of QT, was dissolved in an optimized volume of 90 mL of purified water. Then, by regular exudation of an optimized volume of 10 mL of a tris-ammonium buffer solution, the solution was stirred at 40 rpm for around 30 min until the pH level was attuned to 9. This drop-wise buffer addition was optimized to ensure precise pH control. After 48 h, it was perceived that DA-HCl experienced a self-polymerization process, forming a thin layer of PDA on both sides of the strips. The sensor was then baked in a furnace at 40°C for 30 min to remove moisture. Thereafter, it was rinsed in Millipore water for 5 min to pull out loosely bound particles. This rinsing process creates tiny cavities shaped like the QT template molecule on the polymer's surface. The sensor was then redried in the furnace using the same configurations till it was ready for testing. The NI-2P@C sensor was developed likewise to that followed during MIP preparation, excluding for the incorporation of QT in the solution before the stirring initiation.

B. Experimental set-up

The testing analysis was performed by dipping the sensor (dip length 4.4 cm) into test samples (Fig. 5.3.1). An impedance analyzer (KEYSIGHT, E4990A, 20 Hz-50 MHz), connected with the sensor was employed to investigate the sensor's electrical properties (capacitance, impedance, phase angle) at an ac signal of 1 V magnitude, with a frequency sweep from 20 Hz to 50 kHz, using a logarithmic sweep with 201 points (Fig. 5.3.2). Five trial solutions with increasing QT concentrations (10 ppm, 20 ppm, 30 ppm, 40 ppm, and 50 ppm) were concocted at room temperature of 25°C. Corresponding to each trial solution, ten test runs were considered for

data acquisition corresponding to those three electrical parameters. Between each dip, the sensor was washed in Millipore water for 5 min to eradicate loosely bound particles. Before testing a new solution, the sensor was incubated in that corresponding solution for 10 min. To ensure consistent measurements, especially parallel capacitance (C_{pqt}), all experiments were conducted at ambient temperature using the same 100 mL beaker size. Thus, these masquerading factors neither significantly influence the experimental results nor the sensor's intrinsic characteristics. The 5-min washing time was obtained to be the optimum as the minimum error was obtained in capacitance measurements (less than 0.51%, Table 5.3.1) before and after testing.

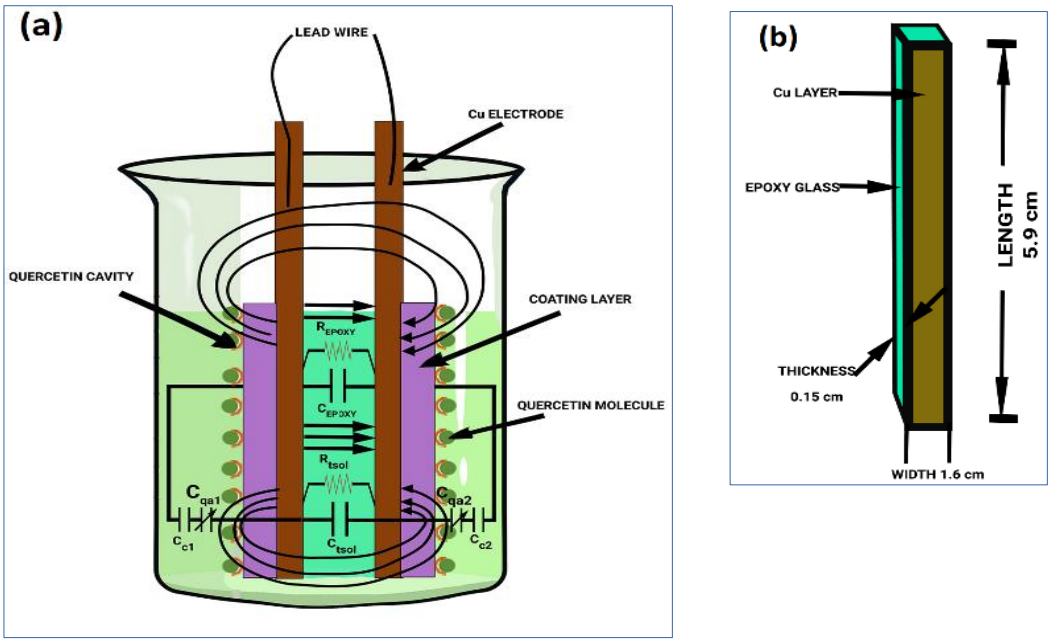

Fig. 5.3.1. Graphic representation of (a) Equivalent circuit of the sensor along with M2P-QT coated Cu strip, and (b) Cu strip**.**

Table 5.3.1

Washing time optimization

Sl No.	Pre-Testing (Max. Capacitance (nF)	Post-Testing		Error (%)
1		**Wash Time (min)**	**Max. capacitance (nF)**	0
2		0	9.37	56.40
3	21.47	3	17.14	20.17
4		**5**	**21.36**	**0.51**
5		10	21.35	0.55
6		15	21.33	0.65

Fig. 5.3.2. Experimental Testing system – electrode coupled with the impedance analyzer.

5.3.1.2 Equivalent electrical theoretical model of the projected sensor

A. Electrical equivalent model: M2P-QT@C sensor

The aforementioned studies lead the way to designing the equivalent electrical circuit of the proposed sensor [51, 65 – 68]. The uncoated sensor is embraced by two Cu plates with FR4 fiberglass epoxy (EP) in between. Circuit elements (C_{para}, C_{epoxy}, R_{epoxy}, C_{c1}, C_{c2}, C_{qa1}, C_{qa2}, C_{sol}, and R_{sol}) as shown in Fig. 5.3.3(a) form the mainstay of the electrical equivalent circuit of the sensor.

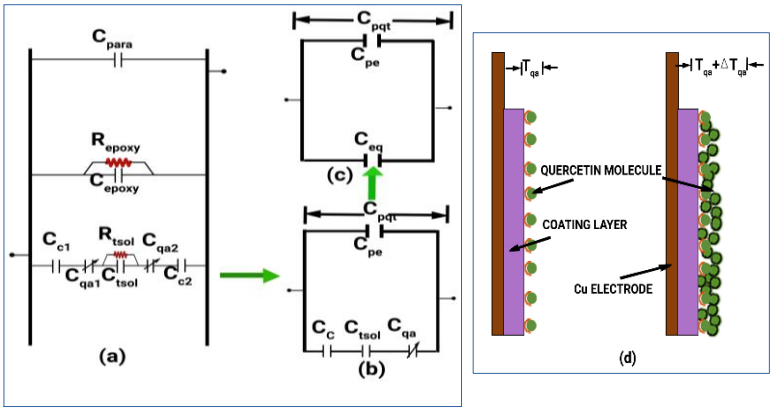

Fig. 5.3.3. (a) Electrical equivalent model, (b) to (c) concise equivalent models, and (d) MIP-coated Cu strips portraying widening of the QT-layer on the electrode surface.

During the operation of the sensor, one of the paths of electric lines of force is most likely to pass unswervingly through the EP-FR4 and the other via the test solution encompassing the sensor. The lines of force are passing through EP - FR4, being straight leads to the rise of C_{epoxy} and R_{epoxy} between a couple of Cu electrodes. Furthermore, from one of the Cu electrodes originates a curved electric field path to another electrode via the test solution environing the

sensor, due to the fringing fields in the vicinity of the sensor edge. R_{tsol} and C_{tsol} define the capacitance and resistance developed in this path. The coating capacitances arising from the coating layers on both sides of the Cu electrode are represented as C_{c1} and C_{c2}. On both sides of the strip, a couple of variable capacitances (C_{qa1} and C_{qa2}) are probably dynamically formed as a result of the absorption of QT molecules to MIP sensor layers. As depicted in Fig. 5.3.3(b) and Fig. 5.3.3(c), R_{epoxy} and R_{tsol} almost act as open circuit paths, and were hence eliminated from the equivalent circuit model courtesy of their high values [51]. The compact circuit model is shown in Fig. 5.3.3(b) and Fig. 5.3.3(c). Regardless of the QT concentration variation in the solution, the thickness of the MIP coating (T_{MIP}) remains unaltered on both sides of the Cu electrode. C_{para} symbolizes the parasitic capacitance, and C_{pe} represents the equivalent capacitance of the Cpara-Cepoxy pair. The compact equivalent circuit of the sensor is shown in Fig. 5.3.3(d). The overall parallel capacitance, $C_{pqt,}$ can be estimated from the following equations:

$$C_{pqt} = C_{pe} + C_{eq} \tag{1}$$

Where $C_{pe} = C_{para} + C_{epoxy}$ (2)

and $C_{eq} = \frac{C_c \times C_{sol} \times C_{qa}}{(C_c \times C_{tsol}) + (C_{tsol} \times C_{qa}) + (C_{qa} \times C_c)}$ (3)

$$\frac{C_c \times C_{tsol}}{C_c + C_{tsol} + \left(\frac{C_c \times C_{tsol}}{C_{qa}}\right)} \tag{4}$$

Here, the variable capacitance due to the adsorption of QT molecules,$C_{qa}$is given by

$$C_{qa} = \frac{C_{qa_1} \times C_{qa_2}}{C_{qa_1} + C_{qa_2}} = \in_o \times \in_{qo} \times \frac{A_s}{2 \times T_{qa}} = f\left(\frac{1}{T_{qa}}\right) \tag{5}$$

where, $\in_{qo}$, and T_{qa} indicate the dielectric constant of QT and the thickness of the absorbed QT molecule layer on the MIP surface.

On the other hand, overall coating capacitance, C_c is given by

$$C_c = \frac{C_{c_1} \times C_{c_2}}{C_{c_1} + C_{c_2}} = \frac{\in_o \times \in_{MIP} \times A_s}{2 \times T_{MIP}} \tag{6}$$

where, T_{MIP} - MIP coating thickness on the Cu electrode on dual sides, A_s- electrode surface area, $\in_o$ and $\in_{MIP}$- dielectric constant of vacuum, and the coated-MIP, respectively.

Therefore,$C_{pqt} = C_{pe} + C_{eq} = \left(C_{para} + C_{epoxy}\right) + \frac{C_c \times C_{tsol}}{C_c + C_{tsol} + \left(\frac{C_c \times C_{tsol}}{f\left(\frac{1}{T_{qa}}\right)}\right)}$ (7)

B. Theoretical Aspect-Capacitance dependency on QT concentration

The MIP technique governs the detection mechanism of the proposed sensor. The PDA-PEG layer of the sensor contains QT-cognizant sites, designed to mimic specifically QT molecules, and attract them from the sample test solutions. When dipped into the solution, QT molecules begin to adsorb to the sensor's surface, forming a layer whose thickness primarily depends on a couple of factors: QT concentration and sensor dipping time. The scope and extent of this molecular adsorption modulated the surface density close to the solid-liquid interface, which most likely alters the effective thickness of the sensor.

This variable layer's thickness affects the C_{pqt} in turn, a measurement of how much electrical charge the sensor can store. As the QT concentration in the solution increases, the thickness of the QT layer on the sensor also increases, T_{qa} to $T_{qa} + \Delta T_{qa}$ (Fig. 5.3.3(d)). This rise in layer thickness leads to a decrease in adsorption capacitance values, C_{qa1} and C_{qa2}. Since other circuit parameters (C_{para}, C_{epoxy}, C_{c1}, C_{c2}, C_{sol}) influencing the overall capacitance (C_{pqt}) remain constant after the sensor is fabricated, any changes in QT concentration in the sample solution will only directly impact the C_{qa1} and C_{qa2}, which in turn affect the overall parallel capacitance (C_{pqt}) of the sensor (Fig. 5.3.4).

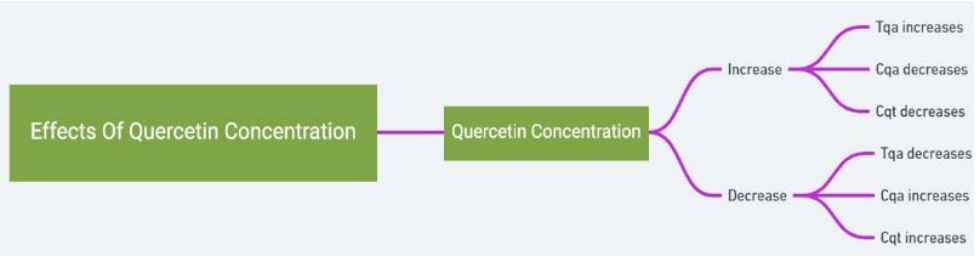

Fig. 5.3.4. Relationship between QT concentration, layer thickness, and overall parallel capacitance

5.3.2 Results with discussions.

5.3.2.1 SEM Insights

Scanning electron microscopy (SEM) analysis was performed to investigate the surface morphology of M2P-QT@C and N2P@C materials (Fig. 5.3.5). The SEM images revealed that M2P-QT@C (Fig. 5.3.5(a)) possesses more globular and uniformly sized particles compared to NI-2P@C (Fig. 5.3.5(b)). This observation signposts a superior dispersion of molecules on the M2P-QT@C sensor surface. As a consequence, M2P-QT@C most likely offers a greater number of binding sites for QT analyte molecules to readily occupy, potentially leading to enhanced sensor performance.

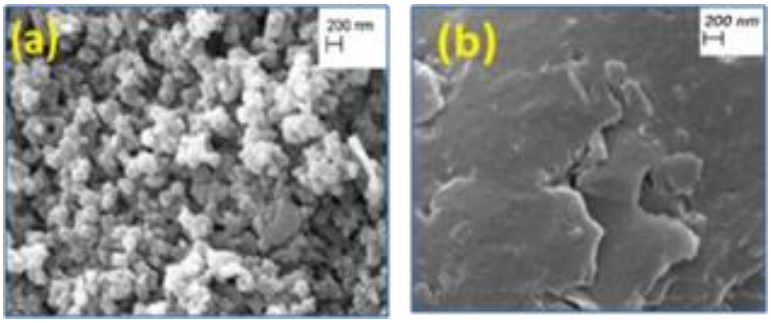

Fig. 5.3.5. SEM insights of (a) M2P-QT@C material, (b) N2P@C material.

5.3.2.2 XRD Investigation

The X-ray diffraction (XRD) analysis has been performed for the M2P-QT@C synthesized material (Fig. 5.3.6). The diffraction pattern revealed a significantly stronger peak at 26.65° (2θ values). This indicates the formation of an amorphous, sturdily-bonded polymer with several DA units interconnected along the polymer chain. This observation is consistent with the previously reported formation of an amorphous PDA polymer in [69].

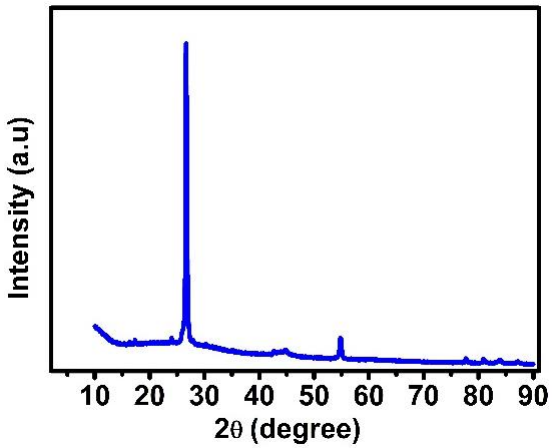

Fig. 5.3.6. X-ray diffraction study of the produced M2P-QT@C composite.

5.3.2.3 Comparative insights: variation of capacitance- M2P-QT@C versus N2P@C

The synthesis of the MIP composite involved a blend of PEG and dopamine (DA). Courtesy of hydrogen bonding between PEG's ether groups and DA's catechol group, a PDA-PEG composite with a uniform distribution of PDA aggregates was produced. PDA is synthesized inherently by the self-polymerization of DA. This newly formed composite is ideal for adhering to the Cu plate owing to the innate adhesiveness of the PDA. PDA has an attractive ability to chelate and reduce copper ions (Cu^{2+}) to metallic Cu in an alkaline environment, which is the collective effect of its catechol and amino groups. Additionally, the higher affinity of Cu^{2+} ions toward amino groups may have emboldened them to coordinate with PDA's amino groups [45].

Fig. 5.3.7 compares the capacitance (C_{pqt}) of M2P-QT@C and N2P@C sensors at a lower frequency range. M2P-QT@C has abundant recognition sites for QT, leading to enhanced analyte adsorption and a thicker adsorption layer (T_{qa}). According to equation (5), a thicker T_{qa} reduces the inter-electrode capacitance (C_{pqt}), resulting in a lower C_{pqt} value. Conversely, N2P@C has minimal molecular adsorption due to the absence of recognition sites, which translates to a thinner adsorption layer (T_{qa}) and a higher C_{pqt} value. As expected, M2P-QT@C exhibits a significantly lower C_{pqt} of about 5.51 times lower than that of NI-2P@C due to the presence of more recognition sites and the resulting thicker adsorption layer.

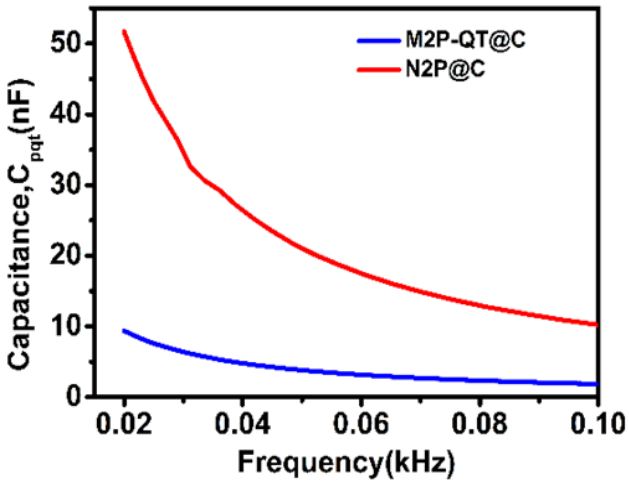

Fig. 5.3.7. Effect of frequency on the capacitance (C_{pqt}) for M2P-QT@C and N2P@C sensors.

5.3.2.4 Impact of different QT concentrations on the Capacitance (Cpqt)

It was explored that the parallel capacitance of the sensor (C_{pqt}) decreases as the operating frequency increases (Fig. 5.3.8 (a)). This trend is consistent with the proposed electrical model in section 2.4 and prior research [51]. Additionally, as steered by equation (7), C_{pqt} was inversely proportional to both the adsorption thickness and QT concentration (P_{qt}), implying a decrease of C_{pqt} as the concentration of QT increases in the test sample.

5.3.2.5 Linearity range exploration with LOD calculation

Fig. 5.3.8(b) shows a straight line (linear plot) depicting the relationship between the maximum parallel capacitance (C_{pqtm}) and the template QT concentration (P_{qt}). The capacitance points were taken at 20 Hz, which is the lowest frequency at which the peak capacitance was observed. The calibration plot demonstrates that the C_{pqtm} increases linearly with increasing P_{qt} concentration from 10 ppm to 50 ppm, following a linear equation of regression.

$C_{pqtm} = -1.72P_{qt} + 11.026$; $R^2 = 0.99$ (8)

The LOD and LOQ of the M2P-QT@C can be evaluated to be 0.035 µg/kg and 0.116 µg/kg, respectively, using the following couple of equations: LOD = $3\sigma_c/ m_c$ and LOQ= $10\sigma_c / m_c$, where σ_c and m_c designate the capacitance (C_{pqt}) standard deviation and calibration curve gradient [70]. The LOD of 0.035 µg/kg as achieved in this case is a noteworthy improvement over that reported in the earlier study [71].

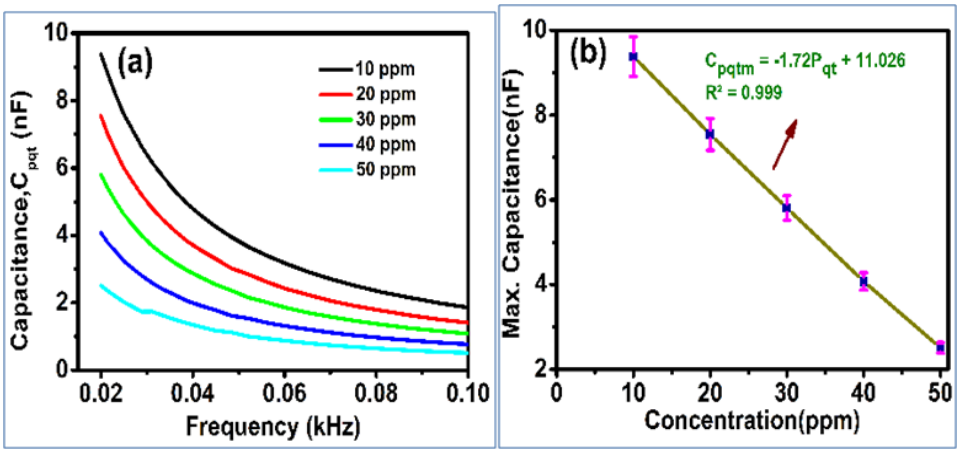

Fig. 5.3.8. (a) C_{pqt} deviation profile with the change of QT concentration in the test solution for 20-100 Hz frequency window and (b) Maximum capacitance (C_{pqtm}) linear variation with QT concentration.

5.3.2.6 Sensor impedance with phase angle variation study for diverse QT concentration

For the RC parallel circuit, the equivalent admittance (Y_{pqt}) can be expressed as

$$Y_{pqt} = \frac{1}{Z_{pqt}} = j\omega C_{pqt} + \frac{1}{R_{pqt}} \quad (10)$$

where R_{pqt} and C_{pqt} represent the resistance and parallel capacitance, respectively.

Impedance (Z) being the reciprocal of admittance(Y), equivalent sensor impedance (Z_{pqt}) can be directly derived from the above equation

$$Z_{pqt} = \frac{R_{pqt}}{1+j\omega C_{pqt}R_{pqt}} = \frac{R-j\omega C_{pqt}{R_{pqt}}^2}{1+\omega^2 C^2 {R_{pqt}}^2} \quad (11)$$

The real part and the imaginary part of Z_{pqt} can be obtained as $Z_r = \frac{R_{pqt}}{1+\omega^2 {C_{pqt}}^2 {R_{pqt}}^2}$ (12)

$$Z_i = \frac{-j\omega C_{pqt}{R_{pqt}}^2}{1+\omega^2 {C_{pqt}}^2 {R_{pqt}}^2} \quad (13)$$

The relationship between the sensor impedance (Z_{pqt}) and the sensor parallel capacitance C_{pqt} is governed by equations (10)-(13). Fig. 5.3.9(a) shows how the variation of the impedance of

the sensor with frequency (up to 100 Hz) for different QT concentrations. The frequency characteristics revealed that the impedance, $Z_{pqt,}$ increases as the concentration of QT increases. It also revealed that the impedance decreases slightly at low frequencies for all concentrations. These couple of observations are consistent with the above-mentioned equations. The phase angle (θ_{pqt}) of the sensor is also affected by frequency and QT concentration. Fig. 5.3.9(b) portrays the phase angle, $\theta_{pqt,}$ versus frequency for different QT concentrations up to 1 kHz. It was observed that the phase angle, $\theta_{pqt,}$ decreases as the frequency increases for all concentrations. Additionally, the phase angle surges for a given frequency as the QT concentration in the test solution is raised. This may be elucidated by the variation of the electrical properties of the sensor evoked by the changes in QT concentration.

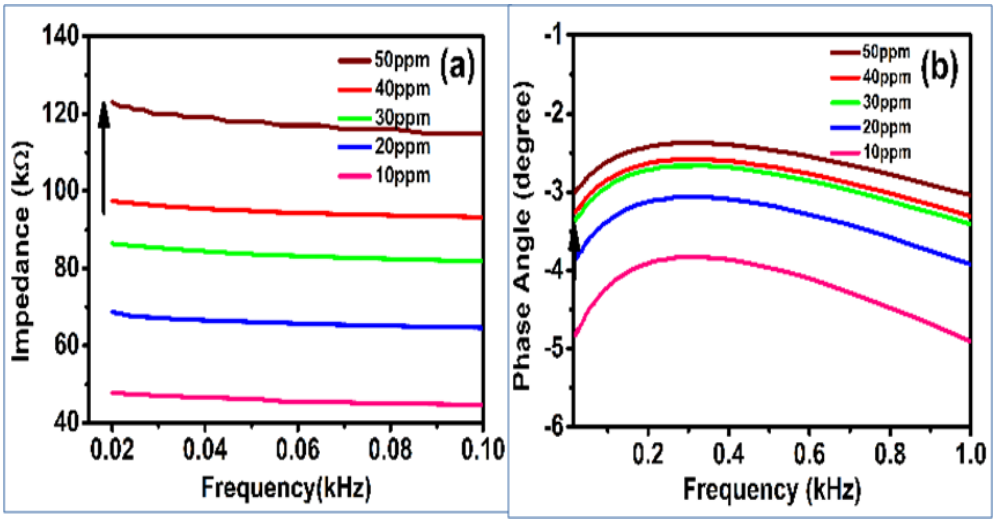

Fig. 5.3.9. (a) Variation of sensor impedance (Z_{pqt}) with frequency (kHz) and (b) Phase angle (θ_{pqt})-frequency profile at different QT concentrations

5.3.2.7 Reliability of: M2P-QT@C Sensor

To explore the sensor's stability, or in other words, reliability, in succession, periodic tests were performed over three months. The maximum parallel capacitance (C_{pqtm}) exhibited excellent stability, with minimal change in the first 30 days, and a slight increase of only 0.4% after one and a half months at a 10 ppm QT concentration (Fig. 5.3.10). This indicates high sensor reliability. The minor increase in C_{pqtm} is likely due to the MIP coating layer thinning slightly over time, which may have obliterated a few template recognition sites on the surface. To avert contamination from the environment, the sensors were gingerly stowed in zip-lock pouches with tissue paper at room temperature.

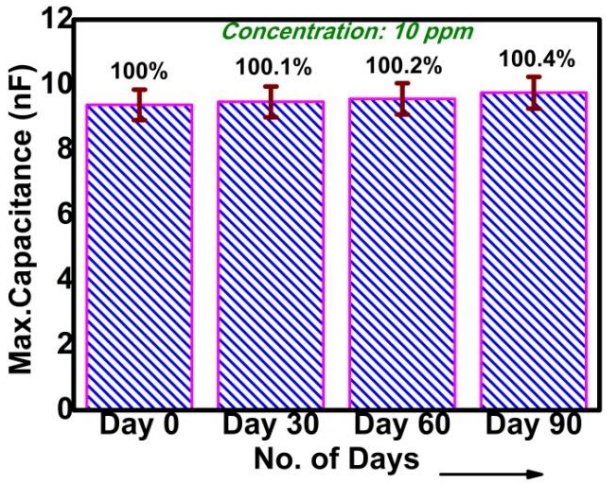

Fig. 5.3.10. Stability Profile of the M2P-QT@C Sensor.

5.3.2.8 Selectivity investigation: M2P-QT@C Sensor

The selectivity efficacy of the M2P-QT@C was examined by sub-immersing the sensor in 10 ppm solutions of QT, gallic acid (GA), syringic acid (SA), catechin (CC), and salicylic acid (SA) one after another for 10 min. The M2P-QT@C sensor was employed to measure the QT content in Oregano (OGN), onion (ON), and spinach (SN). These molecules have been selected based on the structural resemblance and coexistence with the QT molecule in real samples. The results depicted in Fig. 5.3.11 unveiled that the sensor responded best to QT compared to all other molecules. This may be attributed to the following: QT molecules have the same number of hydrogen bond-forming sites as the molecules on the sensor's surface, allowing them to fit snugly into cavities. As more QT molecules were adsorbed onto the sensor, the C_{pqt} decreased, owing to the increase in the adsorption layer (T_{qa}), as discussed earlier.

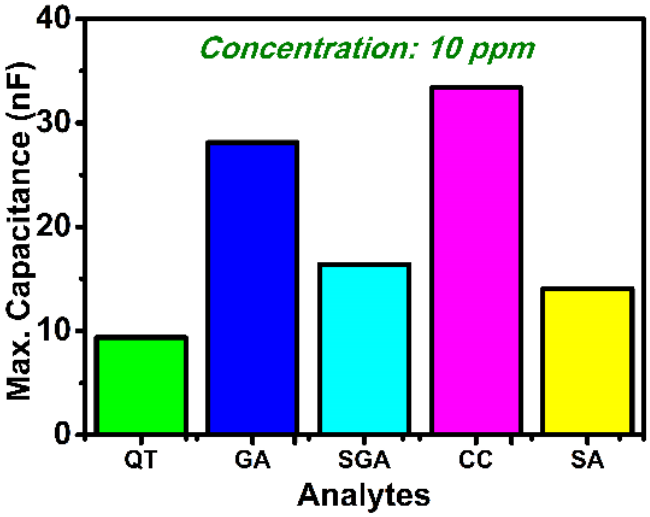

Fig. 5.3.11. Selectivity profile: M2P-QT@C sensor.

5.3.2.9 Real Sample Analysis

The M2P-QT@C sensor was employed to measure the QT content in three samples: Oregano (OGN), onion (ON), and spinach (SN). OGN, ON, and SN, obtained from a local market, were thoroughly washed under running water to remove any dirt or contaminants. The washed samples were air-dried at room temperature for 1h until the moisture content was reduced to a minimal level. After extraction of juices using a standard juice extractor for 5 min, the samples were diluted with 100 mL of distilled water to create a 1:10 dilution. The brewed samples were filtered employing disposable sterile syringe filters (Whatman UNIFLO, 25 mm diameter, 0.22 μm pore size) equipped with polyvinylidene fluoride (PVDF) membranes to eliminate insoluble particles. The final solutions were diluted to a volume of 200 mL using distilled water. This solution was then tested using an impedance analyzer. For each sample, the M2P-QT@C electrode was dipped into the test solution eight times, and the impedance was measured across the entire frequency window of 20 Hz to 50 kHz. This resulted in a data matrix with dimensions of [201 × 10 × 2]. PLSR and PCR were implemented in MATLAB R2017b to analyze and obtain the prediction accuracy. For each QT concentration, 80% and 20% of the data were considered for the training and testing process, respectively. The results are abridged in Tables 5.3.2 and 5.3.3. The accuracy of the M2P-QT@C sensor was compared to HPLC analysis, and both techniques achieved high average prediction accuracies of over 99%. Table 5.3.2 highlights the statistical metrics corresponding to PLSR and PCR models, where R_v^2, R_c^2, and R_p^2 indicate validation, calibration, and prediction coefficients respectively. To further validate the sensor's performance, recovery experiments were conducted. Real samples were spiked with QT concentrations close to their initial measured values. The recovery percentages were then calculated for both PLSR and PCR models. Table 5.3.3 summarizes the spiking and recovery results.

Table 5.3.2

Statistical metrics for both models

Technique employed	Calibration		Validation		Prediction	
	RMSEC	Rc^2	RMSEV	Rv^2	RMSEP	Rp^2
PLSR	0.0075	0.93	0.0078	0.92	0.0083	0.90
PCR	0.0084	0.91	0.0093	0.90	0.0094	0.89

Table 5.3.3

QT content & prediction accuracy: PLSR and PCR model

Sl No.	Reference QT (ppm) (HPLC)	Predicted QT (ppm)		Prediction Accuracy (%)	
		PLSR	PCR	PLSR	PCR
OGN	14.90	13.89	13.81	93.22	92.68
ON	19.38	18.16	17.92	93.71	92.46
SN	10.29	09.61	9.56	93.39	92.90
	Average prediction accuracy			**93.44**	**92.68**

5.3.2.10 Comparative Insights: Proposed Technique with Literature found on QT detection

The proposed sensor offers a superior limit of detection (LOD) and pleasing prediction capability compared to those obtained with the authors' preceding study [72] and other existing works (Table 5.3.4). In three real samples, OGN, ON, and SN, the minimum QT content detectable is 4.7 ppm, 1.327 ppm, and 0.429 ppm, respectively [73 - 74]. These minimum detectable values are significantly higher than the LOD achieved by this sensor.

Table 5.3.4

Comparative Insights

Electrode/ Sensor	Techniques used	Linear range (µM)	LOD (nM)	Refs
CPO/SPCE	DPV	0.08-129.83	3.00	[75]
Co_3O_4/GCE	DPV	0.01-3.00	0.20	[27]
CNU-DAQx	DPV	0.015-230.0	4.00	[26]
HOPNC	DPV	0.1-120.0	30.0	[76]
WS_2/$GdCoO_3$/GCE	DPV	0.001-329.0	3.00	[22]
M-AARGO@G	CV, DPV	0.001-400.0	0.13	[61]
Pt-MXene/GCE	CV,DPV	0.001-0.10, 0.10-1.00	0.92	[77]
SeO_2/rGO/GCE	CV,DPV	0.01-200.0	1.60	[78]
AgNPs@g-CNCV,DPV	CV,DPV	0.01-120.0	6.00	[79]
p[DqCrC]@Co-NC	CV, DPV	0.01-21.40, 1.40-150.0	14.00	[80]
MIP/PSSGR-/GCE	CV,DPV	0.001-0.02	0.50	[81]
Pd/MoS-IL-OMC/GCE	CV, DPV	0.02-10.00	8.00	[82]
CD/AuNPs/MWCNTs/GCE	CV, DPV	0.005-7.00	6.40	[83]
PB-rGO/TCD/AuNPs/GCE	CV, DPV	0.005-0.400	1.83	[84]
M2P-QT@C	**Capacitive**	**33.08-165.43**	**0.11**	**This work**

PUBLICATION STATUS

JOURNAL

- D. Bandyopadhyay, S. Nag, S. Acharya, D. Das and R. B. Roy, "A Novel Molecular Imprinted Dual-Polymer Infused Capacitive Sensor for Quercetin Detection in Agro Products," *IEEE Sensors Journal*, vol. 25, no. 21, pp. 39418-39425, 1 Nov.1, 2025, doi: 10.1109/JSEN.2025.3614749.

5.4 Summary of Developed Quercetin Detection Methods

This chapter meticulously investigated two distinct electrochemical sensing platforms for the accurate and selective quantification of quercetin (QCN) in various food samples, aiming to address the critical need for efficient and accessible analytical tools for phytochemical analysis.

5.4.1 Voltammetric Detection using rGO Decorated MIP-PAA Graphite Electrode

The first method introduced an effective reduced graphene oxide (rGO) decorated Molecularly Imprinted Polyacrylic Acid Graphite Electrode (M-AARGO@G) for the selective detection of QCN. This cost-effective, reproducible, and stable electrode was developed using acrylic acid (AA) as the monomer (chosen for its excellent functional group compatibility and reactivity with QCN) and QCN as the template on a graphite base. The incorporation of rGO was specifically intended to enhance electrocatalytic activities by providing a high surface area and numerous active sites, thereby encouraging molecular adsorption and fast electron transfer. The M-AARGO@G electrode material was thoroughly characterized using UV-visible (UV-vis) spectroscopy and scanning electron microscopy (SEM). The analytical features were assessed via a tri-electrode system employing Differential Pulse Voltammetry (DPV) and Cyclic Voltammetry (CV). Rigorous analysis revealed that the electrode exhibited two broad linearity windows: 0.001 μM to 1 μM and 1 μM to 400 μM. It achieved an impressively low limit of QCN detection of 0.13 nM and LOQ of 0.43 nM, indicating superior sensitivity for trace-level detection. Furthermore, the electrode demonstrated high reproducibility (RSD: 1.47%), good stability (RSD: 1.82%), and high repeatability (RSD: 1.17%). Its effectiveness was further corroborated through testing in real food extracts (onion, oregano, and spinach), where it exhibited high accuracy, averaging 99%, compared to the high-performance liquid chromatography (HPLC) method. Satisfactory statistical results from t-test analysis for mean QCN concentrations in the real samples further validated its performance.

5.4.2 Capacitive Detection using Molecular Imprinted Dual-Polymer Sensor

The second approach presented a novel, cost-effective capacitive sensor utilizing molecularly imprinted dual polymer (MIP) for precise quercetin (QT) detection in agro-products. The core

of this sensor was a special composite sensing material, molecular imprinted polydopamine-polyethylene glycol (M2P-QT@C), deposited onto a copper (Cu) plate. The sensing material's characteristics were extensively explored using scanning electron microscopy (SEM) for structural visualization and X-ray diffraction (XRD) for atomic arrangement information. The study investigated the frequency variation of three key electrical parameters: parallel capacitance (C_{pqt}), impedance (Z_{pqt}), and phase angle (θ_{pqt}). The sensor exhibited a linear response to QT concentrations ranging from 10 to 50 ppm, demonstrating exceptional sensitivity with an LOD of 0.035 µg/kg and an LOQ of 0.116 µg/kg. To predict the amount of QT in real samples, two statistical methods, Principal Component Regression (PCR) and Partial Least Squares Regression (PLSR), were successfully applied, both exhibiting high accuracy exceeding 90% with minimal error (RMSEC: 0.0015). A key finding was the significant decrease in measured C_{pqt} values with increasing QT concentration, consistent with the sensor's equivalent circuit model. A substantial difference in C_{pqt} values was observed between the M2P-QT@C sensor and its non-imprinted version (NI-2P@C) across different frequencies, confirming the effectiveness of the imprinted cavities. The sensor also demonstrated excellent selectivity for QT recognition and remarkable stability, with the maximum parallel capacitance (C_{pqtm})increasing by only 0.4% even after three months of use, indicating minimal performance degradation. Its capacitive nature allowed for direct immersion in infusions without pre-treatment, enhancing usability.

5.5 Conclusion

This chapter successfully developed and validated two innovative and highly effective electrochemical sensing platforms for the precise and selective quantification of quercetin (QCN) in real food samples. The rGO decorated Molecularly Imprinted Polyacrylic Acid Graphite Electrode (M-AARGO@G) demonstrated remarkable sensitivity with exceptionally low nanomolar detection limits and two broad linearity windows, making it suitable for a wide range of QCN concentrations. Its performance was further bolstered by excellent reproducibility, stability, and high accuracy in real food matrices like onion, oregano, and spinach, as confirmed by HPLC comparison and t-test analysis.

Complementing this, the novel Molecular Imprinted Dual-Polymer Infused Capacitive Sensor (M2P-QT@C) offered an equally compelling solution, distinguished by its unique capacitive sensing mechanism and exceptionally low detection limits in the microgram per kilogram range. The sensor's robust linear response, high predictive accuracy via PLSR and PCR, and impressive long-term stability, even after extended use, highlight its significant practical

potential. The ability of both sensors to effectively quantify QCN in real food extracts, with consistent agreement with established HPLC methods, underscores their reliability and suitability for real-world applications. Collectively, these advancements in electrochemical sensing, particularly through the strategic integration of molecularly imprinted polymers and nanomaterials like rGO, offer robust, cost-effective, and user-friendly alternatives to traditional, more laborious analytical techniques. These developed sensors hold significant promise for various applications within the food industry, facilitating efficient quality control, nutritional assessment, and the monitoring of health-beneficial compounds in a diverse array of agroproducts.

References

[1] S. Parasuraman, A. Anand David, and R. Arulmoli, "Overviews of biological importance of quercetin: A bioactive flavonoid," *Pharmacognosy Reviews*, vol. 10, no. 20, pp. 84-89, Nov 2016, doi: 10.4103/0973-7847.194044.

[2] S. C. Gupta, S. Prasad, and B. B. Aggarwal, *Drug Discovery from Mother Nature*. Springer, 2016.

[3] J. Pozo-Martínez, S. Vázquez-Rodríguez, C. Olea-Azar, and M. Moncada-Basualto, "Evaluation of ORAC methodologies in determination of antioxidant capacity of binary combinations of quercetin and 3-(3,4,5-trihydroxybenzoyl) coumarin derivatives," *Arabian Journal of Chemistry*, vol. 15, no. 11, p. 104298, Nov. 2022, doi: 10.1016/j.arabjc.2022.104298.

[4] A. Yarahmadi, F. Zal, and A. Bolouki, "Protective effects of quercetin on nicotine induced oxidative stress in 'HepG2 cells,'" *Toxicology Mechanisms and Methods*, vol. 27, no. 8, pp. 609–614, Jul. 2017, doi: 10.1080/15376516.2017.1344338.

[5] A. Guzel*et al.*, "Protective Effects of Quercetin on Oxidative Stress-Induced Tubular Epithelial Damage in the Experimental Rat Hyperoxaluria Model," *Medicina*, vol. 57, no. 6, p. 566, Jun. 2021, doi: 10.3390/medicina57060566.

[6] Y. Li et al., "Quercetin, Inflammation and Immunity," *Nutrients*, vol. 8, no. 3, p. 167, Mar. 2016, doi: 10.3390/nu8030167.

[7] S. Sadeghi and M. Hosseinpour-Zaryabi, "A sensitive fluorescent probe based on dithizone-capped ZnS quantum dots for quercetin determination in biological samples," *Luminescence*, vol. 35, no. 8, pp. 1391–1401, Aug. 2020, doi: 10.1002/bio.3903.

[8] X. ZHOU, J. SUN, D. ZHU, B. YUAN, and T. YOU, "Quality Analysis of Herbal Medicine Products Prepared from HerbaSarcandrae by Capillary Electrophoresis with Electrochemical Detection," *Chemical Research in Chinese Universities*, vol. 24, no. 2, pp. 148–153, Mar. 2008, doi: 10.1016/s1005-9040(08)60031-8.

[9] L. WANG and M. MORRIS, "Liquid chromatography–tandem mass spectroscopy assay for quercetin and conjugated quercetin metabolites in human plasma and urine," *Journal of Chromatography B*, vol. 821, no. 2, pp. 194–201, Jul. 2005, doi: 10.1016/j.jchromb.2005.05.009.

[10] V. Pilařová et al., "Simultaneous determination of quercetin and its metabolites in rat plasma by using ultra-high-performance liquid chromatography tandem mass spectrometry," *Talanta*, vol. 185, pp. 71–79, Aug. 2018, doi: 10.1016/j.talanta.2018.03.033.

[11] S. Özbilgin, Ö. B. Acıkara, E. K. Akkol, I. Süntar, H. Keleş, and G. S. İşcan, "In vivo wound-healing activity of Euphorbia characias subsp. wulfenii: Isolation and quantification of quercetin glycosides as bioactive compounds," *Journal of Ethnopharmacology*, vol. 224, pp. 400–408, Oct. 2018, doi: 10.1016/j.jep.2018.06.015.

[12] P. K. Jain, S. Jain, S. Sharma, S. Paliwal, and G. Singh, "Evaluation of anti-diabetic and antihypertensive activity of Phoenix sylvestris (L.)Roxb leaves extract and quantification of biomarker Quercetin by HPTLC," *Phytomedicine Plus*, vol. 1, no. 4, p. 100136, Nov. 2021, doi: 10.1016/j.phyplu.2021.100136.

[13] O. A. A. Ahmed, H. M. El-Bassossy, H. M. El-Sayed, and S. S. A. El-Hay, "Rp-HPLC Determination of Quercetin in a Novel D-α-Tocopherol Polyethylene Glycol 1000 Succinate Based SNEDDS Formulation: Pharmacokinetics in Rat Plasma," *Molecules*, vol. 26, no. 5, p. 1435, Mar. 2021, doi: 10.3390/molecules26051435.

[14] H. Qiu, C. Luo, M. Sun, F. Lu, L. Fan, and X. Li, "A novel chemiluminescence sensor for determination of quercetin based on molecularly imprinted polymeric microspheres," *Food Chemistry*, vol. 134, no. 1, pp. 469–473, Sep. 2012, doi: 10.1016/j.foodchem.2012.02.102.

[15] M. Hassan, F. Uzcan, S. N. Shah, U. Alshana, and M. Soylak, "Switchable-hydrophilicity solvent liquid-liquid microextraction for sample cleanup prior to dispersive magnetic solid-phase microextraction for spectrophotometric determination of quercetin in food samples," *Sustainable Chemistry and Pharmacy*, vol. 22, p. 100480, Sep. 2021, doi: 10.1016/j.scp.2021.100480.

[16] N. Altunay, D. Bingöl, A. Elik, and R. Gürkan, "Vortex-assisted ionic liquid dispersive liquid-liquid microextraction and spectrophotometric determination of quercetin in tea, honey, fruit juice and wine samples after optimization based on response surface methodology," *Spectrochimica Acta Part A: Molecular and Biomolecular Spectroscopy*, vol. 221, p. 117166, Oct. 2019, doi: 10.1016/j.saa.2019.117166.

[17] J. -H. Hwang, X. Wang, P. Pathak, M. M. Rex, H. J. Cho and W. H. Lee, "Enhanced Electrochemical Detection of Multiheavy Metal Ions Using a Biopolymer-Coated Planar Carbon Electrode," *IEEE Transactions on Instrumentation and Measurement*, vol. 68, no. 7, pp. 2387-2393, July 2019, doi: 10.1109/TIM.2019.2908045.

[18] R. Zribi et al., "Ag Nanoplates Modified-Screen Printed Carbon Electrode to Improve Electrochemical Performances Toward a Selective H_2O_2 Detection," *IEEE Transactions on Instrumentation and Measurement*, vol. 72, pp. 1-8, 2023, Art no. 6002708, doi: 10.1109/TIM.2023.3253902.

[19] A. Gomes, G. J. Mattos, B. Coldibeli, R. F. H. Dekker, A. M. Barbosa Dekker, and E. R. Sartori, "Covalent attachment of laccase to carboxymethyl-botryosphaeran in aqueous solution for the construction of a voltammetric biosensor to quantify quercetin," *Bioelectrochemistry*, vol. 135, p. 107543, Oct. 2020, doi: 10.1016/j.bioelechem.2020.107543.

[20] Y. Wang, M. Qiao, X. Mamat, X. Hu, and G. Hu, "Hierarchically ordered porous nitrogen doped carbon modified a glassy carbon electrode for voltammetry detection of quercetin," *Materials Research Bulletin*, vol. 136, p. 111131, Apr. 2021, doi: 10.1016/j.materresbull.2020.111131.

[21] V. Mariyappan, N. Karuppusamy, S.-M. Chen, P. Raja, and R. Ramachandran, "Electrochemical determination of quercetin using glassy carbon electrode modified with WS2/GdCoO3 nanocomposite," *Microchimica Acta*, vol. 189, no. 3, Feb. 2022, doi: 10.1007/s00604-022-05219-3.

[22] G. Ziyatdinova, E. Kozlova, and H. Budnikov, "Poly(gallic acid)/MWNT-modified electrode for the selective and sensitive voltammetric determination of quercetin in medicinal herbs," *Journal of Electroanalytical Chemistry*, vol. 821, pp. 73–81, Jul. 2018, doi: 10.1016/j.jelechem.2017.12.071.

[23] S. Bose, S. Radhakrishnan, B.-S. Kim, and H. W. Kang, "Formulation of amorphous carbon embedded CuFeS2 hybrids for the electrochemical detection of Quercetin," *Materials Today Chemistry*, vol. 26, p. 101228, Dec. 2022, doi: 10.1016/j.mtchem.2022.101228.

[24] W. Zhang, L. Zong, G. Geng, Y. Li, and Y. Zhang, "Enhancing determination of quercetin in honey samples through electrochemical sensors based on highly porous polypyrrole coupled with nanohybrid modified GCE," *Sensors and Actuators B: Chemical*, vol. 257, pp. 1099–1109, Mar. 2018, doi: 10.1016/j.snb.2017.11.059.

[25] S. Karakaya and İ. Kaya, "An electrochemical detection platform for selective and sensitive voltammetric determination of quercetin dosage in a food supplement by poly(9-(2-(pyren-1-yl)ethyl)-9h-carbazole) coated indium tin oxide electrode," *Polymer*, vol. 212, p. 123300, Jan. 2021, doi: 10.1016/j.polymer.2020.123300.

[26] N. H. Khand *et al.*, "A new electrochemical method for the detection of quercetin in onion, honey and green tea using Co_3O_4 modified GCE," *Journal of Food Measurement and Characterization*, vol. 15, no. 4, pp. 3720–3730, May 2021, doi: 10.1007/s11694-021-00956-0.

[27] A. Hayat *et al.*, "Organic heterostructure modified carbon nitride as apprehension for Quercetin Biosensor," *Synthetic Metals*, vol. 278, p. 116813, Aug. 2021, doi: 10.1016/j.synthmet.2021.116813

[28] M. Mosleh, S. M. Ghoreishi, S. Masoum, and A. Khoobi, "Determination of quercetin in the presence of tannic acid in soft drinks based on carbon nanotubes modified electrode using chemometric approaches," *Sensors and Actuators B: Chemical*, vol. 272, pp. 605–611, Nov. 2018, doi: 10.1016/j.snb.2018.05.172.

[29] D. Bandyopadhyay, S. Acharya, S. Nag, D. Das, and R. B. Roy, "A Molecular-Imprinted Bipolymer Infused Capacitive Sensor for Inositol Detection in Fruits," *IEEE Transactions on Instrumentation and Measurement*, vol. 72, pp. 1-9, 2023, Art no. 9512409, doi: 10.1109/TIM.2023.3306839.

[30] M. L. Quint, F. S. de Souza, A. Spinelli, and J. B. Domingos, "Low-Range Detection of the Phosphate Group by a Molecularly Imprinted Polymer-Modified Carbon Paste Electrode," *IEEE Sens. J.*, vol. 15, no. 2, pp. 1012–1019, Feb. 2015, doi: 10.1109/JSEN.2014.2359959.

[31] S. Nag, S. Pradhan, D. Das, B. Tudu, R. Bandopadhyay, and R. B. Roy, "Fabrication of A molecular imprinted polyacrylonitrile engraved graphite electrode for detection of formalin in food extracts," *IEEE Sens. J.*, pp. 1–1, 2021, doi: 10.1109/JSEN.2021.3128520.

[32] N. Cennamo et al., "A Novel Sensing Methodology to Detect Furfural in Water, Exploiting MIPs, and Inkjet-Printed Optical Waveguides," *IEEE Transactions on Instrumentation and Measurement*, vol. 68, no. 5, pp. 1582-1589, May 2019, doi: 10.1109/TIM.2018.2879170.

[33] N. Leibl, K. Haupt, C. Gonzato, and L. Duma, "Molecularly imprinted polymers for chemical sensing: A tutorial review," *Chemosensors*, vol. 9, no. 6, p. 123, May 2021, doi: 10.3390/chemosensors9060123.

[34] N. Cennamo et al., "Measurement of MIPs Responses Deposited on Two SPR-POF Sensors Realized by Different Photoresist Buffer Layers," *IEEE Transactions on Instrumentation and Measurement*, vol. 69, no. 4, pp. 1464-1473, April 2020, doi: 10.1109/TIM.2020.2967864.

[35] J. Goossens et al., "Design of a Lab-on-Chip Cartridge for the Optical Detection of Small Molecules Based on Dye-Displacement MIPs," *IEEE Transactions on Instrumentation and Measurement*, vol. 72, pp. 1-9, 2023, Art no. 9511209, doi: 10.1109/TIM.2023.3301040.

[36] D. Das *et al.*, "Electrochemical Detection of Epicatechin in Green Tea Using Quercetin-Imprinted Polymer Graphite Electrode," *IEEE Sens. J.*, vol. 21, no. 23, pp. 26526–26533, Dec. 2021, doi: 10.1109/jsen.2021.3122145.

[37] S. Bahar and R. Mantashloo, "Synthesis of Magnetic Graphene Quantum Dots Based Molecularly Imprinted Polymers for Fluorescent Determination of Quercetin," *SSRN Electronic Journal*, 2022, doi: 10.2139/ssrn 4140008.

[38] X. Hu, L. Liu, Y. Ma, Y. Lei, and T. Zhu, "Thermosensitive molecular imprinted polymer monolith for the selective recognition of quercetin," *Separation Science and Technology*, vol. 54, no. 5, pp. 696–704, Sep. 2018, doi: 10.1080/01496395.2018.1520724.

[39] S. Xu, L. Chen, and L. Ma, "Fluorometric determination of quercetin by using graphitic carbon nitride nanoparticles modified with a molecularly imprinted polymer," *Microchimica Acta*, vol. 185, no. 10, Oct. 2018, doi: 10.1007/s00604-018-3016-y.

[40] T. Swift, L. Swanson, M. Geoghegan, and S. Rimmer, "The pH-responsive behaviour of poly(acrylic acid) in aqueous solution is dependent on molar mass," *Soft Matter*, vol. 12, no. 9, pp. 2542–2549, 2016, doi: 10.1039/c5sm02693h.

[41] A. Sett and T. K. Bhattacharyya, "Functionalized Gold Nanoparticles Decorated Reduced Graphene Oxide Sheets for Efficient Detection of Mercury," in *IEEE Sens. J.*, vol. 20, no. 11, pp. 5712-5719, 1 June 2020, doi: 10.1109/JSEN.2020.2973463.

[42] S. Nag, D. Das, and R. B. Roy, "Voltammetry Application of Molecularly Imprinted Polyacrylamide as Vanillin Receptor in Desserts," *IEEE Sens. J.*, vol. 23, no. 4, pp. 3446–3452, Feb. 2023, doi: 10.1109/jsen 2023.3235933.

[43] M. Catauro et *al.*, "Silica/quercetin sol–gel hybrids as antioxidant dental implant materials," *Science and Technology of Advanced Materials*, vol. 16, no. 3, p. 035001, Jun. 2015, doi: 10.1088/1468-6996/16/3/035001.

[44] E. Laviron, "General expression of the linear potential sweep voltammogram in the case of diffusionless electrochemical systems," *J. ElectroAnal. Chem. Interfacial Electrochem.*, vol. 101, no. 1, pp. 19–28, Jul. 1979, doi: 10.1016/S0022-0728(79)80075-3.

[45] G. Tesfaye, T. Hailu, E. Ele, N. Negash, and M. Tessema, "Square wave voltammetric determination of quercetin in wine and fruit juice samples at poly (safranine O) modified glassy carbon electrode," *Sensing and Bio-Sensing Research*, vol. 34, p. 100466, Dec. 2021, doi: 10.1016/j.sbsr.2021.100466.

[46] D. Bandyopadhyay *et al.*, "Voltammetric Detection of Inositol Using a Platinum-Based Electrode," *Nano LIFE*, vol. 12, no. 02, Mar. 2022, doi: 10.1142/s1793984422500040.

[47] S. Nag *et al.* "A Novel Molecular Imprinted Polymethacrylic Acid Decorated Graphite Electrochemical Sensor for Analyzing Metanil Yellow Adulteration in Food," *IEEE Sens. J.*, doi: 10.1109/JSEN.2023.3300732.

[48] M. Sarkar, S. Khandavilli and R. Panchagnula, "Development and validation of RP-HPLC and ultraviolet spectrophotometric methods of analysis for the quantitative estimation of antiretroviral drugs in pharmaceutical dosage forms", *J. Chromatography B*, vol. 830, no. 2, pp. 349-354, Jan. 2006.

[49] S. Kar, B. Tudu, A. K. Bag and R. Bandyopadhyay, "Application of near-infrared spectroscopy for the detection of metanil yellow in turmeric powder", *Food Anal. Methods*, vol. 11, pp. 1291-1302, May 2018.

[50] S. Biswas, M. Chakraborty, and K. Biswas, "Detection of formaldehyde by an RGO/PMMA-coated sensor," *2020 IEEE International Instrumentation and Measurement Technology Conference (I2MTC)*, May 2020, pp. 1–6

[51] MD. M. Nezami, S. A. Wani, S. A. Khan, N. Khera, and S. Sohail, "An MIP-Based Novel Capacitive Sensor to Detect 2-FAL Concentration in Transformer Oil," *IEEE Sens. J.*, vol. 18, no. 19, pp. 7924–7931, Oct. 2018, doi:10.1109/JSEN.2018.2864793.

[52] A. K. Prusty and S. Bhand, "Molecularly imprinted polyresorcinol-based capacitive sensor for sulphanilamide," *Electroanalysis*, vol. nezami31, no. 9, pp. 1797–1808, Jun. 2019, doi:10.1002/elan 201900099.

[53] W. Wang, A. Zhang, L. Liu, M. Tian, and L. Zhang, "Dopamine-Induced Surface Functionalization for the Preparation of Al–Ag Bimetallic Microspheres," *J. Electrochem. Soc.*, vol.158,no.4,p.D228,2011,doi:10.1149/1.3551496.

[54] S.-C. Chou, W.-A. Chung, T.-L. Fan, Y. Dordi, J. Koike, and P.-W. Wu, "Polydopamine and its composite film as an adhesion layer for cu electroless deposition on SiO2," *J. Electrochem. Soc.*, vol. 167, no. 4, p. 042507, Mar. 2020, doi:10.1149/1945-7111/ab7aa2.

[55] J. H. Waite, "Adhesion a la moule." *Integr. Comp. Biol.*, vol. 42, no. 6, pp. 1172–1180, Dec. 2002, doi:10.1093/icb/42.6.1172.

[56] H. G. Silverman and F. F. Roberto, "Understanding marine mussel adhesion." Mar. Biotechnol., vol. 9, no. 6, pp. 661–681, Dec. 2007, doi:10.1007/s10126-007-9053-x.

[57] W. Wang, Y. Jiang, S. Wen, L. Liu, and L. Zhang, "Preparation and characterization of polystyrene/Ag core-shell microspheres--a bio-inspired poly(dopamine) approach.," *J. Colloid Interface Sci*., vol. 368, no. 1, pp. 241–249, Feb. 2012, doi:10.1016/j.jcis.2011.10.047.

[58] L. Huang, J. Yi, Q. Gao, X. Wang, Y. Chen, and P. Liu, "Carboxymethyl chitosan functionalization of CPED-treated magnesium alloy via polydopamine as intermediate layer," *Surface and Coatings Technology*, vol. 258, pp. 664-671, Nov.2014,doi:10.1016/j.surfcoat.2014.08.020.

[59] H. Lee, S. M. Dellatore, W. M. Miller, and P. B. Messersmith, "Mussel-inspired surface chemistry for multifunctional coatings." *Science*, vol. 318, no. 5849, pp. 426–430, Oct. 2007, doi:10.1126/science 1147241.

[60] J. Yu et al., "Adaptive hydrophobic and hydrophilic interactions of mussel foot proteins with organic thin films." *ProcNatlAcadSci USA*, vol. 110, no. 39, pp. 15680–15685, Sep. 2013, doi:10.1073/pnas 1315015110.

[61] Z. Tapsir and S. Saidin, "Synthesis and characterization of collagen–hydroxyapatite immobilized on polydopamine grafted stainless steel," *Surface and Coatings Technology*, vol. 285, pp.11–16, Jan 2016,doi:10.1016/j.surfcoat.2015.11.02.

[62] J. Wang et al., "Electropolymerization of dopamine for surface modification of complex-shaped cardiovascular stents." *Biomaterials*, vol. 35, no. 27, pp. 7679–7689, Sep. 2014, doi:10.1016/j.biomaterials.2014.05.047.

[63] C. Xu, M. Tian, L. Liu, H. Zou, L. Zhang, and W. Wang, "Fabrication and properties of silverized glass fiber by dopamine functionalization and electroless plating," *J. Electrochem. Soc.*, vol. 159, no. 4, pp. D217–D224, 2012, doi:10.1149/2.056204jes.

[64] P. Qi, M. F. Maitz, and N. Huang, "Surface modification of cardiovascular materials and implants," *Surface and Coatings Technology*, vol.233, pp.80, 90, Oct.2013,doi:10.1016/j.surfcoat.2013.02.08.

[65] D. Schaubroeck, L. Mader, P. Dubruel, and J. Vanfleteren, "Surface modification of an epoxy resin with polyamines and polydopamine: Adhesion toward electroless deposited copper," *Appl. Surf. Sci.*, vol.353, pp. 238–244, Oct. 2015, doi:10.1016/j.apsusc.2015.06.114.

[66] S. Acharya, S. Nag, D. Bandyopadhyay, D. Das, A. Mandal, and R. Banerjee Roy, "A Molecular Imprinted Polymer Tethered Capacitive Sensor for Epicatechin Detection in Green Tea," *IEEE Sens. J.*, vol. 24, no. 4,pp.4213–4220,Feb.2024,doi:10.1109/jsen.2023.334466.

[67] D. Bandyopadhyay, S. Acharya, S. Nag, D. Das, and R. B. Roy, "A Molecular-Imprinted Bipolymer Infused Capacitive Sensor for Inositol Detection in Fruits," *IEEE Transactions on Instrumentation and Measurement*, vol. 72, pp. 1–9, 2023, doi: 10.1109/tim 2023.3306839.

[68] A. Bose and K. Biswas, "Performance Study of Urease-PMMA-Based Aqueous Urea Sensor," *IEEE Sens. J.*, vol. 17, no. 21, pp. 6850–6858, Nov.2017,doi:10.1109/JSEN.2017.275102.

[69] J.-L. Gong, F.-C. Gong, Y. Kuang, G.-M. Zeng, G.-L. Shen, and R.-Q. Yu, "Capacitive chemical sensor for fenvalerate assay based on electropolymerized molecularly imprinted polymer as the sensitive layer." *Anal. BioAnal. Chem*., vol. 379, no. 2, pp. 302–307, May 2004, doi:10.1007/s00216-004-2568-3.

[70] M. Maruthapandi, M. Natan, G. Jacobi, E. Banin, J. H. T. Luong, and A. Gedanken, "Antibacterial Activity Against Methicillin-Resistant Staphylococcus aureus of Colloidal Polydopamine Prepared by Carbon Dot Stimulated Polymerization of Dopamine," *Nanomaterials (Basel)*, vol. 9, no.12, Dec. 2019, doi:10.3390/nano9121731.

[71] M. Moulick, S. Nag, D. Das, B. Tudu, R. Bandyopadhyay and R. B. Roy, "Detection of Tannic Acid using Nd2O3 Modified Graphite Electrode," 2022 *2nd International Conference on Emerging Frontiers in Electrical and Electronic Technologies (ICEFEET)*, 2022, pp. 1-5, doi: 10.1109/ICEFEET51821.2022.9848155.

[72] D. Bandyopadhyay, S. Nag, D. Das, and R. B. Roy, "A Novel rGO-Decorated Molecularly Imprinted Polyacrylic Acid Graphite Electrode for the detection of Quercetin in Food," *IEEE Transactions on Instrumentation and Measurement*, vol. 73, pp. 1–8, Jan. 2024, doi:10.1109/tim 2024.3398119.

[73] G. M. Hussein Alsayadi, J. U. Hamid, P. Patel, and B. D. Kurmi, "Lipid nanoparticles: An advanced delivery system for quercetin," *Pharmaspire*, vol. 14, no. 04, pp. 130–134, 2022, doi:10.56933/pharmaspire 2022.14217.

[74] J. Gupta, A. Gupta, and A. K. Gupta, "Role of dietary flavonoids having antidiabetic properties and their protective mechanism," *International Journal of Current Research in Chemistry and Pharmaceutical Sciences*, vol. 5, no.1, pp.13–21, Jan.2018,doi:10.22192/ijcrcps 2018.05.01.004.

[75] V. Vinothkumaret al., "Preparation of three-dimensional flower-like cobalt phosphate as dual functional electrocatalyst for flavonoids sensing and supercapacitor applications," *Ceramics International*, vol. 47, no. 21, pp. 29688–29706, Nov.2021,doi:10.1016/j.ceramint.2021.07.140.

[76] Y. Wang, M. Qiao, X. Mamat, X. Hu, and G. Hu, "Hierarchically ordered porous nitrogen doped carbon modified a glassy carbon electrode for voltammetry detection of quercetin," Materials Research Bulletin, vol. 136, p. 111131, Apr. 2021doi: 10.1016/j.materresbull.2020.111131.

[77] F. Gao et al., "MXene Nanosheets Decorated with Pt Nanostructures for the Selective Electrochemical Detection of Quercetin," *ACS Applied Nano Materials*, vol. 6, no. 8, pp. 6869–6878, Apr. 2023, doi: 10.1021/acsanm 3c00584.

[78] P. Karuppasamy, A. Karthika, S. Senthilkumar, and V. Rajapandian, "An efficient and highly sensitive amperometric quercetin sensor based on a Lotus flower-like SEO2-Decorated RGO nanocomposite modified glassy carbon electrode," *Electrocatalysis*, vol. 13, no. 3, pp. 269–282, Feb. 2022, doi: 10.1007/s12678-022-00707-9.

[79] P. Veerakumar, C. Rajkumar, S.-M. Chen, B. Thirumalraj, and K.-C. Lin, "Ultrathin 2D graphitic carbon nitride nanosheets decorated with silver nanoparticles for electrochemical sensing of quercetin," *Journal of Electroanalytical Chemistry*, vol. 826, pp. 207–216, Aug. 2018, doi: 10.1016/j.jelechem.2018.08.031.

[80] N. Sabbaghi et al., "Synthesis of poly(dopamine quinone-chromium(III) complex) @hierarchical cabbage flower-like cobalt as a novel mesoporous nanocomposite modifier of graphite paste electrode for electrochemical determination of quercetin in biological samples," *Colloids and Surfaces a Physicochemical and Engineering Aspects*, vol. 643, p. 128739, Mar. 2022, doi: 10.1016/j.colsurfa.2022.128739.

[81] Y. Liang, C. Qu, R. Yang, L. Qu, and J. Li, "Molecularly imprinted electrochemical sensor for daidzein recognition and detection based on poly(sodium 4-styrenesulfonate) functionalized graphene," *Sensors and Actuators B Chemical*, vol. 251, pp. 542–550, May 2017, doi: 10.1016/j.snb.2017.05.044.

[82] B. Xu, L. Yang, F. Zhao, and B. Zeng, "A novel electrochemical quercetin sensor based on Pd/MoS2-ionic liquid functionalized ordered mesoporous carbon," *Electrochimica Acta*, vol. 247, pp. 657–665, Jun. 2017, doi: 10.1016/j.electacta.2017.06.130.

[83] X. Kan, T. Zhang, M. Zhong, and X. Lu, "CD/AuNPs/MWCNTs based electrochemical sensor for quercetin dual-signal detection," *Biosensors and Bioelectronics*, vol. 77, pp. 638–643, Nov. 2015, doi: 10.1016/j.bios.2015.10.033.

[84] Z. Zhou, C. Gu, C. Chen, P. Zhao, Y. Xie, and J. Fei, "An ultrasensitive electrochemical sensor for quercetin based on 1-pyrenebutyrate functionalized reduced oxide graphene /mercapto-β-cyclodextrin /Au nanoparticles composite film," *Sensors and Actuators B Chemical*, vol. 288, pp. 88–95, Feb. 2019, doi: 10.1016/j.snb.2019.02.105.

PUBLICATION STATUS

JOURNAL

- Bandyopadhyay, S. Nag, S. Acharya, D. Das and R. B. Roy, "A Novel Molecular Imprinted Dual-Polymer Infused Capacitive Sensor for Quercetin Detection in Agro Products," IEEE Sensors Journal, vol. 25, no. 21, pp. 39418-39425, 1 Nov.1, 2025, doi: 10.1109/JSEN.2025.3614749.

Towards the development of an integrated, voltametric electrode for the electrochemical sensing of food quality

6

6.1 Introduction

Salicylic acid (ScA, $C_7H_6O_3$, Fig. 6.1), a phenolic phytohormone, is not only naturally present in various plants but also widely utilized as a preservative in the food industry, pharmaceuticals, and cosmetic products [1-3]. Furthermore, it stands as a crucial active pharmaceutical ingredient (API) in numerous pharmaceutical formulations, most notably in the synthesis of acetylsalicylic acid, commonly known as aspirin [4]. Its applications extend to the cosmeceutical industry, where it plays a dynamic role in unclogging pores, abating hyperpigmentation, and waning the appearance of wrinkles [5]. However, ineptitudes in industrial separation processes during ScA production have led to the generation of substantial amounts of ScA-containing industrial wastewater. Recognizing ScA as a water pollutant due to its color and significant ecotoxicity, its detection in sewage and even drinking water poses risks to liver and kidney function, can induce protein denaturation, and may even cause mucosal bleeding [6].

Moreover, the high concentrations of ScA found in such wastewater present challenges for conventional sewage treatment technologies, resulting in the loss of a valuable chemical resource [7]. Consequently, the development of efficient methods for the selective separation and detection of ScA in aqueous environments is of paramount importance from both environmental and economic perspectives [8].

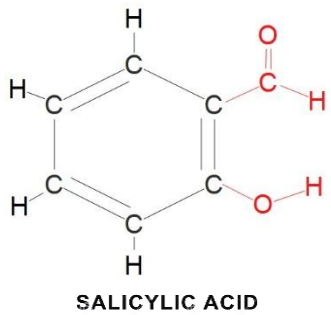

Fig. 6.1 Chemical structure of ScA

Traditional analytical techniques for ScA detection include a variety of methods. Spectrophotometric methods utilize UV-Visible spectrophotometry, occasionally with pH variation, to quantify ScA [9], [10]. Other spectrophotometric techniques include kinetic spectrophotometry

[11], solvent extraction [12], and absorptiometry in aqueous ethanolic solutions [13]. Further, fluorescence spectroscopy [14] and High-performance liquid chromatography (HPLC) are frequently used, sometimes coupled with mass spectrometry (LC-MS) [15], [16], [17]. Reversed-phase liquid chromatography is another variant [18]. Gas chromatography-mass spectrometry (GC-MS) is also used for ScA detection [19]. For pharmaceutical formulations, methods like UV-HPLC have been developed [20]. Ion-selective electrodes (ISEs) are another important electrochemical technique for determining ScA, both in pure form and pharmaceutical formulations, offering a simpler approach in some cases [21-29]. These traditional methods often face challenges such as procedural complexity, high instrumentation costs, and the need for expensive and time-consuming sample pretreatment. Electrochemical sensors offer a compelling alternative, providing a pathway towards simpler, faster, and more cost-effective analysis of ScA.

Electrochemical sensing relies on the measurement of electrical signals—current or potential—resulting from the electrochemical reaction between the target analyte and the electrode surface. A diverse array of electrode materials and configurations has been explored for ScA detection, encompassing modified carbon electrodes, metallic electrodes, and enzyme-based sensors. These sensors offer advantages such as high sensitivity, selectivity, and the possibility of miniaturization, making them suitable for on-site and real-time monitoring.

Molecularly imprinted polymers (MIPs) are highly regarded as robust synthetic materials and artificial receptors. They are created using molecular imprinting technology (MIT), a technique that designs specific recognition sites within a polymer matrix [30]-[35]. These sites are tailored to match the template molecules in terms of size, shape, and the arrangement of functional groups. This biomimetic method is straightforward to use, and it offers benefits such as high selectivity, predictable structure, versatility, excellent physical and chemical stability, and cost-effectiveness. The suitability of MIP-based electrochemical sensors for determining a wide variety of contaminants in complex food and drink matrices has been well-established, making them the preferred choice for decentralized analysis [30]-[41].

Several studies have explored the efficacy of MIPs in ScA recognition. Kang et al. [41] developed an amperometric sensor using an MIP-modified electrode. Baxter et al. [42] detailed a method for identifying and measuring ScA and salicyluric acid in urine. Zhihua et al. [43] investigated the voltammetric determination of ScA using MI film-modified electrodes. As reported in Yang et al. [44] and Xu et al. [45], MIPs have been exploited in photoelectrochemical sensing and for optimizing the adsorption of ScA. Li et al. [46] explored MIP membranes

for selective adsorption of a compound related to ScA. Conventional tri-electrode systems consisting of working, reference, and counter electrodes require separate dipping into the sample with no fixed distance maintained between them during testing or analysis. This positional variability introduces high signal uncertainty. Manually replacing materials with rods and wires for the working electrode is time-consuming, error-prone, and impractical for field use. Additionally, these systems experience material loss during regeneration. Furthermore, single-use formats, such as screen-printed electrodes (SPEs), suffer from rapid sensor fouling and lack recovery capability, leading to significant waste and high operational cost. The inherent lack of long-term stability in these portable formats often necessitates advanced material engineering, such as interface synergistic stabilization principles, to guarantee longevity under operational stress in complex media [48].

Motivated by the limitations of tri-electrode systems, especially in field-based applications, the current research proposes a novel pen-like tri-electrode integrated system for detecting food constituents (additives, nutrients, etc.). This system aims to overcome the challenges of traditional voltammetry, offering advantages such as ease of use, portability, and efficiency in recognizing and quantifying target molecules, ScA in real-food samples. A promising innovation in electrochemical sensing is the integration of three essential electrodes—working, reference, and counter electrodes—into a single, user-friendly, pen-like tri-electrode system. The core innovation lies in its fixed-geometry architecture and a piston-driven regenerative mechanism, designed to offer a truly portable and efficient platform. Furthermore, the proposed integrated design with the fixed and precise inter-electrode geometry parades several key advantages:

- It provides operational simplicity, as the user only needs to immerse the pen-like device into the sample, eliminating the need for complex cell assembly.
- It enhances portability, enabling convenient on-site analysis and rapid measurements in various settings.
- The design will reduce the compulsion for pushing rods manually and disconnecting wires for the electrodes, thereby streamlining the process for user-friendly surface regeneration of the electrodes.
- The integrated design will minimize material losses associated with traditional regeneration, making it a more efficient and material-conservative approach.
- Consistent electrode placement may ensure consistent voltammetric responses for reliable data analysis across multiple measurements.

- The fixed inter-electrode distance not only enhances the precision of current readings and minimizes signal distortion and ohmic drop effects but also serves as the essential hardware prerequisite for integrating advanced computational analysis.

Conventional sensor instability often necessitates complex software compensation. By providing clean, highly reproducible signals, this stable hardware design enables the efficient adoption of techniques like Sensor fault estimation (FE), reducing the computational resources required to maintain system integrity [49]. Moreover, this stability is vital for leveraging advanced Artificial Intelligence (AI) methods, such as machine learning for high-confidence data classification [50] or implementing efficient feature fusion networks [51]. These computational strategies are necessary to process multi-featured voltammetric data and filter noise effectively, ensuring robust quantitative detection of contaminants in complex real-world samples. The proposed system seems to be a crucial innovation for food quality analysis, enabling more accurate, reproducible, and sensitive detection of food molecules. This may pave the way for a revolutionary, feasible tool in field-based food quality and safety monitoring for both laboratory and field applications.

Experimental Section

This section details the fabrication and operation of the pen-like electrochemical system designed for ScA detection. The process encompassed the vigilant construction of its components and their integration into a user-friendly format, with a focus on streamlining electrode surface renewal.

6.2.1 Building the Electrochemical Pen: Electrode Fabrication

The preliminary steps involved the meticulous construction of the individual electrodes that form the core of the pen-like system.

I. **Crafting the Reference Electrode:** A pure silver (Ag) wire served as the foundation for the stable reference point. This wire was electrochemically coated with a layer of silver chloride (AgCl) using an appropriate deposition technique. The AgCl-coated wire was then carefully sealed within the tip of a micropipette casing. A reservoir containing a potassium chloride (KCl) solution, solidified using an agar-agar matrix, was introduced into the micropipette tip to establish a consistent ionic environment, ensuring a reliable and stable reference potential throughout the measurements.

II. **Preparing the Working Electrode Refills:** For the working electrode, the sensing element (MIP(GA-ScA)/G) for ScA interaction, disposable, pen refill-like cartridges

were designed for easy insertion and replacement within the main body of the pen prototype. These refills were prepared by incorporating a molecularly imprinted polymer (MIP) as the sensing material. This involved creating a paste of the MIP, tailored for ScA recognition, using gallic acid (GA) as the monomer. The GA monomer, along with other necessary components, was carefully mixed and polymerized to create a sensing material with a specific affinity for ScA. This MIP(GA-ScA)/G paste was then carefully packed into the refill cartridge. The open tip of this cartridge would then serve as the active sensing surface. The central body of the pen, housing these refills, was fashioned from a syringe, providing a familiar and functional structure.

III. **Integrating the Counter Electrode:** The counter electrode, a platinum rod, was secured within one of the designated external extensions at the bottom of the pen body. This placement ensured proper electrical contact to facilitate the electrochemical reactions at the working electrode. Similarly, the micropipette tip housing the reference electrode was secured in its own designated external extension, positioned to maintain a defined geometry with the working electrode.

6.2.2 The Art of Resurfacing: Electrode Regeneration

An integrated mechanism for regenerating the working electrode surface, ensuring consistent performance, was a crucial design feature. A rotator bolt was employed to engage a linear actuator. Rotation of this bolt drove a piston (either steel or copper) downwards within the working electrode refill. This action gently pushed the sensing material, MIP(GA-ScA)/G, toward the tip, effectively exposing a fresh layer of the MIP to the solution sample. A spring mechanism was integrated to ensure automatic piston retraction after pushing, ensuring a pristine sensing surface ready for subsequent analysis.

6.2.3 Unveiling Salicylic Acid: Voltammetric Measurements

With the integrated-pen system assembled, it was connected to a potentiostat for electrochemical measurements. A carefully controlled voltage sweeps or a sequence of potential pulses was applied between the working electrode (bearing the MIP for ScA) and the stable reference electrode, with the platinum counter electrode completing the electrical circuit. Voltammetric measurements were thus performed directly on the food sample. The resulting current response, indicative of the electrochemical interactions, was then meticulously analyzed to identify and quantify the presence of ScA, the target molecule, within the sample.

As visually summarized in Fig. 6.2, this integrated design, coupled with the pushing mechanism for electrode regeneration, offers a user-centric and efficient approach to on-site analysis of food constituents. The easy replacement of the disposable working electrode refills and the simplified regeneration process promise to minimize material waste and reduce the hands-on effort typically associated with traditional three-electrode setups. The envisioned electrode arrangement is further illustrated in Fig. 6.3.

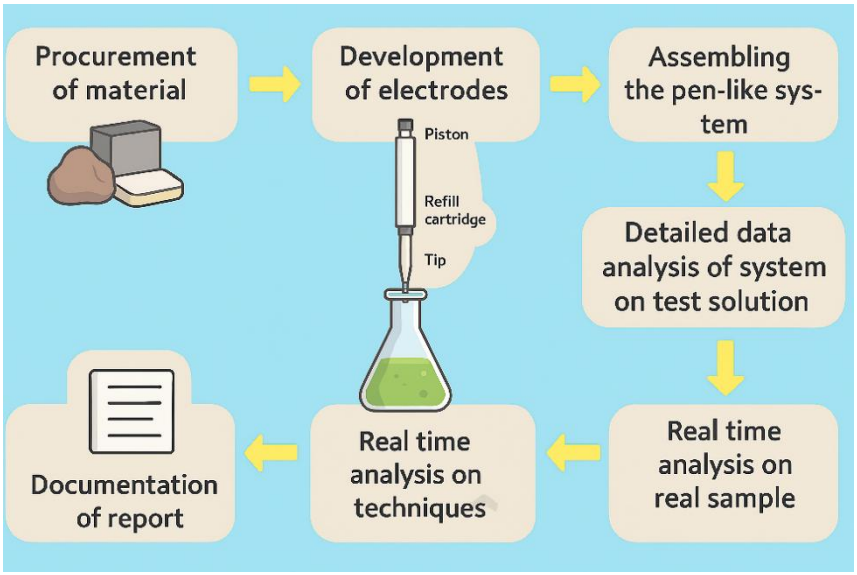

Fig. 6.2. Conceptual methodology flow diagram illustrating the stages of development, from the MIP material synthesis to the final assembly of the integrated pen electrode system.

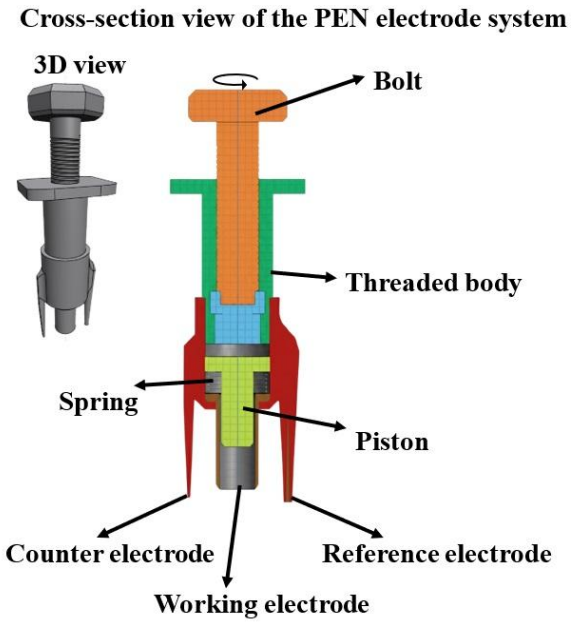

Fig. 6.3. Cross-sectional view of the proposed integrated trielectrode system, highlighting the fixed spatial geometry between the working, reference, and counter electrodes, and the piston-driven, regenerative cartridge mechanism.

6.2.4 MIP(GA-ScA)/G Polymer Preparation

Graphite powder (0.95 g) was dispersed in 15 mL of ethanol and sonicated for 1 hour. Subsequently, 0.05 g of gallic acid (GA) as the monomer and 0.05 g of salicylic acid (ScA) as the template were added, and the mixture was sonicated for another hour. Then, 400 µL of ethylene glycol dimethyl acrylate (EGDMA) as the crosslinker and 1 mg of benzoyl peroxide as the polymerization initiator were added, followed by sonication for approximately 45 minutes. Polymerization was carried out in a water bath with the temperature regulated between 30-40 °C. The resulting polymerized material underwent a washing process using a 70:30 (v/v) ethanol-water mixture to remove the ScA template molecules. Traces of ScA were leached out from the polymerized sample through filtration, yielding the MIP(GA-ScA)/G material. The synthesized material was dried at room temperature and stored for electrode development.

6.2.5 MIP(GA-ScA)/G and NIP(GA)/G Integrated pen Electrode and Traditional Electrode Fabrication

Synthesized powdered polymerized materials (300 mg) were ground in a mortar with the sequential addition of 3-4 drops of paraffin oil (binder) to form a smooth paste suitable for electrode fabrication. This fine paste was then stuffed into glass capillary tubes with an inner diameter of 1.25 mm using a thin metallic rod, thereby forming a traditional sensing glass electrode (Fig. 6.4). Copper wires were inserted into the back of the packed paste to ensure the necessary electrical contact for testing. In a parallel approach, the same synthesized MIP(GA-ScA)/G paste was also stuffed into modified disposable pen refill-like cartridge. This paved the way for the integration of the sensing material into the proposed integrated pen system. The NIP electrode (NIP(GA)/G) was fabricated using the same procedure but without the ScA template, maintaining an identical polymer background while lacking the selective binding cavities.

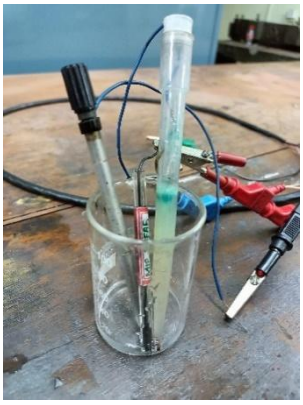

Fig. 6.4. A traditional three-electrode system setup, illustrating the separate, manual positioning of the working, Ag/AgCl reference, and platinum counter electrodes, which introduces variable uncompensated resistance due to positional errors.

6.2.6 Electrochemical Testing

The performance of the fabricated MIP(GA-ScA)/G electrodes was evaluated using an Autolab Potentiostat/Galvanostat PGSTAT101 (Metrohom Autolab, Netherlands) connected to a tri-electrode system. In this setup, the MIP(GA-ScA)/G electrode served as the working electrode, with an Ag/AgCl electrode as the reference electrode and a platinum (Pt) electrode as the counter electrode. Electrochemical measurements, including both differential pulse voltammetry (DPV) and cyclic voltammetry (CV), were conducted within a potential window of 0.1 V to 1.2 V.

To evaluate the performance of the proposed integrated pen system, electrochemical testing was conducted separately for both the traditional tri-electrode system, utilizing the capillary tube-based MIP(GA-ScA)/G electrode, and the pen-like system, incorporating the MIP(GA-ScA)/G modified pen refill. The Autolab Potentiostat/Galvanostat PGSTAT101 was employed for electrochemical measurements in both configurations, allowing for direct comparative analysis of their performance for the detection of ScA.

Electrochemical impedance spectroscopy (EIS) was conducted in 0.1 M PBS at pH 6.0 containing 100 µM ScA over the frequency range of 100 kHz to 0.1 Hz to rigorously probe the interfacial charge transfer kinetics and inherent resistance characteristics of the MIP electrodes [52-54]. As depicted in the resulting Nyquist plots (Fig. 6.5), which delineate the real (Z') versus complex (Z'') impedance, a suppressed semicircle is evident in the high-frequency domain whose diameter reflects the charge transfer resistance (R_{ct}). For the traditional MIP(GA-ScA)/G configuration, the R_{ct} was determined to be 0.598 kΩ. In stark contrast, the novel PEN-MIP integrated system, designed for high-precision detection, yielded a

substantially lower R_{ct} of 0.527 kΩ. This significant 12% reduction in R_{ct} provides empirical validation that the fixed-geometry architecture minimizes positional variability, resulting in a lower uncompensated resistance (R_u) and diminished ohmic drop effects, thus confirming that the mechanical integration fundamentally enhances the electron transfer kinetics and overall precision of the electrochemical measurement system.

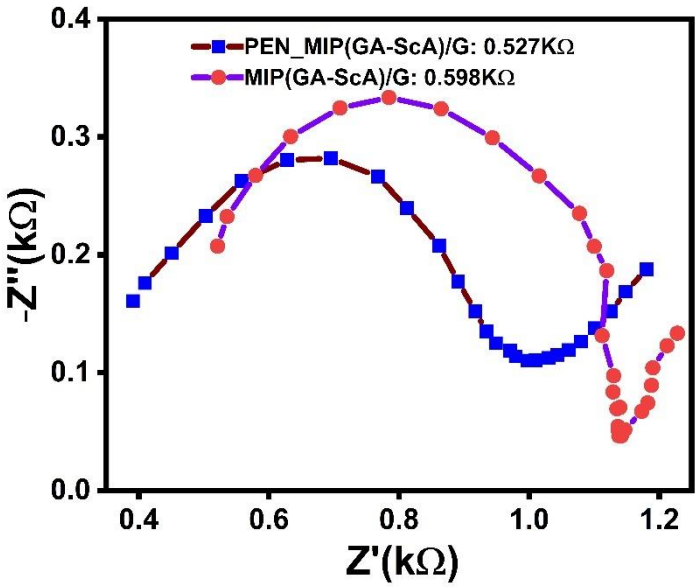

Fig. 6.5. EIS Nyquist plots comparing PEN_MIP(GA-ScA)/G (blue) and the traditional MIP system (red). The PEN configuration exhibits a lower charge-transfer resistance (R_{ct} = 0.527 kΩ) compared to the traditional setup (0.598 kΩ), indicating more efficient electron transfer enabled by the PEN's fixed-geometry design

6.3 Results And Discussions

6.3.1 Monomer Selection

Gallic acid (GA) was selected as the primary functional monomer for its potential to interact with ScA through hydrogen bonding and π–π interactions, owing to its phenolic hydroxyl and aromatic ring structures, respectively. To explore the effect of incorporating a second monomer, maleic acid (MA) was introduced at a 50% molar ratio with GA in the MIP(GA-MA-ScA)/G polymer. MA, with its carboxylic acid groups, could offer additional or alternative interactions with ScA. However, the results indicate that the MIP synthesized solely with GA as the functional monomer (MIP(GA-ScA)/G) demonstrated a higher current response towards ScA oxidation compared to the copolymer-based MIP(GA-MA-ScA)/G. Electrochemical

detection of ScA was performed using cyclic voltammetry with a traditional tri-electrode system, employing MIP-modified electrodes as the working electrode. Fig. 6.6 presents the cyclic voltammograms obtained for MIP(GA-ScA)/G (red line) and MIP(GA-MA-ScA)/G (black line) electrodes in a solution containing ScA. As depicted in that figure, both MIP-modified electrodes exhibited distinct oxidation peaks within the scanned potential window (0.4 V to 1.4 V), indicative of the electrochemical oxidation of salicylic acid at the electrode surface. The MIP(GA-ScA)/G electrode, synthesized using GA as the primary functional monomer, displayed a prominent oxidation peak with a higher current response compared to the MIP(GA-MA-ScA)/G electrode. The MIP(GA-ScA)/G electrode (red line) showed a clear oxidation peak at approximately 1.15 V with a current reaching around 62 µA. In contrast, the MIP(GA-MA-ScA)/G electrode (black line), where a combination of GA and MA was employed as monomers in a 50% ratio, exhibited an oxidation peak at a similar potential (around 1.12 V) but with a noticeably lower peak current of approximately 55 µA. This advocates that under the tested conditions, the interactions facilitated by the GA monomer alone were more effective in the electrochemical detection of ScA. The inclusion of MA did not significantly enhance, and potentially slightly hindered, the overall electrochemical signal. This could be attributed to a less optimal arrangement of binding sites within the polymer matrix when two different monomers are incorporated, potentially reducing accessibility or affinity for the ScA - template molecule.

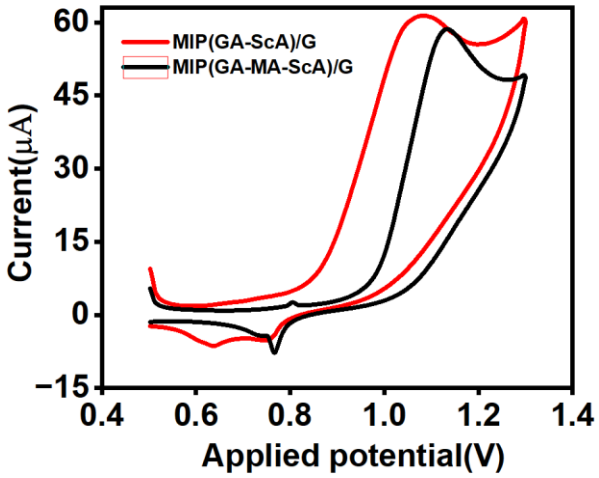

Fig. 6.6. Comparative cyclic voltammograms (CV) of ScA oxidation (100 µM in PBS, pH 7.0) obtained using two different MIP polymer compositions: MIP(GA-ScA)/G (red line) and MIP(GA-MA-ScA)/G (black line). This study determined the optimal formulation (GA-ScA) for subsequent analytical work.

6.3.2 Buffer Selection with pH variation

Electrochemical detection of ScA was further investigated by examining the influence of different buffer solutions and varying pH levels within a phosphate buffer system, engaging both the traditional MIP(GA-ScA)/G electrode and the pen-like PEN_MIP(GA-ScA)/G electrode. Fig. 6.7 presents a comparative analysis of the peak currents obtained under these conditions.

a) **Effect of Buffer Type:** Fig. 6.7(a) illustrates the peak currents observed for ScA detection in three different buffer solutions: ABS, CBS, and PBS, using both electrode configurations. For ABS, the pen-like electrode (yellow striped bar) yielded a slightly higher peak current (approximately 26 μA) compared to the traditional electrode (green solid bar, ~24 μA). In CBS, both electrodes showed relatively lower peak currents, with the pen-like system (~19 μA) again exhibiting a slightly higher response than the traditional one (~18 μA). Notably, PBS resulted in the highest peak currents for both systems, with the traditional tri-electrode showing a significantly higher current (~37 μA) compared to the pen-like electrode (~41 μA). This suggests that the choice of buffer meaningfully impacts the sensitivity of the ScA detection, with PBS appearing to be the most favorable among the tested buffers, irrespective of the electrode configuration. The subtle differences observed between the two electrode systems within each buffer indicate that the electrode geometry also plays a minor role in the overall response.

b) **Effect of pH Variation in PBS:** Fig. 6.7(b) explores the effect of varying the pH of the phosphate buffer (PBS) on the peak current for ScA detection using both electrode systems. The pH values tested were 3, 5, 6, 7, and 9. Both electrode configurations exhibited a trend where the peak current varied with pH. The highest peak currents for both the pen-like (~39 μA) and the traditional (~37 μA) electrodes were observed at pH 6. Deviations from this pH, both towards acidic and alkaline conditions, resulted in a decrease in the peak current. This pH-dependent performance likely reflects the influence of the solution pH on the protonation state of ScA and the functional groups within the MIP, affecting their interaction and the subsequent electrochemical oxidation. The optimal pH of 6 recommends that at this specific acidity, the binding affinity between ScA molecules of the test solution and the MIP, and/or the electrochemical oxidation kinetics of ScA at the electrode surface, seems to be most auspicious. The integrated pen electrode (PEN_MIP(GA-ScA)/G) showed a slightly higher or comparable response to the traditional electrode across the different pH values, particularly at the optimal pH of 6. The overall consistency in trends highlights that the PEN_MIP(GA-ScA)/G

system can be a viable alternative for ScA detection, offering the advantages of portability and ease of use without a significant compromise in sensitivity.

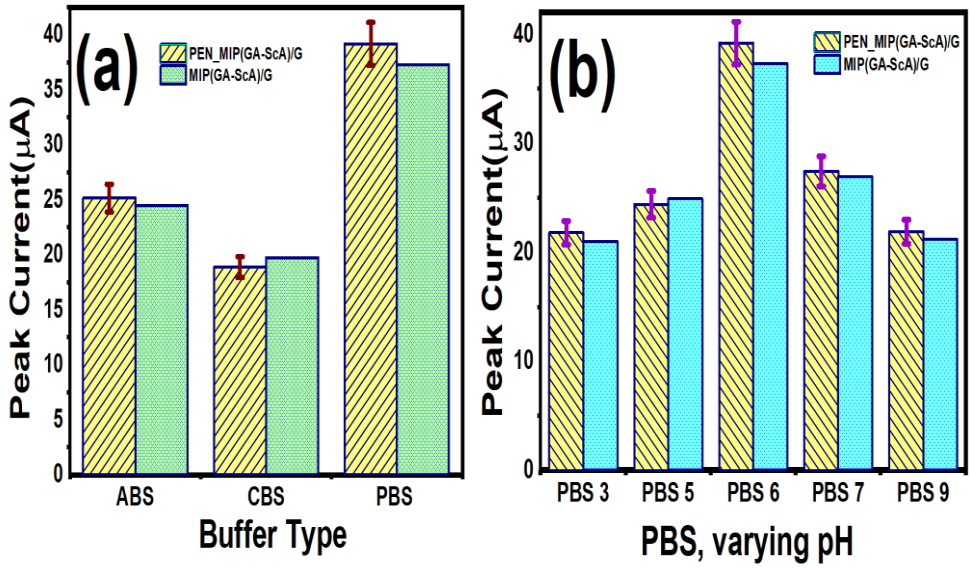

Fig. 6.7. Optimization of experimental conditions for ScA detection (100 μM concentration) via Differential Pulse Voltammetry (DPV). (a) Effect of buffer type (ABS, CBS, PBS) on the peak current. (b) Effect of pH variation in PBS on the DPV peak current, comparing the traditional (green/blue) and pen-like (PEN_MIP, yellow) electrodes to determine the optimal pH for maximum analytical sensitivity

6.3.3 Effect of Scan rate variation and comparative performance of MIP vs. NIP systems

The cyclic voltammograms of ScA at different scan rates (10 mV/s to 500 mV/s) using both the traditional MIP(GA-ScA)/G electrode (a) and the PEN_MIP(GA-ScA)/G electrode (b) have been depicted in Fig. 6.8. As the scan rate increased, the anodic peak current for ScA oxidation also increased for both electrode systems. This comportment is characteristic of surface-confined or diffusion-controlled electrochemical processes.

A visual assessment of Fig. 6.8(a) and 6.8(b) reveals similar trends in the evolution of the oxidation peak with increasing scan rate for both the traditional, MIP(GA-ScA)/G and the PEN_MIP(GA-ScA)/G electrode configurations. The peak potentials also exhibit a slight positive shift with increasing scan rate in both cases, which is often observed in irreversible or quasi-reversible electrochemical reactions. The magnitude of the current response at corresponding scan rates appears comparable between the two systems, further endorsing this.

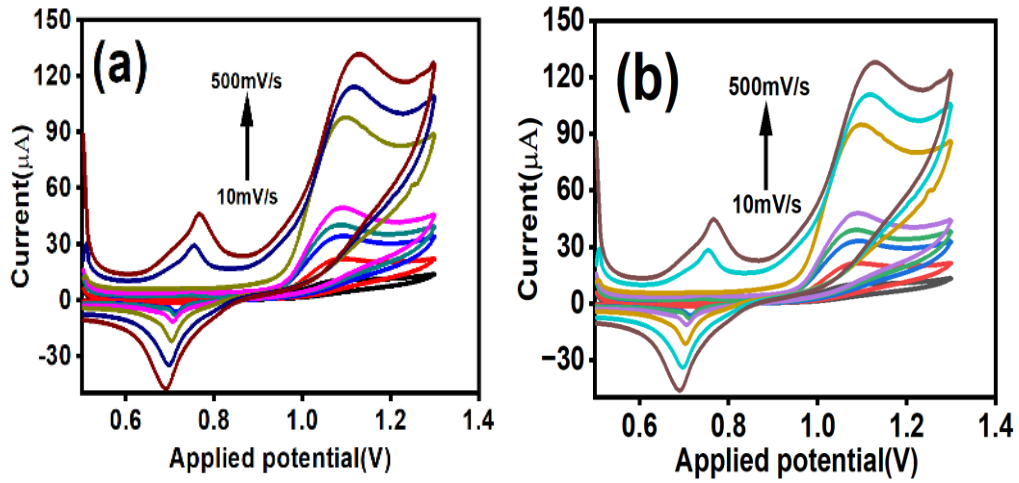

Fig. 6.8. Mechanistic study: CV of ScA oxidation (100 µM in PBS, pH 7.0) at varying scan rates (10-500 mV/s) using (a) the traditional MIP(GA-ScA)/G electrode and (b) the pen-like PEN_MIP(GA-ScA)/G electrode. The linear relationship between current and the square root of the scan rate confirms the diffusion-controlled nature of the reaction for both systems.

The effectiveness of any MIP-based sensor relies on its ability to selectively recognize and enrich the target analyte. To confirm that the enhanced electrochemical response originated from this selective recognition rather than the polymer matrix, the MIP electrode was compared against an identically prepared NIP control. As revealed in Table 6.1, the PEN_MIP system generated a peak current of 39.2 µA for 100 µM ScA, whereas PEN_NIP(GA)/G produced only ~30.7 µA. This notable enhancement reflects the imprinting effect, demonstrating that the MIP layer forms high-affinity sites that capture and pre-concentrate ScA before electrochemical detection. A similar trend was observed in the traditional setup: the Traditional MIP yielded 37.3 µA, while the Traditional NIP(NIP(GA)/G) showed the lowest response at ~28.1 µA. These findings confirm that the imprinting mechanism is consistent across platforms. Notably, PEN_MIP achieved the highest overall current (39.2 µA), indicating that the fixed-geometry PEN design significantly improves the efficiency and analytical performance of the MIP layer. Evidently, the inherent stability of the fixed geometry is substantiated, as even the PEN_NIP(GA)/G electrode demonstrates performance lift over the traditional three-electrode system, validating the overall operational consistency across the entire PEN platform.

Table 6.1. Comparison of MIP and NIP electrode performance across PEN and traditional systems

Hardware Configuration	Electrode System	Peak Current (I_p/µA)	Key Comparison Effect
Integrated Pen System	MIP, PEN_MIP(GA-ScA)/G	39.2	Highest response, reflecting strong MIP selectivity combined with low-loss, highly stable PEN architecture.
	NIP, PEN_NIP(GA)/G	30.7	Represents non-selective background response within the stable PEN platform, indicating minimal non-specific interactions.
Traditional electrode system	MIP, MIP(GA-ScA)/G	37.3	Affirms MIP effect under conventional hardware, though with greater variability compared to PEN system
	NIP, NIP(GA)/G	28.1	Lowest expected current, representing baseline NIP response in more variable traditional setup.

6.3.4 Effect of Concentration variation- Comparative study

The electrochemical response of the (a) traditional MIP(GA-ScA)/G electrode and (b) the PEN_MIP (GA-ScA)/G electrode at varying concentrations of ScA (100 µM to 1000 µM) has been illustrated in. As the concentration of ScA increased, a corresponding increase in the oxidation peak current was observed for both the electrode systems, indicating a concentration-dependent response.

The calibration plot for ScA detection using the PEN_MIP(GA-ScA)/G electrode, shown in Fig. 6.9(c) (green circles), reveals two distinct linear regions within the tested concentration range:

a) Lower Concentration Range (100 µM to 400 µM): Linear regression analysis for this region yielded the equation:

$$I_{p,ScA} = 1.416C_{ScA} + 6.565; R^2 = 0.991$$

b) Higher Concentration Range (500 µM to 1000 µM): Linear regression analysis for this region resulted in the equation:

$$I_{p,ScA} = 0.897C_{ScA} + 6.608; R^2 = 0.998$$

The presence of two linear regions with different slopes suggests a change in the binding affinity or the mass transfer limitations at higher concentrations of ScA on the MIP-modified pen-like electrode (PEN_MIP(GA-ScA)/G). The higher sensitivity (steeper slope) observed in the lower concentration range (1.416 µA/µM) indicates a more efficient binding and/or electrochemical response in this regime. At higher concentrations, the sensitivity decreases (0.897 µA/µM), which could be due to saturation of binding sites on the MIP or increased mass transfer limitations to the electrode surface. The high correlation coefficients (R^2 >0.99) for both linear regions indicate a good fit of the data to the linear models within their respective concentration ranges, suggesting the potential for accurate quantification of ScA using the pen-like sensor in these regimes.

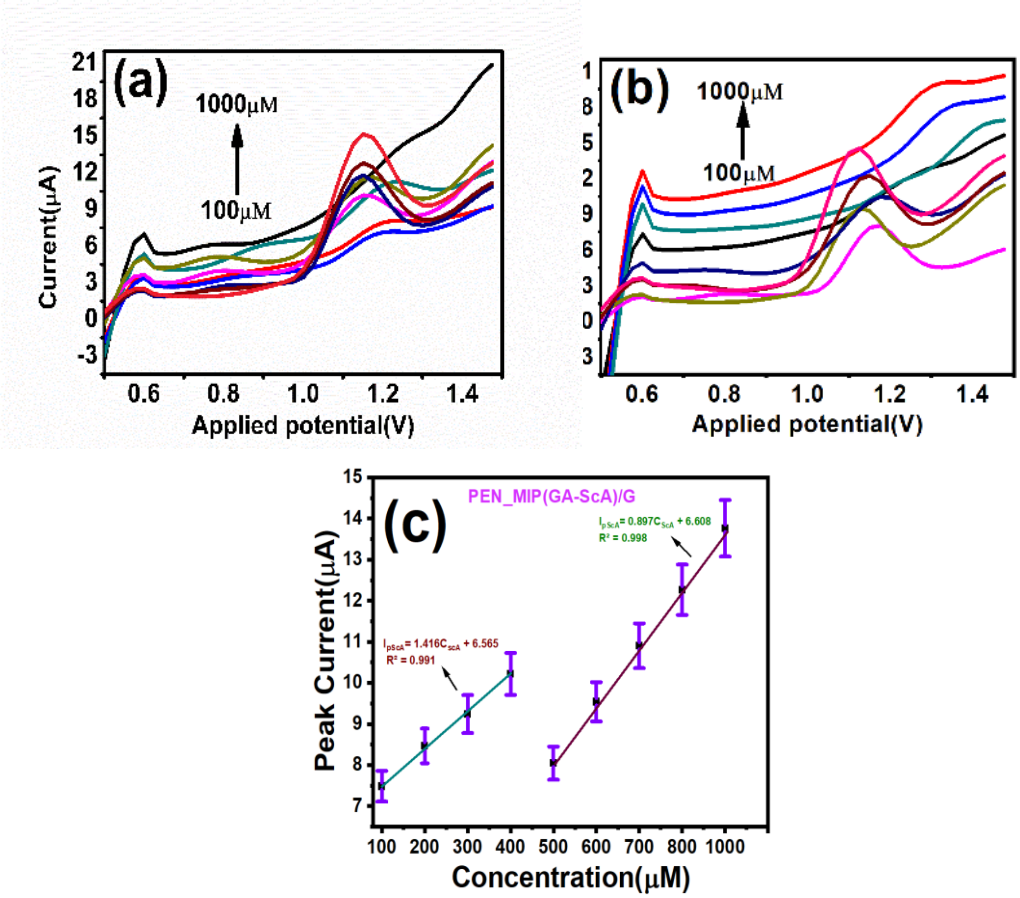

Fig. 6.9. Analytical performance evaluation via DPV. Electrochemical response of the (a) traditional MIP(GA-ScA)/G electrode and (b) the PEN_MIP(GA-ScA)/G electrode across the linear concentration range of ScA (100 µM to 1000 µM) in PBS. An increase in the oxidation peak current was observed with increasing ScA concentration for both electrodes. (c) Calibration plot (peak current vs. concentration) for the integrated PEN_MIP system, demonstrating excellent linearity ($R^2 > 0.99$).

From the lower concentration range, the limit of detection (LOD) was estimated to be approximately 1.06 µM, and the limit of quantification (LOQ) was approximately 3.53 µM from the following equations [55]-[57]: $LOD = \frac{3s_b}{S}$ and $LOQ = \frac{10s_b}{S}$ (Where:s_b is the standard deviation and S is the sensitivity of the slope of the calibration curve.

6.3.5 Operational Durability, consistency, and stability

The transition of the PEN_MIP(GA-ScA)/G sensor from a laboratory concept to a viable field-deployable device necessitated a comprehensive evaluation of its operational durability, inter-device consistency, and storage stability, the results of which are summarised in Fig. 6.10.

Operational durability and repeatability (Fig. 6.10(a)): The consistency of the analytical signal was first confirmed through mechanical regeneration testing (R1, R2, R3, and R4). The unique integrated piston mechanism allows for simple surface renewal without requiring external pre-treatment. To quantify the efficacy of this innovative regeneration method, the Regeneration efficiency (RE) was calculated using the following formula, $RE = \frac{I_{p,Rn}}{I_{p,initial}} * 100$, where $I_{p,Rn}$ is the peak current after the nth regeneration, and $I_{p,initial}$ is the initial peak current before surface regeneration. Using the initial current of 39.20 µA and the subsequent peak currents after each regeneration, the average RE for the four cycles was calculated to be ≈99.86%. This result strongly validates the mechanism, confirming that the piston successfully exposes a near-pristine sensing surface, restoring virtually all of the original electrochemical activity. The measurement consistency achieved with the PEN_MIP(GA-ScA)/G electrode yielded an RSD of 0.84%, marginally superior to the 0.85% obtained for the MIP(GA-ScA)/G traditional setup. These sub-1.0% RSD values, underpinned by the high RE, affirm the structural stability of the molecularly imprinted polymer-carbon composite during repeated use and the reliability of the regeneration mechanism.

Inter-device reproducibility (Fig. 6.10(b)): The mass production viability and operational flexibility were established by comparing the results from three independently fabricated pen cartridges, S1, S2 and S3. This test models the practical scenario where users simply replace the cartridge refill without changing the full system. The PEN_MIP(GA-ScA)/G electrodes demonstrated an excellent inter-electrode relative standard deviation (RSD) of 0.90%. This exceptional consistency, which is slightly better than the 0.94% RSD obtained for the traditional setup, validates the core design advantage: the fixed inter-electrode geometry mitigates the variable uncompensated resistance (R_u) and manual positioning errors associated with conventional setups, thereby ensuring superior manufacturing consistency and operational precision.

Long-term storage stability (Fig. 6.10(c)): The long-term chemical and physical integrity of the sensor was investigated over an extended 60-day period with an interval of 15 days (D1, D15, D30, D45, D60) following dry storage at ambient conditions. Over this duration, the electrode was observed to maintain an outstanding > 96% of its initial electrochemical activity. This exceptional stability figure is comparable to the highest values typically reported for stable polymer-composite sensors and provides critical validation for the intrinsic chemical robustness of the synthesized molecularly imprinted material. The efficacy of the pen-like housing in providing effective environmental protection is confirmed, thereby assuring a reliable, extended shelf life for practical application.

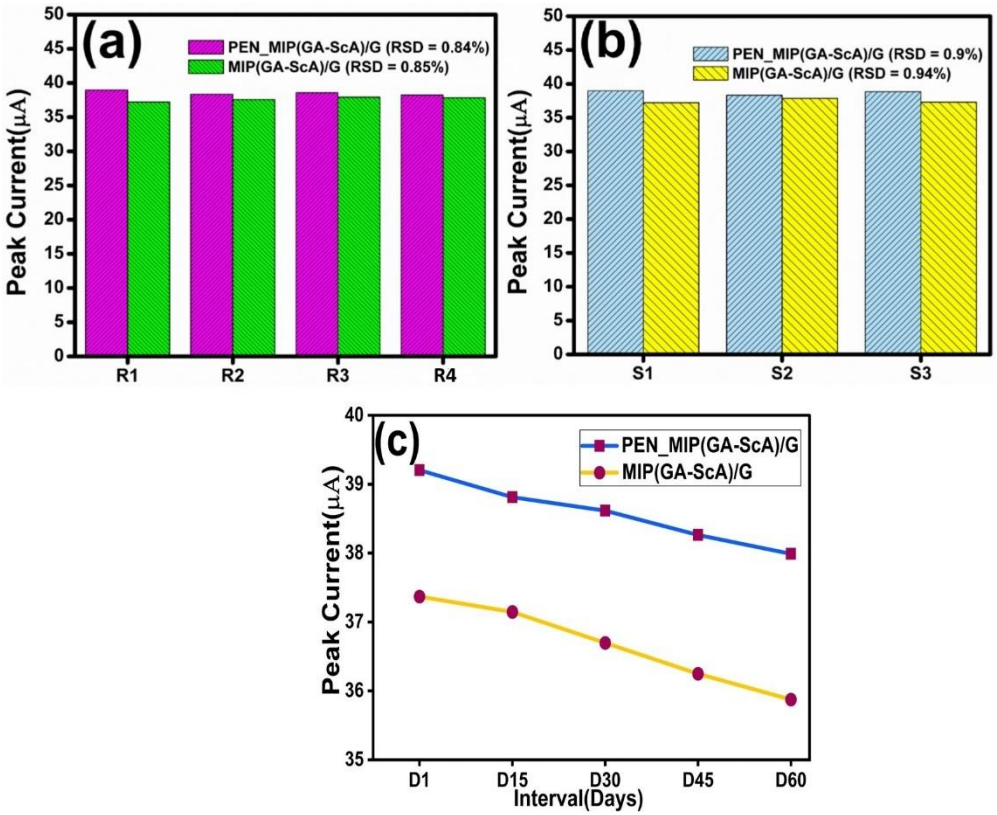

Fig. 6.10. Comparative Analytical Precision of Salicylic Acid (ScA) Electrochemical Sensing, comparing the traditional MIP(GA-ScA)/G electrode architecture with the proposed PEN_MIP(GA-ScA)/G electrode. 9(a) Repeatability: Intraday precision of the electrochemical signal for ScA, demonstrating electrode surface regeneration capability across four successive regeneration cycles (R1, R2, R3, R4). 9(b) Reproducibility: Inter-electrode precision of the electrochemical signal for ScA, measured using three independently fabricated sensors (S1, S2, and S3). 9(c) Stability: Long-term preservation of the electrochemical signal for ScA monitored over 60 days, with measurements taken at 15-day intervals.

6.3.6 Interference Study

The practical utility of any electrochemical sensor is predicated on its ability to selectively quantify the target analyte within a complex, often interfering, matrix. Therefore, a rigorous interference study was conducted to validate the intrinsic selectivity of the MIP recognition sites and to compare the performance consistency between the novel PEN_MIP(GA-ScA)/G integrated system and a conventional MIP(GA-ScA)/G electrode setup. Five critical co-existing compounds were selected based on two key criteria: 1) structural or functional similarity to the target analyte ScA, and 2) their presence as common food matrix components or ubiquitous electroactive species. The study strategically challenged 100 µM ScA with a significant 10-fold molar excess of the five critical co-existing compounds (Table 6.2), including the structural analogues Benzoic Acid (BA) and Phthalate, the common organic and inorganic matrix components Acetic Acid (CH_3COOH) and Phosphoric Acid (H_3PO_4), and the ubiquitous electroactive species Caffeine. As summarised in Table 6.2, the PEN_MIP(GA-ScA)/G electrode exhibited exceptional selectivity, with the current deviation (% Deviation) remaining within a tight range of 0.5% to 2.3% across all interferents. This minimal change confirms that the MIP cavity effectively excludes compounds lacking the precise geometric and electronic characteristics of ScA. Specifically, the strong rejection of BA demonstrates that the ortho-hydroxyl group of ScA is indispensable for high-affinity binding within the GA-templated polymer, validating the successful imprinting mechanism.

Table 6.2. Interference study comparing the electrochemical response of the PEN_MIP GA-ScA-G integrated electrode with the traditional MIP GA-ScA-G electrode, employing 100 µM ScA in the presence of 1.0 mM (10-fold excess) common interfering compounds.

Analyte / Matrix Component (100 µM ScA)	PEN_MIP(GA-ScA)/G Peak Current (I_p/µA)	% Deviation (PEN)	MIP(GA-ScA)/G Traditional Peak Current (I_p/µA)	%Deviation (Traditional)
ScA	39.2	0	37.3	0
ScA + Benzoic Acid (BA)	38.7	1.3	37.5	0.5
ScA + Phthalate	39.5	0.8	38.5	3.2
ScA + Acetic Acid (CH_3COOH)	38.3	2.3	37.9	1.6
ScA + Phosphoric Acid (H_3PO_4)	40.1	2.3	38.1	2.1
ScA + Caffeine	39.4	0.5	38.7	3.7

The comparative data unequivocally advocate the operational superiority afforded by the integrated electrode architecture. Across all five interference conditions, the PEN_MIP(GA-ScA)/G integrated system consistently demonstrated a lower magnitude of signal perturbation than the conventional MIP setup. The maximum observed current deviation for the PEN system was only 2.3 %, a substantially tighter tolerance compared to the 3.7 % recorded for the traditional arrangement. For instance, when challenged by caffeine, the PEN system's signal deviated by only 0.5 %, while the traditional setup exhibited a 3.7 % shift. Furthermore, the overall consistency of the measurements, quantified by the RSD, was 2.01 % for the PEN system—a significantly reduced value compared to the 3.23 % of the traditional setup. This empirical evidence provides strong validation that the fixed inter-electrode geometry efficaciously eliminates the inherent variability of conventional dipping cells, mitigating uncompensated resistance fluctuations and yielding a sensor with superior analytical precision. This successful demonstration of both high selectivity and enhanced precision validates the PEN platform as a robust, viable technology for complex sample analysis.

6.3.7 Real sample- Comparative study

To evaluate the practical applicability of the pen-like PEN_MIP(GA-ScA)/G electrode for real-world analysis, the sensor was employed in the determination of ScA in spiked fruit samples of orange, apple, and grapes.

Sample Preparation: 10 g of each fruit, obtained from the local market, was subjected to grinding using a mixer. The resulting pulp was subsequently mixed with 10 mL of a 100 µM PBS buffer (at pH 6) and then centrifuged for 15 minutes. For dilution, 1 ml of the supernatant (juice extract) was mixed with 9 ml of the same buffer solution, resulting in a 1:10 dilution (juice: buffer) before electrochemical analysis to minimize matrix effects.

Spiking and Recovery Studies: Initially, the native ScA levels in the diluted juice extracts were estimated using both PEN_MIP(GA-ScA)/G and traditional, MIP(GA-ScA)/G electrodes. Following this, known amounts (100 µM and 200 µM) of ScA standard solution were introduced into separate aliquots of the diluted extracts. The spiked samples were then analyzed, and the recovery(R) of the added ScA was calculated and compared for the two systems. The results obtained are summarized in Table 6.3.

Table 6.3. Recovery of ScA from spiked fruit samples using pen-like and traditional MIP(GA-ScA)/G electrodes, showing detected concentrations and recovery percentages after standard 1:10 dilution

Sample	ScA (Pen) (µM)	ScA (Trad) (µM)	ScA Added (µM)	Recov. ScA (Pen) (µM)	Recov. ScA (Trad) (µM)	R_{Pen} (%)	R_{trad} (%)	Pen sys.
Orange	1.18	1.1	100	101.5	100.5	100.32	99.41	Slightly Better
Orange	1.18	1.1	200	201.5	201	100.15	100	Comparable
Apple	0.22	0.31	100	100.3	99.5	100.08	99.19	Slightly Better
Apple	0.22	0.31	200	200.1	199.8	99.94	99.75	Comparable
Grapes	2.10	2.02	100	101.9	101	99.71	98.9	Slightly Better
Grapes	2.10	2.02	200	202.8	202	100.29	99.95	Slightly Better

6.3.8 Comparative analysis of advanced electrochemical sensors for ScA

The development of the PEN_MIP(GA-ScA)/G electrode is a strategic effort to produce a high-performance, reusable sensing platform that directly addresses the limitations of conventional laboratory setups. The core novelty lies in the PEN_MIP(GA-ScA)/G electrode's integrated design, which ensures that any study cited in Table 6.4 that relies on a conventional three-electrode glass cell setup ([58], [60], [62], [64]– [68]) could utilize the PEN_MIP(GA-ScA)/G electrode as a direct, drop-in replacement electrode module. This immediate compatibility demonstrates that the PEN_MIP(GA-ScA)/G electrode is not a deviation from established analytical practice, but rather a superior evolution of the three-electrode system itself. The fixed-geometry architecture of the PEN housing eliminates the alignment, spacing, and contamination variability inherent in manual beaker setups, ensuring enhanced reproducibility. Despite the existence of ultra-trace detection systems ([66]), which are invariably non-portable and require specialized GCE preparation, the PEN_MIP(GA-ScA)/G electrode delivers an excellent LOD of 1.06 µM. This sensitivity is highly competitive with other high-performance lab standards and miniaturized systems, and is more than adequate for most practical monitoring requirements. By integrating the essential MIP recognition element and a fixed-geometry three-electrode system into a robust, handheld form factor, the PEN_MIP(GA-ScA)/G electrode successfully combines high MIP selectivity and regenerability with ease of use. This makes the PEN__MIP(GA-ScA)/G electrode a highly promising, forward-compatible replacement for the core sensing component alternative to miniaturized systems ([59], [63]) and disposable flat formats, such as SCEs ([61], [69]), drastically simplifying experimental setup and preparation while maintaining competitive analytical performance.

Table 6.4. Comparative analysis of LOD and key structural/analytical features of the integrated PEN MIP system versus recent advanced electrochemical ScA sensors.

Electrode System Type & Configuration	Working Electrode Material	LOD (µM)	Key Feature & Relevance to Proposed Pen System	Reference
Integrated Tri-Electrode, Regenerative (Pen-like device)	PEN_MIP(GA-ScA)/G	1.06	Compact & Regenerative. Unique ergonomic form factor for field use. High precision via fixed geometry.	This work
Conventional 3-Electrode Glass Cell	CPE with Ce-ZrO2 Nanoparticles	0.12	High Sensitivity (Benchmark). Non-portable lab-based system with low LOD via highly active nanoparticle modification.	[58]
Miniaturized Tip 3-Electrode System (Pt wire)	MWCNT modified	0.1	Miniaturized for in vivo use. Designed for continuous monitoring, not general field dipping.	[59]
Conventional 3-Electrode Glass Cell	Polypyrrole (PPy) / Banana Tissue Composite	0.089	Extremely Low LOD. Highest sensitivity biosensor, but non-portable.	[60]
Screen-Printed 3-Electrode System (SPCE)	Electrochemically Reduced Graphene Oxide (rGO)	≈2	Low-Cost & Disposable. Excellent model for printed portability, but non-regenerative.	[61]
Conventional 3-Electrode Glass Cell	Multi-Walled Carbon Nanotubes (MWCNT)	0.8	Very Wide Linear Range. High-performance lab benchmark; non-portable.	[62]
Integrated 3-Electrode System in Microchannel	GO/Bi-Enzyme	0.5	Miniaturized & Selective. Requires external fluid control; limits true field	[63]

Chip			portability.	
Conventional 3-Electrode Glass Cell	Ppy MIP on Platinum Plate	72	Lab-Based MIP Benchmark. High selectivity confirmed by DFT. Uses a non-portable electrode configuration	[64]
Conventional 3-Electrode Glass Cell (FTO/TiO2)	MIP on TiO2 Nanorods	0.039	Highly Ordered Architecture. Uses TiO2 nanorod arrays for enhanced performance. Non-portable.	[65]
Conventional 3-Electrode Glass Cell (GCE)	Ppy MIP	0.000035	Ultra-Trace Sensitivity. Achieves the lowest reported LOD using a non-portable lab electrode.	[66]
Conventional 3-Electrode Glass Cell (GCE)	PoPD MIP	20	MIP Benchmark. Early MIP work establishing feasibility on GCE. Non-portable.	[67]
Conventional 3-Electrode Glass Cell (GCE)	GCE/AuNP-Gr-Chi/MIP	0.00013	Ultra-Sensitive Real Sample Analysis. GCE enhanced with nanomaterials. Non-portable.	[68]
Screen-Printed Electrode (SPE)	Cu-MOF/CB Ratiometric Sensor	12.5	Uses ratiometric signal on a flat SPE; highly relevant for practical application and sensor geometry	[69]

Note: AuNP (Gold nanoparticle), CB (Carbon black), Chi (Chitosan), FTO (Fluorine-doped tin oxide), GO (Graphene oxide), Gr (Graphene), MWCNT (Multi-walled carbon nanotubes), PoPD (Poly(o-phenylenediamine)), PPy or Ppy (Polypyrrole), Pt (Platinum electrode), rGO (Electrochemically reduced graphene oxide), and TiO_2 NRAs (Titanium oxide nanorod arrays).

6.3.9 Economic Feasibility and Fabrication Scalability

The successful transition of the integrated device from the lab to field deployment requires strong economic viability and production scalability. The pen architecture was designed for mass production using high-throughput processes. The housing and cartridge components utilize low-cost, durable polymer materials, enabling efficient manufacturing via injection

molding. This ensures high dimensional precision and a low unit cost, positioning the hardware competitively against existing screen-printed sensors. Operational economy is maximized by the regenerative mechanism. By achieving a RE>99%, the PEN_MIP system provides multiple uses from a single cartridge, drastically lowering the cumulative cost per analysis compared to single-use sensors. The internal piston design ensures that only a minimal, controlled volume of the sensing material is consumed per cycle, resulting in inherently low material waste and superior longevity. This fusion of low manufacturing cost and high operational lifespan positions the integrated pen system as an economically optimized tool for high-volume, decentralized food quality monitoring.

Conclusion with future roadmap

The applicability of the developed MIP-based electrochemical sensors for real sample analysis was demonstrated through recovery studies in spiked fruit juice samples. Generally, recovery percentages for both the pen-like (R_{Pen}) and traditional systems (R_{trad}) were found to be close to 100%, indicating acceptable accuracy and minimal matrix interference following a 1:10 dilution (1 ml juice in 9 ml buffer) of the extracts. Upon comparison of the two electrode systems, the PEN__MIP(GA-ScA)/G electrode exhibited performance that was comparable to, and in several instances slightly better than, the traditional MIP(GA-ScA)/G electrode in the detection of ScA across the tested fruit matrices. Beyond these matrix results, the integrated design validated its core advantages by exhibiting exceptional long-term stability (96% current retention over 60 days) and enhanced precision (RSD for reproducibility 0.90%) and tighter tolerance in the interference study compared to the traditional setup. While the system's performance was rigorously validated using a commercial benchtop potentiostat/galvanostat to maintain instrumental control, the next logical step involves the integration of the fixed-geometry architecture with a miniaturized, custom-built potentiostat. This development is necessary to fully realize the potential for a truly self-contained and portable analytical device capable of immediate, non-laboratory deployment. The pen system's modular design offers a significant path for future development. Crucially, by simply tailoring the MIP template layer for a different target analyte without requiring any modification to the core mechanical or electrical housing., the same integrated hardware can be re-purposed for the detection of a wide range of other high-impact analytes, including various phenolic antioxidants, food dyes, or contaminants, enhancing its utility as a versatile, field-deployable platform for broader food quality and safety monitoring. The suitability of use and potential for on-site analysis offered by the integrated pen-like design, coupled with its strong analytical performance, position it as a promising tool for practical applications in food safety and quality control.

References

[1] D. Rahangdale and A. Kumar, "Chitosan as a substrate for simultaneous surface imprinting of salicylic acid and cadmium," *Carbohydrate Polymers*, vol. 202, pp. 334–344, Sep. 2018, doi: 10.1016/j.carbpol.2018.08.129.

[2] J. Ahima, X. Zhang, Q. Yang, L. Zhao, A. M. Tibiru, and H. Zhang, "Biocontrol activity of Rhodotorula mucilaginosa combined with salicylic acid against Penicillium digitatum infection in oranges," *Biological Control*, vol. 135, pp. 23–32, May 2019, doi: 10.1016/j.biocontrol.2019.04.019.

[3] H. Xu *et al.*, "Synthesizing a surface-imprinted polymer based on the nanoreactor SBA-15 for optimizing the adsorption of salicylic acid from aqueous solution by response surface methodology," *New Journal of Chemistry*, vol. 45, no. 14, pp. 6192–6205, Jan. 2021, doi: 10.1039/d1nj00016k.

[4] J. Huang, Y. Hu, Y. Hu, and G. Li, "Disposable terbium (III) salicylate complex imprinted membrane using solid phase surface fluorescence method for fast separation and detection of salicylic acid in pharmaceuticals and human urine," *Talanta*, vol. 107, pp. 49–54, Jan. 2013, doi: 10.1016/j.talanta.2012.12.054.

[5] M. T. Jafari, Z. Badihi, and E. Jazan, "A new approach to determine salicylic acid in human urine and blood plasma based on negative electrospray ion mobility spectrometry after selective separation using a molecular imprinted polymer," *Talanta*, vol. 99, pp. 520–526, Jun. 2012, doi: 10.1016/j.talanta.2012.06.023.

[6] M. Meng *et al.*, "Optimization of surface imprinted layer attached poly(vinylidene fluoride) membrane for selective separation of salicylic acid from acetylsalicylic acid using central composite design," *Chemical Engineering Journal*, vol. 231, pp. 132–145, Jul. 2013, doi: 10.1016/j.cej.2013.07.015.

[7] N. Nakada, T. Tanishima, H. Shinohara, K. Kiri, and H. Takada, "Pharmaceutical chemicals and endocrine disrupters in municipal wastewater in Tokyo and their removal during activated sludge treatment," *Water Research*, vol. 40, no. 17, pp. 3297–3303, Aug. 2006, doi: 10.1016/j.watres.2006.06.039.

[8] X. Yu, X. Mi, Z. He, M. Meng, H. Li, and Y. Yan, "Fouling Resistant CA/PVA/TiO2 Imprinted Membranes for Selective Recognition and Separation of Salicylic Acid from Waste Water," *Frontiers in Chemistry*, vol. 5, Jan. 2017, doi: 10.3389/fchem.2017.00002.

[9] J. I. Routh, N. A. Shane, E. G. Arredondo, and W. D. Paul, "Method for the determination of acetylsalicylic acid in the blood," *Clinical Chemistry*, vol. 13, no. 9, pp. 734–743, Sep. 1967, doi: 10.1093/clinchem/13.9.734.

[10] V. Vs, C. Vp, and R. Mv, "Simultaneous estimation of mometasone furoate and salicylic acid in topical formulation by UV-Visible spectrophotometry," *International Journal of Chemical Sciences*, vol. 15, no. 2, Jan. 2017.

[11] N. Rajendraprasad and K. Basavaiah, "Modified Spectrophotometric Methods for Determination of Iron(III) in Leaves and Pharmaceuticals Using Salicylic Acid," *Indian Journal of Advances in Chemical Science*, vol. 4, no. 3, pp. 302-307, 2016.

[12] Y. Yamamoto, T. Kumamaru, Y. Hayashi, and M. Otsuchi, "Spectrophotometric determination of salicylic acid by solvent extraction with tris (1, 10-phenanthroline)iron(II) chelate cation," *BUNSEKI KAGAKU*, vol. 18, no. 3, pp. 354–359, Jan. 1969, doi: 10.2116/bunsekikagaku 18.354.

[13] M. O. Iwunze, "Absorptiometric determination of acetylsalicylic acid in aqueous ethanolic solution," *Analytical Letters*, vol. 41, no. 16, pp. 2944–2953, Nov. 2008, doi: 10.1080/00032710802440574.

[14] K. W. Street and G. H. Schenk, "Spectrofluorometric determination of acetylsalicylic acid, salicylamide, and salicylic acid as an impurity in pharmaceutical preparations," *Journal of Pharmaceutical Sciences*, vol. 70, no. 6, pp. 641–646, Jun. 1981, doi: 10.1002/jps 2600700617.

[15] K. Wille *et al.*, "Validation and application of an LC-MS/MS method for the simultaneous quantification of 13 pharmaceuticals in seawater," *Analytical and Bioanalytical Chemistry*, vol. 397, no. 5, pp. 1797–1808, May 2010, doi: 10.1007/s00216-010-3702-z.

[16] M. Hefnawy *et al.*, "Fast and sensitive liquid chromatography method for simultaneous determination of methylisothiazolinone, salicylic acid and parabens in cosmetic products," *Current Analytical Chemistry*, vol. 13, no. 5, Mar. 2017, doi: 10.2174/1573411013666170330092426.

[17] E. Protasiuk and M. Olejnik, "Determination of salicylic acid in feed using LC-MS/MS," *Journal of Veterinary Research*, vol. 62, no. 3, pp. 303–307, Sep. 2018, doi: 10.2478/jvetres-2018-0044.

[18] J. L. N. De Aguiar, K. C. Leandro, S. De Mello Pereira Abrantes, and A. L. M. Albert, "Development of a new analytical method for determination of acetylsalicylic and salicylic acids in tablets by reversed phase liquid chromatography," *Brazilian Journal of Pharmaceutical Sciences*, vol. 45, no. 4, pp. 723–727, Dec. 2009, doi: 10.1590/s1984-82502009000400016.

[19] Z.-H. Huang *et al.*, "Simultaneous determination of salicylic acid, jasmonic acid, methyl salicylate, and methyl jasmonate from Ulmus Pumila Leaves by GC-MS," *International Journal of Analytical Chemistry*, vol. 2015, pp. 1–7, Jan. 2015, doi: 10.1155/2015/698630.

[20] A. M. Saeed, M. J. Hamzah, and N. Q. Ahmed, "QUANTITATIVE ASSAY OF ASPIRIN AND (SALICYLIC ACID AND HEAVY METALS AS IMPURATIES) IN IRAQI'S MARKET ASPIRIN TABLETS USING DIFFERENT ANALYTICAL METHODS," *International Journal of Applied Pharmaceutics*, vol. 10, no. 5, p. 167, Sep. 2018, doi: 10.22159/ijap 2018v10i5.26820.

[21] M. M. Ardakani, A. Sadeghi, J. Safari, and F. Shibani, "[Bis(2-hydroxyl imino)1-phenyl, 2-(2-quinoxaline) 1-ethanone]Aluminium(III) Complex as Carrier for a Salicylate-Sensitive Electrode," *Croatica Chemica Acta*, vol. 79, pp. 581-589, 2006.

[22] I. M. Isa *et al.*, "Determination of Salicylate ion by Potentiometric Membrane Electrode based on Zinc Aluminium Layered Double Hydroxides-4(2,4-dichlorophenoxy)Butyrate Nanocomposites," *International Journal of Electrochemical Science*, vol. 8, no. 2, pp. 2112–2121, Feb. 2013, doi: 10.1016/s1452-3981(23)14295-7.

[23] M. Mazloum-Ardakani, M. A. Sheikh-Mohseni, and A. Benvidi, "Determination of Salicylate by Selective and Sensitive Polymer Membrane Electrode: with Internal Solution and Solid Contact," *Anal. Bioanal. Electrochem.*, vol. 2, no. 3, pp. 155-164, 2010.

[24] V. J. F. Ferreira *et al.*, "An electrode of the second kind for aspirin determination in tablet formulations," *Analytical Sciences*, vol. 15, no. 3, pp. 249–253, Mar. 1999, doi: 10.2116/analsci 15.249.

[25] M. R. Ganjali, F. G. Nejad, S. Tajik, H. Beitollahi, E. Pourbasheer, and B. Larijanii, "Determination of salicylic acid by differential pulse voltammetry using ZNO/AL2O3 nanocomposite modified graphite screen printed electrode," *International Journal of Electrochemical Science*, vol. 12, no. 11, pp. 9972–9982, Oct. 2017, doi: 10.20964/2017.11.49.

[26] R. Ansari, Z. Mosayebzadeh, M. Arvand, and A. Mohammad-Khah, "A potentiometric solid state copper electrode based on nanostructure polypyrrole conducting polymer film doped with 5-sulfosalicylic acid," *Journal of Nanostructure in Chemistry*, vol. 3, no. 1, May 2013, doi: 10.1186/2193-8865-3-33.

[27] H. C. Loh, M. Ahmad, and M. N. Taib, "Fabrication and characterization of novel salicylic acid sensors using different reagents (Ferric and Copper)," *Analytical Letters*, vol. 39, no. 7, pp. 1299–1310, May 2006, doi: 10.1080/00032710600666354.

[28] J. C. B. Fernandes, C. A. B. Garcia, L. A. Grandin, G. De Oliveira Neto, and O. E. S. Godinho, "Determination of acetylsalicylic acid in tablets with salicylate ion selective electrode in a Batch Injection Analysis system," *Journal of the Brazilian Chemical Society*, vol. 9, no. 3, pp. 249–251, May 1998, doi: 10.1590/s0103-50531998000300008.

[29] M. N. Ayanoğlu, H. E. K. Ertürün, A. D. Özel, Ö. Şahin, M. Yılmaz, and E. Kılıç, "Salicylate Ion-Selective Electrode Based on a Calix[4]arene as Ionophore," *Electroanalysis*, vol. 27, no. 7, pp. 1676–1684, Mar. 2015, doi: 10.1002/elan 201400737.

[30] J. Wang et al., "Molecularly imprinted fluorescent hollow nanoparticles as sensors for rapid and efficient detection λ-cyhalothrin in environmental water," *Biosensors and Bioelectronics*, vol. 85, pp. 387–394, May 2016, doi: 10.1016/j.bios.2016.05.041.

[31] S. Nag, D. Das and R. B. Roy, "Voltammetry Application of Molecularly Imprinted Polyacrylamide as Vanillin Receptor in Desserts," in *IEEE Sens. J.*, vol. 23, no. 4, pp. 3446-3452, 15 Feb. 15, 2023, doi: 10.1109/JSEN.2023.3235933.

[32] D. Das et al., "Amine Functionalized MWCNTs Modified MIP-Based Electrode for Detection of Epicatechin in Tea," *IEEE Sens. J.*, vol. 22, no. 11, pp. 10323–10330, Jun. 2022, doi: 10.1109/JSEN.2022.3169169.

[33] G. Pan, Y. Zhang, Y. Ma, C. Li, and H. Zhang, "Efficient One-Pot synthesis of Water-Compatible molecularly imprinted polymer microspheres by facile RAFT precipitation polymerization," *Angewandte Chemie International Edition*, vol. 50, no. 49, pp. 11731–11734, Oct. 2011, doi: 10.1002/anie.201104751.

[34] S. Nag et al., "A simple nano cerium oxide modified graphite electrode for electrochemical detection of formaldehyde in mushroom," *IEEE Sensors J.*, vol. 21, no. 10, pp. 12019–12026, May 2021

[35] W. Chen, Y. Ma, J. Pan, Z. Meng, G. Pan, and B. Sellergren, "Molecularly Imprinted Polymers with Stimuli-Responsive Affinity: Progress and Perspectives," *Polymers*, vol. 7, no. 9, pp. 1689–1715, Sep. 2015, doi: 10.3390/polym7091478.

[36] B. Sellergren, "Molekular geprägte Polymere mit einem Gedächtnis für kleine Moleküle, Proteine oder Kristalle," *Angewandte Chemie*, vol. 112, no. 6, pp. 1071–1078, Mar. 2000, doi: 10.1002/(sici)1521-3757(20000317)112:6.

[37] S. Nag, D. Das, H. Naskar, B. Tudu, R. Bandyopadhyay, and R. Banerjee Roy, "Detection of metanil yellow adulteration in turmeric powder using nano nickel cobalt oxide modified graphite electrode," *IEEE Sens. J.*, vol. 22, no. 13, pp. 12515–12521, Jul. 2022, doi: 10.1109/JSEN.2022.3178768.

[38] D. Bandyopadhyay, S. Nag, D. Das, and R. B. Roy, "Detection of syringic acid in food extracts using molecular imprinted polyacrylonitrile infused graphite electrode," *Journal of food composition and analysis*, vol. 132, p. 106280, Aug. 2024, doi:10.1016/j.jfca.2024.106280.

[39] S. Nag, S. Pradhan, D. Das, B. Tudu, R. Bandyopadhyay, and R. B. Roy, "Fabrication of a molecular imprinted polyacrylonitrile engraved graphite electrode for detection of formalin in food extracts," *IEEE Sensors Journal*, vol. 22, no. 1, pp. 42–49, Nov. 2021, doi: 10.1109/jsen.2021.3128520.

[40] D. Bandyopadhyay, S. Acharya, S. Nag, D. Das, and R. B. Roy, "A Molecular-Imprinted bipolymer infused capacitive sensor for inositol detection in fruits," *IEEE Transactions on Instrumentation and Measure*ment, vol. 72, pp. 1–9, Jan. 2023, doi: 10.1109/tim.2023.3306839.

[41] V. Ayerdurai, M. Cieplak, and W. Kutner, "Molecularly imprinted polymer-based electrochemical sensors for food contaminants determination," *TrAC Trends in Analytical Chemistry*, vol. 158, p. 116830, Nov. 2022, doi: 10.1016/j.trac.2022.116830.

[42] J. Kang, H. Zhang, Z. Wang, G. Wu, and X. Lu, "A novel amperometric sensor for salicylic acid based on molecularly imprinted Polymer-Modified electrodes," *Polymer-Plastics Technology and Engineering*, vol. 48, no. 6, pp. 639–645, May 2009, doi: 10.1080/03602550902824499.

[43] G. J. Baxter, J. R. Lawrence, A. B. Graham, D. Wiles, and J. R. Paterson, "Identification and determination of salicylic acid and salicyluric acid in urine of people not taking salicylate drugs," *Annals of Clinical Biochemistry International Journal of Laboratory Medicine*, vol. 39, no. 1, pp. 50–55, Jan. 2002, doi: 10.1258/0004563021901739.

[44] W. Zhihua, L. Xiaole, W. Bowan, W. Fangping, and L. Xiaoquan, "Voltammetric determination of salicylic acid by molecularly imprinted film modified electrodes," *International Journal of Polymer Analysis and Characterization*, vol. 17, no. 2, pp. 122–132, Feb. 2012, doi: 10.1080/1023666x.2012.640429.

[45] X. Yang *et al.*, "Dual Functional Molecular Imprinted Polymer-Modified Organometal lead halide perovskite: synthesis and application for photoelectrochemical sensing of salicylic acid," *Analytical Chemistry*, vol. 91, no. 15, pp. 9356–9360, Jul. 2019, doi: 10.1021/acs.analchem.9b01739.

[46] H. Xu *et al.*, "Synthesizing a surface-imprinted polymer based on the nanoreactor SBA-15 for optimizing the adsorption of salicylic acid from aqueous solution by response surface methodology," *New Journal of Chemistry*, vol. 45, no. 14, pp. 6192–6205, Jan. 2021, doi: 10.1039/d1nj00016k.

[47] X. Li, J. Chen, and C. Yang, "Fabrication of Polyether Sulfone Blend Imprinted Membranes for Selective Adsorption of p-hydroxybenzonic from Salicylic Acid," *Fibers and Polymers*, vol. 19, no. 5, pp. 977–986, May 2018, doi: 10.1007/s12221-018-1106-4.

[48] Y. Hu, H. Du, J. Lu, H. Zhang, S. Li, and X. Du, "Interface synergistic stabilization of zinc anodes via polyacrylic acid doped polyvinyl alcohol ultra-thin coating," *Journal of Energy Storage*, vol. 87, p. 111444, Mar. 2024, doi: 10.1016/j.est.2024.111444.

[49] V. Djordjevic, L. Dubonjic, M. M. Morato, D. Prsic, and V. Stojanovic, "Sensor fault estimation for hydraulic servo actuator based on sliding mode observer," *Mathematical Modelling and Control*, vol. 2, no. 1, pp. 34–43, Jan. 2022, doi: 10.3934/mmc.2022005.

[50] Z. Guan, Y. Sun, Y. He, J. Cao, J. Tian, and Z. Ji, "Machine-learning-assisted nanopore sensing solution for the determination of matrix metalloproteinase," *Biosensors and Bioelectronics*, vol. 288, p. 117752, Jul. 2025, doi: 10.1016/j.bios.2025.117752.

[51] H. Tao, Z. Huang, Y. Wang, J. Qiu, and S. Vladimir, "Efficient feature fusion network for small objects detection of traffic signs based on cross-dimensional and dual-domain information," *Measurement Science and Technology*, vol. 36, no. 3, p. 035004, Feb. 2025, doi: 10.1088/1361-6501/adb2ad.

[52] M. Dhara et al., "TiO2-Graphite Supported Hybrid MIP Sensor for Sensitive Vitamin C Detection in Cosmetics," IEEE *Sensors Journal*, vol. 25, no. 19, pp. 35757-35764, 1 Oct.1, 2025, doi: 10.1109/JSEN.2025.3598128.

[53] M. Dhara et al., "Synthesis of HNQ-Imprinted Poly(Methyl acrylate) using hybrid polymerization for the detection of lawsone in henna powder," *IEEE Sensors Journal*, vol. 25, no. 9, pp. 14598–14605, Mar. 2025, doi: 10.1109/jsen.2025.3550828.

[54] M. Dhara et al., "High performance multilayered graphene-graphite composite-based hybrid molecularly imprinted polymer sensor for vitamin C detection in cosmetic formulations," *Microchemical Journal*, vol. 218, p. 115607, Oct. 2025, doi: 10.1016/j.microc.2025.115607.

[55] J. Krupčík, P. Májek, R. Gorovenko, J. Blaško, R. Kubinec, and P. Sandra, "Considerations on the determination of the limit of detection and the limit of quantification in one-dimensional and comprehensive two-dimensional gas chromatography," *Journal of chromatography A*, vol. 1396, pp. 117–130, Apr. 2015, doi: 10.1016/j.chroma.2015.03.084.

[56] N. A. Epshtein, "Validation of chromatographic methods: Determining the limit of quantification in practice," *Pharmaceutical Chemistry Journal*, vol. 55, no. 1, pp. 91–96, Apr. 2021, doi: 10.1007/s11094-021-02378-0.

[57] S. A. Gegenschatz, F. A. Chiappini, C. M. Teglia, A. M. De La Peña, and H. C. Goicoechea, "Binding the gap between experiments, statistics, and method comparison: A tutorial for computing limits of detection and quantification in univariate calibration for complex samples," *Analytica chimica acta*, vol. 1209, p. 339342, Dec. 2021, doi: 10.1016/j.aca.2021.339342.

[58] T. Alizadeh and S. Nayeri, "Electrocatalytic oxidation of salicylic acid at a carbon paste electrode impregnated with cerium-doped zirconium oxide nanoparticles as a new sensing approach for salicylic acid determination," *Journal of Solid State Electrochemistry*, vol. 22, no. 7, pp. 2039–2048, Feb. 2018, doi: 10.1007/s10008-018-3907-1.

[59] Y. Zhang et al., "Smartphone-based electrochemical microsensor in combination with internet of things for remote monitoring of salicylic acid in plant," *Biosensors and Bioelectronics*, vol. 287, p. 117733, Jul. 2025, doi: 10.1016/j.bios.2025.117733.

[60] M. H. A. Zavar, S. Heydari, and G. H. Rounaghi, "Electrochemical determination of salicylic acid at a new biosensor based on Polypyrrole-Banana tissue composite," *Arabian Journal for Science and Engineering*, vol. 38, no. 1, pp. 29–36, Dec. 2012, doi: 10.1007/s13369-012-0411-2.

[61] B. Kashyap and R. Kumar, "Bio-agent free electrochemical detection of Salicylic acid," 2019 *IEEE SENSORS*, Montreal, QC, Canada, 2019, pp. 1-4, doi: 10.1109/SENSORS43011.2019.8956497.

[62] W.-D. Zhang, B. Xu, Y.-X. Hong, Y.-X. Yu, J.-S. Ye, and J.-Q. Zhang, "Electrochemical oxidation of salicylic acid at well-aligned multiwalled carbon nanotube electrode and its detection," *Journal of Solid State Electrochemistry*, vol. 14, no. 9, pp. 1713–1718, Feb. 2010, doi: 10.1007/s10008-010-1014-z.

[63] B. Kashyap and R. Kumar, "Salicylic acid (SA) detection using bi-enzyme microfluidic electrochemical sensor," *Proc. SPIE 10662, Sensing for Agriculture and Food Quality and Safety X*, 106620K, May 2018. doi: 10.1117/12.2305124.

[64] G. Zvirzdine et al., "Electrochemical salicylic acid sensor based on molecularly imprinted polypyrrole," *ACS Applied Materials & Interfaces*, vol. 17, no. 41, pp. 57475–57485, Oct. 2025, doi: 10.1021/acsami.5c11951.

[65] X. Xiong et al., "In situ grown TiO2 nanorod arrays functionalized by molecularly imprinted polymers for salicylic acid recognition and detection," Journal of Electroanalytical Chemistry, vol. 873, p. 114394, Jun. 2020, doi: 10.1016/j.jelechem.2020.114394.

[66] W. Zhihua, L. Xiaole, W. Bowan, W. Fangping, and L. Xiaoquan, "Voltammetric determination of salicylic acid by molecularly imprinted film modified electrodes," *International Journal of Polymer Analysis and Characterization*, vol. 17, no. 2, pp. 122–132, Feb. 2012, doi: 10.1080/1023666x.2012.640429.

[67] J. Kang, H. Zhang, Z. Wang, G. Wu, and X. Lu, "A novel amperometric sensor for salicylic acid based on molecularly imprinted Polymer-Modified electrodes," *Polymer-Plastics Technology and Engineering*, vol. 48, no. 6, pp. 639–645, May 2009, doi: 10.1080/03602550902824499.

[68] L. Ya MA, S. S. Miao, F. F. Lu, M. S. Wu, Y. C. Lu, and H. Yang, "Selective electrochemical determination of salicylic acid in wheat using molecular imprinted polymers," *Analytical Letters*, vol. 50, no. 15, pp. 2369–2385, Jun. 2017, doi: 10.1080/00032719.2017.1291654.

[69] L. Yang et al., "Ratiometric electrochemical sensor for accurate detection of salicylic acid in leaves of living plants," *RSC Advances*, vol. 10, no. 64, pp. 38841–38846, Jan. 2020, doi: 10.1039/d0ra05813k.

PUBLICATIONS

JOURNALS: D. Bandyopadhyay, D. Bandyopadhyay, S. Nag, J. Naskar, and R. B. Roy, "Towards the development of an integrated, user friendly, voltammetric electrode for the electrochemical sensing of food quality," *Measurement*, vol. 260, p. 119776, Nov. 2025, doi: 10.1016/j.measurement.2025.119776.

Conclusions and Future Scopes

7

7.1 Introduction

Food constituents, including vital nutrients, are chemical substances naturally present in food or intentionally added to enhance specific properties such as preservation, flavor, or nutritional content. Historically, traditional methods were employed to preserve and enrich food. However, with the rapid evolution of the food processing industry, there's a growing demand for a diverse range of compounds to create modern food products, from nutrient-fortified items to convenient ready-to-eat meals. These substances serve various functions, including nutritional supplementation, processing aids, or sensory enhancements, with many exhibiting multiple roles.

The safety and efficacy of these food constituents, particularly nutrients and compounds affecting food quality, are rigorously assessed through extensive investigations. These studies involve meticulous monitoring of the effects of various substances on biological parameters in test animals to establish the No-Observed-Effect Level (NOEL). This NOEL is then used to determine the Acceptable Daily Intake (ADI) for human consumption, ensuring public health and safety.

Global awareness regarding the quality and safety of food, especially concerning its nutritional value, is continuously increasing. This has spurred researchers worldwide to develop innovative methods for improved food quality evaluation. While traditional analytical techniques like High-Performance Liquid Chromatography (HPLC) and Gas Chromatography-Mass Spectrometry (GC-MS) are highly effective for precise quantification in laboratories, they are often costly, time-consuming, and require sophisticated instrumentation. Consequently, there is a pressing need for the development of low-cost, portable, and non-destructive sensor probes capable of evaluating food nutrient levels and overall food quality directly in the field. Such field-deployable sensors represent a crucial advancement for real-time monitoring.

This thesis addresses this critical need by focusing on the development of functionalized electrodes for the rapid and accurate detection of several key food nutrients and related compounds that impact food quality. The core of this research involved designing novel electrochemical sensors, which were then rigorously tested across diverse applications. The development of these sensor materials primarily utilized two strategic approaches: metal oxide modification and Molecularly Imprinted Polymer (MIP) technology. The MIP method harnesses the principle of an engraved polymer-based approach, where meticulously crafted recognition cavities within the polymer matrix are designed to precisely match the target molecule in terms of size, shape, and chemical functionality. This strategy offers notable advantages for agro-industrial applications due to:

a) Cost-effectiveness and Accessibility: The developed electrodes present a highly beneficial alternative to expensive existing analytical equipment. Unlike noble metals or other costly electrode materials, all precursors employed in MIP synthesis are readily available and economically viable.

b) Ease of Fabrication and Real-Time Application: The straightforward fabrication methods, coupled with rapid response-recovery capabilities, render these electrodes particularly practical and advantageous for real-time, in-situ applications, crucial for monitoring nutrient content.

Throughout this thesis, specific sensors have been conceived, constructed, and validated to accurately determine the concentration of important food nutrients, including inositol, syringic acid, and folic acid, as well as other significant compounds affecting food quality like quercetin and salicylic acid, in various food products.

7.2 Summary of Findings

Extensive literature reviews reveal numerous studies focused on the distinct electrochemical detection of various analytes. This thesis has made significant contributions to this field, with the key findings summarized in Table 7.1. Notably, the detection limits achieved in each investigated case have shown marked improvements compared to many earlier reports. The strategic integration of metal oxide and MIP approaches, consistently employed in the fabrication of all developed electrodes, resulted in significantly lower LOD values compared to many conventional electrochemical methods. Furthermore, in contrast to some previous procedures for

electrode fabrication that were time-consuming or required expensive precursors, this research prioritized by utilizing affordable precursors to ensure the developed MIP electrodes are stable, biocompatible, and environmentally benign. These advancements position the developed electrodes as effective, environmentally friendly sensors for target analyte detection in real samples, contributing to the assessment of nutritional quality.

Table 7.1. Major Findings of the Thesis

Sl. No.	Target Compound	Electrode	Precursors	Linear Range	LOD	Ref.
1	Inositol	Pt (Electrochemical)	Platinum	50 to 400 µM	19.28 µM	[Chapter 2]
		MI-2P-IS@C (Capacitive)	Molecular Imprinted Polydopamine-Polyethylene Glycol (PDA-PEG)	0.125 - 1 ppm	1.8 ppb	[Chapter 2]
2	Syringic Acid	UV-Vis Spectroscopy	N/A (Spectroscopic method)	N/A (Qualitative discrimination)	N/A	[Chapter 3]
		MIP-AN@G (Electrochemical)	Monomer: Acrylonitrile, Template: Syringic acid	10 to 100 µM	0.32 µM	[Chapter 3]
3	Folic Acid	MAN@G (Electrochemical)	Monomer: Acrylonitrile, Template: Folic acid	20 to 400 µM	18 nM	[Chapter 4]
4	Quercetin	M-AARGO@G (Electrochemical)	Monomer: Acrylic acid, Template: Quercetin, rGO (Reduced Graphene Oxide)	0.001 to 1 µM; 1 to 400 µM	0.13 nM	[Chapter 5]
		M2P-QT@C (Capacitive)	Monomer: Polydopamine-Polyethylene Glycol (PDA-PEG), Template: Quercetin	10 to 50 ppm	0.035 µg/kg	[Chapter 5]
5	Salicylic Acid (ScA)	Pen-like Trielectrode System	Monomer: Gallic acid (GA) for MIP(GA-ScA)/G working electrode	100-400 µM; 500-1000 µM	1.06 µM	[Chapter 6]

The detailed findings from each relevant chapter of the thesis are outlined below:

a) Chapter 2: Electrochemical Detection of Inositol in Food Samples

This chapter explored two distinct electrochemical sensor designs for the detection of inositol, a crucial non-reducing sugar alcohol with significant health implications.

The first approach involved the development and optimization of a platinum (Pt) electrode-based electrochemical system for rapid inositol detection. Utilizing Differential Pulse Voltammetry (DPV), this system demonstrated efficacy over a wide linear range of operation from 50 to 400 μM, achieving a limit of detection (LOD) of 19.28 μM. This LOD is notably lower than the recommended inositol limit for children (27.7 μM, equivalent to 50mg/kg per day) [19], underscoring its sensitivity for practical applications. Chemometric analysis, specifically Principal Component Analysis (PCA), successfully discriminated between different inositol concentrations, yielding an impressive class separability index (SI) of 142.91. Furthermore, Partial Least Squares Regression (PLSR) and Principal Component Regression (PCR) models exhibited high prediction accuracies of 93.69% and 93.71%, respectively. The sensor's practical utility was validated by achieving a satisfactory recovery rate of 96.18% when tested on real orange juice samples. These results collectively highlight the potential of the Pt electrode-based electrochemical system for reliably detecting varying traces of inositol in everyday food items like fruits and fruit juices.

The second approach introduced a novel, inexpensive, reusable, and stable molecularly imprinted polymer (MIP) technology-based capacitive sensor designed for inositol (IS) detection in fruits. The sensitive material comprised molecular imprinted polydopamine-polyethylene glycol (PDA-PEG) introduced onto copper (Cu)-clad FR-4 plates. The sensor's performance was rigorously investigated across an IS concentration range of 0.125 - 2 ppm. A key finding was the sensor's exceptional linearity from 0.125-1 ppm and a significantly lower LOD of 1.8 ppb, which is superior to many previously reported methods for inositol detection in infusions. Experimental analysis revealed a consistent reduction in parallel capacitance (Cpis) with increasing IS concentration, aligning well with the sensor's equivalent circuit model. The study also elucidated the distinct variations in (C_{pis}) with frequency for both the MI-2P-IS@C (molecularly imprinted) and NI-2P@C (non-imprinted) sensors, along with the impact of frequency on sensor impedance and phase. Predictive modeling using PCR and PLSR techniques

yielded remarkably high average prediction accuracies of 99.91% and 99.90%, respectively. Beyond its high sensitivity and accuracy, the sensor demonstrated excellent selectivity for IS and maintained high stability even after three months of usage. These attributes position the proposed MI-2P-IS@C capacitive sensor as a highly feasible and promising prospect for the quantitative detection of inositol in fruits and other food samples

b) Chapter 3: Quantification of Syringic Acid Using Novel Electrochemical Sensors

This chapter explored two effective methods for the quantification of syringic acid (SGA). The first approach utilized Ultraviolet-visible (UV-Vis) spectroscopy coupled with multivariate analysis. Data measurements performed in the 200-400 nm range, followed by Principal Component Analysis (PCA), confirmed effective clustering of samples with a high-class separability index of 313.52. For quantitative prediction, Principal Component Regression (PCR) and Partial Least Squares Regression (PLSR) analyses were performed, demonstrating high average prediction accuracies of 99.78% and 99.69% respectively, and a high correlation factor (CF) of 0.99 for both models. This primary investigation recommends UV-Vis spectroscopy with multivariate analysis as a viable approach for detecting and assessing SGA.

The second approach involved the development of a highly sensitive and selective molecularly imprinted polymer (MIP) based electrochemical sensor using an acrylonitrile (AN) MIP over graphite (MIP-AN@G electrode). Characterization was performed using UV-Vis, FTIR, and SEM. The sensor exhibited a wide linearity window from 10 µM to 100 µM with a satisfactory lower limit of SA detection (LOD) of 0.32 µM. It showed high repeatability (RSD: 1.11%), reproducibility (RSD: 1.16%), and good stability (RSD: 1.89%). When tested in real food extracts (cauliflower, oregano, black olives), high accuracies (99.34% to 99.79%) were achieved compared to HPLC, with satisfactory t-test results. This confirmed the MIP-AN@G electrode as a promising candidate for SA detection.

c) Chapter 4: Quantification of Folic Acid in Food Extracts Using Molecularly Imprinted Polyacrylonitrile Imbued Graphite Electrode

This chapter elucidated the effectiveness of a molecularly imprinted polyacrylonitrile-imbued graphite-base electrode (MAN@G) for the selective detection of folic acid (FA). Fabricated using acrylonitrile (AN) as the monomer and FA as the template, the electrode was characterized by UV-Vis spectroscopy and SEM. Using DPV and CV techniques, the electrode exhibited

a widespread linearity window from 20 µM to 400 µM concentrations with an acceptable lower limit of detection (LOD) of 18 nM and a limit of quantification (LOQ) of 60 nM. It also demonstrated high reproducibility (RSD: 1.72%), good stability (RSD: 1.32%), and high repeatability (RSD: 1.19%). Tested in food extracts (orange, spinach, papaya, soybean, and cooked rice), it showed high accuracy compared to HPLC, with satisfactory t-test analysis results, establishing its potential for FA detection in food industries.

d) Chapter 5: Advanced Electrochemical and Capacitive Sensors for Quercetin Detection in Food Products

This chapter presented two novel approaches for quercetin (QCN) detection.

The first work described a novel rGO decorated Molecularly Imprinted Polyacrylic Acid Graphite Electrode (M-AARGO@G). Using acrylic acid (AA) as the monomer and QCN as the template, with rGO decoration, the electrode exhibited two broad linearity windows (0.001 µM to 1 µM; 1 µM to 400 µM). It achieved an exceptionally low LOD of 0.13 nM and LOQ of 0.43 nM, alongside high reproducibility (RSD: 1.47%), good stability (RSD: 1.82%), and high repeatability (RSD: 1.17%). Validation in real food extracts (onion, oregano, spinach) showed high accuracy (average 99%) compared to HPLC, with satisfactory t-test results.

The second work introduced a novel Molecular Imprinted Dual-Polymer Infused Capacitive Sensor (M2P-QT@C) for precise QT detection in agro-products. This sensor utilized a molecularly imprinted polydopamine-polyethylene glycol (M2P-QT@C) composite. It showed a linear response to QT concentrations from 10 to 50 ppm, with exceptional sensitivity (LOD: 0.035 µg/kg, LOQ: 0.116 µg/kg). Principal Component Regression (PCR) and Partial Least Squares Regression (PLSR) showed high prediction accuracy exceeding 90%. The sensor demonstrated excellent selectivity and remarkable stability (0.4% performance degradation after three months), making it a valuable contender for QT determination in agro-products.

e) Chapter 6: Towards the development of an integrated, voltammetric electrode for the electrochemical sensing of food quality

This chapter introduced a novel pen-like trielectrode integrated system designed for the detection of salicylic acid (ScA), aiming to overcome limitations of traditional voltammetric analysis in field applications. The system consists of a working electrode with a disposable refill cartridge (MIP(GA-ScA)/G), a reference electrode within a micropipette tip, and a platinum

counter electrode, all integrated to maintain a fixed inter-electrode geometry for enhanced accuracy and reproducibility.

Comparative studies on scan rate variation demonstrated that as the scan rate increased from 10 mV/s to 500 mV/s, the anodic peak current for ScA oxidation consistently increased for both the traditional MIP(GA-ScA)/G electrode and the novel PEN_MIP(GA-ScA)/G electrode. This behavior is characteristic of surface-confined or diffusion-controlled electrochemical processes. The similar trends observed in oxidation peak evolution and comparable current responses between the two systems further validate the viability of the pen-like electrode for ScA recognition.

Investigations into concentration variation revealed that for both the traditional and pen-like electrodes, an increase in ScA concentration from 100 µM to 1000 µM resulted in a corresponding increase in the oxidation peak current. For the PEN_MIP(GA-ScA)/G electrode, the calibration plot exhibited two distinct linear regions: a lower concentration range (100 µM to 400 µM) and a higher concentration range (500 µM to 1000 µM). The presence of these two regions with differing sensitivities (steeper slope in the lower range, 1.416 µA/µM, versus 0.897 µA/µM in the higher range) suggests a change in binding affinity or mass transfer limitations at higher concentrations, possibly due to saturation of MIP binding sites. High correlation coefficients (>0.99) for both linear regions indicate strong linearity and the potential for accurate ScA quantification. The system demonstrated promising analytical performance with an LOD of approximately 1.06 µM and an LOQ of approximately 3.53 µM. Comparative studies in real-world food samples yielded high recovery results (around 99%), highlighting the significant potential of this proposed electrode system for food additive and nutrient recognition in non-laboratory settings.

7.3. Recommendations

Based on the comprehensive findings derived from the developed electrodes presented in this thesis, the following recommendations are put forth for their application in agro-industries and related sectors, with a particular emphasis on food nutrient assessment:

a) Cost-Effective Replacement for Traditional Methods: These electrodes offer a significant advantage for agro-industries by overcoming the limitations of traditional analytical methods in terms of high cost and limited portability. Their affordability and ease of deployment make them a viable alternative for nutrient analysis to expensive existing laboratory equipment.

b) In-situ Measurement Capabilities for Nutrient Profiling: The developed sensors enable the in-situ measurement of various critical food nutrients (viz. inositol and folic acid), as well as other compounds (viz. syringic acid, quercetin, and salicylic acid) that are naturally present in or affect the quality of nutrient-rich foods. This capability is crucial for real-time quality control directly at the point of need, whether in fields, processing units, or retail environments, to ensure optimal nutritional content.

c) Commercial and Health Sector Potential: Given the significant impacts of the tested compounds on human health and product quality, particularly concerning their nutritional value, the developed sensors possess immense potential for profitable utilization in both business and health sectors. There are substantial opportunities for adding value to products through improved quality assurance, nutrient monitoring, and safety assessment.

7.4. Future Scopes of Research

To further enhance the suggested sensing approaches and expand the scope of this research, the following future directions are recommended:

a) Enhanced Economic Viability and Deployability: Further efforts should focus on making the sensors even more economically viable for easier deployment in industrial and agricultural sectors. This could be achieved through the development of screen-printed electrodes or disposable paper-based electrodes. The use of disposable electrodes would also eliminate the need for repeated washing of the sensor surface, thereby ensuring consistently high repeatability and accuracy in nutrient detection.

b) Advanced Predictive Modeling for Nutrient Quantification: For higher accuracy in designing prediction models to quantify relevant food nutrients and other beneficial or quality-impacting food constituents, advanced machine learning methods such as deep learning and convolutional neural networks(CNN) may be employed. This would enable more robust and complex data analysis, leading to more precise quantification of nutritional profiles.

c) Broader Analyte Detection for Comprehensive Nutrient Analysis: While this thesis focused on specific analytes (inositol, syringic acid, folic acid, quercetin, and salicylic acid), future research can extend to creating sensors for other substantial essential nutrients, vitamins, minerals, or bioactive compounds that significantly impact health and the overall nutritional quality of food.

d) Development of Portable, Integrated Devices for On-site Analysis: A significant future research scope involves the development of portable, low-cost, and integrated devices for

comprehensive food quality evaluation, with a strong focus on nutrient assessment. Such devices could combine multiple sensor units with user-friendly interfaces, potentially leveraging wireless connectivity for data logging and remote monitoring. The goal is to develop reliable prototypes that allow users to obtain an overall chemical fingerprint related to the nutritional and quality profile of food products directly in the field.

7.5. Conclusion

This thesis successfully introduces and validates advanced electrochemical sensor technology for the quantitative assessment of several critical food nutrients (inositol, folic acid) and other important food constituents (syringic acid, quercetin, salicylic acid) that influence the quality and safety of food products. Despite the early stage of some of the described studies, there is no dispute that this work has added a new dimension to the approach for evaluating diverse food samples, particularly concerning their nutritional integrity. The developed sensor electrodes are lightweight, inexpensive, and compact, making them ideal for use in field settings. Consequently, the widespread adoption of these tools would be highly feasible, benefiting both producers in maintaining food's nutritional quality and final consumers in assessing product quality prior to purchase. Overall, the manufacturing process for the sensors described in this thesis demonstrates effectiveness with multiple different food analytes, holds immense promise for usage with molecules of a similar kind, and is anticipated to usher in a new, more accessible approach to nutrient and quality control for food products.

Dipan Bandyopadhyay

Professor
Dept. of Instrumentation & Electronics Engg
Jadavpur University
Salt Lake, 2nd Campus
Kolkata-700 106